Explosibility of Coarse Biomass Powders

David John Frank Slatter

Submitted in accordance with the requirements for the degree of
Doctor of Philosophy

The University of Leeds
School of Process, Environment and Materials Engineering

October, 2015

The candidate confirms that the work submitted is his own, except where work which has formed part of jointly-authored publications has been included. The contribution of the candidate and the other authors to this work has been explicitly indicated below. The candidate confirms that appropriate credit has been given within the thesis where reference has been made to the work of others.

List of publications

1. **Pulverised Biomass Explosions: Investigation of the Ultra Rich Mixtures that give Peak Reactivity. H. Sattar • G. E. Andrews • D. Slatter • B. M. Gibbs • H. N. Phylaktou – 26, JULY 2012 Conference: IX International Symposium on Hazards, Prevention, and Mitigation of Industrial Explosions (IX-ISHPMIE)**

(some content of this publication are in chapters 2 and 6)

Hammed Sattar was lead author on this paper. I, together with Hammed Sattar, preformed the $1m^3$ tests used in this research, identified the post combustion residue as mostly appearing unburned and theorised about the possibility of wall contact preventing complete combustion of the dust. Herodotos N. Phylaktou, Bernard M. Gibbs and Gordon E. Andrews helped with supervision of the writing of this paper.

2. **X-ISHPMIE- Biomass explosion testing: Accounting for the post-test residue and implications on the results - February 2015 • in the Process Industries - David J. F. Slatter • Hamed Sattar • Clara Huéscar Medina •Gordon E. Andrews • Herodotos N. Phylaktou • Bernard M. Gibbs X International Symposium on Hazards, Prevention, and Mitigation of Industrial Explosions (X-ISHPMIE) Journal of Loss Prevention**

(some content of this publication are in chapters 3 and 7)

I was lead author on this paper, Hamed Sattar and Clara Huéscar helped me run the tests, set up the vessel and extract the residue. All analysis and writing was done by myself. Herodotos N. Phylaktou, Bernard M. Gibbs and Gordon E. Andrews helped with supervision of the writing of this paper.

3. **Flame Propagation of Pulverised Biomass Crop Residues and their Explosion Characteristics August 2015 Muhammad Azam Saeed • Gordon E. Andrews • Herodotos N. Phylaktou • David Slatter • Clara Huéscar Medina • Bernard Gibbs 25th International Colloquium on the Dynamics of Explosions and Reactive Systems (ICDERS), University of Leeds, Leeds, UK; 08/2015**

(some content of this publication are in chapter 5)

Muhammad Azam Saeed was lead author on this paper. I, together with Muhammad Azam Saeed and Clara Huéscar Medina, performed the $1m^3$ tests used in this research and computed flame speeds. Herodotos N. Phylaktou, Bernard M. Gibbs and Gordon E. Andrews helped with supervision of the writing of this paper.

4. **Comparison of the explosion characteristics and flame speeds of pulverised coals and biomass in the ISO standard 1 m3 dust explosion equipment Clara Huescar Medina • Brian MacCoitir • Hamed Sattar • David J. F. Slatter • Herodotos N. Phylaktou • Gordon E. Andrews The 10th European Conference on Coal Research and its Applications, Fuel, Volume 151, 1 July 2015, Pages 91–101**

(some content of this publication are in chapter 6)

Clara Huéscar Medina was lead author on this paper. I, together with Hammed Sattar and Clara Huéscar Medina, performed the $1m^3$ tests used in this research. Prior to this work I supervised and carried out a complete replacement the thermocouples in the vessel. Herodotos N. Phylaktou, Bernard M. Gibbs and Gordon E Andrews helped with supervision of the writing of this paper.

5. **Agricultural Waste Pulverised Biomass: Lean Flammability and Flame Speed as a Measure of Reactivity June 2014 M. A. Saeed • C. Huescar Medina • G. E. Andrews • H. N. Phylaktou • D. Slatter • B. Gibbs Tenth International Symposium on Hazard, Prevention and Mitigation of Industrial Explosions (X ISHPMIE); 06/2014**

(some content of this publication are in chapters 5)

Muhammad Azam Saeed was lead author on this paper. I, together with Muhammad Azam Saeed and Clara Huéscar Medina, performed the Hartmann tube tests used in this research and computed flame speeds. This paper used results from my tests as well as observations on the dust distribution during these tests. Herodotos N. Phylaktou, Bernard M. Gibbs and Gordon E. Andrews helped with supervision of the writing of this paper.

6. **Ignition Sensitivity of Coal / Waste /Biomass Mixtures August 2015 Nieves Fernandez-Anez • David J. F. Slatter • Muhammad Azam Saeed • Herodotos N. Phylaktou • Gordon E. Andrews • Javier Garcia-Torrent Proceedings of the 8th Int. Conference on Sustainable Energy and Environmental Protection (SEEP2015), University of the West of Scotland, Paisley, Scotland; 08/2015**

(some content of this publication are in chapter 5)

Nieves Fernandez-Anez was lead author on this paper. I, together with Muhammad Azam Saeed and Nieves Fernandez-Anez, performed the Hartmann tube tests used in this research and computed flame speeds. I set up and developed the use of the high speed camera for this research. Herodotos N. Phylaktou, Bernard M. Gibbs, Javier Garcia-Torrent and Gordon E. Andrews helped with supervision of the writing of this paper

7. **The Influence of Particle Size and Volatile Content on the Reactivity of HC and HCO Chemical and Biomass Dusts D. J. F. Slatter • C. Huescar Medina • H. Sattar • G. E. Andrews • H. N. Phylaktou • B. M. Gibbs Proceedings of the Seventh International Seminar Fire and Explosion Hazards; 01/2013, 109, D. Bradley, G. Makhviladze, V. Molkov, P. Sunderland, F. Tamanini.**

(some content of this publication are in chapters 2, 6 and 7)

I was lead author on this paper, Hamed Sattar and Clara Huéscar helped me run the tests. All analysis and writing was done by myself. Herodotos N. Phylaktou, Bernard M. Gibbs and Gordon E. Andrews helped with supervision of the writing of this paper.

8. **Improvements to the Hartmann Dust Explosion Equipment for MEC Measurements that are Compatible with Gas Lean Limit Measurements Muhammad A. Saeed, Gordon E. Andrews, Herodotos N. Phylaktou, Hamed Sattar, Clara Huescar-Medina, David Slatter, Herath, P. & Bernard M. Gibbs Proceedings of The 10th Asia-Oceania Symposium on Fire Science and Technology; 10/2015, 87.**

(some content of this publication are in chapter 2)

Muhammad A. Saeed was lead author on this paper and wrote it. I helped to put it together and do the literature search on this paper as well as consulting regularly on the progress and direction of the work. Herodotos N. Phylaktou, Bernard M. Gibbs and Gordon E. Andrews helped with supervision of the writing of this paper.

Acknowledgements

This research has been carried out by a team which has included Hamed Sattar, Clara Huéscar, Muhammad Azam Saeed, Nieves Fernandez-Anez, Herodotos N. Phylaktou, Gordon E. Andrews, Bernard M. Gibbs and Robert Boreham.

I want to thank my supervisors Herodotos N. Phylaktou, Gordon E. Andrews and Bernard M. Gibbs for consultation and guidance on the direction of the research and the writing of my thesis.

Thanks are due to Mr. Robert Boreham, for providing technical support and maintenance of the experimental system in order to carry out the research work.

I want to thank my fellow research students; Hamed Sattar, Clara Huescar and Muhammad Azam Saeed for their help in operating equipment and running and maintaining the laboratory.

I want to thank my Mother and Father who experienced all the ups and downs of my research. I know, they will be happy to see me complete this degree.

Abstract

Pulverised biomass is being used in electric power generation, either co-fired with coal or increasingly as 100% biomass. However, there is minimal information in the literature on the mechanism of flame propagation in pulverised biomass. In the present work the explosion technique was used to obtain fundamental information on the rate of flame propagation, the lean limits of flame propagation and related explosion characteristics of coarse biomass.

A large part of this research involved the modification of the ISO $1m^3$ method to enable it to be used with coarse fibrous biomass powders. The technique that worked was to follow the Hartmann method and place the dust inside the vessel using a hemispherical bowl and then disperse this dust with a blast of air. This was demonstrated to work with coarse woody biomass and the calibration was established using cornflour and referenced to the standard method.

The MEC and K_{st} for dusts were shown to have a dependence on the particle size. However, very coarse particles still propagated a flame, with no evidence that this was due to preferentially burning of the finer particles. Biomass particles of 300-500µm were shown to be flammable, i.e. as large as kerosene mist and large than coal particles will propagate a flame. For coarse woody biomass the K_{st} values were very low <20 bar m/s in many cases, but the peak pressure was high and hence the explosion would destroy biomass handling plant.

This work found that the unburnt material was compressed into a layer against the wall of the vessel ahead of the flame front, thus preventing it from interacting with the flame front. It was postulated that large particles lagged the main flame due to interaction with the explosion induced wind. This led to large particles being pyrolysed behind the flame front and then to arrive last at the wall and so appear as on outer pyrolysed layer on the material compressed against the wall. This explanation also enabled an explanation to be given for the very rich mixtures that could burn with dusts than could not burn if the material was a gas.

Table of contents

List of publications iii

Acknowledgements vii

Abstract viii

Table of Contents ix

List of Tables xv

List of Figures xvii

1 Introduction 1

1.1 Biomass 1

1.2 Green Energy 3

1.3 Biomass Energy generation 5

1.4 Environmental Legislation 13

1.5 Implementation concerns for biomass electricity 15

1.6 Safety legislation 18

1.7 Problems with existing data 19

1.8 Aims 21

2 Literature review 23

2.1 Woody biomass 23

2.2 Dust explosions 31

2.2.1 Definition 31

2.2.2 Types of Flame Propagation 35

2.2.3 Safety regulations 39

2.2.4 Protection systems 42

2.2.5 Dust combustion compared to gas combustion..... 45

2.2.6 Mode of Dust Flame Propagation..... 47

2.3 Explosibility 52

2.3.0.1 Stoichiometric air to fuel and equivalence ratio for H and CH type gases..... 54

2.3.0.2 Stoichiometric fuel to air and equivalence ratio for CHO type dust..... 56

2.3.1 Minimum explosive concentration 59

2.3.2 Maximum explosive concentration 65

2.3.3 Max Pressure and K_{ST} generation 67

2.3.4 Flame speed and burning velocity..... 72

2.3.5 Turbulence and turbulent burning velocities in dusts 73

2.3.6 Laminar burning velocity for dusts..... 76

2.3.7 Particle size..... 78

2.3.8 BIOT number..... 86

2.3.9 Moisture content..... 90

2.3.10 Sources of Ignition..... 91

2.3.11 Test vessels 92

2.3.12 Minimum ignition energy 99

2.3.13 Limiting oxygen concentration..... 100

2.3.14 Combustion residue 100

2.3.15 Secondary assessment of aims 102

Chapter 3 Equipment and Experimental Methodology 104

3.1 Fuels tested..... 104

3.1.1 Sample preparation..... 106

3.1.2 Milling..... 106

3.1.3 Sieving 107

3.2 Residue 108

3.2.1 Residue collection and separation procedures 109

3.2.2 Residue separation equipment 113

3.3 Material analysis 114

3.3.1 Elemental analysis 114

3.3.2 Proximate analysis 115

3.3.3 Calorific values 117

3.3.4 Particle size distribution 118

3.3.5 Surface morphology – SEM 119

3.4 Hartmann tube apparatus and its modifications 120

3.4.1 MEC definition in Hartmann 122

3.4.2 Thermocouple results 123

3.4.3 Rate of pressure rise 125

3.4.4 High speed video 126

3.5 The 1m^3 dust explosion vessel set-up 132

3.5.1 Ignition system 137

3.5.2 Pressure transducers 138

3.5.3 Thermocouples 141

3.5.4 Flame speed measurements 1m^3 146

3.5.5 Thermocouples maintenance and separation 150

3.5.6 Vacuum Pump 152

3.5.7 Mixing control panel 153

3.5.8 Data acquiring and logging 153

3.5.9 Reasons for injector modifications 155

3.6 Experimental procedures 156

3.7 Procedure for dusts explosions in the modified Hartmann tube apparatus 156

3.8 Procedure for dust explosions in the Leeds 1m^3 explosion vessel - C-ring 157

3.8.1 Dust explosions in the Leeds 1m^3 explosion vessel – wall mounted 160

3.8.2 Dust explosions in the Leeds 1m^3 explosion vessel – in vessel dust storage/dispersion 161

3.8.3 Repeatability of tests 163

3.9 Procedure for gas explosions in Leeds 1m^3 explosion vessel 164

3.9.1 Turbulent gas explosions tests 166

3.9.2 Laminar gas explosions tests 166

3.10 Mass burned concentration 167

4 Biomass composition and characteristics 169

5 Influence of particle size on MEC and mixture reactivity using the Hartmann equipment. 173

5.1 Introduction 173

5.1.2 Hartman flame speed and rate of pressure rise 180

5.2 Hartman tests with High speed video 183

5.2.1 Hartman flame propagation 185

5.2.2 Hartman single particle combustion/spread 191

5.2.3 Single particle combustion and propagation video 194

5.2.4 Single particle combustion – separation distance 197

5.3 MEC 202

5.4 Discussions 206

5.5 Conclusions 211

6 1m^3 Explosion vessel tests and disperser calibration 215

6.1 Disperser designs and Testing 215

6.1.1 Disperser designs 216

6.1.2 Calibration and timing alterations 220

6.2 Fibrous biomass tests 222

6.2.1 Biomass explosibility 222

6.2.2 Effect of elemental composition 226

6.2.3 Particle size effect 227

6.2.4 Flame speeds 231

6.2.5 Mass burnt 234

6.3 Cake formation 237

6.4 Disperser limitations 242

6.5 Future work on dispersers and 1m^3 vessel 244

6.6 Conclusions 246

7 Residue separation and analysis 252

7.1 Separated samples 253

7.1.1 Differences between layers 254

7.1.2 Size analysis of what burnt 262

7.1.3 Future work on equipment 268

7.2 Conclusions 269

8 Further discussion and comparisons 273

8.1 Hartmann comparison against 1m^3 273

Chapter 9. Conclusions and future work. 280

9.1 Effect of particle size on the combustion behaviour of Biomass with reference to coal. 281

9.2 Combustion behaviour of Biomass. 282

9.3 Reasons for extended rich limit in biomass. 284

9.4 1m^3 improvements 286

9.5 Hartmann improvements 288

9.6 Future work 289

9.7 Equipment improvements 291

References 292

List of tables

Table 1.1 Total % renewables (DUKES, 2014b). 5

Table 1.2 Total Generation (DUKES, 2014b). 6

Table 1.3 Fuel used for renewable energy (DUKES, 2014a). 8

Table 1.4 Closure of power stations in the UK (DUKES, 2014a)..... 9

Table 2.1 Biomass Lignin, Cellulose and hemicellulose composition (Bergman, 2011, Couhert et al., 2009, Tillman, 1978). 25

Table 2.2 Polymer and hemicelluloses composition of the hardwood against softwood (Bergman, 2011). 26

Table 2.3 The chemical composition of four biomass of biomass (Bergman, 2011) 27

Table 2.4 Proximate composition of coal and biomass (Wilén, 1999). 34

Table 2.5 Typical explosion values per material and the factors that affect them (Ramírez, 2009). 35

Table 2.6 Categorisation of dusts based on K_{st} and Pmax (Foulke, 2007). 42

Table 2.7 Elemental composition of coal and biomass (Wilén, 1999). 57

Table 2.8 MEC equivalence ratios for various materials, calculated from elemental and proximate analysis (Wilén, 1999). 58

Table 2.9 Collection of CHO, CH and coal dust MEC data. 61

Table 2.10 MEC shown to be dependent on the particle size for coal (Cashdollar, 1996). 63

Table 2.11 MEC as a function of particle size 80

Table 2.12 The Biot number for the oak size fractions tested. 89

Table 2.13 Compilation of 20L sphere and hartman tests. 92

Table 2.14 MEC from 20L spher compared to 1m^3 vessel (Wilén, 1999). 94

Table 2.15 K_{st} values from differnt sets of test equipment Eckhoff (2003). 96

Table 2.16 Comparison of 5 different materials by 4 different labs Eckhoff (2003). 97

Table 2.17 Hartman MEC compared to 1m^3 MEC showing good agreement 97

Table 2.18 MEC compared from different sources (EPRA, 2011) 99

Table 2.19 MIE for various dusts 100

Table 3.1 Thermocouple distences within vessel 151

Table 3.2 repeat tests with the new disperser 163

Table 4.1 Particle size of as recived and post combustion fuel samples with corresponding MEC's. 169

Table 4.2 Materials analysied by TGA and Proximate analysis 170

Table 4.3 Residue materials analysied by TGA and Proximate analysis 171

Table 4.4 Residue materials analysied by TGA and Proximate analysis 172

Table 5.1 <500µm fractions pine and oak particle size compared 206

Table 5.2 Effect of milling on oak <500 µm 210

Table 7.1 Seperated residue samples 253

Table 8.1 1m^3 MEC against hartmann MEC 273

List of figures

Fig 1.1 Particle shape and size differences between coal dust and woody biomass (Laddha, Zink-Sharp, 1997). 3

Fig 1.2 Renewable electricity generation (MacLeay, 2015). 4

Fig 1.3 Green electricity, heat and transport fuels (DUKES, 2014b). 5

Fig 1.4 Pressure rise and flammability limits of methane gas compared to coal and polyethylene dust (Cashdollar, 2000). 22

Fig 2.1 Chemical structure of cellulose polymer (Lentini, 2006). 23

Fig 2.2 Chemical structure of hemicellulose monomers (Huiling, 2015). 24

Fig 2.3 Chemical structure of lignin polymer (Lentini, 2006). 24

Fig. 2.4 Fresh willow milled in the cutting mill with bottom sieve of 250µm (Bergman, 2011). 28

Fig. 2.5 The structure of a woody biomass cell wall. (a) part of the cell wall and middle lamella, primary wall and secondary cell wall, (b) macro fibril mutual structure, (c) micro fibril structure, (d) individual cellulose polymers including micelles (Bergman, 2011). 29

Fig 2.6 Image of flame front (in pink) propagation in dust cloud showing disappearance of dust particles ahead of flame front (Proust, 2006). 33

Fig 2.7 Different inerting agents and their effect on the flammability limits of coal (Dastidar, 2002). 44

Fig 2.8 Volatile concentration in a solid fuel needed to produce combustion in fly ash, with varied concentration (Dastidar, 2002). 44

Fig 2.9 Time frame for pyrolosis in relation to temperature (Proust, 2006). 49

Fig 2.10 Low concentration Hydrogen and graphite 2 stage explosion (Denkevits, 2007). 50

Fig 2.11 High hydrogen medium graphite dust single stage explosion. (Denkevits, 2007) 51

Fig 2.12 Dust/gas hybrid MEC with varied volatile and gas concentration (Eckhoff, 2003). 52

Fig 2.13 MEC against average particle size for a large number of biomass samples (Wong, 2013). 62

Fig 2.14 Volatile content against MEC (Eckhoff, 2003). 64

Fig 2.15 UFL and LFL for gasses as a function of carbon number, gasses -blue, liquids - red, solids - green (Jechura, 1987). 66

Fig 2.16 Pressure rise and flammability limits of magnesium dust 70

Fig 2.17 Rate of pressure rise and flammability limits against concentration for general dust. (BSEN, 2004) 71

Fig 2.18 Burning velocity at different temperatures and pressures (Bradley and Mitcheson, 1976). 73

Fig 2.19 Flame speed and K_{st} as a function of turbulent velocity (Phylaktou, 2001). 75

Fig 2.20 Pressure rise for material against ignition delay for dust (Phylaktou, 2010). 76

Fig 2.21 Mist droplet flammability with droplet size (Cook, 1977). 81

Fig 2.22 Droplet flammability as a function of size (Zabetakis, 1965). 82

Fig 2.23 Inter particle force against particle size (Shao, 2008). 85

Fig 2.24 Surface area : volume ratio of cylinder against surface area : volume ratio of sphere for varying cylinder height. 86

Fig 2.25 Maximum pressure from 20L spher and $1m^3$ vessel (Wilén, 1999). 95

Fig 2.26 One of many variations of 1m3 chamber that are in use (Dastidar, 2001). 98

Fig 2.27 (A) Feedstock (B) Tubular reactor residue (C) Wire-mesh reactor residue (Cetin, 2004). 101

Fig 2.28 Drop-tube furnace residue (Cetin, 2004). 102

Fig 3.1 Retsch SM100 cutting mill 107

Fig 3.2 Material trapped between the bag layers. 110

Fig 3.3 12L separator 111

Fig 3.4 Separation equipment used 111

Fig 3.5 Separation equipment schematic 112

Fig 3.6 Top fraction filter paper 113

Fig 3.7 Bottom fraction filter paper 113

Fig 3.10 Leeds University Leo 1530 Gemini and attached computers. 119

Fig 3.11 Hartmann dispersion device. 120

Fig 3.12 Leeds University Hartman vessel. 121

Fig 3.13 Pressure and thermocouple readouts from the hartmann apperatus for lycopodium powder 123

Fig 3.14 Thermocouple responces at and around the vent bursting .. 124

Fig 3.15 Rate of pressure rise against thermocouple flame speeds ... 125

Fig 3.16 Without dust (red), With dust - coarse and ignition (green) and With dust - fine and ignition (blue). 125

Fig 3.17 Image of dust distribution around the spark at ignition <63µm oak 127

Fig 3.18 Ignition delay for different particle size materials in the hartmann apperatus as a function of equivlance ratio. 128

Fig 3.19 Oak <500µm (Ø=1= 218.9) 1 g, 750g/m^3, Ø=3.44 129

Fig 3.20 Oak <500 (Ø=1= 218.9) 0.5 g, 375g/m^3, Ø=1.71 129

Fig 3.21 Oak <500 (Ø=1= 218.9) 0.25 g, 187.5g/m^3, Ø=.86 129

Fig 3.22 Oak <63µm (Ø=1= 218.9) 1 g, 750g/m^3, Ø=3.44 130

Fig 3.23 Oak <63µm (Ø=1= 218.9) 0.5 g, 375g/m^3, Ø=1.71 130

Fig 3.24 Oak <63µm (Ø=1= 218.9) 0.25 g, 187.5g/m^3, Ø=.86 130

Fig 3.25 Oak <63µm (Ø=1= 218.9) 0.08 g, 60g/m^3, Ø=0.275 131

Fig 3.26 Flame speeds of oak <63µm at different concentrations. 131

Fig 3.28 Leeds 1m3 vessel from front and side 133

Fig 3.29 Dust pot for Leeds 1m3 vessel 133

Fig 3.30 C-ring injector system. 135

Fig 3.31 Pressure loss in injection pot and corresponding pressure rise in explosion vessel due to explosion (BSEN, 2011). 136

Fig 3.32 Two 5KJ igniters with blast cup. 138

Fig 3.33 Curve from the experimental results for the pressure-time trace of an explosion test methane cornflour and EFB in the 1m^3 vessel. 139

Fig 3.34 <63µm oak dp/dt and pressure traces from 1m^3 vessel. 140

Fig 3.35 Vertical and horizontal thermocouple array. 141

Fig 3.36 Cross section of a K-type thermocouple. 142

Fig 3.37 Mount used to secure thermocouple to 1m^3 vessel..... 142

Fig 3.38 Different thermocouple responces from same test (cornflour). 144

Fig 3.39 Response of thermocouple against dust particle size (A) EFB (B) cornflour. 145

Fig 3.40 10% methane laminar test - pressure with thermocouple 15-22 activation times. 146

Fig 3.42 Thermocouple locations within vessel 150

Fig 3.43 Edwards two stage high vacuum pump 152

Fig 3.44 Sequence generator. 154

Fig 3.45 Globe disperser side 160

Fig 3.46 Deflection plate disperser from ISO standard 160

Fig 3.47 dispersion cup 161

Fig 3.48 Disperser made from dispersion cup design 162

Fig 4.1 TGA volatile release rates against temperature for all biomasses and coal tested by this group. 169

Fig 4.2 Oak 150-300µm 169

Fig 4.3 Oak 63-150µm 170

Fig 4.4 Oak <63µm 171

Fig 4.5 Oak <500µm 171

Fig 4.6 Pine 300 - 500µm 172

Fig 4.7 Wood as received 172

Fig 5.1 Milled pine sieved into different size fractions 174

Fig 5.2 Un-milled pine sieved into different size fractions 176

Fig 5.3 Comparason of oak and pine MEC at size distrubution <63µm. 177

Fig 5.4 Comparason of oak and pine MEC at same size size distrubution <500µm. 177

Fig 5.6 MEC (equivalence ratio) of materials tested against d_{10} 179

Fig 5.7 MEC (equivalence ratio) of materials tested against d_{50} 179

Fig 5.8 MEC (equivalence ratio) of materials tested against d_{90} 180

Fig 5.9 Rate of pressure rise and MEC for oak and pine size ranges tested 181

Fig 5.10 rate of pressure rise against particle size 182

Fig 5.11 Oak less than 63µm (Ø=1= 218.9) 0.5 g, 375g/m^3, Ø=1.71 184

Fig 5.12 Lycopodium 37.5g/m^3, Ø= 0.307 close up 186

Fig 5.14 Oak 300 -150µm (Ø=1= 218.9) 0.5 g, 375g/m^3, Ø=1.71 188

Fig 5.15 Oak <63µm 375g/m^3, Ø=1.71 Lycopodium powder 375g/m^3, Ø= 3.07 188

Fig 5.16 Coconut trunk <500µm 0.5g 375 g/m^3, 1.75 Ø 189

Fig 5.17 A - Oak <63µm 0.25g and B - Oak 63µm 0.08g 190

Fig 5.18 Oak less than 63µm (Ø=1= 218.9) 0.5 g, 375g/m^3, Ø=1.71 191

Fig 5.20 Seperation distences oak 63-150µm fraction. 193

Fig 5.21 Seperation distences oak 150-300µm fraction. 193

Fig 5.24 Particle to particle propagation in 150-300µm oak..... 196

Fig 5.25 Images used to scale the magnified particle to particle propagation images. 197

Fig 5.26 Particle to particle propagation A-B. 198

Fig 5.27 Particle to particle propagation A-C. 199

Fig 5.28 Single particle burnout time from video. 201

Fig 5.29 Inert material content against MEC from the Hartmann. 203

Fig 5.30 MEC of materials tested against d_{10}, d_{50}, d_{90} and D3/2. 204

Fig 5.31 MEC of materials tested against D 3/2. 205

Fig 5.32 MEC of materials tested against D3/2 without <500µm. 206

Fig 5.33 Ignition proberbility of all hartmann tests 209

Fig 5.34 MEC and dp/dt againse D 3/2. 210

Fig 6.1 K_{st} produced from various disperser designs with 750 g/m^3 cornflour. 216

Fig 6.2 Maximum pressure produced from various disperser designs with 750 g/m^3 cornflour. 217

Fig 6.3 (A) hemispherical disperser, (B) hemispherical lip disperser, (C) hemispherical lip perforated disperser. 218

Fig 6.4 (A) spherical disperser 30 holes 2cm, (B) spherical disperser 30 1.4cm holes..... 219

Fig 6.5 750g/m^3 cornflour flame propagation in drilled pipe hemispherical disperser. 220

Fig 6.6 Ignition delay changes for drilled pipe hemispherical disperser 221

Fig 6.7 ignition delay changes for hemispherical disperser 221

Fig 6.8 Maximum pressure as a function of the (A) injected and (B) burned equivalence ratio 222

Fig 6.9 K_{st} as a function of the (A) injected and (B) burned equivalence ratio. 222

Fig 6.10 Maximum pressure as a function of the (A) injected and (B) burned equivalence ratio 223

Fig 6.11 K_{st} as a function of the (A) injected and (B) burned equivalence ratio. 224

Fig 6.12 <63µm oak dp/dt and pressure trace 228

Fig 6.13 <500µm oak dp/dt and pressure trace 228

Fig 6.14 Pressure trace from <63µm (blue) and <500µm oak (green). 229

Fig 6.15 MEC against d_{10}, d_{50}, and d_{90} and D 3/2 230

Fig 6.16 K_{st} against d_{10}, d_{50}, and d_{90} and D 3/2 230

Fig 6.18 Oak <63 µm 500g/m^3 232

Fig 6.19 Oak <63 µm 1000g/m^3 232

Fig 6.20 Pine <500µm -1500 g/m^3 233

Fig 6.21 Oak 150 - 300µm - 1500 g/m^3 233

Fig 6.22 Mass burnt against nominal mass. 235

Fig 6.23 Mass of powder burned as a function of mass injected in equivalence ratio. 235

Fig 6.24 (A) Milk powder "cake", wall-touching side (B) Milk powder "cake" flame-touching side 238

Fig 6.25 Rate of pressure loss for methane and corn flour 239

Fig 6.26 Pressure loss rate, after the peak pressure as a function of the calculated dust wall layer thickness. 240

Fig 6.27 Rate of pressure decay as a function of the adiabatic flame temperature at constant pressure. 241

Fig 6.28 Rate of pressure loss as a function of the burned dust Ø 242

Fig 6.29 3000g/m^3 wood after explosion. 243

Fig 6.31 Mass injected against mass burnt 244

Fig 6.32 Igniters post ignition (A) partial failure of igniter shell (B) complete failure of igniter shell 246

Fig 7.1 Cenosphere's in residue. 255

Fig 7.2 Fully combusted particle. 256

Fig 7.3 Secondary material loss. 256

Fig 7.4 Cenosphere 257

Fig 7.5 150 – 300 3 (A) and 4 (B) Image of cenosphere's in the residue 257

Fig 7.6 632 (A) and 631 (B) Image of cenosphere's in the residue 258

Fig 7.7 Residue 632 top (A) bottom (B) 259

Fig 7.8 1533 top (A) bottom (B) 259

Fig 7.9 Pine nut top (A) bottom (B) 260

Fig 7.10 Trapped material from vacuum bag. 261

Fig 7.11 <63µm size analysis, logarithmic scale, normal distribution 263

Fig 7.12 <63µm size analysis, cumulative distribution 263

Fig 7.13 63 – 150µm size analysis, logarithmic scale, normal distribution. 264

Fig 7.14 63 - 150µm size analysis, cumulative distribution. 264

Fig 7.15 150 - 300µm size analysis logarithmic scale normal distribution. 265

Fig 7.16 150 - 300µm size analysis cumulative distribution. 265

Fig 7.18 <500µm size analysis, cumulative distribution. 267

Fig 7.19 1533 top separation filter paper 269

Fig 8.1 Hartmann and 1m^3 rate of pressure rise nominal concentration 275

Fig 8.3 Maximum rate of pressure rise recorded 277

Fig 8.5 Rate of pressure rise from different vessels at different concentrations 278

Fig 9.1 USBM 20 L explosibilty test chamber (Cashdollar, 1996). 287

1 Introduction

1.1 Biomass

Eventually, fossil fuel reserves will decrease to the point that they become financially unviable. By this point, the world will have had to move towards more sustainable, non-environmentally toxic energy sources such as wind, solar and biomass. The combustion of sustainably produced biomass for electric power generation or thermal heat is one of the green technologies that have been developed in recent years, primarily for electric power generation in existing coal fired power plants. The use of biomass for thermal heat is also being encouraged in the UK where it has not been a significant source of industrial process heat for many years.

Any use of biomass for power generation or heat has to be sustainable and criteria for this are set out in EU legislation. The key criterion is that new biomass must be planted to replace that harvested. For wood this means the whole of an existing forest cannot simply be felled for biomass. If the growing cycle for a mature tree is say 50 years then only 2% of an existing forest can be felled per year and that 2% has to be replaced. Agricultural wastes are a more obvious bio-energy source as they are based on annual crops and the waste is currently not fully utilised. However, here the energy source is distributed over a large area and the collection and transport costs are high. Currently most use of biomass for energy is forest trees and forest waste. Waste wood from the construction industry is also a significant source of biomass, but has more restrictions on its use due to the presence of contaminants. Additionally, any additional preparation and handling (particle milling, intermediate shipping or torrefaction) will consume energy, reducing the energy savings of biomass against fossil fuels. Therefore if a power station is built next to a forest and the fuel is sustainably harvested this biomass will have lower carbon footprint that biomass collected from scattered sources. Further, the finer the biomass is milled prior to combustion the higher the carbon footprint that biomass.

Carbon dioxide is captured from the atmosphere through the biological processes of photosynthesis by plants; this is then burnt as bio-mass to produce energy. This method does not release any additional CO_2 into the atmosphere as the biomass

has drawn its carbon content from the atmosphere through photosynthesis and so is only re-releasing what was drawn from the atmosphere when burnt. This differs from fossil fuels that re-introduce previously trapped C into the atmosphere in the form of CO_2.

Each year around the world, photosynthesis generates 6-7 times as much energy that is then stored as biomass, than we consume in the same time frame. Therefore biomass is the fourth largest energy source available after solar, wind and geothermal (A. Garcia-Maraver, 2015) and could in the foreseeable future become one of our main energy sources.

Biomass also has the significant advantage over other green or renewable energy sources; it can be utilised as a solid, liquid or gas. Biomass can be gasified like coal to produce syngas that can be used in the Fischer-Tropsch process to produce diesel fuel while butanol is a fermentation product and fit for use in petrol engines. Wood dust/chips or torrefied material can replace coal in fluidised bed coal burners (or axial/rotary burners if the particles are small enough), while syngas can be burnt in gas turbines. So unlike any other energy source biomass has the ability to fit into our current energy infrastructure with relatively few modifications.

However, problems exist in the processing of biomass for use as a fuel source. The first of these is the low energy density combined with the relatively high moisture content. This makes transport in bulk quantities expensive, for raw biomass such as logs or hay bales. The second is that woody biomass is very fibrous and tough, making the production of biomass particles $\leq$500 μm or 0.5mm a difficult and energy consuming process. This creates a problem in burning biomass as it is these large particles that are currently being fed to burners in coal boilers.

Figure 1.1 compares pulverised coal with pulverised wood. The particle length/diameter ratio (L/D) is about 1 and relatively round. For pulverised wood particles small fibres are generated with a long cylindrical shape and large L/D of typical 10 or more.

Fig 1.1 Particle shape and size differences between coal dust and woody biomass (Laddha, Zink-Sharp, 1997).

Woody biomass for power generation started with co-firing with coal in existing coal fire power station burners such as Drax near Leeds in the UK. Proportions of biomass started at 10% and were increased as more supplies became available to 50%. However, due to changes in UK government support for biomass, the highest subsidy was restricted to 100% biomass plants and these are now in operation, such as at Drax.

Co-firing biomass with coal can have a substantial impact on the emissions of sulphur compounds (SOx) and nitrogen oxides (NOx). SOx emissions are reduced when biomass is fired with coal, as most biomass fuels contain far less sulphur than coal. Similarly NOx emissions are reduced due to lower N content of biomass.

Cellulosic materials are widely used in today's manufacturing processes in dust form. Sawdust is used for chip board and all the wood processing industry's produces sawdust, other materials are used in dust form to make animal feed pellets. In agriculture biomass type dusts occur in grain silos and in the manufacture of food products such as sugar and flour. All these materials have an explosion risk and more information is known about this type of products than is known about the hazards of sawdust. The main reason for this is that the experimental equipment for investigating dust explosions do not work adequately with fibrous sawdust. This will be discussed in more detail in the literature review.

1.2 Green energy

Over the last 13 years the growth in renewable energy in the UK has been significant (10TWh to 53.6TWh, a 536% increase in capacity) as is shown in **Figure**

1.2 (MacLeay, 2015). This shows that the growth in renewable energy is mainly due to growth in solar, wind and biomass. However, while solar and wind are weather dependent biomass is a continuous reliable source of renewable energy, making it more desirable from the point of view of a green supply of electricity when it is required rather than when the wind blows or sun shines. Landfill gas utilization prevents the release of methane, a far more damaging gas to the environment than CO_2 and harvests an otherwise wasted energy source. The methane is collected by pipes into the landfill site and fed into a gas turbine for combustion, 1.45% of the UK's electricity generation now comes from landfill gas combustion and is effectively a bioenergy source as the gas comes from biological microbe actions in the landfill waste once the site is capped off.

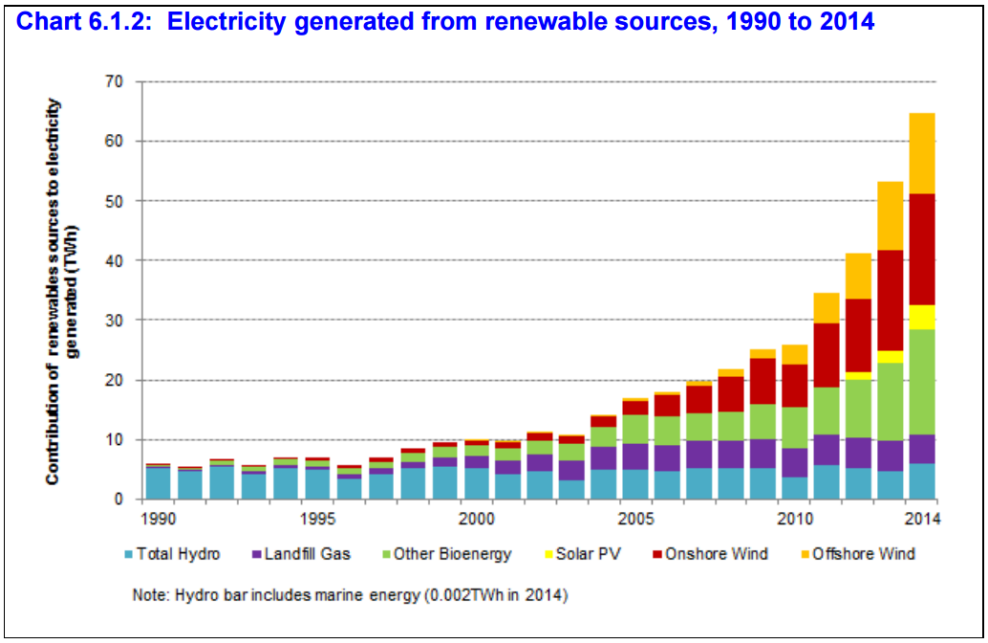

Fig 1.2 Renewable electricity generation (MacLeay, 2015).

A more detailed breakdown of the UK's renewable energy generation is shown in **Figure 1.3** (DUKES, 2014b). This shows that renewable electricity is the dominant use of green generation technology and that biomass for heat is significant but much lower than for electricity and biofuels for transport is smaller than biomass for heat. This is in spite of heat being the largest energy utilisation sector and transport the second largest. The EU target for renewables by 2020 is 20% of total energy NOT 20% of electricity, but it is only.in electricity that the target might be met.

Figure 1.3 shows that biomass for electricity has nearly twice as much fuel imported as is grown in the UK and there is a significant contribution from animal

biomass and waste burning for electricity generation. Biomass based electricity with all sources included is just behind that of all wind energy in 2014.

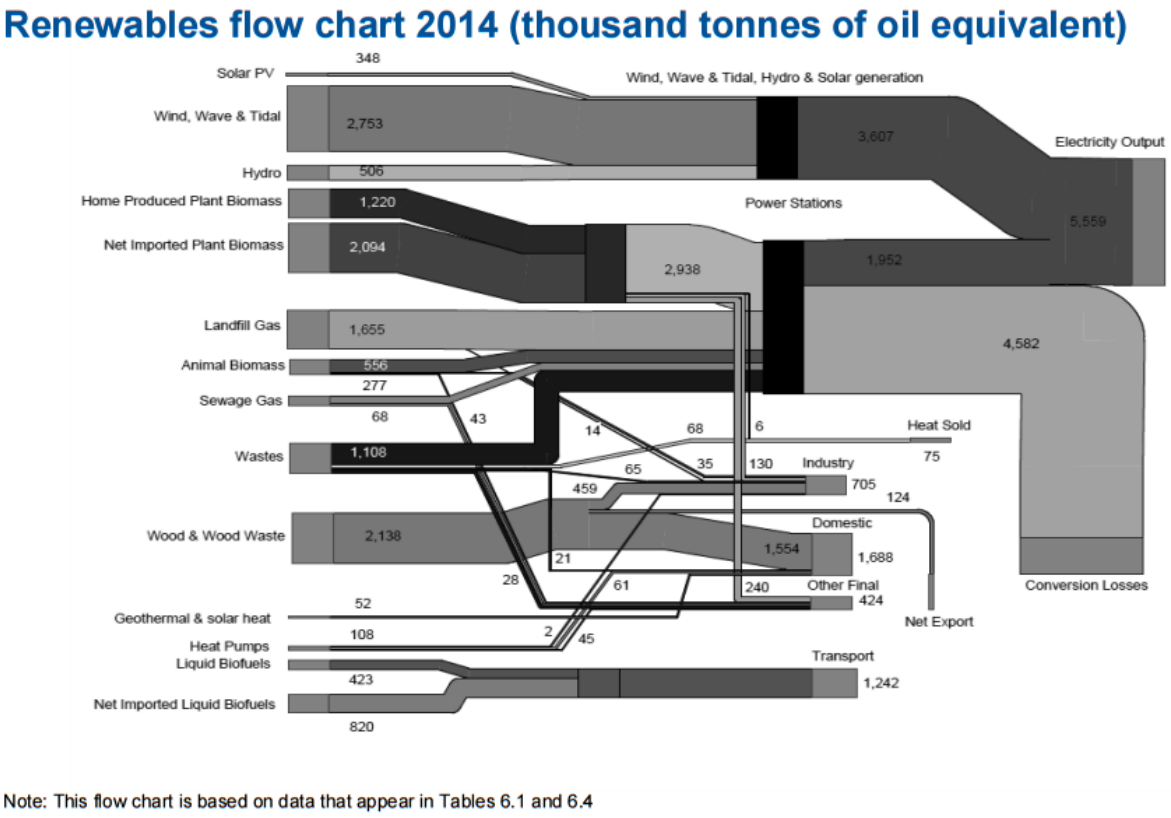

Note: This flow chart is based on data that appear in Tables 6.1 and 6.4

Fig 1.3 Green electricity, heat and transport fuels (DUKES, 2014b).

1.3 Biomass energy generation

Between 2010 – 2014 the energy derived from renewables in the UK increased by 280%, **Table 1.1**.

Table 1.1 Total % renewables (DUKES, 2014b).

Table 6A: Percentages of electricity derived from renewable sources	2010	2011	2012	2013	2014
Overall renewables percentage (international basis)	6.8	9.4	11.3	14.8	19.1
Percentage on a Renewables Obligation basis	7.0	9.8	11.9	15.5	19.8
Percentage on a 2009 Renewable Energy Directive basis (normalised)	7.4	8.8	10.7	13.8	17.8

A breakdown of these figures is given in **Table 1.2** from (DUKES, 2014a). Using this and **Table 1.3** (DUKES, 2014a) the total renewable electricity generation was **64.65GWh** (19%), and of this **13.1GWh** came from woody “plant” biomass (20%). It may also be shown that **35.1%** of all renewable electricity in the UK comes from

bioenergy, but only **6.54%** of total energy production in the UK is from bioenergy. **57.2%** of total bioenergy production was from fibrous biomass and **3.9%** of total energy production in the UK is from fibrous or “plant” biomass**.** This shows that the UK is well adrift from the 20% target for renewable energy, but that biomass plays a significant role in the renewable energy that has been generated**.** The equivalent figures for 2010 were 6.7% of total energy from renewables with 3.1% from bioenergy and 0.79% from fibrous or plant biomass.

Table 1.2 Total Generation (DUKES, 2014b).

GWh

	2010	2011	2012	2013	2014
Electricity production					
Total production *(6)*	**378,622r**	**364,516r**	**360,612r**	**356,264r**	**336,043**
Primary electricity					
Major power producers	**73,051r**	**86,414r**	**91,711r**	**98,174r**	**95,146**
Nuclear	62,140	68,980	70,405	70,607r	63,748
Large scale hydro *(6)*	2,505	4,291	3,898	3,348	4,333
Small scale hydro	198	303	272r	261	301
Wind *(7)*	8,208r	12,840r	17,137r	23,958r	26,763
Other generators	**2,951r**	**4,142r**	**5,169r**	**7,551r**	**10,555**
Nuclear	-	-	-	-	-
Large scale hydro	587	698	733	678	720
Small scale hydro	275r	388r	382	415r	530
Wind, wave and solar photovoltaics *(7)*	2,090r	3,056r	4,054r	6,459r	9,304
Secondary electricity					
Major power producers	**271,645r**	**243,141r**	**233,592r**	**223,647r**	**202,794**
Coal	103,941	104,797	140,164	130,204	100,158
Oil	2,271	1,074	1,132	745	530
Gas	161,748	132,753	86,229	82,891r	88,871
Renewables	3,685r	4,518r	6,067r	9,285r	12,707
Other	-	-	-	522	528
Other generators	**30,975r**	**30,818r**	**30,139r**	**26,892r**	**27,549**
Coal	3,753	3,774	2,992	564	549
Oil	2,532	2,043	1,439	1,346r	1,351
Gas	13,908	13,767	13,931r	13,137r	12,057
Renewables	8,236r	8,435r	8,581r	8,873r	9,995
Other	2,545r	2,799r	3,196r	2,971r	3,597
Primary and secondary production *(8)*					
Nuclear	62,140	68,980	70,405	70,607r	63,748
Hydro	3,565r	5,680r	5,285	4,702r	5,885
Wind, wave and solar photovoltaics	10,297r	15,896r	21,191r	30,417r	36,068
Coal	107,694	108,571	143,156	130,768r	100,707
Oil	4,803	3,117	2,571	2,091r	1,881
Gas	175,656	146,520	100,160r	96,028r	100,928
Other renewables	11,921r	12,953r	14,648r	18,159r	22,702
Other	2,545r	2,799r	3,196r	3,493r	4,125
Total production	**378,622r**	**364,516r**	**360,612r**	**356,264r**	**336,043**

The largest increase in biomass usage in the UK comes from plant biomass (**Table 1.3**) and over the same time there is a large decrease in the use of co-firing biomass. This is due to the ROC credits (2009-2017) being set up as follows:

- From 1 April 2009 until 31 March 2010 the ROC for fuel derived from energy crops was 0.25 ROC
- From 1 April 2010 until 31 March 2011 this increases to 0.5 ROC
- From 1 April 2011 until 31 March 2016 it increased further to 0.75 ROC

- From 2017 onwards co-firing will no longer be eligible for ROC's and only 100% biofuel firing will be eligible. However the ROC scheme has been phased out and contract for difference (CfD) introduced and only 100% biomass is eligible.

In 2014 5.8% of the UK's supplied electricity was generated from pulverised biomass mainly used in existing coal fired power stations. This was a 25.7% increase on 2013 and in 2014 was 19.69 MOTE (Million Tonnes of Oil Equivalent). It was the fastest growing renewable electricity source between 2013 and 2014 (MacLeay, 2015).

Renewable energy has been encouraged by the UK Government using various subsidies, paid for by the users of electricity through higher electricity costs. CfDs (contract for difference) will be available to new projects from some time in 2014, while the Renewables Obligation Certificate (ROC) scheme will remain until 31 March 2017, as outlined above. Contract for difference will no longer be covering co-firing of biomass and will only be available for 100% biomass in the future. This aims to drastically increase the volume of biomass being burnt in the UK and to stimulate greater production of domestically produced energy crops and a more robust domestic biomass supply chain.

Table 1.3 Fuel used for renewable energy (DUKES, 2014a).

	2010	2011	2012	2013	2014
Installed Capacity (MW) *(1)*					
Wind:					
Onshore	4,060r	4,629r	5,904r	7,519r	8,486
Offshore	1,341	1,838	2,995	3,696	4,501
Marine energy (wave and tidal stream)	3	3	7	7	9
Solar photovoltaics	96r	995r	1,756r	2,851r	5,377
Hydro:					
Small scale	184	202	218r	231r	246
Large scale *(2)*	1,459r	1,477r	1,477r	1,477r	1,477
Bioenergy:					
Landfill gas	1,009r	1,052r	1,037r	1,043r	1,051
Sewage sludge digestion	193	198	204	198	208
Energy from waste *(3)*	424r	505r	517r	550r	696
Animal Biomass (non-AD)*(4)*	111	111	111	111	111
Anaerobic digestion	30	71	119	164	216
Plant Biomass *(5)*	315	1,149	1,171r	1,955r	2,244
Total bioenergy and wastes	2,083r	3,085r	3,159r	4,021r	4,526
Total	9,225r	12,230r	15,515r	19,801r	24,623
Co-firing (6)	266	338	204	35r	16
Generation (GWh)					
Wind:					
Onshore *(7)*	7,182r	10,503r	12,232r	16,950r	18,611
Offshore	3,073r	5,149r	7,603r	11,472r	13,404
Marine energy (wave and tidal stream) *(8)*	2	1	4	6	2
Solar photovoltaics	41	244	1,352r	1,989r	4,050
Hydro:					
Small scale *(7)*	473r	691r	654r	676r	832
Large scale *(2)*	3,092	4,989	4,631	4,026	5,053
Bioenergy:					
Landfill gas	5,031r	5,085r	5,145r	5,160r	5,045
Sewage sludge digestion	697	764	719	761	846
Biodegradable energy from waste *(9)*	1,530r	1,503r	1,774r	1,649r	1,950
Co-firing with fossil fuels	2,332	2,964	1,783	309	133
Animal Biomass *(4)*	627	615	643	628	614
Anaerobic digestion	111	273r	501r	722r	1,009
Plant Biomass *(5)*	1,593	1,749	4,083	8,929r	13,105
Total bioenergy	11,921r	12,953r	14,648r	18,159r	22,702
Total generation	25,783r	34,529r	41,124r	53,277r	64,654
Non-biodegradable wastes *(10)*	987r	1,085r	1,429r	1,481r	1,951
Total generation from sources eligible for the Renewable Obligation *(11)*	21,830r	28,919r	33,406r	44,948r	52,745

Alongside these developments in the use of biomass has been the implementation of the EU Large Combustion Directive. This brought in regulations for drastic NOx and SO_2 emissions. For existing coal fired power stations this would require very expensive selective catalytic reduction (SCR) of NOx using ammonia as the reducing agent. In addition flue gas desulphurisation using limestone reactions with SO_2 to form gypsum would have to be installed. This is a major capital expenditure for 40 year old power stations. As a consequence the power station operators have chosen to close the coal fired power stations with only a few of the more efficient

stations remaining open. The coal fired power stations closure programme is summarised in **Table 1.4** (DECC, 2014). This closure programme reduces the opportunities for biomass conversion and those stations that had opted to close were not subsequently allowed (i.e. they were not given contract for difference agreements for biomass) to convert to biomass and stay open. Ironbridge in **Table 1.4** has closed recently even though it was operating with 100% biomass but did not have a CfD contract.

Also in **Table 1.4** are the nuclear power stations due to close through old age and the CCGT natural gas fired power stations that have closed or are mothballed due to the high price of gas, in the 2011-14 period. All these closures with no replacement of the generating capacity makes the security of supply of electricity in the UK much more precarious. A growth in biomass use in the remaining coal fired power stations is one way of avoiding power cuts over the next few years.

Table 1.4 Closure of power stations in the UK (DUKES, 2014a).

Site	Fuel	Status	Previous Capacity (MW)	New Capacity (MW)	Year of closure, capacity reduction or conversion
Fife	CCGT	Closed	123	0	2011
Derwent	CCGT-CHP	Closed	228	0	2012
Shotton	CCGT-CHP	Closed	210	0	2012
Kingsnorth A	Coal/Oil	Closed	1,940	0	2012
Grain A	Oil	Closed	1,300	0	2012
Oldbury	Nuclear [1]	Closed	434	0	2012
Wylfa (Reactor 1)	Nuclear [2]	Partially Closed	980	490	2012
Keadby	CCGT	Mothballed	749	0	2013
Kings Lynn	CCGT	Mothballed	340	0	2013
Roosecote	CCGT	Mothballed	229	0	2013
Cockenzie	Coal	Closed	1,152	0	2013
Drax	Coal [3]	Partially Converted	3,870	3,870	2013
Ironbridge	Coal [4]	Converted	940	360	2013
Tilbury B	Coal [5]	Closed	750	0	2013
Didcot A	Coal/Gas	Closed	1,958	0	2013
Fawley	Oil	Closed	1,036	0	2013
Teesside	OCGT [6]	Closed	45	0	2013
Ferrybridge C	Coal [7]	Partially Closed	1960	980	2014
Uskmouth	Coal [8]	Closed	363	0	2014

1. Reactor 2 with capacity of 217 MW closed on 30 June 2011, reactor 1 with capacity of 217 MW closed on 29 February 2012
2. Reactor 2 with a capacity of 490 MW closed on 30 April 2012
3. Partly converted to biomass. Overall capacity remains at 3,870 MW (coal 3,225 MW, biomass 645 MW)
4. Converted from coal to dedicated biomass in 2013 (at 900 MW), before reducing to 360 MW in April 2014.
5. Converted from coal at 1,063 MW capacity to dedicated biomass at 750 MW capacity in 2011 before closing in 2013.
6. Reduced capacity from 1,875 MW (CCGT 1,830 MW / OCGT 45 MW) to 45 MW (OCGT) in 2011 before closing in 2013.
7. Two units (980 MW) closed in April 2014.
8. One unit (120 MW) closed in April 2013, with the remaining two closing in April 2014.

There are 5 main types of biomass:

- Existing Resources:- Non-food or Waste: forest residue/debris, waste and co-products from the agriculture, however due to the scattered nature collection would increase the overall cost. Waste straw/slurry as well as wood wastes from commercial and industrial activities (rubber and plastic waste from rubbish as well as landfill methane). Waste from the lumber industry normally accounts for 50-75% of the tree's volume. The paper industry already use waste from the process to power the plant by burning it in a generator on site.

- Food crops used for biofuel:- different parts of the crop can be used to make energy, corn ears are used to make bioethanol and wheat straw and other husks are burnt, for electricity generation.

- Dedicated Energy Crops:- elephant grass (miscanthus) and coppiced willow are exclusively grown for use as biomass fuels, generally on unused land.

- Conversion of Algal biomass to transport fuels:- here the algae is grown in tanks, allowing for higher growth rate than conventional crops, this is then harvested and fermented into ethanol for transport fuel. There are a number of companies around the world attempting to commercialise this sustainable energy technology. The Algenol system which is being commercialized by the company BioFields utilizes seawater, industrial exhaust and algae to produce ethanol. The algae release it naturally; there is no killing or harvesting of the algae.

Now the 5 main types of biomass have been identified the various methods of converting biomass into electricity, fuels and heat, the methods currently in use or under review include:

- Direct Combustion for Electricity:- using solid pulverised biomass to generate steam to drive a steam turbine to drive an electricity generator. For this application pulverised biomass is used in a similarly way to the use of coal and using the same equipment. The biomass can be co-fired with coal or used as 100% biomass, as is currently being used at Drax power station in Yorkshire. This research project is directed at the 100% use of pulverised biomass as it relates to flame propagation in clouds of woody biomass dusts.

- Direct Combustion for Heat:- using solid fuel as logs or pellets. A bed of logs or pellets burns with air blown through the bed. Generally staged combustion is used with the bed operated fuel rich and secondary air or over fire air used to complete combustion. This application is not considered in the present work.

- Gasification:- solid biomass converted by heating with steam and a small amount of oxygen into a combustible gas mixture of CO and hydrogen plus nitrogen if air is used for gasification. In the present work very rich mixtures of biomass are investigated for their explosion characteristics and these mixtures will produce CO and hydrogen in the combustion products.

- Pyrolysis:- heating biomass without oxygen, to produce combustible gas, liquid and solid fuels. This is not relevant to the present work and very little biomass is actually used for these processes, as shown in the above review of biomass uses.

- Fermentation process:- sugar/biomass is converted to bioethanol.

- Esterification/Trans-esterification processes: vegetable oil conversion to biodiesel.

- Anaerobic Digestion:- the bacterial breakdown of organic waste into CO_2 and methane, also known as biogas. Sewage and landfill biogas can also be burnt as an energy source; biogas is most commonly burnt in a gas turbine.

In order to meet the renewable energy goals for the UK there is a requirement for a major increase in UK biomass production. The UK Biomass Strategy (DECC, 2012) states that this could be done by:

- Sourcing an additional 1 million dry tonnes of wood per annum from forests and unused land. However the scattered nature of this resource presents a challenge for collection and transport while still remaining “green”.

- Increasing the amounts of permanent energy crops in the UK to up to 17% of total UK arable land (1 million hectares).

- Increased supply from organic waste materials (manure). This may lead to an increase in man-made fertilizer production to compensate for lost circulation of nutrients in the land.

However, the problem of sourcing biomass in the UK instead of importing it from abroad (hence reducing its carbon footprint) is far from solved. In 2005 a total of 1.4 million tonnes of biomass was co-fired compared to a total of 52 million tonnes of coal for electricity generation (BEC, 2005). Of the biomass used for co-firing 81% was imported,

- 33% was imported palm products: co-products of the palm oil industry (palm kernels and residues such as empty fruit bunches and fibre)

- 21% was imported olive products: co-products of the olive oil industry (olive cake and pellets)

- 20% was wood products including sawdust, wood shavings, pellets and chips, predominantly imported

- 7% was straw and other co-products of cereal production.

Figure 1.3 (DUKES, 2014b) shows that the percentage of solid biomass burnt in the UK that is sourced abroad was down to 64% in 2014.

For biomass to be eligible for ROCs or CfD or for heating applications within the renewable heat incentive, the biomass must be shown by the supplier to be sustainable. For example forest based wood cannot simply be chopping down an existing forest leaving a bare hillside. If a tree takes say 50 years to reach maturity and it is then cut down then a sustainable forest will not cut more than 2% of the wood and new trees will be planted and this must be audited. Also land currently used for agriculture to produce food crops cannot be converted to biomass production. Both the USA and Europe have detailed procedures to ensure that biomass sources are sustainable and do not impact on food production. There is concern from some environmentalist that these procedures are not robust enough in their policing, but there is now clear intent that biomass and biofuels will be sustainable.

Burning raw biomass is known as a 1st generation fuel, it is using seed oils to produce biodiesel. It should be emphasised that these are the only biofuels currently in use. There is ongoing research into what is referred to as 2nd generation biofuels which normally involve the gasification of cellulosic biomass and use of the gas in a gas turbine or synthesis into a liquid fuel using a similar process to that Shell uses to convert natural gas into a pure n-alkane liquid fuel. Fuels derived from algae are often referred to as 3rd generation biofuels. However, these future processes to produce liquid fuels use the feedstock of farm waste and woody biomass that is currently used in burning to generate electricity and/or heat. Also none of these future biomass energy sources have any significant production base as the cost of implementation is in the billions of pounds. For the foreseeable future second generation biofuels will be used for electric power generation or heat production from solid biomass.

1.4 Environmental legislation

The UK Governments Biomass Strategy (DECC, 2012) states that the UK intends to push a major rise in the use of biomass for energy generation (up to 10 -12%) and policy goals, most significant of which are:

- An EU target of 20% renewable energy (*not just electricity)* by 2020. (14.9% for electricity in 2013 and 19.1% in 2015 but only 7.2% renewables in terms of total energy (EU energy policy, 2010)).

- The UK's Climate Change Act - a legal obligation on future governments to cut carbon dioxide pollution by 80% or more by 2050. This has no funding to assist in meeting the target and sets up a Quango, (the Climate Change Committee) that has funding for its own expenses! This Act sets intermediate GHG reduction target on the way to 80% reductions by 2050 (referenced to 1990).

- The EU Large Combustion Plants Directive (LCPD) for existing power generation facilities mean that by 2016, all major pulverised coal fired power plants in the UK will have to install Flue-Gas Desulfurization (FGD) (for >90% removal of sulphur dioxide SO_2) and Selective Catalytic Reduction (SCR) (for >85% nitric oxide(s) NO_x removal).

This legislation combined with public pressure has led to the growth in green energy over the last 13 years as shown in **Figure 1.2**.

The LCPD has had a massive effect on the landscape of UK power generation as 50% of the power generation closed down in the UK in the last 4 years was coal fired power stations. This is due to the cost of the retrofits that the LCPD demanded being greater than the cost of the electricity generated. The main factor on the UK's drive to reduce CO_2 emissions is what the UK decides to build to replace the power stations that have closed. The only new power stations built in recent years (apart from wind farms) are natural gas fired Combined Cycle Gas Turbines (CCGT). However, due to the current high price of gas in the UK some of these have been mothballed and the ones that are less efficient that were installed in the 1990s have been closed. The existing CCGT are capable of burning biogas either directly or mixed into the mains gas and this route to bio-electricity is being progressed with CfD agreements. However, currently biogas generation is not very significant apart from landfill gas and sewage gas. The problem is that although there is plenty of food and farm waste that is the feedstock of biogas generation, the collection of this and transport to large scale biogas generation plants is expensive. This is potentially an area of future growth via the natural gas grid as the carrier for biogas.

The replacement of the closed power stations is urgently required, but none are currently being built. No new coal plant even with carbon capture and storage (CCS) have been built or are planned to be built – this is because the government has stated that it will not approve any new coal fire power stations without CCS, but no CfD agreement on CCS has been reached which is the main reason why none have yet been built. Two have been approved to be built as demonstrators but the grants from the government (which came from an industrial energy efficiency scheme from which the government took the funds that should have been returned to industry as a payment for saving energy – the funds are not from government tax revenues) do not cover the costs and EU grants which they also have also do not cover the costs. Thus funds have to be borrowed from banks who will not lend until there is a guaranteed price for the higher cost of coal fired power plant electricity with CCS (roughly double the current price) (Hackett, 2015). One 3.5GW nuclear plant renewal has been approved, but the finance for this is still in doubt and no construction work is underway. This new nuclear has already been guaranteed twice the current price of electricity as a CfD. The capital cost of new nuclear is

roughly 10 times that of an equivalence CCGT power station and the interest on the commercial cost of borrowing this money is part of the higher cost of electricity.

New coal with CCS and new nuclear power stations take about 10 years to build and so no reduction in CO_2 from these initiatives can occur before 2025. Retrofitting new CCS to old coal is hardly sensible as the youngest coal fired power station at Drax is 30 years old. In contrast biomass burnt in existing coal fired power stations is achieving CO_2 reductions today and the capital investment and plant alteration costs are much smaller than building CCS. It is thus likely that biomass for power generation in existing coal fired plants will continue to expand. The present UK Government has recently cut CfD funding for onshore wind power and only offshore wind power will be supported. This is likely to lead to a reduction in the growth of renewable electricity in this area in the future. Coupled with this feed in tariff support for solar power is being cut and renewable energy will essentially have to compete on costs with no subsidies in the future. Biomass is also having its subsidy removed by this government and will have to compete on costs. The future for renewable energy in the UK under the current Government is bleak (Arbon, 2015).

1.5 Implementation concerns for biomass electricity

The supply of biomass is a key area, which is not the subject of this thesis. However, it should be realised that the quantities of biomass involved are enormous. A 660 MWe boiler at Drax with a thermal efficiency of 40% requires 1650 MWth of biomass and with a typical GCV of 18 MJ/kg this is 91.7 kg/s or for a typical 10 hour use per day is 3.3 kTonnes per day. For a typical bulk density of 300 kg/m^3 this is 11,000 m^3 per day. A one week supply; which is the minimum fuel reserve; is thus 77,000 m^3. At Drax power station pellet storage silos of 100,000 m^3 have been constructed. These are the world's largest silo stores and they need to be filled every week. Drax intends to have three of their 660MW boilers operating on biomass by 2017 and this will be the UKs largest source of biomass electricity. Three boilers will remain on coal.

The sourcing of these large quantities of biomass is on a very large scale and includes ships arriving fully loaded with pellets, some from the USA – but they are sourced from all over the world, a ship arrives every day and is unloaded onto trains that take the biomass to Drax. This uses the same system as for delivering imported coal to Drax.

For coal the bulk density is higher so the storage volume required is less. However, coal can be stored in the open as it does not absorb rain water excessively. Biomass cannot be stored in the open as pellets, as they absorb moisture and rot and hence there is the necessity to build large fuel storage silos. This storage creates auto-ignition hazards and dust explosion hazards during the filling of the store and during the extraction of the biomass for feeding to the mills, as this also creates a biomass power explosion hazard. The transport of the biomass to the mills and from the mills to the burners creates further explosion risks. Unfortunately, these risks are shown to be high as there have been several biomass power plant explosions.

This is illustrated by the compilation of recent accidents, most of which occurred once changes to original system had been made or when working with biomass for the first time.

- 2005, Chetwynd mill, British Columbia, Canada. Work on a shutdown burner created a cloud of dust that was ignited by cutting torches. At least one worker was injured and taken to hospital. (Hoekstra, 2012)

- 2008, Pacific Bioenergy's pellet plant, Prince George, Canada. An explosion in the pellet plant in March. (Hoekstra, 2012)

- February 2008 , Imperial Sugar Company, Georgia. An overheated bearing on a conveyor initiated an explosion and fire lead to 14 fatalities. (CSHIB, 2008)

- June 2009, University of South Carolina's wood-burning boiler, an explosion followed two previous smaller explosions and a series of mechanical breakdowns. (Wayne, 2011)

- August 2009, Pinnacle Pellet in Armstrong, Canada. The company experienced an explosion at its Williams Lake plant. That explosion was caused by a combination of air, dust and a spark, said the company. (Hoekstra, 2012)

- February, 2010, Brilon, Germany. A biomass plant exploded killing three workers and causing a subsequent fire. (Forum)

- December 2010, Pacific Bioenergy's pellet plant in Prince George in Canada. An explosion caused extensive damage where dust was cited as a factor ignited by a spark (Hoekstra, 2012).

- January 2011, Tolko's Soda Creek sawmill, Williams Lake, Canada. An explosion was caused by dust in one of the mill's motor control centres. (Hoekstra, 2012)

- February 2011, Babine Forest Products, Canada. A small explosion took place that was fed by unusually dry sawdust, according to a B.C. Safety Authority report. (Hoekstra, 2012)

- 20 June, 2011, Georgia Biomass plant. A dust explosion was caused by an overheated roller/bearing assembly in a pelletizer that sparked causing the explosion at the factory that had been online for just over a month. (Stepzinski, 2011)

- April 2011 Pinnacle Pellet in Armstrong, Canada. Explosion was caused a fire that quickly spread into the basement and into the attic. (Hoekstra, 2012)

- 30 October, 2011 Tyneside port biomass storage facility in South Shields stored biomass, which is used at Drax power station Yorkshire. 25 tonnes of which caught fire in storage. (BBC, 2011)

- February, 2012 fire at Tilbury biomass power station burnt for days and needed 100+ firemen to control the fire, caused by run-away heating in a hopper. (Mail, 2012)

- A very recent tragic incident of wood floor mill explosion in UK (17 July 2015) was the Bosley Mill sawdust explosion in Macclesfield. There were 4 deaths and the plant was almost completely destroyed. (BBC, 2014)

When biomass power stations were first developed in the UK the operators intended to use biomass delivered as logs or bales of hay. However, it was found that the milling of the biomass on site was a key problem area and that different mills were required for wood and agricultural biomass. A problem with the use of whole logs was that of transport. Even dried logs would have around 5% moisture

and this would mean that for a ship the transport costs were paying for water to be moved to the power station. Thus it was realised that the wood should be dried. Also logs do not fill a closed volume easily and this led to the transport costs being too high as the mass of biomass moved per ship or lorry load was too low.

The solution was to move the pulverisation and biomass drying operations to the source of the biomass – the forest or near a group of farms. This has been done for the large power stations such as Drax where large biomass pulverisation plants have been built on the forest sites in the USA used for sourcing the biomass. The pulverised biomass is then dried in a fired kiln and then compressed into pellets. The shipping of dried pellets reduces the transport of water and also the packing density of pellets is greater than that of logs, so a ship of the same volume carries greater biomass energy in pellet form. These pellets at the power station are fed directly to the coal mills where the pellets are broken up to yield the pulverised particles that the pellets were manufactured from. This process has been reproduced in the present work with biomass supplied as pellets broken up in a small mill at Leeds so that the particles investigated were typical of those being burnt in power stations. It will be shown that these particles are relatively large and this led to a theme of this research on the influence of particle size on biomass dust cloud flame propagation.

1.6 Safety legislation

There are two European Directives pieces of legislation that have been implemented in the UK in the explosion safety area:

- Directive 99/92/EC (ATEX 137); Regulations on the Minimum Requirements for Improving the Safety and Health Protection of Workers Potentially at Risk from Explosive Atmospheres. The emphasis is on the owner to carry out adequate risk assessment and safety measures to protect his workers, to whom he has a duty of care. This covers plant operation, the equipment and personnel in each area and how these operate together with regard to explosions.

- Directive 94/9/EC (ATEX 95); Directive on the Approximate of Laws of the Member States relating to Devices and Protection Systems for Use in Explosive Environments. It covers the standard to which any equipment

made for compliance within the 99/92/EC directive must be constructed, produced and marketed.

The Dangerous Substances and Explosive Atmosphere Regulations (DSEAR) implement the above Directives in the UK. The HSE has also offered further guidance: precautions against explosions HSE HSG103 2nd Ed.2003. This provides practical advice on the prevention of dust explosions and fires, the publication outlines the relevant legislation, it also provides advice on how to prevent dust explosions.

To comply with this legislation a number of details are needed, the Minimum Explosive Concentration, the maximum K_{st} and the maximum Pressure rise. The MEC is used for determining the risk of explosions in a given area (zoning areas).

The K_{st} and P max is used to calculate the vent size needed to prevent building and personnel damage as well as being used to calculate building separation and the volume of inert material needed to prevent propagation of the explosion. Additionally K_{st} is used to classify dust into reactivity categories [St1 (<200 Bar m/s), St2 (201-300200 Bar m/s) and St3 (301+200 Bar m/s)]

Additionally, premixed air/dust transfer ducts from the mills to the burner or the mill itself, may be at risk of explosion. Normally 20% of stoichiometric (Ø = 1) air is used to transport the mixture, meaning it is transferred at Ø = 5 or ƛ of .2 (ƛ = 1/Ø), which for some types of coal and biomass will be shown in this work to be flammable concentrations. The explosion risk is both in the biomass storage system, the transfer system to the hoppers that feed the mills, inside the mills or in the connecting pipes from the mills to the burner (an explosion here occurred at Ironbridge in 2012).

1.7 Problems with existing data

The literature (prior to the recent work of the Leeds group) has scant data for biomass dusts and their explosive profiles. This data refers to ‘wood’ with no composition given, the test method is often not given and the total amount of data is very small and more data is required, which was an objective of the present work.

There are several reasons for this lack of information:

- There has been no widespread use of pulverised biomass for power generation until recently and the only other wood dust explosion hazard was in the wood working industry through the sawdust explosion risk and dust extractor systems.

- The characteristics of laboratory tested materials:- moisture, particle size and size distribution may differ from those of the actual materials used by industry. These parameters have a significant influence on the explosion characteristics of the material when tested. Therefore where ever possible tests will be carried out on samples of materials currently in use by the industry in order to provide accurate and relevant data on explosion risk of the materials.

- A large proportion of data doesn't give the chemical composition of many agricultural materials tested. This is important as environment; soil composition and fertilizers used differ over the time and from one country/area to another. Hence crops cultivated in one area may be significantly different, even when dealing with plants of the same species.

- Some of the apparatus and test methods used have become obsolete; an example would be data showing Maximum Explosion Pressure and Maximum Explosion Pressure rise rate values from the Hartmann device which has been proved to underestimate these values.

- The dust found on industrial sites is frequently a mixture of several different dusts that had been stored/used previously. Therefore the composition, particle size distribution and ignition energy of this mixture depend on the amalgamation of its constituent parts. In addition, more and more new materials are being used which have not been used before and, therefore, their explosive properties have not yet been studied.

Literature sources (Beck, 1997) provide a large volume of data showing a wide spread of data, the K_{st} values for maize dust vary from 7- 75 bar m/s, P_{max} from 4.0 - 9.4 and the Lower Explosive Limit (LEL) also referred to as the Minimum Explosive Concentration (MEC) for icing sugar from 60 - 500 g/m^3.

There may be data that isn't publically available, it may exist in a company's possession but they are unwilling to share it. Relevant data is needed that is

publically available. Power generators that are using pulverised biomass may have commissioned their own explosion safety measurements, but these are not in the public domain. The data may exist in a company's possession but they are unwilling to share it as it would waste all the money spent on the research and development. In the UK Chilworth Technology has undertaken most of these tests using their 20 L sphere test equipment. There is very little data obtained on the ISO 1m^3 test equipment and it is the purpose of the present research work to produce this data for a range of pulverised biomass.

1.8 Aims

The aim of the project is to investigate the characteristics of fibrous biomass (fine <63µm and as received with large particles) dust explosions – Maximum K_{st}, maximum pressure rise, lower flammability limit, upper flammability limit and flame speed. The influence of particle size on flame propagation is a specific theme of this research for woody biomass. As currently most pulverised biomass used for power generation is of relatively large size up to 1mm and sometimes greater.

With the increase in interest in biomaterials in industry it is possible that the absence of data could leave people and processes at risk. The risks arise due to the fact that without data the ATEX guidance cannot be applied correctly and therefore will not function properly.

- Vents may not be of the right size.
- Maximum pressure produced is underestimated.
- Both of which risk pressure vessel rupture.

All published data for dusts and pulverised biomass shows that the peak reactivity occurs at around 500-1000g/m^3. When this is converted into an equivalence ratio for dusts, then these most reactive mixtures are all at least an equivalence ratio of 4. No gas behaves like this, as shown in **Figure 1.4** (Cashdollar, 2000), and this research investigates why this occurs.

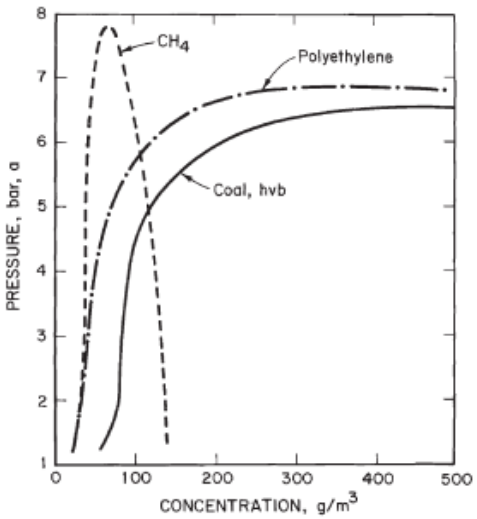

Fig. 7. Explosion pressure data for high volatile bituminous (hvb) coal and polyethylene dusts, compared with those of methane gas.

Fig 1.4 Pressure rise and flammability limits of methane gas compared to coal and polyethylene dust (Cashdollar, 2000).

The present work also enables the flame speeds to be determined and this is required for pulverised biomass burner designs. The turbulent flame speed has the same combustion physics as in flames in power station boilers with 100% biomass. Thus the information is of relevance to the design of burners and the understanding of flame propagation in biomass flames as well as being required for explosion hazard evaluation.

Therefore to find out what is happening, part of the intended focus of the research is on the residue of the (fibrous biomass) explosions to find out what is actually taking place in the combustion process. While; at the same time comparing the explosion itself to others from various materials therefore creating a more expansive base of biomass data.

2 Literature review

2.1 Woody biomass

There are two main sources of biomass: wood (including waste wood) and agricultural biomass (including waste agricultural products such as palm oil nut shells and Olive Stones). The combustion properties are related, but this research is concentrated on woody biomass. Biomass has a structure made from different proportions of cellulose, hemicellulose and lignin, as shown in **Figure 2.5**. These three structures have been the main focus for most studies aimed at the understanding of the thermal decomposition mechanisms in biomass. Most of this work was carried out on studies of torrefaction and pyrolysis of biomass. However, it should be applicable to biomass combustion if the higher rate of heating is allowed for (Ubhayakar et al., 1977, Cetin, 2004, Kobayashi et al., 1977).

In biomass cellulose is the largest single group on a mass basis. Its purpose within the cell is to support the cell structure of the plant as it forms the main load bearing component of the cell walls. It provides mechanical strength and toughness to a plant's structure therefore providing the opportunity for the plant to grow in height to achieve optimal light exposure and therefore photosynthesis. Lignin is the more rigid structure that along with cellulose gives the cell wall its strength and Hemicellulos provides cross linking between cellulosic fibrils.

The chemical structure of these three biomass constituents is –

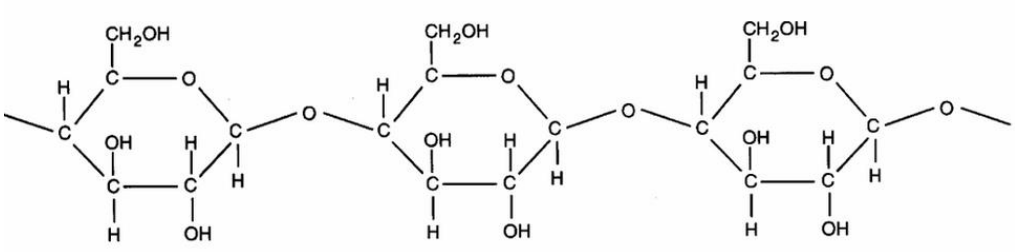

Fig 2.1 Chemical structure of cellulose polymer (Lentini, 2006).

$CH_{1.5}O_{0.833}$ A/F = 5.12

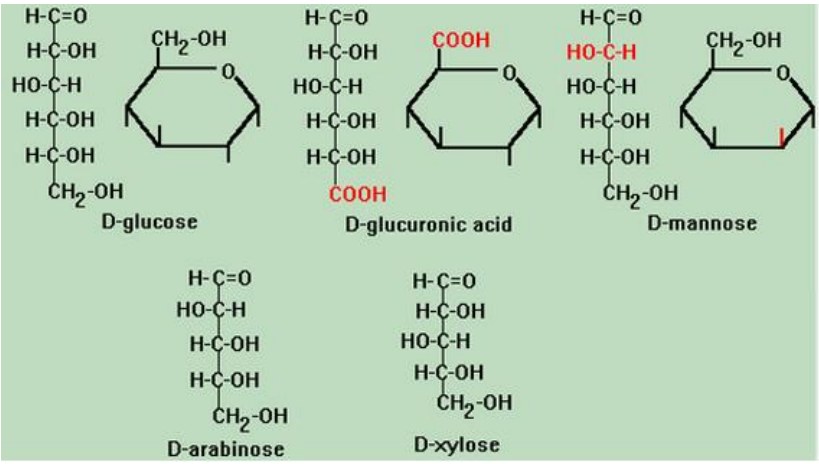

Fig 2.2 Chemical structure of hemicellulose monomers (Huiling, 2015).

$CH_{1.167}O$, CH_2O, $CH_{1.67}O_{1.1167}$ A/F = 3.15 – 4.6

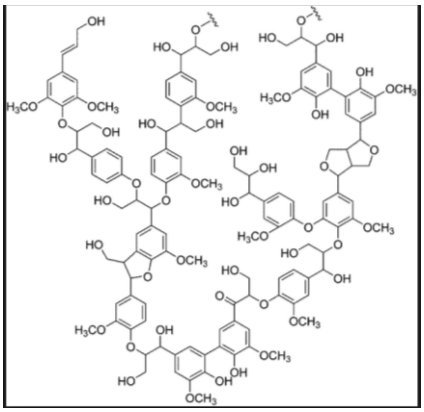

Fig 2.3 Chemical structure of lignin polymer (Lentini, 2006).

$CH_{1.11}\ O_{0.22}$, $CH_{1.2}O_{0.3}$, $CH_{1.27}O_{0.364}$ A/F = 8.2 – 11.1

Woody biomass, excluding straw type, falls into two categories, softwood (larch) and hardwood (beech, willow). In general, hardwood comes from a deciduous tree and softwood comes from evergreen. Hardwoods tend to be slower growing, and are therefore usually denser. Along with these groups are herbaceous species, agricultural wastes or straw type of biomass.

The three groups of biomass are related by their Lignin, Cellulose and hemicellulose content as shown in **Table 2.1** (Bergman, 2011, Couhert et al., 2009, Tillman, 1978). This is determined by wet chemistry with a series of hot solvent mixtures which remove lipids, proteins, lignin, and hemicelluloses (Updegraff, 1969).

Table 2.1 Biomass Lignin, Cellulose and hemicellulose composition (Bergman, 2011, Couhert et al., 2009, Tillman, 1978).

Polymer	Lignin (wt%)	Cellulose (wt%)	Hemicelluloses (wt%)
hardwood	18-25	40-44	15-35
softwood	25-35	40-45	20-32
straw	14	34	27
beach	22.1	45.2	32.7
white spruce	27.1	48.5	21.4
eastern white cedar	30.7	48.9	20.4
grass	3	69	38
bark	44	25	30
rice husk	23	42	35
beach wood	22	46	32
spruce and fir	28	47	23

As can be seen in **Figure 2.4**, softwood biomass generally has a higher lignin content compared to hardwood biomass and especially when compared to herbaceous or straw species of biomass. The most relevant difference between hardwood and softwood however is not in the amount of lignin but the composition of their hemicelluloses fractions. Hardwood hemicellulose is made up predominantly of 4-O methyl glucuronoarabinoxylan hemicelluloses, softwood predominantly consists of Glucomannan hemicellulose (Bergman, 2011).

Table 2.2 Polymer and hemicelluloses composition of the hardwood against softwood (Bergman, 2011).

Composition hemicelluloses	**hardwood**	**softwood**
4-O methyl glucuronoxylan (wt%)	80-90	5-15
4-O methyl glucuronoarabinoxylan (wt%)	<1	15-30
Glucomannan (wt%)	1-5	60-70
Galactoglucomannan (wt%)	<1	1-5
Arabinogalactan (wt%)	<1	15-30
Other galactose polysaccharides (wt%)	<1	<1
Pectin (wt%)	1-5	1-5

It should be noted that these differences occur through different structural arrangements and bonds of the atoms present in these materials rather than different compositions as shown in **Table. 2.3** (Bergman, 2011). The difference between “hardwood” and “softwood” comes more from the speed at which they grow, leading to hardwood being denser than softwood. However, these differences appear to lead to no marked difference in devolatilization behaviour at significantly high heating rates as found in explosions (Couhert et al., 2009).

Table 2.3 The chemical composition of four biomass of biomass (Bergman, 2011)

Biomass	MC (% wt.)	Size bin (mm)	Shape	C (% wt.)	H	N	O	Ash	LHV_{daf} (MJ/kg)
Willow	8.6	< 10 10 – 30 30 – 50	Cylindrical, (including bark)	47.2	6.1	0.34	44.8	1.6	17.7
Beech	8.1	2 – 16	Flat chips, debarked	47.2	6.0	0.40	45.2	1.2	17.0
Larch	9.8	10	Cubic, debarked	48.8	6.1	0.10	44.9	0.1	18.2
Straw	10.7	powder		44.3	5.8	0.40	42.4	7.1	16.1

Short rotation woody biomass is generally sourced from fast growing softwood trees, although hardwood willow is also used that are harvested within five to eight years of planting. Woody biomass also includes poplar, willow, silver maple, cottonwood, green ash, black walnut, sweet gum, and sycamore.

One of the main problems with woody biomass is the difficulty in reducing the particles to sizes that can be used in pulverised biomass burners. Woody biomass has a fibrous structure that does not pulverise easily as the fibres do not shatter by brittle fracture in the way that coal does. Woody biomass produces relatively long thin particles when milled, as shown in **Figure 2.4** (Bergman, 2011).

Fig. 2.4 Fresh willow milled in the cutting mill with bottom sieve of 250µm (Bergman, 2011).

To try to understand why this occurs a typical cell structure for biomass is shown in **Figure 2.5** (Bergman, 2011). The consistency of the tubular make up throughout the material is shown. All the fibrous cells are orientated in the same direction, making this structure very hard to break up in the direction transverse to the fibres. While the woody biomass fibres can be cut in rotating blade cutting mills, this is very energy intensive when compared to friable materials such as coal which break up easily in ball mills.

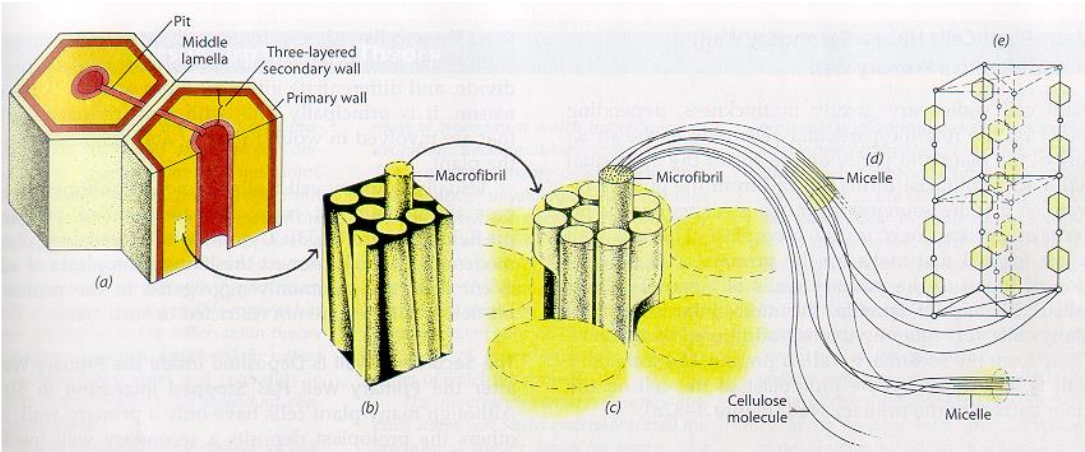

Fig. 2.5 The structure of a woody biomass cell wall. (a) part of the cell wall and middle lamella, primary wall and secondary cell wall, (b) macro fibril mutual structure, (c) micro fibril structure, (d) individual cellulose polymers including micelles (Bergman, 2011).

The fibrous nature of woody biomass creates a problem in its use as a pulverised fuel as, even with rotating blade cutting mills, achieving fine particle sizes is difficult and current power stations are burning a relatively coarse biomass size distribution compared with pulverised coal. This thesis investigates the influence of woody biomass particle size on the rate of flame propagation. However, for a standard characterisation of any pulverised material or dust the ISO standard (BSI, 1991) requires that it is milled and sieved to <63µm and this is very difficult to do for woody biomass. Also such fine biomass is not what is being burned in power stations and hence there is a need to determine flame propagation rates in practical particle size distributions, where fibres may be up to 1mm in length (Livingston, 2013).

In order to study pulverised coal and biomass combustion the powder has to be dispersed in air and standard equipment has been developed to do this using the closed vessel explosion technique. There are three common experimental techniques: Hartmann explosion tube (used in this work); 20 litre sphere (not used in this work) and the ISO 1m^3 vessel. These three experimental techniques are outlined here and their development and problems discussed in more detail later (sections 3.4 and 3.5). Other methods of investigating flame propagation in powders are in an open vertical tube with the powder shaken from the top and falling under gravity and ignited at the bottom (Proust, 2006, Han et al., 2000). However, this type of method has not been adopted as a standard test due to the influence of buoyancy on the results.

The Hartman vessel is a Perspex tube (L=300mm, D=80) fitted with a 10J spark ignition source located 1/3rd of the way up the tube, it has a tin foil vent at the top and dispersion of the dust at the bottom using compressed air.

The 20L sphere is a closed spherical explosion vessel fitted with either the rebound or C-ring injection system; the dust is ignited in the centre of the vessel using a 10kJ pyrotechnic igniter.

The 1m^3 vessel is a closed explosion vessel fitted either with the rebound or C-ring injection system; it is a cylinder with rounded ends and a length to diameter ratio of 1. Ignition is in the centre of the vessel using a 10kJ pyrotechnic igniter.

An explosion is deemed to have taken place in each piece of equipment if:

- **1m^3 vessel**: Overpressure relative to the initial pressure Pi is ≥ 0.3 bar (Pi is the pressure of the vessel before the ignition) (BSEN, 2011)

- **20L sphere**: Overpressure relative to the initial pressure Pi is ≥0.5 bar (BSEN14034-3, 2006).

- **Hartmann vessel**: Overpressure relative to the initial pressure Pi is ≥0.1 bar or activation of 2nd thermocouple, this was compiled as an amalgamation of the two definitions of an explosion taking place given in the European gas flammability criteria, method T and B.

(BSi, 2012) also establishes two methods for defining if an explosion has taken place in a tube and bomb apparatus similar to the Hartman and 20L sphere respectively:

- **Method T (tube)**: the upward movement of the flame from the spark gap for at least 100 mm. Dimensions of tube very similar to Hartmann's tube.

- **Method B (bomb)**: measured explosion overpressure is equal to or greater than the overpressure created by the ignition source alone in air, plus (5 ± 0,1) % of the initial pressure (0.5 bar overpressure).

All the above three standard dust flame propagation methods used the closed vessel explosion technique and measure the rate of reactivity of the dust from the rate of pressure rise in the vessel. In the present work in addition to this,

methodology has been developed to determine the flame propagation speed as well as the rate of pressure rise. However, the standards that accompany the use of the above equipment all specify that <63µm powders are used. The 20L sphere and 1m^3 test vessels have powder injection systems that do not work on fibrous biomass – even when milled to <63µm. However, the Hartmann equipment places the powder inside the vessel and this dispersion method does work with coarse woody biomass powders, which is why it was extensively used in the present work.

Woody biomass cannot be properly tested in the 1m^3 ISO vessel *(Wilén and Rautalin, 1996)* due to the fibrous particle shape causing blockage of the C ring (the standard disperser). A major part of this research project was the development of modifications to the dust injection system of the ISO 1 m^3 equipment that will enable it to operate with coarse fibrous woody biomass.

Currently computer models are being developed to predict the influence of particle size distribution/concentration on pulverised woody biomass explosions (Callé et al., 2005). However in order to produce reliable predictions these programs must be validated against experimental explosions and this work aims to provide this data.

2.2 Dust explosions

The three requirements for combustion are fuel, oxidising agent (usually air) and an ignition source that is equal to or above the fuel's minimum ignition energy (MIE). This is often called the "fire triangle". The fuel source can be any material that reacts rapidly and exothermically with an oxidising agent. For a dust or gas explosion to take place the dust or gas must be dispersed in the air, at a concentration between its lean and rich flammability limits while an ignition source is present. The dust flame propagation in the fuel-air mixture in a closed volume leads to an increase in the vessel pressure. The reaction rate of a dust explosion is determined by the rate of pressure rise in the closed vessel and in the present work by direct measurement of the flame speed.

2.2.1 Definition

Current data on and understanding of dust combustion is based primarily on work by (Bartknecht, 1989, Bartknecht, 1981 , Field, 1982 , Verakis, 1983, Cashdollar,

1987 , Eckhoff, 2003). There are two distinct mechanisms for dust combustion (Hertzberg, 1992): heterogeneous and homogeneous. The difference centres on the physical state of the fuel at the moment, leading up to and of combustion.

- In the heterogeneous combustion mechanism, the reaction with the fuel takes place at the particles surface in a solid/gas reaction. However according to (Proust, 2006) “the contribution of heterogeneous type combustion in the flame propagation process (for non-metals) should be discarded”. This mechanism is only viable for metals and other high melting point materials where the reaction of the oxygen and the reactant takes place at the particle surface.

- In homogeneous combustion there are three processes:

  heating and devolatilization *(Cashdollar, 2000, Lewis, 1987)* of the dust particles ahead of the flame front; mixing of those volatiles with the air surrounding the particle and gas phase combustion of the volatile air mixture by the flame front.

In homogeneous dust combustion an insensitivity of the lean limit to particle size (for fine dusts), this shows that flame propagation is restrained by sufficient fuel being present. A particle size dependence of the minimum explosion concentration (MEC) or lean flammability has been found to be a function of the particle size (Pilão et al., 2004, Pilão et al., 2006) and (Hertzberg, 1982). The reason for this is that the propagation control is shifting from the total fuel (for fine particles sizes) available for combustion to the fuel that can be devolatilised in time from large particle sizes.

It will be shown in this work that conventional modelling of dust explosions may not apply to biomass and other CHO dusts as results will be shown that clearly show that flame propagation lean limits cannot be explained by a model based on flame propagation in hydrocarbon volatiles released from the dust. A model of double flame structure combustion of the devolatilised material at the leading flame front followed by an oxygen controlled diffusion flame around the particle may be necessary for large particles (Han, 2001, Gao, 2015).

Tomographic techniques (Proust, 2006) were used to investigate this using laser sheet analysis starch particle combustion as shown in **Figure 2.6**. This shows that

the particle can be seen to disappear well ahead of the flame front where combustion takes place. For fine particles it isn't only the volatile material that can participate in a dust explosion propagation as there is adequate time for the fixed carbon to participate in the combustion which is contrary to the conclusion of Cashdollar (2000) as shown by the complete disappearance of particles ahead of the flame front.

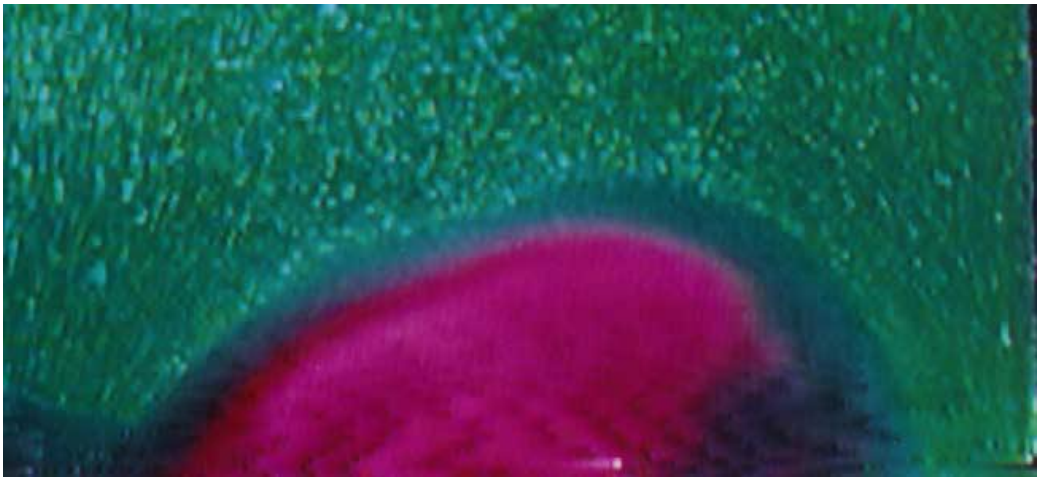

Fig 2.6 Image of flame front (in pink) propagation in dust cloud showing disappearance of dust particles ahead of flame front (Proust, 2006).

The conventional view of dust flame front propagation is that conduction and radiation from the flame front heats the particles and releases volatiles that then ignite and the flame propagates as a gas flame. However, it is easy to see that the volatiles for biomass and agricultural dusts cannot be methane, as is usually modelled for coal dust flame propagation, as there is insufficient hydrogen in the fuel to account for the very large proportion of volatiles released from biomass fuels. Other gases must be involved principally carbon monoxide and hydrogen (Corella, 1988, Commandré, 2011) are thought to be released. It will be shown in the present work that for fine particles there is little evidence of the production of char that remains after the explosion. This indicates that all the biomass powders are vaporised under the rapid heating of the flame front. This is different to coal where there is always a char (fixed carbon +ash) remaining after flame propagation. Biomass dusts and coal have an inert ash content and this is left as a residue after flame propagation.

The volatile content of biomass is usually determined using thermal gravimetric analysis, TGA, (see Chapter 3) which involves relatively slow heating of the biomass compared with that in flames. Some results for biomass using this method

are shown in **Table 2.4** (Wilen, 1999). This method shows that the volatile gases can contribute up to about 70-80% of the total mass of biomass powders and 30-50% for coal (depending on the type). **Table 2.4** shows that typical values for woody biomass are:

Wood: volatile matter (80%), fixed carbon (19.4%) and ash (0.4%)

Bark: volatile matter (74.7%), fixed carbon (24%) and ash (1.3%)

Table 2.4 Proximate composition of coal and biomass (Wilén, 1999).

Dust sample	Humidity %	Ash %	Volatile matter %	Lower heating value (LHV) MJ/kg
Wood	1.65	0.39	81.87	18.16
Bark	5.75	1.70	68.55	19.83
Forest residue	5.30	2.55	73.25	19.73
Spanish pine	7.40	0.25	78.15	18.52
Barley straw	15.35	4.20	63.30	17.18
Miscanthus	7.00	1.00	73.20	18.32
Sorghum	6.55	5.25	70.40	17.59
Rapeseed straw	11.50	5.40	50.95	17.06
German lignite	9.85	3.85	46.10	23.52
Spanish lignite	16.65	17.10	36.60	17.23
Mixture 1	9.50	3.10	53.00	22.34
Mixture 2	14.65	14.10	47.50	17.87

In the flame propagation the fixed carbon of the biomass particles may be pyrolysed and so contribute to the combustion process. However, rather than direct combustion of carbon or char (at the particle surface) it is possible that under rapid heating the fixed carbon is converted to CO (Lewellen, 1977) and so would react in the gas phase.

There is relatively little work on the composition of the volatiles released from biomass under the relative low temperature heating that releases the volatiles (300 – 400^{o}C). Most work on the pyrolysis of biomass used high temperature heating with pyrolysis of the fuel into tar, gases and char. The degree to which the solid particles are pyrolysed will depend on the temperature of the flame front and the residence time (dictated by the flame speed and flame thickness) of the particles within it. And could lead to real term volatile yields of 90 - 100% from biomass powder and 60 - 70% for coal (Commandré, 2011).

Table 2.5 taken from Ramírez (2009) lists the factors that affect an explosion and will be reviewed in more detail later in this paper.

Table 2.5 Typical explosion values per material and the factors that affect them (Ramírez, 2009).

factors that affect reactivity	
factor	the maximum value of dP/dt corresponds with
particle size	the finest
dust concentration	much higher than LEL
energy of ignition source	strong sources
location of ignition source	central position
initial temperature	high
initial pressure	high
turbulence	high
presence of gasses	flammable gasses

There are two loss mechanisms that can quench flame propagation in dust combustion *(Hertzberg, 1982).*

(1) Natural convection/buoyancy, that occurs in lean mixtures.

(2) Heat loss to dust particles/objects (Dastidar, 2001) that aren't completely devolatilised as occurs in rich mixture situations or don't take part in combustion (vessel walls).

The steps taken to allow for and minimise these losses are discussed later in this work.

2.2.2 Types of flame propagation

Deflagration is the term used to describe a subsonic combustion that propagates through a mixture of fuel and oxidant (usually air) by thermal convection and gaseous species diffusion heat transfer to the mixture ahead of the flame. The rate of flame propagation relative to the unburnt gas is the burning velocity which may be laminar or turbulent depending on the flow conditions in the oxidant. For dust flame propagation it has to be turbulent in order to keep the dust in suspension. The magnitude of the burning velocity is a measure of the mixture reactivity and if a turbulent test rig is used, as for all the dust flame propagation test equipment discussed earlier, then the turbulence must be held constant as the dust

composition is varied. This is the principle of operation of the three dust explosion test methods discussed earlier. For a stable flame at the end of a burner pipe the mixture must be fed along the burner tube at a flow rate that balances the burning velocity so that a stationary flame occurs.

The flame speed is another measure of mixture reactivity and this is the speed at which a flame propagates relative to a stationary observer. Thus in a burner with a stable flame the flame speed is zero. If the fuel/air mixture is in a closed volume and is stationary, then a central ignitor will produce a spherical flame that propagates through the mixture at the flame speed which is measured in the present work on dust explosions.

This situation occurs in explosion hazards following a gas or liquid aerosol leak or dust dispersion in a closed volume. For closed volumes the flame propagation will be accompanied by a pressure rise. Explosions can occur if there is a gas leak or dust dispersion in the open with no confinement and then a flash fire occurs that is only dangerous if people are engulfed in the flash fire, there is normally no significant pressure rise. This scenario can become dangerous if there are turbulence creating obstacles ahead of the flash explosion, which interact with the propagating flame to create turbulence and accelerated the flame. In large scale spillages on chemical plants this can result in what is known as an Unconfined Vapor Cloud Explosion (UVCE), but these are not the subject of this research.

The flame speed, S_s, is related to the burning velocity, S_u, by Eq. 1.

$S_s = S_u \rho_u/\rho_f = S_u E_p$ for constant pressure flame propagation – (1)

Where ρ is the gas density with subscript u for the unburnt gas and f for the burnt gases. This density ratio is known as the expansion coefficient E which has two values, one for combustion at constant pressure E_p and one for combustion at constant volume, E_v. E_v is greater than E_p as the adiabatic flame temperature in constant volume combustion is greater than that at constant pressure, due to differences in specific heat at constant volume and constant pressure. For constant pressure the temperature is lower than the constant volume temperature because some of the energy is utilized to change the volume of the system. The difference is of the order of 10%, but is mixture specific. This is important if the measurement of the mixture reactivity is made in a constant volume explosion, as it is in dust tests. In this case the expansion of the gas is confined and the pressure increases so that

the peak pressure, P_m, as a ratio of the initial pressure, P_i, which is normally atmospheric pressure, is given by Eq. 2.

$$P_m/P_i = E_v \qquad (2)$$

For dusts of variable composition the computation of the adiabatic flame temperature is not easy and often E_v is measured in constant volume spherical vessel explosions, normally the 20L or $1m^3$ dust explosion vessels. Cashdollar (1987) has provided measurements of E_v for a wide range of dusts. For gases E_v and E_p can be calculated. It is the confinement of flammable mixtures that give rise to pressure rise that causes damage in accidental explosions.

A further feature of flame propagation in initially stationary oxidants is that the expansion of the burnt gases behind the flame front produces a wind in the unburnt mixture ahead of the flame, which is predicted by Eq. 3.

$$S_s - S_u = S_g \qquad (3)$$

Where S_g is the wind ahead of the flame front. This was first measured in a gas/air explosions by Andrews and Bradley (1973) as a means of measuring S_u by the measurement of S_s and S_g. Eq. 2 and 3 by be combined to give Eq. 4 for S_g:

$$S_g = [1-(1/ E_p)] S_s \qquad (4)$$

In UCVCE the acceleration of S_s by turbulence increases S_g and this causes more turbulence to be generated by interaction with obstacles. In the present work S_g is important as it is postulated that this wind entrains large particles of dust from ahead of the flame front during propagation and blows them onto the vessel walls just before the flame contacts the wall. This results in the concentration at the propagating flame front being leaner than the overall initial dust/air mixture concentration.

In a closed vessel explosion the flame initially starts off at constant pressure as the explosion pressure does not increase until there has been significant burning of the initial mass of dust and air. For a flame in a spherical vessel the flame is halfway across the vessel and the pressure rise is only 1.5% of the maximum pressure rise as only 1.5% of the initial mass has been burnt, as shown in Eq. 5.

Flame diameter D_f, vessel diameter D. If D_f = 0.5 D then, assuming that the pressure rise is proportional to the mass burnt (Lewis, 1987) then:

$$P/P_m = (D_f/D)^3 / E_p = (0.5/1)^3/8 = 1/(8 \times 8) = 1.5\% \qquad (5)$$

Where E_p has been taken as 8 which is typical of hydrocarbon flames at stoichiometric concentration. In the present work flame speeds in the $1m^3$ are measured in the constant pressure period of flame propagation, hence the flame speeds and the burning velocity derived from them are at constant pressure.

For an explosion in a closed vessel there is another parameter that is used to characterize the mixture reactivity and that is the deflagration parameter, K_G for gases or K_{st} for dusts (the German word for dust is Staub, which is where the St suffix comes from, as this method of characterization of mixture reactivity in explosions originates with Bartknecht [1989, 1993] in Germany. The definition of K_G or K_{st} is given by Eq. 6.

$$K_G \text{ or } K_{st} = (dP/dt)_{max} V^{1/3} \qquad (6)$$

However, the maximum rate of pressure rise in a closed vessel explosion occurs just before the flame touches the vessel walls and is clearly a reactivity parameter measured under flame temperature conditions of constant volume with expansion ratio E_v. Thus the present measurements of flame speed are at constant pressure and K_{st} is at constant volume. Andrews (2010) showed that the burning velocity and K_G are directly related by Eq. 7

$$K_G = V^{1/3}[0.98\, P_m/P_i - 1] / ((D/4) / S_u\, E_p) = 3.16(P_m/P_i - 1)S_u E_p \ \text{m/s} \qquad (7)$$

Eq. 7 results from an assumption that the flame speed is constant across the diameter of flame travel; which is not quite true, but the variation is only about 20%. Eq. 7 also shows how a burning velocity can be derived from a K_{st} measurement and a measurement of P_m/Pi.

There is one further combustion parameter that occasionally occurs in accidental release of gases and this is detonation. Detonation is a supersonic propagation accelerating through a medium that results in a supersonic shock wave radiating from it. The shock wave generates sufficient temperature rise to ignite the mixture and the expansion of the reaction pushes the shock wave into a detonation at speeds in excess of the original shock wave. Detonations are normally formed by

explosives (military explosives and demolition), but can also happen in reactive gases. Gaseous detonations normally occur in confined systems but are occasionally observed in large gas/vapor clouds (Buncefield). The most common method for generating a detonation is in long pipes where the explosion induced wind creates pipe flow turbulence ahead of the flame and this causes the flame to accelerate, which generates more turbulence. Eventually the wind ahead of the flame in the pipe reaches sonic speed and causes a detonation. Detonations rarely occur outside of confined pipes, but can occur in accidently leaks in VCE (Vapour Cloud Explosions) and are considered to have occurred at Buncefield. In this work only deflagrations were investigated and detonations will not be considered further.

2.2.3 Safety regulations

In the US regulation/legislation to control explosion hazards is largely achieved by following National Fire Protection Association (NFPA) standards:

• NFPA 51B - Standard for Fire Prevention During Welding, Cutting, and other Hot Work.

• NFPA 61 – Standard for the Prevention of Fires and Dust Explosions in Agricultural and Food Processing Facilities.

• NFPA 68 – Standard on Explosion Protection by Deflagration Venting.

• NFPA 69 – Standard on Explosion Prevention Systems.

• NFPA 499 - Recommended Practice for the Classification of Combustible Dusts and of Hazardous (Classified) Locations for Electrical Installations in Chemical Process Areas.

• NFPA 654 – Standard for the Prevention of Fires and Dust Explosions from the Manufacturing, Processing, and Handling of Combustible Particulate Solids.

• NFPA 664 – Standard for the Prevention of Fires and Dust Explosions in Wood Processing and Woodworking Facilities

NFPA 664 identifies “deflagrable wood dust” as “wood particulate with a mass median particle size of 500 microns or smaller”. Although as will be shown later

(**Table 2.11**) wood dust with an average particle size up to 1250µm has been found to propagate an explosion.

The use of mass median particle size is a poor method as mass median particle size can be drastically altered by the volume contribution of the largest particles. A mixture of equal parts 1000µm and 10µm by mass will give an average particle size of 505µm. This was demonstrated with a 50/50 mixture of fine and coarse (too coarse for combustion) oak particles in chapter 5.

In Europe the ATEX Directive's guide the development of explosion protection. ATEX Directive 94/9/EC, is concerned with the manufacturers of equipment intended to be used in potentially explosive atmospheres of various types and severity's. In the UK, the requirements of this Directive were put into effect through BIS Equipment and Protective Systems Intended for Use in Potentially Explosive Atmospheres Regulations 1996 (SI 1996/192). Incidentally it also allows easy trade of such passive protection systems within member states due to the uniform requirements. Products that fall within this Directive are divided into two sectors by use:

- Group I, equipment intended for use in mines.
- Group II, equipment intended for use in other locations.

Within these categories there is further division based on the level of duration/protection required.

Group I
Category 1 - Equipment in this category is required to remain functional with an explosive atmosphere present.
Category 2 - This equipment is intended to be de-energised in the event of an explosive atmosphere forming.

Group II
Category 1 - Equipment in this category is intended for use in areas in which explosive atmospheres are present continuously or for long periods.
Category 2 - Equipment in this category is intended for use in areas in which explosive atmospheres are likely to occur.
Category 3 - Equipment in this category is intended for use in areas in which

explosive atmospheres are unlikely to occur and if so, it's only infrequently and minor.

This covers such things as inability to propagate an explosion from within the casing, minimum energy of device discharge below minimum ignition energy of risk gas and ability to shut down in presence of gas without risk.

The other ATEX Directive (1999/92/EC) is concerned with safety in the workplace following the principles: prevention of the formation of explosive atmospheres or where the nature of the activity does not allow that, avoidance of ignition while constantly working on the mitigation of the effects of any explosion that should take place to ensure the health and safety of workers at all time. This ATEX Directive stipulates that measures must be based on a risk assessment carried out by the responsible person. This is enacted into UK law by regulations 7 and 11 of the Dangerous Substances and Explosive Atmospheres Regulations 2002 (DSEAR).

Requirements in this directive are that wherever an explosive environment could develop the area must be classified into hazardous and non-hazardous areas. Hazardous areas are then classified in terms of "Zones" (EPRA, 2011) on the basis of the frequency and duration of the occurrence of an explosive atmosphere, as follows:

- ***Zone 20*** *A place in which an explosive atmosphere in the form of a cloud of combustible dust in air is present continuously, or for long periods or frequently.*

- ***Zone 21*** *A place in which an explosive atmosphere in the form of a cloud of combustible dust in air is likely to occur in normal operation occasionally.*

- ***Zone 22*** *A place in which an explosive atmosphere in the form of a cloud of combustible dust in air is not likely to occur in normal operation but, if it does occur, will persist for a short period only.*

In addition to this all dusts are categorised into one of three categories based on the maximum pressure rise and the deflagration index, K_{st} (**Table 2.6**) (Foulke, 2007).

Table 2.6 Categorisation of dusts based on K_{st} and Pmax (Foulke, 2007).

The higher a dusts' classification the more stringent the safety procedures and restrictions put upon its use/storage. As will be shown later, biomass/coal materials always fall into the St 1 area while St 3 materials are almost exclusively made up of metal dusts.

2.2.4 Protection systems

These consist of two categories, passive and active-

- Passive protection are devices whose construction is defined by ATEX Directive 94/9/EC. These operate by preventing ignition from themselves, that is to say passive fire/explosion protection systems are operated in combustible environments but cannot ignite them.

- Active fire/explosion protection systems actively fight the propagation of a flame front or the pressure build up; there are two main methods of active explosion protection, venting and inerting.

Venting - Venting is a protection method by which the explosion overpressure is allowed to escape the enclosed volume of the building/vessel it is in. This normally takes the form of a vent with a burst pressure (normally 100mBar) to protect the building/vessel that will normally have a threshold of sustaining damage at approximately 300mBar. Therefore the vent has to be able to vent the pressure rise to below 300mBar from 100mBar. The mixture reactivity determines the value of S_g which determines the flow through the vent and in vent design the deflagration index, K_G or K_{st}, is used as the reactivity parameter when sizing vents. Consequently any differences in the $K_{st,}$ or burning velocities of the likely fuel affects the venting performance. The present work aims to provide K_{st} data for woody biomass dusts of practical biomass size so that explosion protection vents can be adequately designed, this data was not available at the start of this research.

Inerting – Inerting of the atmosphere using nitrogen, carbon dioxide or argon has been used for many years to prevent explosions in gas or vapour explosions and can be used in dust explosion prevention. The principle is that the inert gas acts as a heat sink and reduces the flame temperature. The effect is determined on a lean flammability equipment such as the Hartmann for MEC determinations with an inert gas present (Eckhoff, 2003). The LEL of a HC gas occurs at a flame temperature of about 1400K and inerting is used to reduce the stoichiometric flame temperature to below 1400K by adding nitrogen or CO_2. CO_2 is the most effective gas as it has the highest specific heat capacity. 25% CO_2 will inert most hydrocarbon gas/air explosions, in comparison 30% of water and 40% of N_2 are required to do the same. As the P_m/P_i measured in dust explosions is a measure of the flame temperature to initial temperature the higher the maximum P_m/P_i the more inert gas is required in dust explosion prevention.

Suppression – Suppression of explosions using inert powders as a heat sink, limestone dust is commonly used for this in coal mines. However, it has been found that solids that endothermically decompose when heated give greater cooling and less mass of suppressant is required to extinguish a dust explosion. Sodium bicarbonate and MAP are typical of such solid powder inerts with endothermic decomposition and their superiority to limestone dust as a purely heat sink inert is shown in **Figure 2.7** (Dastidar, 2002).

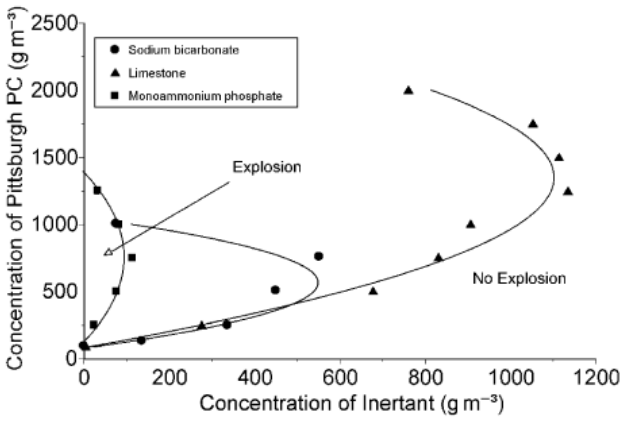

Figure 2. Inerting envelope for Pittsburgh pulverized coal dust with sodium bicarbonate, monoammonium phosphate and limestone as inertants. Experiments conducted in a spherical 1-m^3 chamber using two 5-kJ ignitors as ignition source.

Fig 2.7 Different inerting agents and their effect on the flammability limits of coal (Dastidar, 2002).

In biomass dust there is a natural solid and liquid inert: the ash and water content. Thus variabilities in these reduce the reactivity of the biomass and affect the MEC. The fixed carbon in biomass may also act as an inert as the reactivity of carbon or char is very low compared to that of the volatiles. The effect of this would be to expect that the MEC of a biomass dust would be richer than the equivalent MEC of a pure hydrocarbon dust that had no inerts that would reduce its reactivity. It will be shown that the evidence for this is weak and only where the biomass dust is high in ash and moisture is the MEC less than that for a pure hydrocarbon gas. As the volatile component of coal or biomass dust is trapped within a particle together with fixed carbon and solid ash and liquid water, Dastidar et al. (1997) postulated that there was a critical level of volatiles below which a flame cannot propagate, as shown in **Figure 2.8** (Dastidar, 2002).

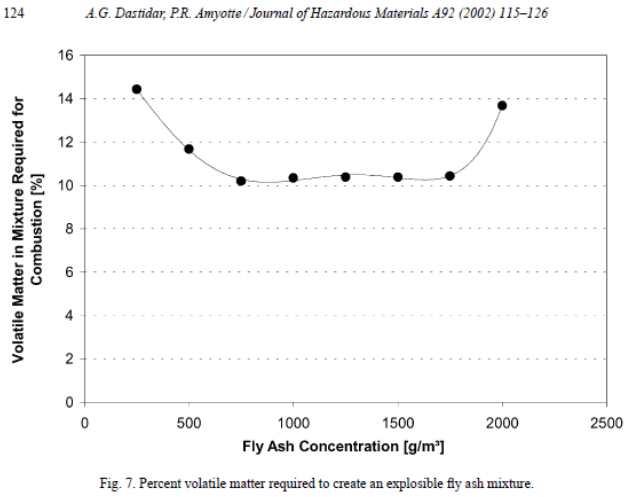

Fig 2.8 Volatile concentration in a solid fuel needed to produce combustion in fly ash, with varied concentration (Dastidar, 2002).

Dastidar (2002) carried out experiments on the amount of volatile material required to create a combustible mixture as shown in **Figure 2.8**, which was approximately 10% (21% added coal dust by mass). The results also showed that as the inert materials particle size was decreases, less of it is required to inert a set explosion. The mass of inert material was concentration (**Fig. 2.7**) and particle size dependent. Dastidar (2002) also found that the amount of inert required reduced as the dust concentration was increased beyond that for the maximum K_{st}. The maximum K_{st} was assumed to occur when the volatile/air mixture was at stoichiometric ratio.

Therefore a link can be drawn between the concentration of fuel and the amount of inert required, as shown in **Figure 2.7**. The reason for this could be that for rich dust/air mixtures, beyond the mixture for maximum K_{st} and P_m/P_i, the addition of more dust could be acting as a heat sink and this would then require more volatiles to overcome the effect, as shown in **Figure 2.8**.

An effect of biomass particle size is that large particles in a dispersion of various particle sizes may act as an inert or heat sink and reduce the flame reactivity. Thus the presence of fines in the mixture may propagate the flame but the coarse particles act as a heat sink that reduces the reactivity and the MEC and enhances the proportion of coarse particles in the residue after the explosion.

2.2.5 Dust combustion compared to gas combustion

The most obvious difference between dust and gas combustion is that the dust has first to release volatiles following heating by the propagating flame front, whereas the gas is already present in a gas explosion. The energy required to release the volatiles from the solid dust has to come from a the CV of the fuel and hence results in a lower flame temperature than for an equivalent gas explosion. However, a simple interpretation of dust explosions as dust heating to release hydrocarbon volatiles does not explain the results in **Figure 2.15**, where very high, rich concentrations of dust do not have a reduced peak pressure in explosions, whereas for gases rich concentrations have reduced peak pressure and reduced flame temperature. Gaseous fuels have narrow flammability limits from a stoichiometric value of 0.5 to 1.5-2.5 for most gasses, as shown in **Figure 1.4**, while as will be elaborated on in Section 2.3.2, this is not the case with dust explosions that show no rich limit. Even if the particles are very fine and at very rich concentrations (Deguingand and Galant, 1981) there is still no rich limit and little reduction in peak pressure for rich mixtures.

Due to the physical differences between them it is impossible to have dust explosions in a laminar environment as can be done with gas explosions. Dust explosions are initiated using chemical igniters, creating a centralised hot ball of gases from the chemical ignitor heat release, the temperature of this zone is well above the temperature necessary to heat the dust and release volatiles and ignite them. For the flame to propagate from this central ignition zone the flame front has to transfer heat by conduction and radiation (Yao B. Yang and Jenny M. Jones,

2008) to the dust ahead of the flame so that it is rapidly heated and releases volatiles that propagate the flame. The burnt gases behind the flame front expand due to their high temperature and this increase in volume and lowers the density of the burnt gases pushing the spherical flame outward. This creates an explosion induced 'wind' ahead of the flame (Andrews and Bradley, 1972) and in a dust explosion this wind may act more on large particles than the small particles. Small particles <10μm would behave like a gas and move with the flow, but larger particles would have inertia and would lag behind and thus be heated by the burnt gases of the flame propagating in the fine particles. This could be a mechanism that enables biomass dust with coarse particles to propagate a flame and this was a major aspect of the present research, to show that coarse particles were an explosion risk and to decide if this explanation was supported by the evidence.

This influence of the explosion wind on particle size distribution ahead of the flame and behind the flame front, has not been recognised in dust explosion literature prior to this. The effect may be to make the hot gases behind the flame front locally richer when large particles are present. For rich mixtures the large particles behind the flame front are burnt in a mixture with low gas phase oxygen and the oxygen that is contained in the biomass. In the Hartman high speed video the initial flame front appears leaner (for large particles) by virtue of the flames being less luminous due to less soot formation. This means there will be oxygen left in the air behind the flame front. If large particles lag the flame front and are then heated in the burnt gases then there is an equivalence ratio distribution at the flame front with the initial combustion lean and a rich combustion zone in the burnt gases. This could be the mechanism of very rich mixtures propagating flames in dust explosions. The rich mixtures in the hot gases behind a lean initial flame (for rich overall mixtures with large particles) would undergo gasification reactions where the equilibrium products are hydrogen and CO (Commandré, 2011). After these burn in the remaining oxygen the remaining particle mass will continue to devolatilise but there is now no oxygen to burn these gases, therefore the volume increase of these gases would increase the peak pressure as they are released into a constant volume. Eventually, as the mass of particles increase the physical cooling of the gas due to their heating would reduce the temperature behind the flame front and eventually the peak pressure would start to fall. This explains the results in **Figure 1.4** and similar results found in this research.

This explanation fits with previous experimental data for coarse biomass mixtures that have been shown to be capable of producing strong explosions (Wilén, 1999, Wong, 2013). The above model of biomass dust combustion explains the observed results of very rich combustion for the most reactive mixture.

2.2.6 Mode of dust flame propagation.

There is a general similarity between dust particle combustion and that of premixed gas flames; they all propagate on gaseous products (excluding metal dusts). For dusts the propagation derives from thermal convection (Proust, 2006, Essenhigh and Csaba, 1963, Bidabadi and Rahbari, 2009, Gao, 2015, Han, 2001) ahead of the flame, producing gasification/pyrolysis of the particles. Then upon flame arrival the heat release takes place in the gaseous phase. (Gao, 2015, Han et al., 2000) observed a double flame structure in biomass and liquid mist combustion where the initial flame front propagated on the devolatilised material while the remaining droplets/particles burn in an envelope diffusion flame around the droplets/particles behind the flame front.

There appear to be two distinct methods of flame propagation in dust clouds, one is continuous the other discontinuous. However (Han, 2001, Gao, 2015, Han et al., 2000) observes lycopodium combustion to be discontinuous. This is therefore probably true for all dusts with particle size smaller than this and of the same relative composition and so covers all materials tested here. This is not the case with metal dusts, these propagate in a continuous manner (Proust, 2006) and due to extremely high reported luminosity may have radiative heat transfer involved in their propagation mechanism (Proust, 2006).

For small flame thickness's radiation is not significant but it is for thick flames, Proust (2006) proved with starch dust that this was not happening, but for larger particles and richer mixtures this may change. Han et al. (2000) puts the thickness of lycopodium flames at 20mm and Proust (2006) comments on the observation of turbulent flames "thickening". So it is possible that radiation could be playing a role in rich, large particle dust explosions as was suggested by Yao B. Yang and Jenny M. Jones (2008). It is also likely that the flame thickness in large particle dust explosions is thicker than was found for lycopodium due to large particles lagging the flame front. Glinka (1996) have reported about 5–16 mm for the preheated

zone in lycopodium particles and in the order of a few centimetres for wheat dust particles.

Discontinuous propagation (Bidabadi and Rahbari, 2009, Han et al., 2000, Han, 2001, Gao, 2015) is characterised by a flame front composed of 3 regions – the preheat zone where the solid particles are devolatilised to gaseous material. The reaction zone where the gasses burn and then a convection zone where the last of the heat release takes place in an oxygen controlled environment.

Tomographic techniques have been used by Proust (2006) to investigate and verify this. Starch particles (28µm), illuminated by the laser sheet, disappear abruptly well ahead of the combustion zone, where combustion is taking place (shown in red/pink) **Figure 2.6**.

The temperature rises as soon as the reaction zone (**Fig. 2.6**) (shown in pink) of the flame arrives although the luminous (radiation) signal begins to grow ahead of this. However, there is no sign of the dust particles ahead of the flame heating up due to radiation from the flame front. The likely explanation is that particles are being pyrolysed by heat convected from the flame front, prior to the combustion that then proceeds in the gas phase. This implies that the concentration of the gaseous, devolatilised material ahead of the flame front will depend on the particle size; particles that fully devolatilise ahead of the flame front will produce gaseous concentrations as that for the dust. However large particles will only devolatilise part of their mass, therefore the flame front will be initially lean with a rich secondary stage when the large particles burn in the products of the first flame front with the remaining air hence the double flame structure in biomass that has been observed (Gao, 2015, Han et al., 2000).

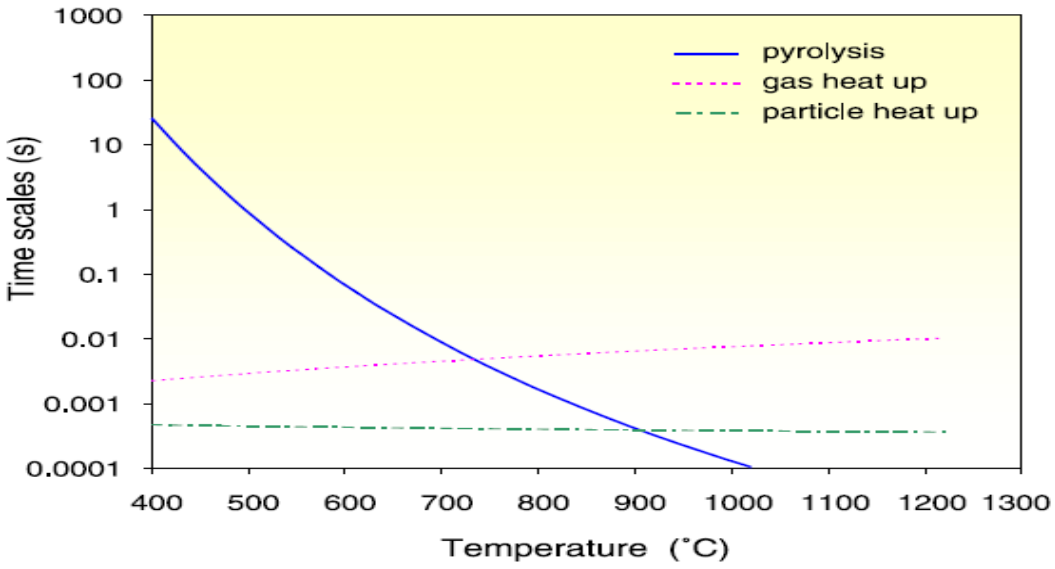

Fig. 5. The time scales in a starch (28 μm) dust–air flame.

Fig 2.9 Time frame for pyrolosis in relation to temperature (Proust, 2006).

The pyrolysis plot (**Fig. 2.9**) (Proust, 2006) crosses the heat transfer curve at about 750C^{o} suggesting that the particles (of this material and size) should disappear as soon as 750C^{o} is reached which is exactly what the flame propagation image shows. This occurs at a residence time of about 5ms from (**Fig. 2.9**).

The same phenomenon has been seen for sulphur dust flames, Proust (1993) and other fuels Gao (2015). For small droplets of tetralin, diameter ≤10μm, Burgoyne and Cohen (1954) showed that droplets vaporize completely before the flame front reaches them. The flame then propagates into and upon a vapour-air mixture. The flammable limits were found to be the same as the corresponding vapour-air system for tetralin (at the slightly elevated temperature necessary to vaporise the droplets). While after a droplet size of >40μm the flame becomes individually burning droplets and the flame propagation becomes discontinuous.

This indicates that there is no significant difference between the combustion of a gas and a liquid vapour other than its surface area and more significantly the percentage of its mass that can be liberated to the gas phase to burn in the time available. If this is applied to dusts it would indicate that the most significant difference between a CH or CHO gas and its solid equivalent is the density and heat of vaporisation. When a solid or liquid is vaporised it creates a locally rich zone, allowing for the material that is not vaporised, this could explain why dust combustion appears to have no upper flammability limit. Therefore general flame

propagation in fine dust flames, with particles able to gasify at low temperature is similar to that in premixed gases (Proust, 2006, Gao, 2015).

Explosibility of hydrogen–graphite dust hybrid mixtures, carried out by Denkevits (2007) could be used as a representation of the different constituents of dust combustion, volatile and solid as biomass particles tend to be much bigger than 28µm so likely don't all devolatilise ahead of the flame as was found by Proust (2006). This kind of additive experiment has also been performed with methane and coal dust (Tominaga, 1987, Foniok, 1985) which increased the explosibility of the solid coal. This effect is most pronounced for dusts with low volatile content. Depending on the mixtures make up the explosion proceeds as one or two stages.

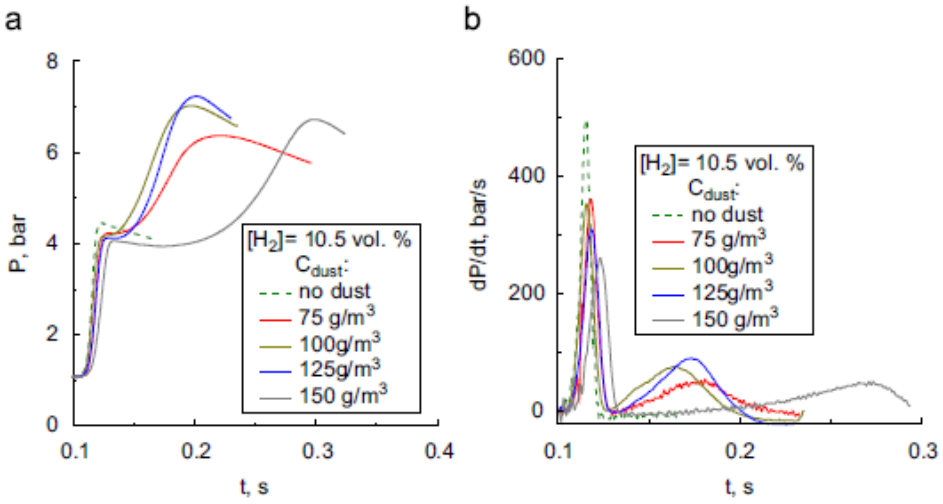

Fig 2.10 Low concentration Hydrogen and graphite 2 stage explosion (Denkevits, 2007).

In two-stage explosions (**Fig. 2.10**) Denkevits (2007) (occurring at low hydrogen and dust concentrations), the reaction creates first a fast hydrogen explosion followed by a slower dust explosion. With increasing dust concentration, the dust reacts faster and can catch up to the hydrogen-explosion stage. Graphite dust is very difficult to get to react and it has no volatile content, the reaction is initiated by the hydrogen flames leaving plenty of oxygen to react with the graphite.

At higher hydrogen concentrations with higher flame temperatures, the hybrid mixtures react more rapidly as shown in **Figure 2.11** (Denkevits, 2007).

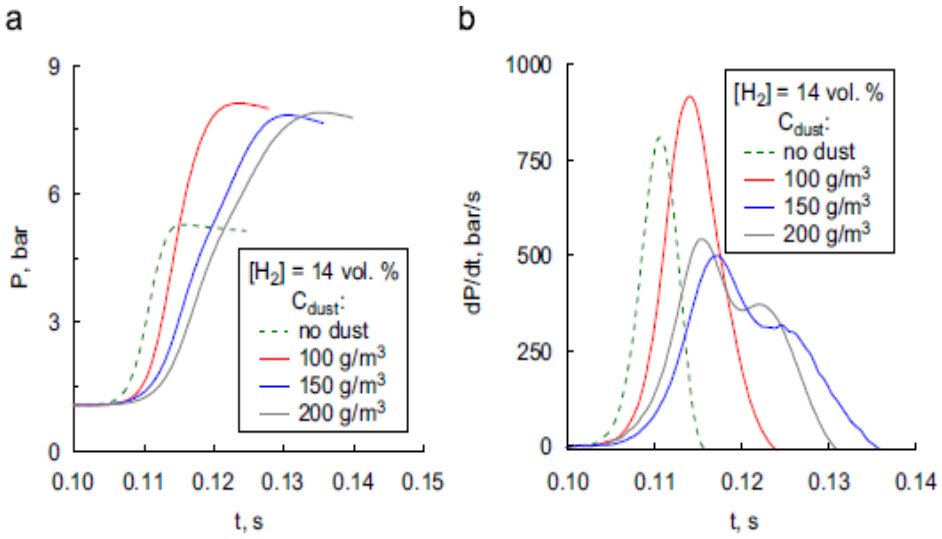

Fig 2.11 High hydrogen medium graphite dust single stage explosion. (Denkevits, 2007)

This demonstrates that with sufficient energy (hydrogen) it is possible to burn graphite rapidly. The maximum overpressure in all the tests with the dust involved in the explosion is substantially higher than that without dust as the 14% hydrogen does not burn all the O_2 in the mixture. Maximum rates of pressure rise are lower in two-phase explosions and higher in one-stage explosions as all the energy is released at once from both the gas and dust. The rate of pressure rise in **Figure 2.11** is slightly higher for 100g/m^3 of graphite dust with hydrogen than for hydrogen alone and appears to react as a single propagation, suggesting a synergistic relationship at this concentration. For all other tests the rate of pressure rise is lower with the addition of graphite and the explosion propagates as two stages while the total pressure rise increases for all tests with the addition of graphite.

Lower hydrogen concentrations resulted in the hydrogen burning out first and then the dust starts to react with the remaining oxygen. With 12% H_2 and greater, the energy released at the start of the hydrogen combustion, is enough to ignite the graphite. The hybrid explosions proceed in 2 stages one fast stage (the gas explosion) the other slower; the time delay between these stages is reduced with increasing H_2 concentration.

The single stage explosion (**Fig. 2.11**) may represent a high volatile dust and its fixed carbon content, where the volatile hydrogen in the flame front is energetic enough to burn the solid (graphite) particle at the same rate as the gasses. However this would not allow for the Oxygen contained within the elemental

composition of the biomass that is lacking here. This could lead to a thicker flame front as the oxygen contained in the fuel will slow the time taken to reduce the oxidant concentration to 0, the governing factor in this part of the reaction.

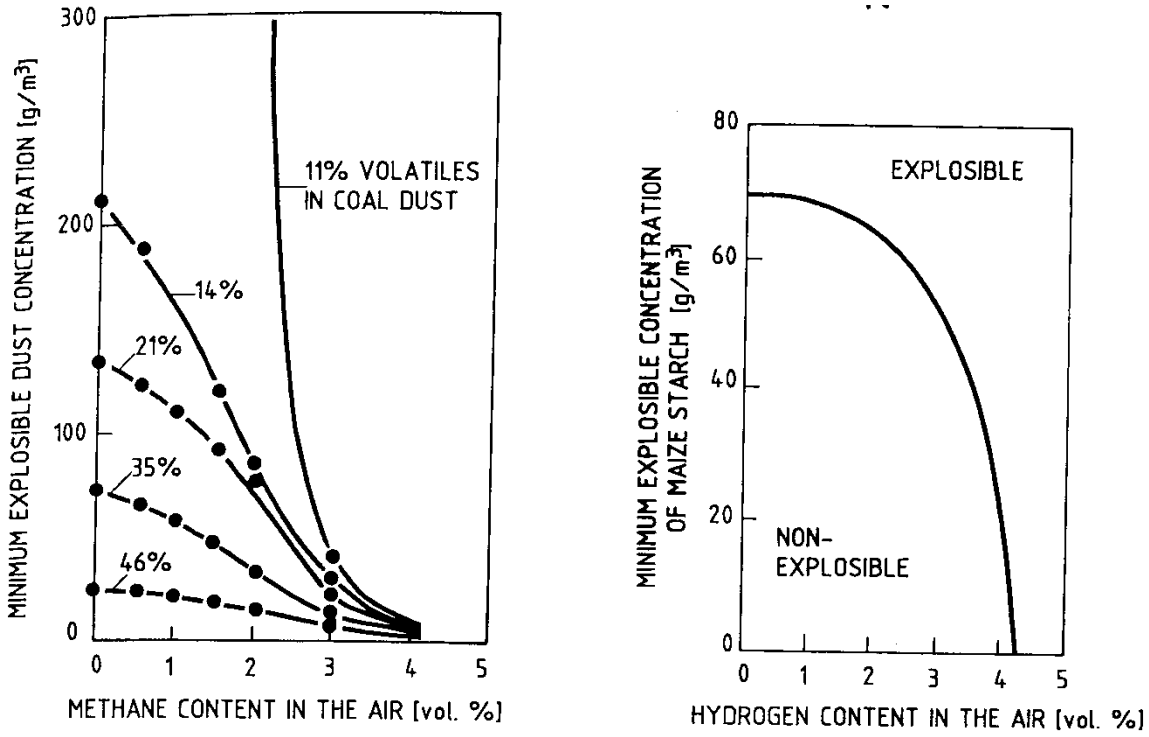

Fig 2.12 Dust/gas hybrid MEC with varied volatile and gas concentration (Eckhoff, 2003).

Figure 2.12 from (Eckhoff, 2003) indicates that volatile concentration in a dust affects the MEC a dust , this was also observed by Gao (2015) who noted that low volatile dusts produce more “blue spots”, thought to be caused by lean combustion of devolatilised material from large particles at the leading edge of the flame front. The richer the fuel mixture is the more solid particles will be in the flame front, theoretically increasing the radiation; this may also be true if the particle size is increased.

There is currently no data to indicate how thick a HC flame front has to become to make radiation a viable mode of flame propagation.

2.3 Explosibility

In discontinuous propagation the volatile fraction of the material will be the first part to take part in the combustion, therefore the percentage of volatiles in a material is

important to understanding its combustion behaviour (**Fig. 2.12** and **2.14**). However the mass of volatiles released by a material will depend heavily on the rate of heating it is subject to.

Comparing the total volatile yield for different heating rates Kobayashi et al. (1977) shows that altering this affects the species and amount of volatiles released from a given mass of solid material. Un-like coal however this percentage is less variable. "The amount of volatiles produced by burning woody biomass is high and usually varies between 76% and 86% of dry weight, depending on the raw material composition " (Van Loo, 2002). However this is the volatile yield from a TGA analysis at exceptionally low heating rates referenced to those found in explosions.

However in the literature (Ubhayakar et al., 1977, Cetin, 2004, Kobayashi et al., 1977) the "volatile" yield is highly dependent on the rate of heating used. The mass lost for lignite (Kobayashi et al., 1977) was recorded as 36% in the standard proximate analysis but yielded 65% mass loss in the highest heating rate tests. Thus it is likely that the volatile yields of biomass on a Dry Ash Free (DAF) basis (**Table 2.4**) are more likely to be around 95-100% for all biomasses given the TGA yield is 76- 86% (Van Loo, 2002).

A propagating flame front in an explosion is the highest heating rate that a dust particle can encounter. At a preheat zone thickness of 6-7mm (Han et al., 2000) and a turbulent burning velocity is around 0.44m/s the residence time is 13.6ms (0.006/0.44 = 0.0136), the temperature rise is then of the order of 2000K which produces a heating rate of 147,000k/s. Turbulent burning velocity of 0.625m/s were reported by (Sattar, 2012) and this gave a residence time of 9.6ms and a particle heating rate of 208,000 K/s, which is very hard to reproduce in any laboratory test. Cetin (2004) did some work at heating rates of 1×10^5 k/s which is the highest rate found (1.47- 2.1 times lower than predicted for real combustion here) but this is the only work to use this. The TGA analyser used in the present work for example has heating rates of 25K/min or 0.4K/s compared with 147000-208000K/s in a flame front. Thus the decomposition of a solid biomass particle in a flame front is likely to be quite different from that produced in the TGA.

Heating rate affects the volatile species released, producing more hydrogen and fewer hydrocarbons (as shown for tyres (Williams et al., 1990) and biomass (Corella, 1988, Commandré, 2011) when preformed in inert environments). Hydrogen has a much lower MEC equivalence ratio of 0.14Ø, as it has a critical

flame temperature that is lower than that of hydrocarbons (700K v 1500K). This may explain how biomass produces such low MEC results (**Table 2.7**). It is postulated that under the high heating rates in flame fronts, gasification reactions can take place inside biomass particles even though the particle is in an oxidizing atmosphere. This then results in the release of hydrogen and this controls the biomass flammability. The influence of particle size is then related to the much slower heating rates of larger particles as the thermal inertia is linked to the particle mass, which scales with the radius cubed. This could give a factor of 1000 reduction in the heating rates for a factor of 10 change in particle size. This could result in large particles releasing hydrocarbons under relatively slow heating and the fine particles releasing hydrogen under much faster heating rates. This type of behaviour would be very difficult to verify, but it does give a qualitative explanation of the present results. It is possible that for biomass particles the rapid heating in the flame front results in particle internal gasification and the release of hydrogen and CO, which gives the measured very lean and rich flammability limits seen for biomass.

2.3.0.1 Stoichiometric air to fuel and equivalence ratio for H and CH type gases

One of the core principles behind an explosion is the molar ratio of fuel to air which can also be described as the mass of fuel available to the mass of air. This relationship dictates the flame temperature, maximum pressure and the rate of pressure rise.

Consider the following reaction for hydrogen;

$2\ H_2 + O_2 = 2\ H_2O$

1 mole of hydrogen requires 1/2 mole of oxygen

1 mole of hydrogen requires 0.5 / .21 = 2.4 moles of air as Oxygen is only 21% of the volume of air. Therefore due to the universal gas law that dictates that all gaseous atoms occupy the same area per mole of material.

Stoichiometric A/F = 2.4/1 = 2.4

To turn this from a mole ratio to a volume percentage

Percent of hydrogen = [number of moles of fuel (hydrogen) / number of moles of reactant (air + fuel)] x 100

Percent hydrogen = [1/3.4] x 100 = 29.4%

The equivalence ratio is defined as what percentage of the Stoichiometric A/F is present in the mixture currently being described.

So let's say for 50% extra hydrogen,

$=(A/F_{stoich})/(A/F_{actual}) = 2.4/(2.4/1.5) = 1.5$

Therefore any value of ≥1 is a rich mixture and all ≤1 are lean.

If we move on to the next (simple) hydrocarbon up, methane with oxygen then it goes like this;

$CH_4 + 2O_2 = CO_2 + 2H_2O$

1 mole of methane requires 2 moles of oxygen

1 mole of methane requires 2/.21 = 9.52 moles of air

Stoichiometric A/F = 9.52/1 = 9.52

Percent of methane = (1/10.52) x 100

Percent of methane = 9.5%

Say for 20% extra methane,

Equivalence ratio $=(A/F_{stoich})/(A/F_{actual}) = 9.52/(9.52/1.2) = 9.52/7.93 = 1.2$

Similarly, the equivalence ratios can be found at the other concentrations and for other hydrocarbon gases, e.g.

$C_2H_2 + 1.5\ O_2 = CO_2 + H_2O$

$C_2H_6 + 3.5\ O_2 = 2CO_2 + 3H_2O$

$C_3H_8 + 5\ O_2 = 3CO_2 + 4H_2O$

2.3.0.2 Stoichiometric fuel to air and equivalence ratio for CHO type dust

However there is a further factor, in biomass there is oxygen bound into the material that will take part in the combustion. This oxygen then will not have to be sourced from the air, allowing the air to fuel ratio to be reduced below that of pure CH materials.

Consider a general formula CHO type dust = $C\alpha H_{\beta}O\gamma$.

This would normally be expressed in terms of H/C and O/C ratios. So, let

So, let the fraction of hydrogen in fuel = H/C = y

and the fraction of oxygen in fuel = O/C = z

The general combustion reaction can be written as;

$CH_yO_z + {}_aO_2 \rightarrow {}_bCO_2 + {}_cH_2O$

Applying

carbon balance; 1 = b

hydrogen balance; y = 2c

oxygen balance; z + 2a = 2b + c

a = [(2 + y/2) – z]/2

Thus, Oxygen/fuel by volume = [[2+y/2]-z]/2

Oxygen/fuel by mass = ([[2+y/2]-z]/2) x ([2 x 16]/[12 + y + 16z])

Air/fuel by mass = ([[2+y/2]-z]/2) x ([2 x 16]/[12 + y + 16z]) x 4.31

Air/fuel by mass = ([[2+y/4]-z/2] x 137.94) /]/[12 + y + 16z]

Dry ash free air/fuel by mass = ([[2+y/4]-z/2] x 137.94) /]/[12 + y + 16z] x [1/ (100 – (%Ash + % H_2O))

Stoichiometric fuel/air in g/m^3 =1200/(Air/fuel by mass). The 1200 is the actual density of air at a standard atmosphere and 21^{o}C).

Stoichiometric concentrations calculated from fuel compositions given in **Table 2.4** and **Table 2.7** (Wilén, 1999). An example as to how to calculate the theoretical A/F ratio and MEC is carried out below-

Table 2.7 Elemental composition of coal and biomass (Wilén, 1999).

dust sample	S %	C %	H %	N %
Wood	0.01	47.31	6.25	0.18
Bark	0.03	50.87	5.96	0.26
Forest Residue	0.05	49	6.24	0.81
Spanish Pine	0.01	47.35	6.43	0.1
Barley Straw	0.08	43.65	6.11	1.21
Miscanthus	0	46.01	6.21	0.43
Soghum	0.06	49.39	6.05	1.3
Rapeseed Straw	0.38	40.01	6.27	0.7
German Lignite	0.3	58.5	5.3	0.83
Spanish Lignite	2.3	43.71	5.16	0.7

For “wood” the air to fuel ratio is calculated by first normalising the chemical composition to carbon. To do this the elemental balance must be done first, so the O_2 % = (100 – (47.31+6.25+1.65+0.35+moisture+ash) = 44.4% (Harker, 1981). So 47.31% C, 6.25% H and 44.4% O becomes 0.4731/12 = 0.0394 C, 0.4625/16 = 0.02775 O and 0.0625/1 = 0.0625 H. Normalising to C gives C = 1 H = 1.59 O = 0.704 or $CH_{1.59}O_{0.704}$.

The air to fuel ratio is now calculated using A/F = [(1+ y/4)-z/2]137.94/(12+y+16z) where y and z are the ratios of hydrogen and oxygen to carbon respectively. So for “wood” A/F = [(1+ 1.59/4)- 0.704 /2]137.94/(12+1.59+16x0.704) = 142.147/25.34 = 5.61.

This is translated in to g/m^3 by 1200/(A/F) so for “wood” 1200/ 5.61 = 214 g/m^3. This has been done for all the materials in **Table 2.7** (Wilén, 1999) as well as adding in the MEC data. The measured MEC (g/m^3) was then compared to the calculated stoichiometric A/F then an (experimentally confirmed) value of MEC in stoichiometric equivalence ratio was found.

Table 2.8 MEC equivalence ratios for various materials, calculated from elemental and proximate analysis (Wilén, 1999).

Biomass	MEC	0/C	H/C	Stoich	Stoich	MEC	Mean Particle
	daf 1m^3	z	y	A/F	g/m^3	Ø	Size
						daf	µm
Wood	29.4	0.734	1.59	5.61	214	0.138	95
Bark	27.8	0.637	1.42	6.03	199	0.14	57
Forest Residue	55.3	0.672	1.53	4.78	251	0.22	102
Spanish Pine	83.1	0.729	1.63	5.69	211	0.394	247
Barley Straw	72.5	0.705	1.68	5.91	201	0.357	253
Miscanthus	110.4	0.771	1.62	5.42	221	0.498	143
Soghum	105.8	0.647	1.45	6.02	199	0.531	178
Rapeseed Straw	174.5	0.986	1.88	4.54	264	0.661	318
German Lignite	51.8	0.45	1.09	7.12	169	0.307	58
Spanish Lignite	59.6	0.826	1.42	4.88	246	0.242	40

The elemental composition gave a mean chemical composition of the biomass, this gave a stoichiometric air/fuel ratio by mass and this converts at ambient air conditions (density 1200 g/m^3) to a concentration. This concentration was used to determine the equivalence ratio by dividing the measured dust concentration at MEC by this stoichiometric concentration in g/m^3 units. This is the conventional definition of equivalence ratio for CH and HCO materials such as coal and it is not the equivalence ratio of the volatile fraction. The use of equivalence ratio is rare in dust explosion literature, so that the dust concentrations at the lean limit or the most

reactive mixture has never been given in equivalence ratio terms and hence it has not been appreciated how lean the MEC was for many HCO dusts was and how rich the most reactive mixture was (Andrews, 2010).

2.3.1 Minimum explosive concentration

Often called the Lower Explosive Limit (LEL), or Minimum Explosible Concentration (MEC) it is a measure of the minimum amount of a set material that will explode when dispersed in a set amount of air and ignited.

It is directly related to how easily a fuel particle releases its gaseous components (Eckhoff, 2003) as this is what determines the maximum distance between particles before the fuel is too scarce too propagate a flame. Without explosion protection operating at 25% of the MEC is quite a common requirement in the UK HSE guidance (Andrews, 2010), therefore the MEC must be accurately defined to abide by this.

The MEC for dusts should be measured to the same accuracy with the same definition of the lean limit as for gas/air explosions (Standard, 2003) and currently this is not the case. For gases the LEL has historically been defined as the lowest concentration at which an explosion can occur (Zabetakis, 1965., Lewis, 1938) and the same criteria has not been applied to dust MEC determination (Eckhoff, 2003). Here it was (till 2011) defined (in BSEN 14034-3:2006- Determination of explosion characteristics of dust clouds — Part 3: Determination of the lower explosion limit LEL of dust clouds) as the maximum concentration at which an explosion CANNOT occur (BSEN, 2011), in 2013 this was changed to the minimum concentration at which an explosion CAN occur (NFPA, 2013). If for example there is an explosion with >0.3 pressure rise at 60 g/m^3 and there is no explosion with >0.3 bar pressure rise at 30 g/m^3, then the MEC is 30 g/m^3 (BSEN, 2011) and there is no requirement to test intermediate concentrations and hence determine the actual MEC. While if there is an explosion with >0.3 pressure rise at 60 g/m^3 and there is no explosion with >0.3 bar pressure rise at 30 g/m^3, then the MEC is 60 g/m^3 (NFPA, 2013, BSi, 2012). In this work the MEC was defined as - the minimum concentration at which an explosion CAN occur. The reason for this decision is that NFPA 68 2013 and gas explosion data are done in the minimum concentration at which an explosion CAN occur so this way they can be related to each other.

Some of the MEC data in the literature was measured as the leanest mixture that DID propagate a flame (Wilén, 1999, Wong, 2013). Indeed the reference MEC data in the European standard (BSi, 2012) is for this definition of MEC, the leanest mixture that did propagate a flame (BSi, 2012). The major issue is that the definition differs depending on the standard used and very few literature sources reference this.

The value for the last ignition should be reported and the concentration gap that was tested with no ignition should be within 10% of the last flammable concentration. In equivalence ratio, Ø, terms hydrocarbon–air mixtures have a lean limit that is about Ø=0.5 and so the resolution of this limit should be to Ø<0.05. Most reported LEL for gases resolve the lean limit better than this and normally report to 0.01Ø. In dust concentration terms the <0.05Ø resolution for a pure hydrocarbon dust such as polyethylene is <4g/m^3 and for a cellulose or biomass type dust with a stoichiometric A/F ratio of 6/1 by mass (200 g/m^3) it would be a resolution of the MEC to <10 g/m^3.

The resolution for the determination of the MEC for dust is very coarse in the European dust explosion MEC standard (BSEN, 2011). The requirement is to test the dust air mixture with the following concentrations of dust: for <500 g/m^3 each successive concentration tested is 50% of the previous one and above 500 g/m^3 the concentration is increased in 250 g/m^3 increments. This means that for most dusts the only concentration tested in the near limit mixture region are 1000, 750, 500, 250, 125, 60 and 30g/m^3. This is why in tabulations of dust MEC there are so many dusts with MEC of 15, 30, 60 or 125 g/m^3, (Eckhoff, 2003).

This data can be used to tailor prevention methods (housekeeping, operating below MEC, etc.) to the combustible dust that is likely to be involved in the explosion. **Table 2.8** shows that for finely ground wood, bark and forest residue, where the mean average particle size was 57 – 102µm the MEC was Ø = 0.14 – 0.22, this is much leaner than for any hydrocarbon/air mixture (excluding H_2).

Coarser particles produced deterioration in the lean limit but even Spanish Pine and Barley straw with mean particle sizes of 250µm have MEC's leaner than for gaseous hydrocarbons of 0.394Ø and 0.357Ø respectively (**Table 2.8**).

More results from various sources were collected and have been added to support the previous calculations from **Table 2.8** and display the same sub 0.5Ø MEC values for CHO vs CH materials (**Table 2.9**).

Table 2.9 Collection of CHO, CH and coal dust MEC data.

Material CH_yO_z	y=H/C	z=O/C	Ø=1 A/F	Ø=1 g/m^3	MEC g/m^3	MEC Ref.	$Ø_{MEC}$
Cellulose	1.67	0.833	5.12	234	55 60	Maisey Eckhoff	0.235 0.256
Poly-Methyl Acrylate (PMA)	1.50	0.50	7.27	165	30	Eckhoff	0.182
Poly-Methyl-Meth-Acrylate PMMA	1.60	0.40	8.28	145	30	Maisey	0.207
polyethylene	2.0	0	14.8	81	30	Maisey Eckhoff	0.37
polypropylene	2.0	0	14.8	81	35	Maisey	0.43
Polyethylene terephthalate (PET)	0.8	0.4	7.18	167	40	Maisey	0.24
Polyvinyl acetate	1.5	0.5	7.22	166	40	Maisey	0.24
Pine Pitch (Tillman)	1.46	0.416	8.09	148	30-60	Eckhoff	~0.3
Spruce (Tillman)	3.58	1.55	3.83	313	20-70	Field	~0.14
Carbon	0	0	11.5	104	60	NFPA Eckhoff	0.55
Bituminous Coal	0.78	0.073	12.7daf	94.5daf	55	Maisey	0.58

MEC data from Wong (2013) shows MEC for large particle mixtures as high as >5000 g/m^3, if approximately 200 g/m^3 is assumed to be stoichiometric then this is >25 Ø which is ridiculously high.

This MEC data was sorted by moisture content and then plotted against average particle size (**Fig. 2.13**). To see how well the MEC correlated with average particle size.

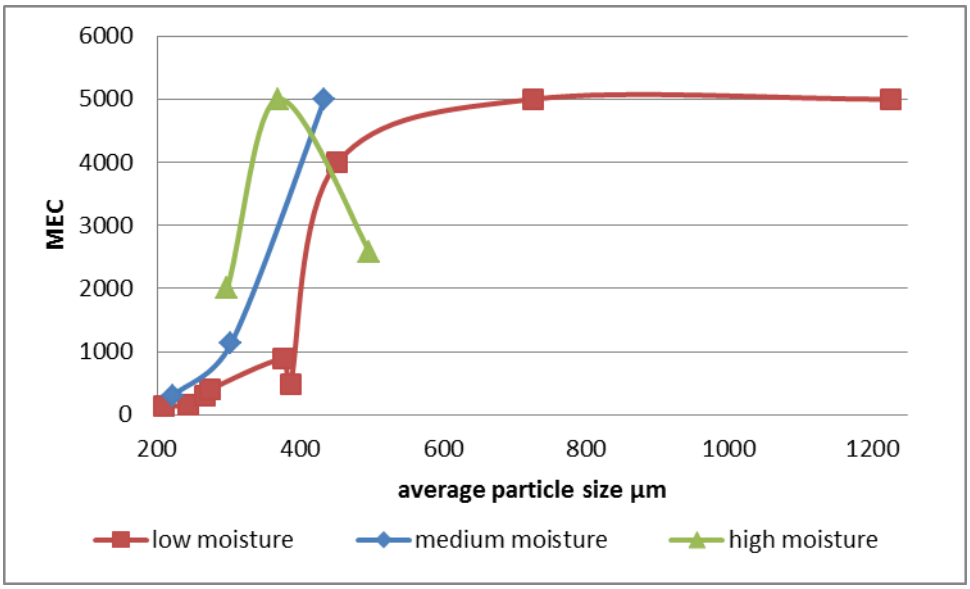

Fig 2.13 MEC against average particle size for a large number of biomass samples (Wong, 2013).

However these calculations are ideal, all the combustible material burns, vaporises and disperses perfectly. However as mentioned for dusts most materials appear to produce experimental data with massive variation as shown in **Table 2.9**.

This wide variation of data is due the MEC being a function of particle size (**Fig. 2.13**, **Table 2.10**) and other factors including (as shown later in section 2.3.11) the apparatus used and volatile component of the fuel.

It has been proposed that the volatile content of a material, being the most easily liberated part should be the only part considered when evaluating a likely MEC for a material (Eckhoff, 2003).

Table 2.10 MEC shown to be dependent on the particle size for coal (Cashdollar, 1996).

Table 3 Size analyses and explosibility data of Pocahontas low volatile coal

	Poc-1 −120M	Poc-2 1/78	Poc-3 3/88-4	Poc-4 6/80	Poc-5 3/88-2,3	Poc-6 2/88-1	Poc-7 fines
$< 20\ \mu m$ (%)	10	27	38	40	46	67	83
$< 75\ \mu m$ (%)	~75	65	75	86	86	94	100
$\bar{D}_g$ (μm)	~48	39	32	26	24	15	11
σ_g	1.9	3.0	3.2	2.6	2.8	2.4	1.9
$\bar{D}_{med}$ (μm)	~52	47	30	27	22	14	10
$\bar{D}_w$ (μm)	~58	63	60	41	40	23	13
$\bar{D}_s$ (μm)	39	19	18	17	15	11	9
$\bar{D}_s(\%T)$ (μm) @ 100–200 g m^{-3}	17–34	9–14	—	6–10	—	—	—
$\bar{D}_s(\%T)$ (μm) @ 300–600 g m^{-3}	20–40	14–27	—	—	—	—	—
MEC (g m^{-3})	120	130	~100	~90	80	80	~80
P_{max} (bar)	6.0	~6.3	—	6.3	6.2	6.5	6.5
$(dP/dt)V^{1/3}$ (bar m s^{-1})	17	~16	—	~26	—	34	31
Amount of rock dust to inert (%)	60	64	76	78	77	82	83

Dashes indicate that no data were available.

Taking the average volatile content of ”wood” as 70-80% (Wilén, 1999) (from the TGA) this means that the MEC stated should actually be 0.138 *.7 = 0.094Ø or 20.7g/m^3 using the volatile theory (and this value of MEC). This value is far leaner than all gasses including Hydrogen burn. This suggests that more than just the TGA volatile yield are burning, supporting the work of (Ubhayakar et al., 1977, Cetin, 2004, Kobayashi et al., 1977) that TGA volatile yields are unsuitable for use in explosion/combustion situations. However even assuming a 100% volatile yield, MEC values of 0.138Ø suggest that unless this is pure H_2 volatiles this value appears ridiculously low and needs more consideration (vessel used, comparison to other data, etc.).

For coal the volatile model does work qualitatively and quantitatively. If only the HC volatiles (mass from TGA) burn, (30% by mass) then the lean limit should be about 200 - 280g/m^3 ((120/2)/0.3) to ((170/2)/0.3), which is not the case for the standard Pittsburgh pulverized coal where the MEC’s are about 80-90 g/m^3 (Cashdollar, 1996, Jensen, 1994, Chawla et al., 1996). However Cashdollar (1996) (**Table 2.10**) indicated that the MEC of coal is linked to its fine particle concentration (possibly excluding mass in large particles) and (Kobayashi et al., 1977) demonstrated that at real heating rates coal has a volatile content of 60-65% not 30% as the TGA suggests. This was supported by Lewellen (1977) work on cellulose which predicts nearly 100% devolatilization in a flame front.

Lignite is 60% volatiles (Kobayashi et al., 1977) so if elemental Ø = 246 and 169 then the mass needed to create Ø with only volatiles would be (German Lignite)

169/0.6 = 281 g/m^3 and (Spanish Lignite) 246/.6 = 415 g/m^3 which is approximately the concentration where the maximum reactivity is found for coal (Sattar, 2012, Huescar et al., 2012b) indicating that this is correct. As stated the measured MEC's are about 80-90 g/m^3 (MEC = 0.645 - 0.72) (80/120 to 90/120) which is what it should be if only volatiles were combusting (0.72*0.65= 0.468Ø, very near the MEC of methane). This indicates that the MEC appears to be controlled by the volatile material percentage, which is not that given by the TGA.

Figure 2.14 is taken from (Eckhoff, 2003) to prove the volatile model for coal, which is supported by (Jensen, 1994) "Research has shown that volatile content is the most significant variable in determining coal dust explosibility." However if only the coal points (**Fig. 2.14**) are viewed there is not a great fit, as the line seems to more closely follow the polyethylene-graphite points than any other. This may be as the volatile mass is directly from the TGA and therefore is lower (additionally at higher heating rates some coals may release more volatiles from char reactions meaning this would not be a uniform loss across the samples).

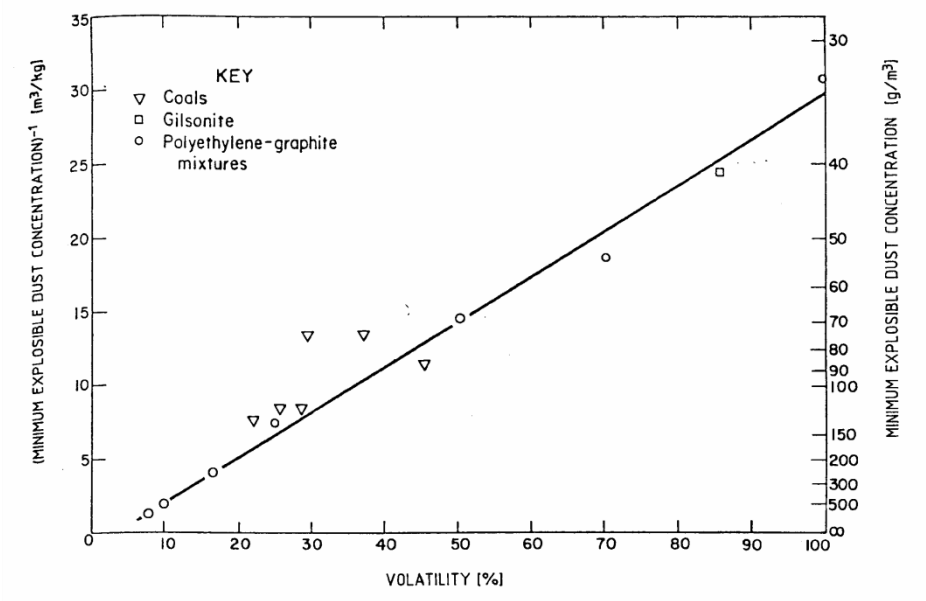

Fig 2.14 Volatile content against MEC (Eckhoff, 2003).

Using the European Standard (2003) method (method T) methane and n-hexane have a lean limit of 0.47Ø (0.53Ø method B), for propane it is 0.43Ø (0.55Ø method B) and for ethylene it is 0.38Ø (0.48Ø method B). Polypropylene has a lean limit of 0.43Ø (0.54Ø method B) which is the same as that for gaseous propane, indicating possible pyrolysis of the dust in the flame front to yield propane. Similarly,

polyethylene dust has a lean limit of 0.37Ø (0.43Ø method B) which is very close to the value for gaseous ethylene of 0.38Ø. Thus for pure hydrocarbon dusts the model that the flame propagates as a gaseous hydrocarbon (with 100% volatile content) appears to be valid.

For CHO materials however CO, and H_2 are the main gas species produced (Commandré, 2011) with higher heating rates promoting the production of H_2 over CO. At pyrolysis temperatures of 950^{o}C the molar ratio of H_2/CO is close to 0.4 therefore H_2 + 4CO = A/F = 2.5 and calculated MEC = 0.258Ø. In this research Commandré (2011) also noted that the ratio H_2/CO increased markedly with temperature, (also noted by Corella (1988)) suggesting that this could be even higher in actual flame fronts, resulting in a gaseous mixture at the flame front with an MEC <0. 258Ø. Values in this range are found repeatedly in the literature (**Table 2.9**).

Observations have been made (for certain dusts) that for extremely fine particles the MEC appears to increase, this may be caused by the fineness of the particles increasing the absorbed energy below the critical flame temperature or particle agglomeration due to static.

2.3.2 Maximum explosive concentration

Often called the Upper Explosive Limit (UEL) is a measure of the maximum amount of a set material that will explode when dispersed in a given amount of air and ignited. It is thought to be directly related to how much of and how easily a fuel particle releases its gaseous components as this is what determines the minimum distance between particles before oxygen is too scarce to propagate a flame. This is of interest as industry often assumes that dust has the same flammability limits as gaseous fuel. A good example of this is in burners, where the fuel is pneumatically moved to the burner with 1/5 of the combustion air, this concentration isn't flammable in gaseous fuel mixtures but appears to be for dusts.

Here oxygen availability and the rate of volatile release are the limiting factors. However in practice the rich limit only appears to apply to gasses as dust mixtures burn even at equivalence ratios of 25+ (Wong, 2013) as was calculated earlier. Deguingand and Galant (1981) reported encountering no rich limit for coal at a stoichiometric concentration of 30 for 2 samples with particle sizes 13µm and

50µm. While Cashdollar (1996) reported encountering no rich limit for coal or polyethylene dust up to 4500g/m^3 (equivalence ratio 15 - 22).

The flammability limits for gasses with varying length C chains (only the alkanes) were plotted (**Fig. 2.15**) (Jechura, 1987) as ((UFL (volume concentration) /stoichiometric (volume concentration)) x 100), to show the widening in the rich limits with increasing chain length. At this point the reason for this is currently unknown. However it is thought that the long chain hydrocarbons result in localised rich burning around these molecules therefore producing high soot yields trapping a large amount of the combustible carbon in the solid phase, effectively lowering the fuel concentration.

It is possible that due to the increasing chain length some of the added carbon content is not fully combusting (insufficient oxygen therefore soot formation or char formation), that would give the impression of an extended rich limit while keeping the LFL constant as is seen for these fuels. The only exception to this is hydrogen, carbon monoxide and methanol which have wider UFL and LFL than other hydrocarbon materials tested.

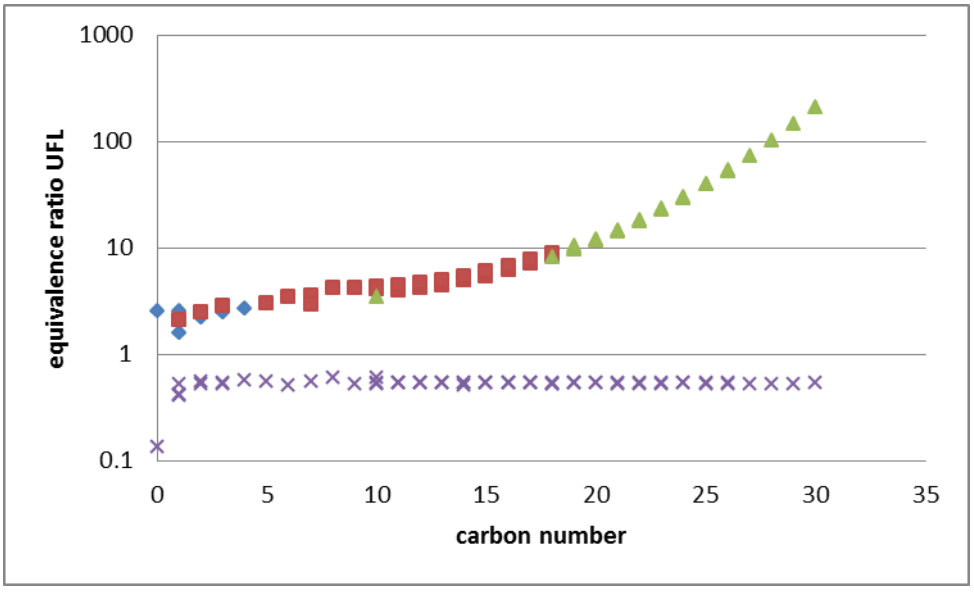

Fig 2.15 UFL and LFL for gasses as a function of carbon number, gasses - blue, liquids - red, solids - green (Jechura, 1987).

As has been mentioned for dust there is no evidence of any UFL. This could be due to some unknown mechanism of flame propagation, however it appears more likely that a portion of the fuel (Carbon backbone) is unable to mix with sufficient oxygen

to fully combust therefore, allowing the oxygen to be utilised by other fuel molecules, stretching the rich limit.

This combined with the step change seen in the MEC in **Figure 2.13** at an average particle size of 400µm may indicate that the dust is undergoing a change from thermally thin to thermally thick at this point, hence the massive increase in MEC. This would combine with the fact that as the particles get bigger the locally rich zone that would be created by their complete devolatilization has increased in size. Therefore it may be that the lack of a rich limit for dusts is due to a stratified gaseous mixture with the rich zones taking the place of the particles as was suggested by Burgoyne and Cohen (1954). When the particle size increases above this thermally thick/thin size boundary the whole particle no longer vaporises, therefore trapping a large quantity of the solid fuel in the solid phase and excluding it from the reaction and pushing the MEC up dramatically.

2.3.3 Maximum pressure and K_{ST} generation

So in a constant volume system an explosion is easiest to understand in terms of the ideal gas law:

$$PV = nRT = \frac{m}{M}RT \quad (8)$$

Where P is the absolute pressure, V is the volume and T is the absolute temperature. The constants are the number of moles, *n*, and the universal gas constant, *R*.

For a “normal dust explosion”, air is the most common oxidant. Because air is mostly made up of nitrogen that doesn’t take part in the combustion, there is little change in the total number of moles of gaseous materiel during combustion. Therefore an explosion or rapid combustion reaction in a constant volume system can be assumed to result in:

$$\frac{P_{max}}{P_o} = \frac{T_b}{T_o} \quad (9)$$

Where P_{max} is the maximum absolute explosion pressure, P_o is the initial absolute pressure, T_b is the absolute temperature of the burned gas and T_o is the initial absolute temperature.

The faster the explosion propagates, the more adiabatic the flame front will be, and so the closer the actual maximum explosion pressure will be to the ideal maximum pressure. This is due to there being less time for heat losses to occur as the faster the reaction is the less likely it is that the flame front will touch the wall before all the mixture is burnt.

For the ideal case, absolute pressure as a function of time, P(t), in a constant volume, spherical explosion is related to the fraction of mass burnt in the fireball during the time taken for propagation- t, as follows:

$$\frac{P(t)-P_o}{P_{max}-P_o} = \frac{M(t)}{M_o} \quad (10)$$

Where M_o is the initial mass and $M(t)$is the mass burnt at time (t).

For spherical propagation from a point source:

$$\frac{M(t)}{M_o} = \left[\frac{r(t)}{r_o}\right]^3 = \left[\frac{Ss}{r_o}\right]^3 \quad (11)$$

Where r(t) is the radius of the flame front, r_0 is the chamber radius, and S_s is the flame speed given by:

$$S_s = \frac{dr(t)}{dt} = \left(\frac{\rho_u}{\rho_f}\right) S_u \quad (12)$$

Where $\left(\frac{\rho_u}{\rho_f}\right)$ is the density ratio of unburned to burned gases at constant pressure. The burning velocity, S_u, is the rate of flame propagation relative to the unburned gas ahead of it and is assumed to remain constant throughout the whole of the propagation. The flame speed, S_s, is relative to a fixed reference point.

The pressure rise in a closed vessel is a linear function of the proportion of the initial mass of fuel that has been burnt. In a spherical vessel, consider the situation when the flame, diameter D_f, has propagated half way across the vessel diameter, D.

Mass burnt / Initial Mass = $(D_f/D)^3 \left(\frac{\rho_u}{\rho_f}\right)$ (13)

Where ρ_u is the un-burnt gas density and ρ_b is the burnt gas density. This density ratio is inversely proportional to the temperature ratio. For lean hydrocarbon type mixtures Ø<1 the flame temperature is about 1500K for a 300K inlet temperature therefore the ratio is ~5. Therefore the density ratio is ~ 1/5. As stated D_f/D=0.5. So at this point only .125 x 1/5=0.025 or 2.5% of the initial mass has been burnt. For stoichiometric Ø=1 the temperature increases to 2100K so the density ratio is ~1/7 so this 0.125 x 1/7=0.017 or ~2% of the initial mass has been burnt. Therefore in a spherical vessel explosion there is little pressure rise in the first half of the flame travel distance and 98% of the total adiabatic pressure rise, occurs in the last half of the flame travel.

The peak pressure is influenced by the constant volume flame temperature. GasEq calculation of the adiabatic flame temperature shows higher flame temperatures under constant volume conditions than at constant pressure. This is important as flame speeds are measured in the 1m^3 vessel in the constant pressure period of flame propagation and hence the conversion from flame speed to burning velocity should use the constant pressure expansion ratio. The constant volume flame temperature is higher than that at constant pressure, which is due to the differences in specific heats at constant volume and constant pressure due to work done.

K_{st} is the (vessel) size normalized maximum rate of pressure rise. As it is size normalized, it allows for calculation for any vessel geometry, K_{st} is used in the design of explosion venting safety systems (NFPA, 1998). This is true for conditions where the vessel size is large compared with either the dust flame thickness or the igniters flame volume, this is true in the 1 m^3 ISO vessel, and the Leeds explosion vessel

As shown in section 2.2.2 -

$$K_{st} = \left[\frac{dP}{dt}\right]_{max} V_o^{1/3}$$

The units of which are meters per second (m/s) in this dimensionless pressure formulation, but bar m/s is more usually used.

K_{st} is the rate of pressure rise created by combustion. Therefore the K_{st} is related to the flame speed, and the higher the K_{st} the higher the corresponding flame speed should be. The maximum K_{st} normally occurs for a higher dust concentration than the P_{max}. However both occur for very high dust concentrations (relative to gasses),

typically between- 0.5 - 1 kg/m^3, which is a very rich mixture. For most standard CH dusts it has been proven that Ø=1 is around 80 g/m^3. P_{max} and $\left[\frac{dP}{dt}\right]_{max}$ occur at concentrations equal to or greater than 500 g/m^3 or ≥ Ø=6. At this point CH gasses are not flammable at this level of richness as shown by methane (**Fig. 1.4**).

The same is also true for metal dusts. For the magnesium dust the dusts actual stoichiometric concentration is 417 gm^{-3}. Magnesium, dust behaves the same as most other dusts including CH dusts with the maximum pressure rise occurring very rich, 3.5 times the stoichiometric concentration (**Fig. 2.16**) (Li et al., 2009). This would seem to indicate that the phenomenon of very rich mixtures producing peak reactivity is a factor of solid particle dust combustion rather than a feature of any type of dust.

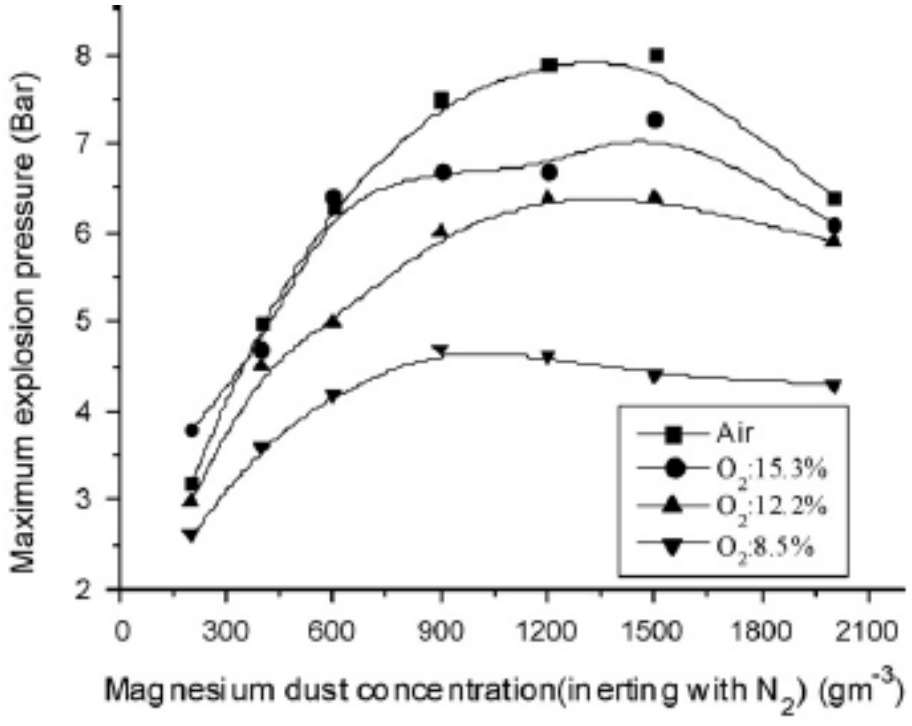

Fig 2.16 Pressure rise and flammability limits of magnesium dust

Figure 2.17 (BSEN, 2004) shows the general trend in dusts for high Ø for maximum Pressure (although no drop in pressure after the maximum is seen as is seen here), and how the value of $\left[\frac{dP}{dt}\right]_{max}$ is found from this. It also shows the general concentration around which the maximum pressure rise and maximum rate of pressure rise is found (750 g/m^3) for most fine dusts. Which would be 854g in the Leeds 1.138 m^3 vessel.

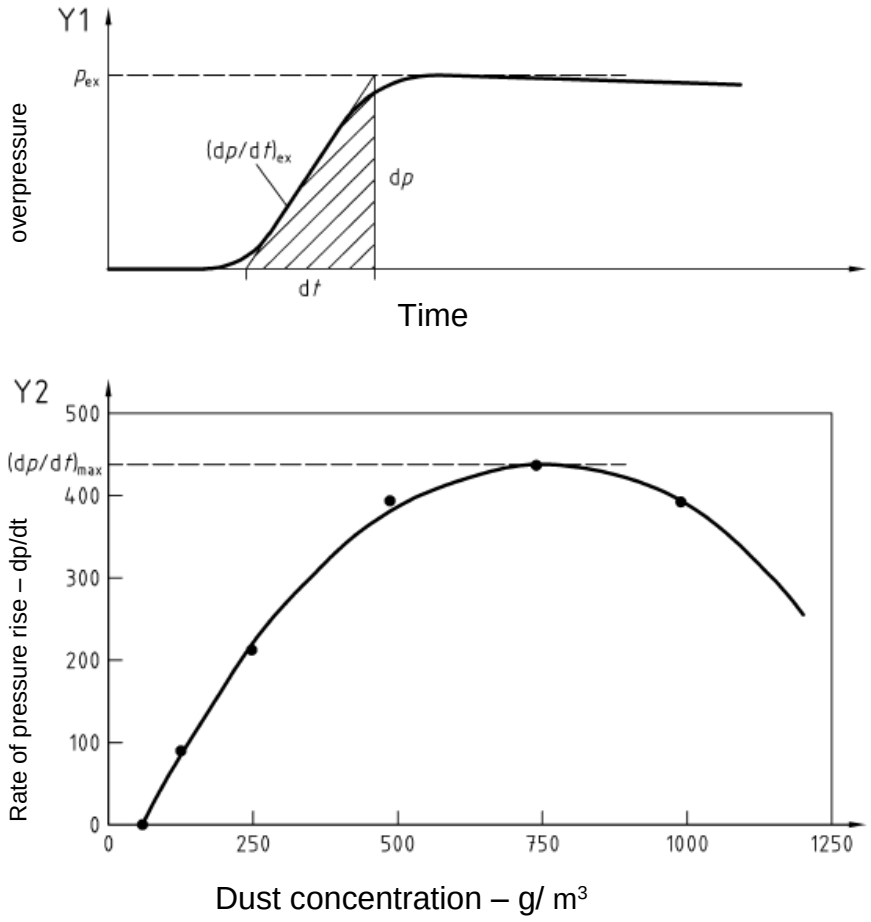

Fig 2.17 Rate of pressure rise against concentration for general dust. (BSEN, 2004)

For gas explosions the test is carried out with a laminar mixture and there is no injection turbulence. Hence, the rate of pressure rise for gasses (K_G) can be considered a fundamental property of the fuel, if the $\left[\frac{dP}{dt}\right]_{max}$ is determined in a spherical vessel with no flame contact with the walls until the end of the explosion so that adiabatic flame propagation occurs.

The K_{st} parameter however has to be empirical as it is a turbulent explosion for dusts and the turbulence level and distribution is determined by the test method and is not a property of the dust. Therefore it was decided to use the actual measurements of Pmax/Pi as the expansion factor for dusts as this was the procedure recommended in the literature (Zabetakis, 1965., Cashdollar, 2000).

So, as the 1m^3 ISO test vessel has a fixed turbulence level under standard operating conditions the K_{st} could by described as β times the equivalent laminar K_G. The laminar burning velocity of a dust is S_{uL} therefore the turbulent burning velocity is S_u, where β is the turbulence intensity.

$S_u = \beta S_{uL}$ (14)

where β is the increase in the reactivity of the same mixture due to turbulence. It is now possible to derive an approximate relationship between K_{st} and the corresponding laminar burning velocities as shown in equation 7 by adding in β as has been done in equation 15 for laminar K_{st}.

$$K_{stl} = \beta \left[\frac{dP}{dt}\right]_{max} \times V_o^{1/3} = \beta 3.16(P_m/P_i - 1)S_{ul}E_p \quad (15)$$

2.3.4 Flame speed and burning velocity

The flame speed is a function of the burning velocity which is an intrinsic measure of the reactivity of a material as it dictates the rate of energy release from the fuel.

One of the assumptions in section 2.3.3 is that S_u does not vary throughout the explosion propagation. However this is not a valid assumption as, as the explosion progresses the pressure and temperature in the un-burnt gases ahead of the flame front change, therefore altering the S_u. However, as will be shown this is a small effect, an approximate 20% increase in S_u at the end of the deflagration. It is know that as the un-burnt gas ahead of the flame is compressed the pressure and temperature rise and both of these factors influence the laminar burning velocity. The pressure and temperature dependence on burning velocity for hydrocarbon/air mixtures are in opposite directions and the net effect is a 20% increase in S_u over the period of the deflagration. However it is not a large amount and the assumption of constant S_u is an acceptable approximation for the purpose of K_{st} results. **Figure 2.18** shows the influence of increasing P and T on the S_u (Bradley and Mitcheson, 1976).

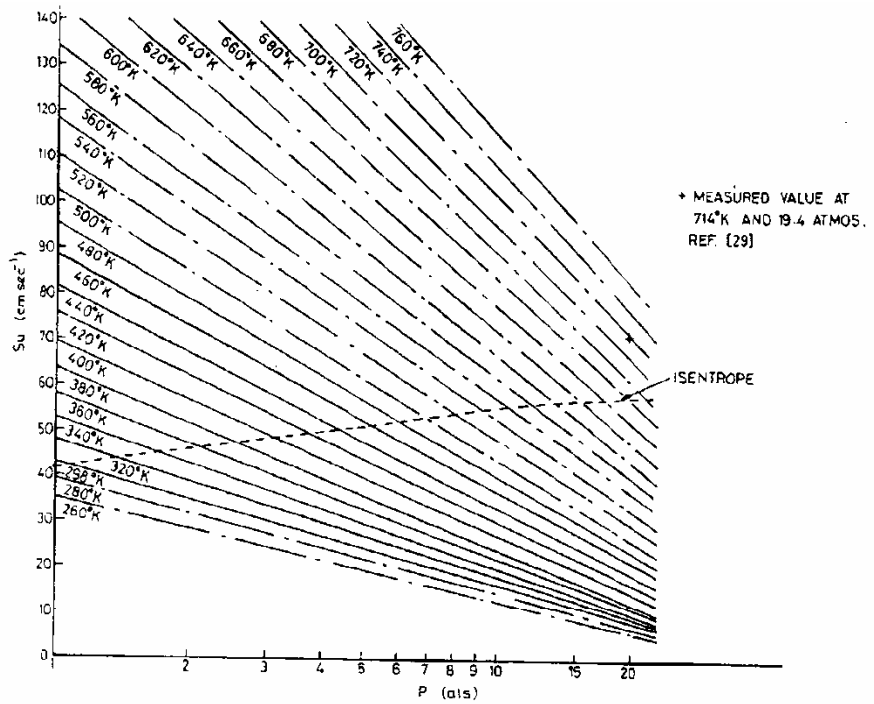

Fig. 2. Burning velocity of 9.5% CH_4—air mixture at different temperatures and pressures.

Fig 2.18 Burning velocity at different temperatures and pressures (Bradley and Mitcheson, 1976).

Flame speed can also be increased by turbulence as will be explained in the next section; this is represented in equation 14.

2.3.5 Turbulence and turbulent burning velocities in dusts

As has been shown turbulence increases both flame speed, K_{st} and P_{max} (due to less time for heat loss to the vessel in the case of P_{max}) in proportion to its intensity, but what is turbulence? It is recognized that the state of a dust cloud just prior to ignition has a strong influence on the ease of ignition and speed at which the flame front propagates through the mixture. This is due to a number of factors affecting the dust and its combustion characteristics- the dust concentration, dispersion and turbulence level.

So what is turbulence in the context of flame propagation and dust explosions? In some instances the main turbulence mechanism is the movement of burning particles relevant to un-burnt ones. So, in this situation where combustion is mainly taking place on or close to the particle surface the particles movements and interactions are in fact in a more fitting measure of turbulence than any movement of the gas around the particles. However this depends on the burning

characteristics of the dust being used. Very fast de-volatilization, resulting in combustion taking place largely as gas combustion, is an extreme case, yet here the gas movement is the more appropriate measure of turbulence.

However most dusts exhibit characteristics of both as CH gasses are devolatilised and propagate the flame front. Yet the particles themselves also partake in the deflagration and raise the pressure through combustion, but also contribute ash that acts as an inert. So for most dusts it is considered best to use the standard method of defining and measuring turbulence as the movement of the gas phase as this is predominant.

There are different circumstances in which turbulence can occur, that caused before and after ignition. Pre-ignition turbulence is created by the air blast that dispersed the dust, lifting it off the surface it was on and creating a dust suspension, while post-ignition turbulence is created by objects in the path of the flame front or by sudden expansion/release of gases, as found during venting of an explosion.

When, as in this case, comparing maximum pressure and K_{st} in a closed vessel, only the pre-ignition turbulence is considered. However the thermocouple array in this $1m^3$ vessel may actually produce some post ignition turbulence by obstruction of the flame front, therefore causing self-acceleration of the flame front. However as there is currently no way around this or of quantifying it, this will be added to the pre ignition turbulence value as it should be nearly constant.

Turbulent flows, once created are always losing energy, so when no further input energy is provided the turbulence decays rapidly, within a couple of seconds in the $1m^3$ vessel. In decaying turbulence, as is found in the $1m^3$ vessel, the large scale eddies die away first as there is no energy to sustain them now the injection has finished. The smaller eddies, therefore, decay away after this as the energy from the large scale eddies is no longer coming in to sustain them. So as can be seen during decaying turbulent flow field, the entire series of eddy sizes changes continuously.

Turbulence is usually defined by a number of components, the most essential of which, are as follows-

- The diffusivity of the turbulence or length scale - This is the mixing of material by turbulent eddies that increase transfer of heat, mass and momentum.

The length scale or mixing of the turbulence increases slowly during turbulent decay.

- The intensity - Turbulence is a trait of the fluid flow itself, not the fluid and is regarded as a strong three-dimensional velocity. Mechanical energy is absorbed from the main turbulent flow by large eddies, these transfer their energy to smaller scale eddies. These then, lose their energy to their surroundings by collapsing, dissipating their energy over large areas. The intensity or strength decreases rapidly during turbulent decay, therefore the turbulent decay pattern can be described as not linear but logarithmic decay. In conflagrations a reduction in turbulent intensity produces a proportional decrease in the burning velocity found. This reduction is brought about by less mass and heat transfer by the turbulence. When eddies that are large by comparison to the flame thickness are met by the flame front, they tend to wrinkle or fold it. These folds increase the area of the flame front, which, in turn raises the burning velocity. Eddies smaller than the flame thickness increase the rates of heat and mass transfer within the flame front itself but only slightly, so are normally ignored. Increasing the burning velocity therefore increases both values of K_{st} and P_{max} correspondingly for the reasons discussed earlier. This effect is shown well on the graphs (**Fig. 2.19**) (Phylaktou, 2001).

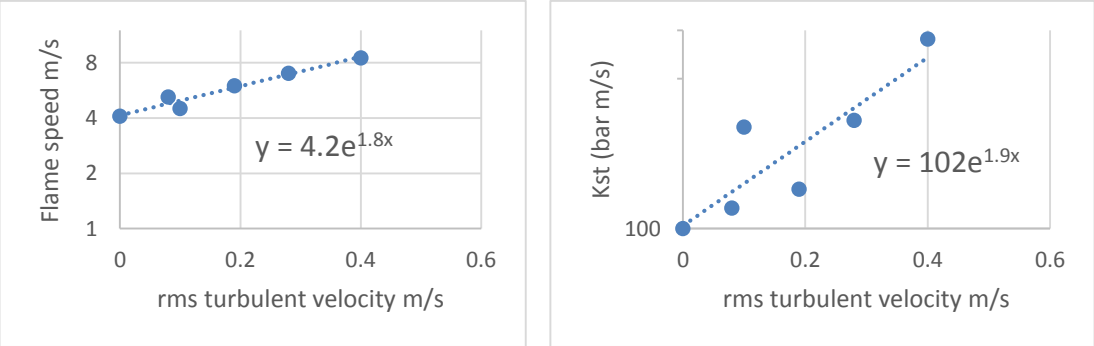

Fig 2.19 Flame speed and K_{st} as a function of turbulent velocity (Phylaktou, 2001).

The turbulence or β value for the Leeds 1m^3 ISO vessel was found by combusting propane at laminar and turbulent (without and with injection of air through C-ring) conditions and then the magnitude of the increase in the Kst value is the value of β, this was found to be 4.03 for the C-ring injector.

2.3.6 Laminar burning velocity for dusts

The laminar burning velocity, S_{SL} of a material is a primary measure of the rate of flame propagation which defines the reactivity of a mixture. This is difficult enough to measure for dusts but as yet no standard method of measurement for gases has even been agreed upon. However it is known, as was shown in section 2.2.2, that $S_S = \beta S_{SL}$, where β is the increase in the reactivity due to the turbulence – $\beta = S_S/S_{SL}$. β = 4.03 is the order of magnitude of the turbulence factor in the $1m^3$ dust tests.

The vessel has in the past been used to attempt to measure the S_{SL} by using a long ignition delay to try to generate laminar conditions. However, it has the problem that during the long ignition delay to get laminar conditions the dust falls out of suspension due to gravity and therefore the mass burnt is less than that injected by the time the ignition occurs. Consequently any result achieved would be for leaner mixtures than intended. This reduces the total energy release due to the fall out of larger dust particles from suspension and therefore gives a lower pressure rise (**Fig. 2.20**) (Phylaktou, 2010).

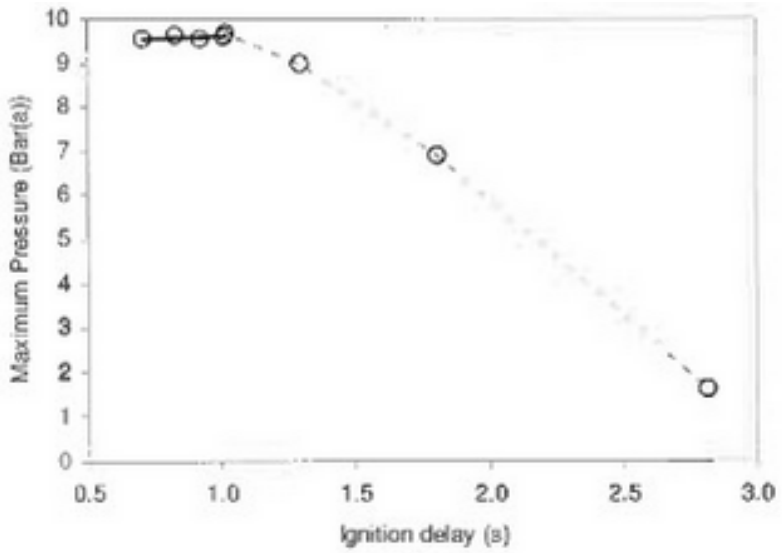

Fig 2.20 Pressure rise for material against ignition delay for dust (Phylaktou, 2010).

The problems with the arbitrary turbulence involved in the $1m^3$ ISO standard dust explosion test vessel has led to investigating other methods to measure the laminar dust explosion flame speeds and burning velocities. To get a laminar dust cloud

most investigators have used various versions of the vertical tube equipment with the dust shaken from the top and free falling under gravity. The bottom end of the tube is normally open and the top closed; with ignition at the bottom so that burnt gases flow out of the tube at the bottom and there is no pressure rise. The flame speed is then measured using high speed video or by optical/thermal probe sensors and the burning velocity calculated from this. The assumptions made for this method are as follows:

- Burnt gases free to exit the tube, no burnt gas expansion to induce an un-burnt gas velocity ahead of the flame.

- No heat losses to the walls.

- Hemispherical flame area – A_f (or the flame area is determined from photography)

- No buoyancy effect on the flame.

The method can be improved by measuring the actual flame area, but the best method is to directly measure the flame speed and un-burnt gas velocity on the centreline of the flame, well removed from the wall heat sink. This method uses tracking of the dust particles with high speed photography to determine the gas velocity ahead of the flame. This is called the ‘direct’ method. Unfortunately the assumption of a no burnt gas expansion induced in the un-burnt gas velocity ahead of the flame is not valid, mainly due to the fact that most of this force is buoyant flow and, as such, is unable to be vented in a downwards direction.

In the tube technique with free falling dust, it is more difficult to control the dust concentration and an internal light obscuration detector is often used to determine the dust concentration. Also the dust concentration often has a gradient from top to bottom. This is the problem of having no turbulence to inject, disperse and mix the dust.

As has been shown there is no current method for measuring S_{SL} for a dust. As such the only option is to derive a value through calculation.

$$K_{st} = \beta\ 3.16(P_{max}/P_o - 1)S_{SL}\ E$$

Where $\mathrm{E} = \left(\frac{\rho_u}{\rho_f}\right)$ = 5 - 8, β = 4.03 (for the 5L pot with C-ring), K_{st}, P_{max} and P_o will be found through experimentation.

2.3.7 Particle size

Although ISO standards states to only to test <63µm particles it has been shown that particles bigger than this will ignite and propagate an explosion (**Fig. 2.13** and **Table 2.9**).

Finer particle size dusts are likely to react quicker than larger particle sizes of the same material due to larger surface area/volume ratio. Also a particles' shape and porosity can have a great effect on the overall particle surface area and correspondingly the reaction rate. Therefore, a particles size and shape are very important to its dusts explosion characteristics. A common definition of what is a dust is defined as a material with particles of ≤420µm. NFPA 654 defined combustible dust as a "finely divided solid material ≤420µm in diameter that presents a fire or explosion hazard when dispersed and ignited in air" (NFPA, 2012). OSHA used this definition in earlier combustible dust guidance, such as its 2005 safety and health information bulletin. Some NFPA standards still use a size criterion in defining combustible dust, such as NFPA 61 (2013) and NFPA 704 (2012). Other NFPA standards, however, have changed their combustible dust definition to remove the size criterion, but discuss size in their explanatory notes. In general the notes concerning particle size state that dusts of combustible material with a particle size of ≤420µm can be presumed to be combustible. However, certain particles, such as fibres, flakes, and agglomerations of smaller particles, may have dimensions >420µm but still have a surface-area : volume ratio sufficient to pose a deflagration hazard. In the most recent revisions, the explanatory notes in many of the NFPA standards have moved from a <420µm to <500µm size threshold. These include NFPA 484 (2013), NFPA 654 (2013), NFPA 664 (2012) and FM Global Data Sheet 7-76 (2013).

It is the high surface area/volume ratio dust particles that heat up fastest to release volatiles, therefore reacting faster and releasing more (of their potential energy) energy than the larger particles. The finer dust particles are also more easily dispersed in air and remain airborne longer due to the added drag created by their large surface areas and low weights, just mentioning particle size is a simplification

of the actual situation. Particle shape and surface structure are also important parameters that must be considered together with the particle size distribution.

The influence of these parameters can explain why sometimes a powder with a larger (median) particle size can produce a higher explosion severity and/or higher ignition sensitivity than an apparently finer dust. However, no simple correlations exist to allow for all these parameters.

There are currently many problems comparing results from different dusts due to there rarely being any mention by the authors of particle shape/size used or distribution of the sizes present within the sample. This is clearly demonstrated by **Table 2.11**, the differences between the values of biomass materials given in each is believed to be the result of different particle sizes being used. The larger the surface area of the material per unit mass the more reactive the material becomes due to larger area for reactions to take place upon. **Table 2.11** clearly shows that the pre-established trend of higher K_{st}'s for smaller particle sizes is true here (Wong, 2013).

Table 2.11 MEC as a function of particle size

Dust Source	Sawmill Sample Location	Moisture Content (% wet basis)	Average Particle Size (µm)	P_{max} (bar)	$(dP/dt)_{max}$ (bar/s)	K_{st} (bar * m /s)	MIE (mJ)	MIT-Cloud (°C)	MEC (g/m^3)
MPB	Under belt return	5	207	8	150	41	1000-10,000	470-480	140-160
MPB	Under belt return	5	210	7.7	151	41	1000-10,000	460-470	140-160
MPB	Under belt return	5	271	7.3	62	17	1000-10,000	550-560	350-400
MPB	Under belt return	5	277	7.7	67	18	1000-10,000	510-520	450-500
MPB	Under belt return	25	298	7	56	15	1000-10,000	480-490	2000-3000
MPB	Under belt return	24	369	5	20	5	1000-10,000	50-530	>5000
MPB	Under belt return	5	414	6.8	59	16	1000-10,000	550-560	>5000
MPB	Under belt return	30	420[4]	0	0	0	NI	NI	NI
MPB	Under belt return	5	490	6.7	42	11	1000-10,000	550-560	3000-4000
MPB	Under belt return	5	726	6.9	36	10	1000-10,000	590-600	>5000
SPF	Vibrating conveyor	5	196	8.1	227	62	1000-10,000	460-470	140-160
SPF	Under trimmer/sorter	5	198	6.4	148	40	1000-10,000	470-480	180-200
SPF	Dust conveyor dump flow	19	221	7.5	166	45	1000-10,000	470-480	180-200
SPF	Trimmer/sorter waste chain	5	267	6	76	21	1000-10,000	480-490	300-350
SPF	Dust conveyor dump flow	19	294	7.1	64	17	1000-10,000	470-480	250-300
SPF	Vibrating conveyor	17	313	7	85	23	1000-10,000	470-480	2000-3000
SPF	Under main chip belt	5	334	6.9	50	14	1000-10,000	520-530	160-180
SPF	Dust conveyor dump flow	5	410	6.9	64	17	1000-10,000	430-440	300-350
SPF	Under trimmer/sorter	5	415	4.8	52	14	1000-10,000	400-410	1000-2000
SPF	Dust conveyor	19	434	6.5	39	11	1000-	470-	>5000
SPF	Under main chip belt	29	481	4.7	19	5	1000-10,000	510-530	160-180
SPF	Vibrating conveyor	28	513	5.5	25	7	1000-10,000	530-540	>5000
SPF	Dust conveyor dump flow	20	993	0	0	0	NI	NI	NI
SPF	Trimmer/sorter waste chain	5	1227	4	18	5	1000-10,000	560-570	>5000
SPF	Vibrating conveyor	29	1276	0	0	0	NI	NI	NI
Douglas-fir	Under trim saws	5	183	6.9	73	20	1000-10,000	450-460	180-200
WRC	In-feed of end dogger	5	189	7.9	216	59	1000-10,000	440-450	100-120
Hem-fir	Under waste conveyor	5	244	8.1	158	43	1000-10,000	460-470	160-180
WRC	In-feed end dogger	5	380	7.5	111	30	1000-10,000	480-490	160-180
Hem-fir	Under waste conveyor belts	5	356	6.8	45	12	1000-10,000	510-520	1200-1300
Douglas-fir	Under trim saws	5	393	7.3	54	15	1000-10,000	470-480	1300-1400

While this data set is far from perfect, (particle shape, size distribution, elemental and proximate results not specified) it has far more information than most literature sources, recording the MEC, maximum K_{st}, maximum Pmax and average particle size for many different biomass (sawdust) samples.

Of most interest are two tests with an average particle size of >1200µm, one of which did ignite and one of which did not. The only significant difference between them was a difference in moisture content that was believed to result in the failed ignition of the wetter sample.

Considering NFPA 664 states that a deflagrable wood dust is – "… Wood particulate with a mass median particle size of 500 µm or smaller" this wood sample would appear to break this along with another that ignited with an average particle size of 726µm.

This is very dangerous as people could apply the guidelines and then think it is all safely dealt with while in actual fact it is still an explosive environment. It is believed that the ability to propagate a flame may be strongly linked to the finer fractions of dust present in the mixture (Man and Harris, 2014). This is backed up by the MEC for some of these materials being >5000g/m^3 (biomass stoichiometric concentration is around 200 - 230g/m^3) which is roughly 25 x the stoichiometric concentration. This could be caused by a low fines percentage therefore needing a lot of material to reach the flammability limit or could be a need for a fixed surface area of material to be available (this would change for different particle size and composition materials).

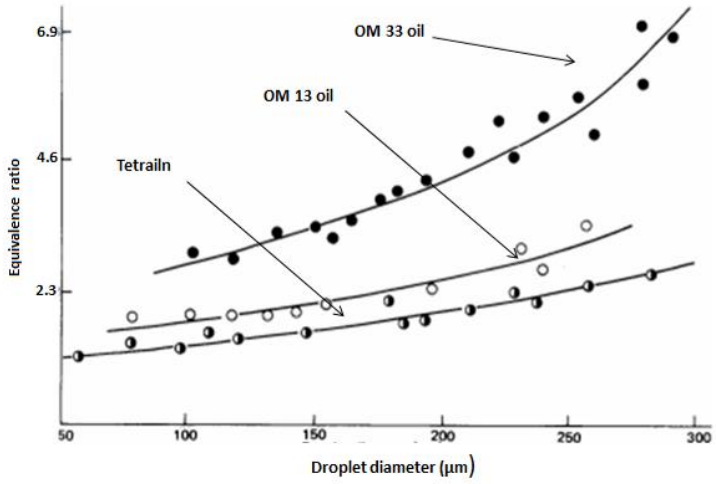

Fig 2.21 Mist droplet flammability with droplet size (Cook, 1977).

For vapours and mists Cook (1977) shows (**Fig 2.21**) that for OM 13 oil, OM 33 oil and tetrailn (1,2,3,4-tetrahydronaphthalene - $C_{10}H_{12}$) combustion will not take place in particles with a mean diameter larger than 300µm.

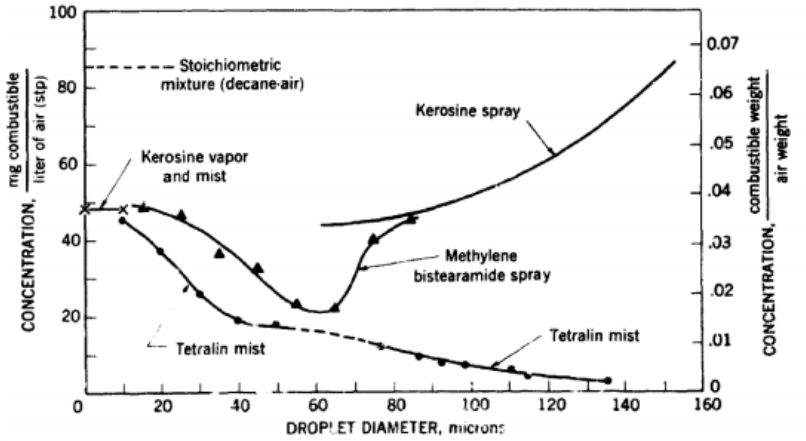

Fig 2.22 Droplet flammability as a function of size (Zabetakis, 1965).

Zabetakis (1965) reported that kerosene droplets are flammable up to 150µm droplet size, however he also puts the limit for tetrailn at 140µm droplet size, half as big as Cook (1977). Man and Harris (2014) stated that for coal there is strong evidence that particles 212µm and above are very difficult to ignite and generally do not deflagrate in explosion vessels up to 1m^3. The paper also speculates that "the explosion is largely controlled by the amount of the finer-size component, probably 150µm or smaller", the coarsest sample run by (Man and Harris, 2014) had an average particle size of 342 µm (43% - sub 212 µm of which 20% - sub 75 µm) while for biomass dusts materials with average particle size up to 1227µm (24% - <420 µm of which 11% - <250 µm) will ignite (Wong, 2013).

Particle size affects not only the flammability of a mixture but also how it and its component particles behave during injection and subsequent suspension in air.

Dispersion forces – During injection the particles will be subjected to many different forces, it is vital to understanding how the flame propagated to understand how this affected the varying particle sized materials.

In physical chemistry, the van der waals forces are the sum of the attractive and repulsive forces between molecules other than those due to bonds, or the interaction of ionic bonds (Hydrogen bonds). These (mainly attractive) forces adhere the particles together, therefore effectively creating bigger particles due to agglomeration, reducing the surface area exposed to the flame front.

For spherical particles, the van der Waals forces can be thought of as made up of:

- Force between two permanent dipoles (Keesom, 1921).
- Force between a permanent dipole and a corresponding induced dipole (Debye, 1920).
- Force between two instantaneously induced dipoles (Eisenschitz and London, 1930).

All molecules have dipole moments and are attracted to other neighbouring molecules by, at least the instantaneously induced dipoles. Additionally the resistance from abrasive particle friction is ignored with spherical particles.

The van der Waals interaction energy between spherical bodies of radii R_1 and R_2 and with an assumption of smooth surfaces was approximated (Eisenschitz and London, 1930) as:

$$U(z;R_1,R_2) = -\frac{A}{6}\left[\frac{2R_1R_2}{z^2-(R_1+R_2)^2} + \frac{2R_1R_2}{z^2-(R_1-R_2)^2} + \ln\left(\frac{z^2-(R_1+R_2)^2}{z^2-(R_1-R_2)^2}\right)\right]$$

(Eq.16)

where A is a constant (~10^{-19} - 10^{-20} J) that is governed by the material properties and *z* is the center-to-center distance, $z = R_1 + R_2 + r$. Where r = distance between particles

Therefore the first equation simplifies to:

$$U(r;R_1,R_2) = -\frac{AR_1R_2}{(R_1+R_2)6r}.$$ (Eq.17)

When r << R_1 or R_2

As the spheres are sufficiently large compared to the distance between them

The van der Waals force between two spheres of constant radius is a function of separation since the force on an object is the negative of the derivative of the potential energy function.

$$F_{VW}(r) = -\frac{dU(r)}{dr}$$ (Eq.18)

This yields:

$$F_{VW}(r) = -\frac{AR_1R_2}{(R_1+R_2)6r^2}.$$ (Eq.19)

The van der Waals forces between objects with other geometries ranging in size from 1μm to 200μm, have been tested, generally the forces measured, scale directly with the particle size as expected (Johnson, 1971).

For aerodynamic force

$$F_D = \tfrac{1}{2}\rho u^2 C_D A$$

F_D is the drag force

ρ is the density of the fluid

u is the flow velocity relative to the object

A is the reference area

C_D is the drag coefficient – a dimensionless coefficient related to the object's skin friction and form drag.

From the expressions above, it is seen that the van der Waals force decreases with decreasing particle size. However, gravitational force is proportional to d^3, aerodynamic force is proportional to d^2 (Area) and cohesive force is proportional to *d*. All three decrease with *d*, but as expected the gravitational and aerodynamic forces decrease fastest due to the squared and cubic relationship to *d*. **Figure 2.23** (Shao, 2008) demonstrates that at a velocity of 0.4m/s, for particles <10 μm the cohesive force is predominant, for >10 μm < 300μm, aerodynamic forces is dominant while gravitational force is dominant for particles >300μm.

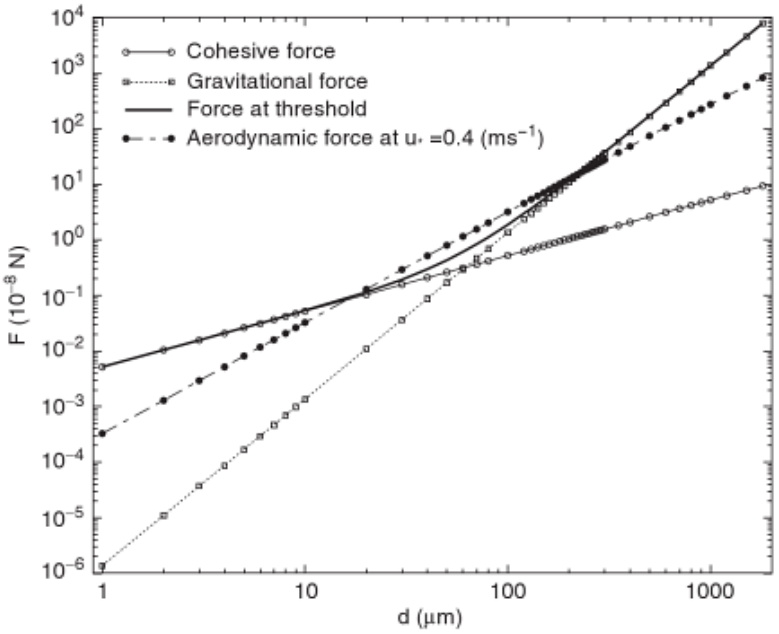

Fig. 5.14. Comparison of the relative importance of the gravity force, the cohesive force and the total aerodynamic force at $u_* = 0.4$ m s^{-1}, as a function of particle size. For fine particles, the cohesive force dominates over the gravity and the aerodynamic forces; for medium sized particles, the aerodynamic force is the largest, and for large particles the gravity force becomes dominant

Fig 2.23 Inter particle force against particle size (Shao, 2008).

This suggests that in a mixture of particle sizes the largest (>300μm) will begin falling out of suspension immediately after the injection inertia has dissipated. The intermediate particles (>10 μm <300μm) will fallout once the gas velocity entraining them (turbulence) falls below their aerodynamic force threshold (different for particles within the >10 μm <300μm range). While <10μm particles will take a very long time to settle out as the particle drag and inter particle attractions between them is larger than the gravitational force pulling them down.

Size separation at the flame front may also occur, not primarily through aerodynamic means but simply through thermal inertia. Large particles may not be sufficiently heated in the flame front, which is driven by the finer particles. These larger particles are then burnt in the combustion products of the finer dust particles where they are flash heated and for lean flame front mixtures there is surplus oxygen to burn them in.

Particle shape is also significant as biomass particles are cylindrical as opposed to coal which produced roughly spherical particles. As the height/radius ratio is increased for cylindrical particles the surface area : volume ratio reduces, meaning

that the longer a cylinder is the lower the surface area : volume ratio and the less reactive the material should be.

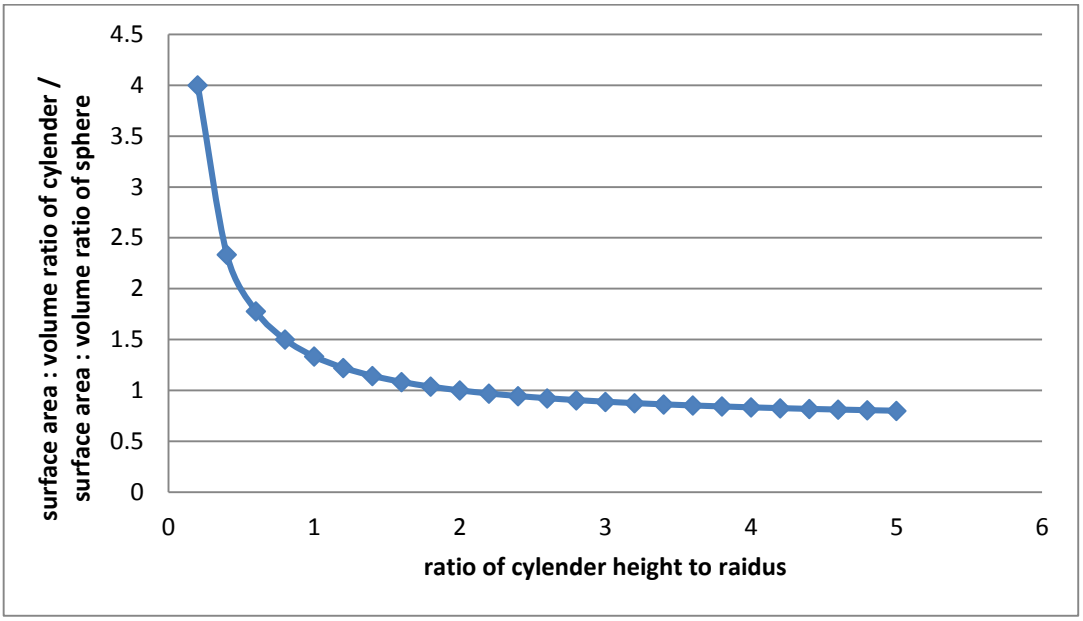

Fig 2.24 Surface area : volume ratio of cylinder against surface area : volume ratio of sphere for varying cylinder height.

This is true as the particles being used are separated based on a constant radius (size shaker mesh separation based on radius). For biomass the finer the particle size the higher the height : radius ratio is and therefore the less reactive the material should be in reference to another spherical particle of the same radius.

Particle shape also plays a major role in dust explosion severity, the explosion hazard from irregularly shaped particles is greater than for spherical particles of the same size. Buschart (1999) found that spherical particles made of plastic were less hazardous than irregularly shaped particles of the same material (Buschart, 1999).

2.3.8 Biot number

The Biot number defines heat transfer characteristics through a particle, specifically it is used to determine whether or a not an object is thermally thick or thin.

If the thermal resistance of the solid/gas interface exceeds the thermal resistance of the interior the Biot number will be lower than one. Where it is much lower than one, the interior of the solid may be assumed to have uniform temperature. This

temperature may change, as more or less heat energy enters the solid from the gas.

If the object is large this causes the length (radius for spherical particles) to increase to the point that the Biot number is >1, now temperature differences within the particle become important. If the particle is made of a thermally insulating material, such as wood the interior resistance to heat transfer will exceed that of the solid/gas boundary. Due to the effects of these variables it is possible to get the Biot number >1 for low conductivity materials with a much smaller particle size than in large conductivity materials

When the thermal resistance to heat transferred into the object is larger than the resistance to heat being diffused completely within the object, the Biot number <1. In this case, particularly for Biot numbers which are very small, the assumption of uniform temperature within the object can begin to be used. If the Biot number is lower than 0.1 then it may be regarded as being "thermally thin", the entire particle will be the same temperature with the only significant difference being at the solid/gas boundary.

This may explain the difference in minimum particle size needed for flame propagation found between coal and biomass dust particles.

The Biot number is defined as:

$$\mathrm{Bi} = \frac{hL_C}{k_b} \quad (20)$$

where:

- h = convective heat transfer coefficient W/(m^2•K)
- LC = characteristic length
- k_b = Thermal conductivity of the body (W/(m·K))

k_b is constant = 0.16 -0.12 *(W/(m.K))(ToolBox)*

0.09*(W/(m.K))*) - (William Simpson, 1999.)

0.16 *(W/(m.K))*) - (Haynes and Lide, 2011)

In the case of a sphere or cylinder “L = R”. L is the “typical” length scale that heat in the solid particle must diffuse to get to the centre (L. W. Kula, 1991). However other sources use Lc = r/2 and this was found to give better agreement with the calculation by Hayhurst (2013).

This was assumed as 0.000063m for the <63µm fraction and was then increased by the ratio of the D[3/2] of the next sample to the last multiplied to this.

Characteristic length = oak - 63 µm = $1.57*10^{-5}$ m

Oak – 63 150 µm = $9.5*10^{-5}$ m

Oak – 150 - 300 µm = $3.55*10^{-4}$ m

Oak – < 500 µm = $2.25*10^{-4}$ m

Convective heat transfer coefficient - $h = (Nu \times \lambda_{ext})/D$

λ_{ext} = thermal conductivity of the hot gas = 0.12 (W/m K) at 1800k

D = diameter of particle = from mastersizer.

$Nu = 2 + (0.4Re^{.5} + 0.06Re^{2/3})Pr^{0.4}(\mu/\mu_s)^{.25}$ (Mason, 2015)

$Re = (U \times D)/ V$

V = kinematic viscosity of hot gasses = 0.00002722 m^2/s

U = particle velocity relative to that of gas

Pr = 0.71 (Mason, 2015)

µ = dynamic viscosity at flame temperature = 5.65×10^{-5} kg/m s

μ_s = dynamic viscosity at particle surface temperature = 1.85×10^{-5} kg/m s

for the 4 different particle sizes of oak tested the Biot number was calculated.

Table 2.12 The Biot number for the oak size fractions tested.

Lc = r/2	U=0.01			k = 0.16	k = 0.09
D	Re	Nu	h	Bi	Bi
3.15E-05	0.02	2.1	3953.8	0.39	0.69
1.09E-04	0.08	2.1	1181.7	0.40	0.71
4.01E-04	0.29	2.3	341.4	0.43	0.76
2.52E-04	0.19	2.2	529.1	0.42	0.74
D	U=1			Bi	Bi
3.15E-05	2.3	2.8	5375.6	0.53	0.94
1.09E-04	8.0	3.6	1973.8	0.67	1.19
4.01E-04	29.5	5.2	772.4	0.97	1.72
2.52E-04	18.5	4.5	1064.2	0.84	1.49
D	U=5			Bi	Bi
3.15E-05	11.6	3.9	7470.0	0.74	1.31
1.09E-04	40.0	5.7	3155.3	1.07	1.91
4.01E-04	147.3	9.5	1425.1	1.79	3.17
2.52E-04	92.5	7.8	1869.8	1.47	2.62

Convective heat transfer was assumed to be the dominant mechanism of heat transfer as was found by Proust (2006) and covered in section 2.2.6.

Yao B. Yang and Jenny M. Jones (2008) puts this transition from thermally thin to thermally thick at 200-250µm for spherical biomass and 150-200µm for cylindrical biomass particles; while Proust (2006) states that particles over 100µm can be considered thermally thick. These calculations (**table 2.12**) indicate that the particle size and the particle velocity relevant to the carrier gas are key to calculating the Biot number for a particular fuel mixture. However theses to values are inter-related in reality, this is not represented in this equation and would require more work generate accurate values of U with changing particle diameter. The current work

though shows a difference between the particles Biot numbers between 63 - 150µm and 150 - 300µm size fraction after a velocity of 1m/s.

The thermal conductivity for coal is 0.22 – 0.48 (Herrin and Deming, 1996). Making it likely to absorbed more energy from the flame front than biomass. While theoretically this should help in the liberation of volatiles it is known that coal has a higher temperature of volatile release (**Fig. 4.1**) than biomass and the interaction of these two variables is unknown but could be responsible for the lower particle size flammability limit and higher MEC found for coal.

A different equation for the Biot number is used if the particle velocity is the same as the gas velocity – "when there is a negligible relative velocity between a gas stream and a tiny particle, carried along by the flow, as in a combustor burning pulverised fuel, small enough to be entrained in the gas" Hayhurst (2013).

$Bi = 0.6 \times (\lambda_{ext} / \lambda_{solid})$

$\lambda_{ext} = 0.12$ (W/m K) (Mason, 2015)

$\lambda_{solid} = 0.16$ (W/m K)

$Bi = 0.45$

The current standards for coal dust in power stations is 70% passing − 200 mesh or 74 microns (Malav et al., 2008). While Bradley et al. (2014) observed that for tetrailn, droplets with diameter below 10 µm, combustion was as in the gas phase, while >40 µm each droplet burned individually in its own envelope of air. This suggests that the <63µm fraction of oak dust should be assessed using the second equation.

2.3.9 Moisture content

The effects of moisture content on dust explosion hazards have been covered, M. Traoré (2009) reported that lowering moisture content increases the explosion risk of materials. Dust explosion statistics from the United States show that most accidents happened during low atmospheric humidity, this is thought to be due to higher potential for static sparks and less inert moisture to act as a heat sink in the atmosphere.

According to Eckhoff (2003), there are three main ways moisture affects dust combustion characteristics;- dust ignition energy, explosion severity and said dusts affinity for dispersion

- Internal heat sink is increased by the energy taken to heat and vaporise the water.
- Oxygen and combustible gasses are diluted by water vapour.
- Water prevents dispersion of dust particles due to clumping together of particles therefore making them less reactive.

Eckhoff (2003) provided a summary of the work of van Laar and Zeeuwen showing the effect of moisture content on the measured Minimum Ignition Energy (MIE) for several organic dusts. The results showed that increasing moisture caused a significant increase in MIE. Similarly,Traoré et al. (2009) looked at the effect of moisture content on the MIE of magnesium stearate which was increased three fold when its moisture content was increased from zero to 90%.

The moisture content of a dust itself is determined by the dusts -

- Natural moisture bound into the structure.
- How hydrophobic the material is.
- Environmental moisture in which the material is stored and how long it is kept there.

2.3.10 Sources of ignition

According to Eckhoff (2003) the most common sources of ignition for combustible dust explosions are:

- Burning or smouldering material.
- Heat from mechanical impacts, electrical arcs or discharges.
- Hot work and hot surfaces such as those found on heaters and hot lines.

- Overheated bearings.

Burning/smouldering material can occur as a result of exothermic reactions in stored material. Single impacts are capable of creating an impact spark, however, the evidence does not indicate that a single impact is capable of producing enough energy to ignite a dust cloud (Abbasi and Abbasi, 2007). Repeated impacts, such as a damaged bucket elevator where a single spot is repeatedly stuck can eventually build up sufficient heat to ignite material. Electrostatic discharges can also ignite dust clouds Glor (2003), this occurs when electrostatic charges are not safely dissipated prior to a discharge.

The ignition system in the Hartman apparatus is similar to an electrical arc while the 2, 5kJ igniters in the $1m^3$ are similar to a blow/cutting torch flame present in hot work.

2.3.11 Test vessels

The literature has shown that measurements (Eckhoff, 2003, Wilén, 1999, Maisey, 1965, Field, 1983) of biomass dusts using the $1m^3$, 20L sphere and Hartman equipment have found MEC's that convert to Ø = 0.14 – 0.3. **Figure 2.15** demonstrates that this should not be possible as no CH or CHO gas will burn this lean (excluding acetylene and hydrogen) therefore it was deemed necessary to compare various explosion vessels to see if this was the cause of these anomalies.

Table 2.13 Compilation of 20L sphere and hartman tests.

Material CH_yO_z	y=H/C	z=O/C	Ø=1 A/F	Ø=1 g/m^3	MEC g/m^3	Equipment	MEC Ref.	Mean Particle size µm	$Ø_{MEC}$
Spruce	3.58	1.55	3.83	313	20 – 70	-	(Field, 1983)	-	~0.14 (0.06-0.22)
Cellulose	1.67	0.833	5.12	234	55	Hartmann	(Maisey, 1965)	-	0.235
Rapeseed Straw	1.88	0.986	4.54	264	210	$1m^3$	(Wilén, 1999)	318	0.79
Spanish Lignite	1.42	0.826	4.88	246	90	$1m^3$	(Wilén, 1999)	40	0.36
Miscanthus	1.62	0.771	5.42	221	120	$1m^3$	(Wilén, 1999)	143	0.54
Carbon monoxide	0	0.75	3.45	-			(Jun et al., 2010)	-	0.406
Wood	1.59	0.73	5.61	214	30	$1m^3$	(Wilén,	95	0.14

		1					1999)		
Spanish Pine	1.63	0.729	5.69	211	90	1m^3	(Wilén, 1999)	247	0.43
Barley Straw	1.68	0.705	5.91	201	90	1m^3	(Wilén, 1999)	253	0.45
Forest Residue	1.53	0.672	4.78	251	60	1m^3	(Wilén, 1999)	102	0.24
Bark	1.42	0.637	6.03	199	30	1m^3	(Wilén, 1999)	57	0.15
Sorghum Straw	1.45	0.647	6.02	199	120	1m^3	(Wilén, 1999)	178	0.6
German Lignite	1.09	0.450	7.12	169	60	1m^3	(Wilén, 1999)	58	0.355
PMA	1.50	0.50	7.27	165	30		(Eckhoff, 2003)	-	0.182
Polyvinyl acetate	1.5	0.5	7.22	166	40	Hartmann	(Maisey, 1965)	-	0.24
Pitch Pine	1.46	0.416	8.09	148	30-60	-	Eckhoff (2003)	-	~0.3 (0.20 – .40)
PMMA	1.60	0.40	8.28	145	30	Hartmann	(Maisey, 1965)	-	0.207
Polyethylene-terephthalate (PET)	0.8	0.4	7.18	167	40	Hartmann	(Maisey, 1965)	-	0.24
Bituminous Coal	0.778	0.073	12.7	94.5	55	Hartmann	(Maisey, 1965)	-	0.58
Polyethylene	2.0	0	14.8	81	30	Hartmann	(Maisey, 1965)	-	0.37
Polypropylene	2.0	0	14.8	81	35	Hartmann	(Maisey, 1965)	-	0.43

Both the 1m^3 and Hartmann equipment gave MEC values <0.4, this indicates that if the low MEC values are a product of unequal distribution of the dust within the vessels this is present in both pieces of apparatus. It should also be noted that Wilén (1999) recorded MEC values of 0.43Ø for particles of an average size of 247µm in the 1m^3 ISO vessel using rebound nozzle injection which was not possible to replicate in the Leeds 1m^3 ISO vessel. However he made no mention in the literature of re-calibrating the vessel to allow for the change in disperser as is specified in the ISO standard “The test apparatus and the procedure shall be verified every 12 months, or following any significant maintenance or repair.” (BSEN, 2011).

Wilén (1999) used both the 20L sphere and 1m^3 vessels (**Table 2.14**), allowing for side by side comparison using the same dust samples. No other literature sources like this were found as while many labs tested substances with the same name, i.e.

“cornflour” the samples came from different sources and therefore had potentially different feedstock’s, particle sizes and moisture contents resulting in a wide variation in values between laboratories (**Table 2.13, 2.14, 2.15, 2.16, 2.17** and **2.18**).

In **Table 2.14** (Wilén, 1999) the 20L sphere produced MEC values slightly lower (Spanish lignite) to 9.6 times larger (sorghum) that that found in the $1m^3$ vessel. The 20L sphere was consistently producing larger MEC values than the $1m^3$ vessel by an average factor of 2-3 fold.

Table 2.14 MEC from 20L sphere compared to $1m^3$ vessel (Wilén, 1999).

material	Stoichiometric concentration g/m^3	Average particle size µm	20L MEC	$1m^3$ MEC
Wood	214	95	0.46	0.138
Bark	199	57	0.5	0.14
Forest Residue	251	102	0.59	0.22
Spanish Pine	211	247	1.6	0.394
Barley Straw	201	253	1.24	0.357
Miscanthus	221	143	2.04	0.498
Soghum	199	178	9.66	0.531
Rapeseed Straw	264	318	2.84	0.661
German Lignite	169	58	0.35	0.307
Spanish Lignite	246	40	0.24	0.242

This may indicate that there is a problem in the distribution of dust in the 20L sphere, however the 20L sphere used in this testing was run similarly to the Hartmann equipment with in vessel dust storage and dispersion from a nozzle at the bottom of the vessel. The MEC values produced from the 20L sphere are far closer to the MEC values of gaseous materials than those from the $1m^3$. It is speculated that the $1m^3$ that was run using the rebound nozzle may have imparted directionality to the injection creating a locally rich zone around the ignition location.

Table 2.11 (Wong, 2013) has a large number of tests carried out on coarse biomass in the 20L sphere, due to lack of elemental or proximate data a stoichiometric concentration is impossible to derive exactly so a general value of $220g/m^3$ is assumed. Using this the lowest MEC achieved in this equipment was Ø =0.63, similar to the 20L sphere in **Table 2.13** (Wilén, 1999) and far higher than the $1m^3$ results in the same table.

At the same time the 20L vessel was producing lower maximum pressures from the same materials **Figure 2.25** (Wilén, 1999). It has been theorised that the 20L sphere is the erroneous equipment, with regard to pressure generation due to-

- Overcharging with igniters – the 10kJ ignition source used in this vessel creates a pressure rise of 1.1bar before propagation begins resulting in the recorded test actually being run at higher than atmospheric pressure.
- Andrews and Bradley (1972) have recommended 250mm diameter vessel as a minimum to enable the flame front to reach a one dimensional plane. The diameter of a spherical 20L vessel is 337mm and if the flame needs a 250mm diameter to attain a one dimensional plane, then it would have already travelled 74% of the vessel diameter. After this distance the burning velocity starts to be effected by the compression of unburned gases ahead of the flame (Andrews, 2010).

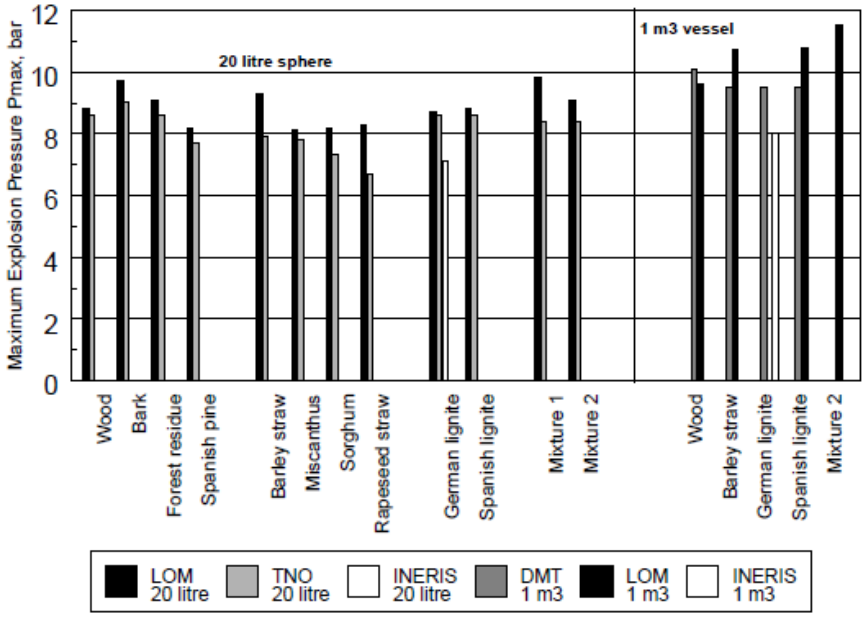

Fig 2.25 Maximum pressure from 20L spher and 1m^3 vessel (Wilén, 1999).

In **Table 2.15** (Eckhoff, 2003) the same dust (starch) is tested in apparatus of different volumes (no mention of shape or geometry is made), it should be noted that the K_{st} varies from 3 to 209 for the same material depending on the vessel. The largest K_{st} values are found for the largest vessels, supporting the maximum pressure data in **Figure 2.25**. However, the 20L sphere, which is a true sphere, gave higher K_{st} values than the 1m^3, this is thought to be due to the quenching of

the flame front during the last stage of flame propagation where the highest rate of pressure rise is found. There are some companies that have built true 1m^3 spherical vessels (FIKE Corporation, 2013) but the present Leeds vessel is built to the ISO specification and is the standard measurement method for dust reactivity in both the USA and Europe.

Table 2.15 K_{st} values from differnt sets of test equipment Eckhoff (2003).

Investigator	$(dP/dt)_{max}$ [bar/s]	Volume V of apparatus [m^3]	K_{St} [bar·m/s]
Bartknecht (1978)	680	0.0012	73
Nagy and Verakis (1983)	612	0.0012	66
Eckhoff et al. (1987)*	220	0.0012	23
Nagy and Verakis (1983)	413	0.009	86
Aldis et al. (1983)	320	0.020	87
Eckhoff et al. (1987)*	365	0.020	100
Yi Kang Pu (1988)	10-20	0.026	3-6
Yi Kang Pu (1988)	60-80	0.026	20-25
Nagy and Verakis (1983)	272	0.028	83
Bond et al. (1986)	50	0.33	34
Kauffman et al. (1984)	72	0.95	71
Kauffman et al. (1984)	20	0.95	20
Nagy and Verakis (1983)	136	3.12	200
Nagy and Verakis (1983)	110	6.7	209
Nagy and Verakis (1983)	55	13.4	131

*Arithmetic mean values, 11% moisture in starch.

12 materials were tested by Wilén (1999) and for every test except one the MEC from the 20L vessel was higher than that from the 1m^3. This suggests that there is an intrinsic difference between these 2 vessels, the fact that the 1m^3 consistently produced lower MEC values than the 20L sphere may indicate that the 1m^3 vessel used in these tests produces locally rich/stratified mixtures. Possibly as a result of the injector change without re-calibration. The comparison of the same 2 vessels (**Table 2.16**) Eckhoff (2003) came to a different conclusion with the 20L sphere here producing the lower average MEC values.

Table 2.16 Comparison of 5 different materials by 4 different labs Eckhoff (2003).

Test method / Dust	20-litre sphere					1 m³	Nordtest Fire 011
	Lab. 1	Lab. 2	Lab. 3	Lab. 4	Arithm. mean	Lab. 1	Lab 3.
Lycopodium	30 (0.5)	20 (0.2)	15 (0.1)	40 (0.5)	26	30 (0.4)	35 ± 6*
Maize starch (11-12% moisture)	60 (0.5)	50 (0.3)	90 (0.2)	90 (0.2)	73	80 (0.3)	130 ± 14* [76 ± 4]
Light protecting agent 'Tinuvin'	30 (1.3)	10 (0.2)	20 ((0.2)	20 (0.1)	20	40 (0.3)	27 ± 3*
Spanish coal (36% volatiles)	40 (0.6)	30 (0.4)	25 (0.3)	30 (0.1)	31	70 (0.2)	98 ± 20* [73 ± 5]
Zinc	600 (0.9)	600 (0.3)	400 (0.3)	400 (0.1)	500	650 (0.8)	565 ± 65*

*Standard deviation.

Other authors have reported values for materials that appear identical given the information available that agree with each other over all three pieces of equipment, **Table 2.17**.

Table 2.17 Hartman MEC compared to 1m³ MEC showing good agreement

Dust	Hartmann – g/m³ Maisey, Field	Eckhoff g/m³ 20L or 1m³	NFPA 68 g/m³ 1m³
Sugar	45	60	200 and 60
Milk Power	50	60	60
Aluminium	30 (6µm) – 40(17µm)	30 (29-22 µm) – 60 (10 – 43 µm)	30 (29µm)
Cellulose	55	60	60
Wheat Starch	45	60	30
Polypropylene	30-35	30-200	30

This would seem unlikely given that the Hartman tube has far more quenching losses due to the geometry of its shape compared to the 1m³ and especially the 20L sphere. This loss of energy from the flame front to the walls is especially important at near limit mixtures where the flame is approaching the critical flame temperature. Therefore it would seem likely that the agreement and in some cases lower values for MEC found in **Table 2.17** between the Hartmann apparatus and other vessels are likely caused by distribution differences causing localised distribution as will be shown later on for the Hartmann vessel.

A possible reason for the disagreement between vessels could be the pneumatic dust dispersion and the use of high energy ignitors causing turbulence, which as covered enhances heat and mass transport at the flame front (Kang Pu et al., 1989), therefore the turbulence in each vessel would have to be empirically altered to produced agreement across the vessels. However due to different vessel geometry's and injectors the exact length scale and pattern of the turbulence differs between vessels. This turbulence accelerates the combustion process but can result in incomplete combustion at near lean limit mixtures.

The high intensity and small scale turbulence is associated with small vessel confinement and does not occur to the same magnitude in larger scale test vessels. It was determined that turbulent mixing at the flame front in the small scale is too rapid, resulting in lower maximum pressure values (as was displayed in **Figure 2.25**). Consequently explosion data obtained in a 950L vessel have been proven to be more reliable than results from smaller vessels. The problem, however, does not stop there, with many vessels that are similar in volume having different geometry's, injector size/number or orientation (**Fig. 2.26**) (Dastidar, 2001).

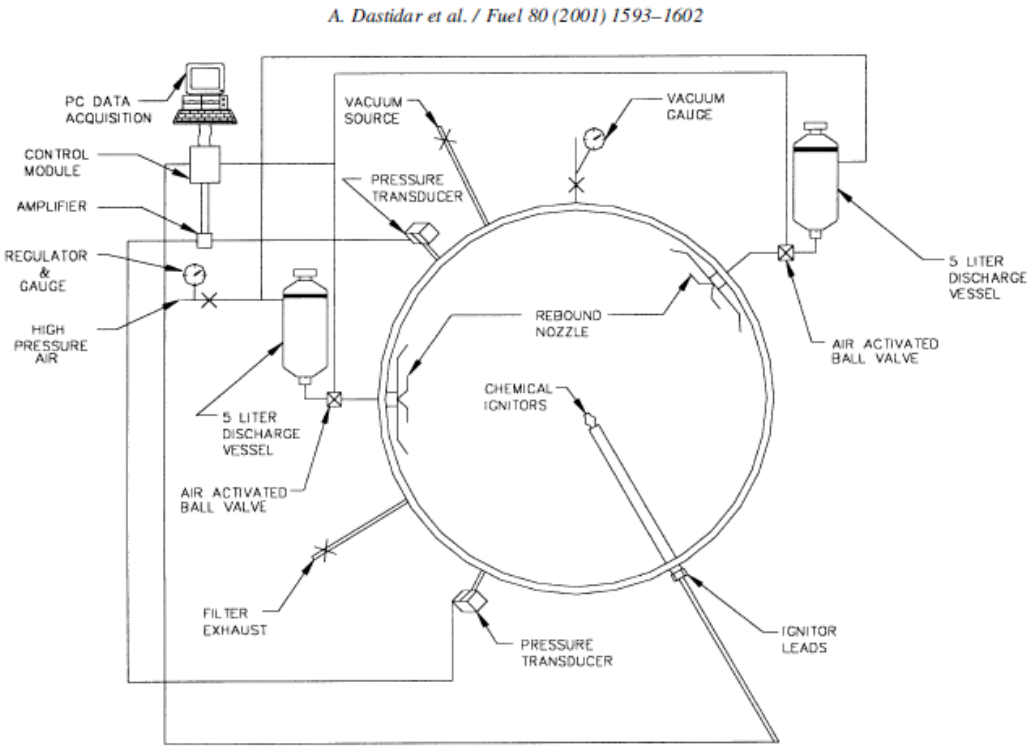

Fig 2.26 One of many variations of 1m3 chamber that are in use (Dastidar, 2001).

In summery none of the data is comparable with other sets due to changes in the injector's, timing, particle size, vessel geometry and ignition source. Maisey (1965) recorded an MEC of 0.58Ø for bituminous coal and an MEC =0.235Ø for cellulose in the same vessel while Wilén (1999) has the biomass samples more reactive than coal in the $1m^3$ vessel but less reactive in the 20L sphere.

All the issues raised are illustrated in **Table 2.18** (EPRA, 2011), the MEC has been measured in 50% intervals, there is an 11.3% variation in the Pmax and a 35% variation in K_{st} (for those that gave actual values). This data was all generated from the standard 20L sphere vessel with no mention of deviation from the standard operating/injection method.

Table 2.18 MEC compared from different sources (EPRA, 2011)

	MEC g/m^3	P bar	K_{st} bar meters/s
Phenolic resin	15	9.6	198
Phenolic resin	30	9.4	156
Phenolic resin	15	9.3	129
Phenolic resin	30	-	St2
Phenolic resin	30	9.8	168
Phenolic resin	30	8.7	185
Phenolic resin	30	-	St1

2.3.12 Minimum ignition energy

A dust cloud suspension that is within flammable limits will not ignite unless sufficient energy is available to ignite it. The minimum energy of an electrical spark that's capable of igniting the explosive dust/air mix is the Minimum Ignition Energy MIE value. The MIE is strongly dependent on particle size Eckhoff (2003) and moisture content of the dust, and will affect the ability of a dust cloud to ignite. An increase in moisture content pushes the MIE up. The moisture works in several ways, evaporating as it absorbs energy from the flame front and once evaporated, the vapour mixes with pyrolysis gases and reduces the reactivity of the gas produced.

Some ignition energy's for various materials from Maisey (1965) are used to illustrate how small these values are in millionths of a joule.

Table 2.19 MIE for various dusts.

Dust	Minimum ignition energy (mJ)
Corn starch	40
Grain dust	30
Sugar	30
Rubber	50
Cellulose	80
PMMA	20
Pittsburgh coal	60
Sawdust (Wong, 2013)	1000

All of these values are below the 4J spark of the Hartman and well below the 10KJ of igniters used in the $1m^3$ and 5KJ of the 20L sphere. Therefore these materials should have no issues with being run on this equipment as there MIE is above that produced by the vessel.

2.3.13 Limiting oxygen concentration (LOC)

LOC is the maximum oxygen content in a mixture of flammable material at which the mixture ceases to allow combustion, below this limit adding fuel would not form an explosive mixture.

Different materials possess different LOC values based on their chemical composition and burning characteristics. Woods with the largest amounts of oxygen and H atoms in their composition have the lowest LOC values, this is due to the oxygen present in the materials structure taking part in the reaction, this therefore means that less oxygen is needed in the surrounding atmosphere to allow combustion to take place. The H content partly determines the reactivity of the material, and higher reactivity materials require less oxygen to allow combustion to take place as well as requiring less oxygen to fully react than carbon therefore lowering the LOC.

2.3.14 Combustion residue

Cetin (2004) carried out work on the effect of the heating rate on char formation in three different pieces of apparatus

(1) Wire-mesh reactor for generating high pressure chars at relatively high heating rates of about 500°C/s and pressures of up to 100 bar.

(2) A tubular reactor for performing low heating rate under atmospheric pressure at 950 °C

(3) A drop-tube furnace for extremely high heating rates (≈1×10^5 °C/s)

Virgin Radiata pine sawdust was used as the feedstock; a typical particle is made of solid cells strongly bounded but with evident cavities (slits), which continue inside the particle **Figure 2.27A**. The particle retains its shape with only slightly deeper openings after devolatilization in the tubular reactor at low heating rates, **Figure 2.27b**. At high heating rates in the Wire-mesh reactor the cell structure is completely destroyed after devolatilization with the apparent melting of the cell structure being observed **Figure 2.27C**.

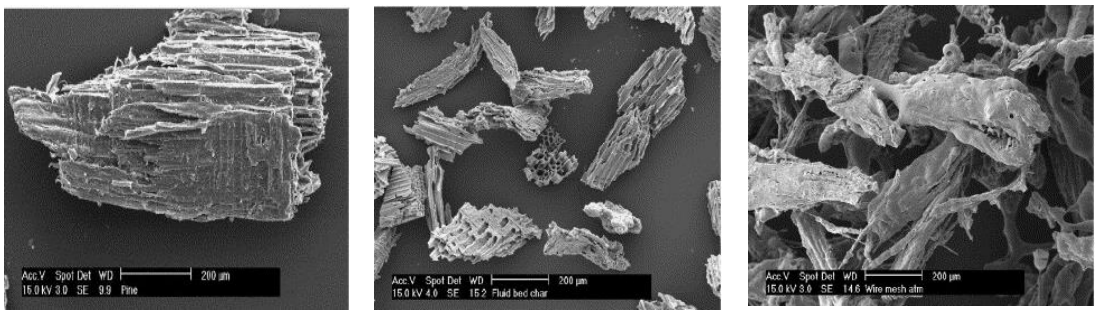

Fig 2.27 (A) Feedstock (B) Tubular reactor residue (C) Wire-mesh reactor residue (Cetin, 2004).

Investigations carried out on chars from the drop-tube furnace at 1000°C showed that even at short residence times melting still occurs at very high heating rates as was seen in **Figure 2.27C**, although it is more pronounced and coupled with the appearance of pores throughout the material (**Fig. 2.28)** (Cetin, 2004).

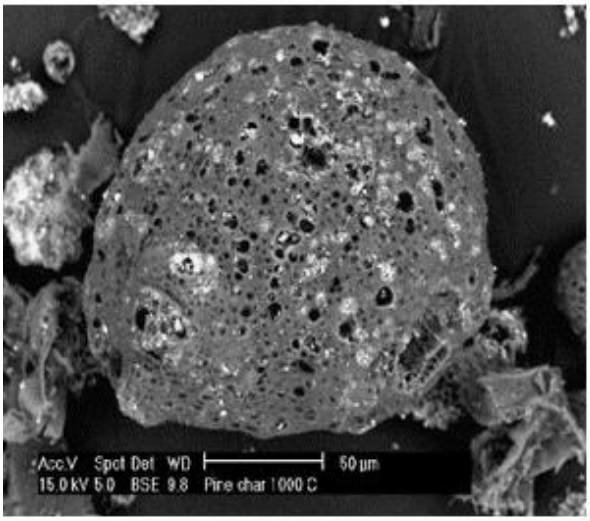

Fig 2.28 Drop-tube furnace residue (Cetin, 2004).

These pores result from the devolatilised gasses bubbling out of the molten particle leaving the char structure that consists of fixed carbon and ash. When these particles are broken they are hollow and made up of many macrospores with very thin cell walls.

A product of combustion in coal and biomass furnaces are aluminosilicate microspheres or “cenosphere’s”, these are formed in temperatures of 1400 -1700^{o}C (Fenelonov, 2010). This rather narrow temperature band would, if they are found in test sample residue allow for approximate determination of the temperature range the material was exposed to in said test.

2.3.15 Secondary assessment of aims

To create date with a full set of data – particle size (d.1,d.5,d.9), elemental, proximate analysis, MEC, a full set of Pressure and K_{st} (as a function of concentration as per the ISO standard) values will be generated. This is particularly important as most of the data currently available only has some of this data therefore making it impossible to reproduce the results achieved in most cases.

Both Maisey (1965) and Wilén (1999) tested coal and biomass samples on the same equipment and for similar particle sized samples found biomass to have an MEC approximately half that of coal. This indicates an increase in reactivity of the biomass in reference to coal, the fuel it is meant to replace. Therefore it would be beneficial to know if this increased reactivity holds true for particle size too, as large

particles are far more common in industry especially for biomass. If this is true it could be that previous safety practices (particle size extraction in dust extractors) or equipment could not be sufficient for safety requirements when using biomass.

Design and build a disperser that can disperse large particle fibrous biomass, as none currently exists that will uniformly disperse coarse biomass particles in the $1m^3$. The work prior to this at one point used a hemispherical disperser that is/was the most successful to date, therefore this will be the basis for this work.

Due to ambiguity on the mechanism of flame propagation between particles high speed video will be used to get pictures of large particle biomass combustion and try to determine whether this is heterogeneous and/or homogeneous combustion as was observed for lycopodium.

To try and determine what material is being consumed by the flame front during propagation it is planned to use residue analysis after combustion to try to determine what was left after the flame has passes through the mixture. Measuring the actual mass burnt during the test will also be part of this too try and explain how dust combustion displays no measurable upper flammability limit.

Figure 2.15 – CO and H_2 (gas species detected in biomass devolatilization in inert atmospheres (Commandré, 2011)) had both leaner and richer limit than methane (the gas species modelled in coal devolatilization) this offers a possible explanation for the MEC results less than 0.5Ø (the MEC of all HC gasses). To this end more tests will be carried out on both the $1m^3$ and Hartman vessels to try and replicate these <0.5Ø results and provide reasons for them.

Chapter 3 Equipment and experimental methodology

3.1 Fuels tested

Due to the long residence times found in solid fuel burners and the energy required to mill biomass, biomass feed stocks used in power generation plants are often large particles, fibrous in nature such as wood or straw type materials. These particles can be 1-2 cm long and are generally elongated and narrow in shape. However, this type of coarse, voluminous and poorly flowing dust samples would not pass through the standard C-tube dust injection system present in the Leeds ISO 1m^3 dust explosion vessel, (actual volume of 1.138 m^3) designed using the engineering drawing in the ISO standard.

One of the main objectives of the present work was the construction of a new fibrous dust feeding systems that can inject fibrous biomass into the 1m^3 test vessel and yet still produce K_{st} and Pmax results comparable to the standard C-ring. This calibration was done using methane and cornflour as a reference dust as was used by Sattar in the work prior to this. The use of reference dusts that would work on the existing and new injection systems was to enable the turbulence levels in the new injection system to be adjusted via the ignition delay to give the same K_{st} as the standard injection system.

The choice of biomass dust samples for the main body of tests was influenced by the need to use biomass materials that are currently being used for power generation alongside traditional fuels such as coal.

Cornflour, oak sawdust (<63µm, 63 -150µm, 150 – 300µm, 300 -500µm and <500µm), Empty Fruit Bunches (EFB) (<500µm) pellets and pine wood pellets (<500µm) (mixture consisting mainly of pine wood) were used in the 1m^3 vessel for this project. Kellingley coal and pine wood pellets were provided by the Drax power station, UK. Kellingley coal was provided as the pulverised sample collected after the milling process. Pine wood pellets were collected from the pellet storage facility after being broken up in water, and were then milled in the cutting mill at Leeds university. Oak sawdust was purchased from a furniture manufacturer in London, where it was a waste problem and this was further milled in the cutting mill.

Oak sawdust (<63µm, 63 -150µm, 150 – 300µm, 300 -500µm and <500µm), EFB (<500µm) pellets and pine wood pellets (<500µm) mixture (consisting mainly of pine wood), Oil Palm Trunk (OPT) (<500µm), lycopodium, rice husk pellets (<500µm) and Coconut Trunk (CT) (<500µm) were run on the Hartman apparatus with high speed video. This produced MEC and flame speeds for the samples for comparison with the $1m^3$ results as well as flame development images to try to understand visually the combustion, which is impossible in the $1m^3$.

These materials were characterised on an as received basis, using elemental analysis, TGA-proximate analysis, particle size analysis and SEM imaging. Standard explosion indices (Pmax and K_{st}), MEC and flame speeds were determined in the Leeds ISO $1m^3$ vessel with the residue after the explosion being collected and weighed, the procedure for which will be discussed later in this chapter. These residues were characterised on an as received basis, using elemental analysis, TGA-proximate analysis, particle size analysis and SEM imaging. This is the first time that the large unburned dust fraction in ISO $1m^3$ dust explosions has been acknowledged and investigated, although discussions at conference's with other users indicate that it is a well-known and unreported problem (personal communication with Rolf Eckhoff, 2012).

Additionally any powder in the external injection pot that was not injected into the explosion vessel was collected and weighed. These measurements enabled the actual mass of dust that participated in the explosion to be determined. Together with the elemental analysis used to determine the stoichiometric concentration of the dust in g/m^3, the equivalence ratio of dust that participated in the flame propagation was determined.

This is the first time that this has been done in dust explosion literature, as all previous publications on dust explosions have measured parameters plotted as a function of the nominal dust concentration, g/m^3. This nominal dust concentration was the mass of dust loaded into the external pot divided by the total volume of the explosion vessel (1.138 of the Leeds $1m^3$). The literature has never converted the g/m^3 concentration into equivalence ratio and so the literature never commented on the fact that the peak reactivity for dust explosions was almost always about 2- 3 times richer than the stoichiometric value (Andrews, 2010). It also makes no mention of the MEC values for dusts from the literature that are lower than the MEC value for most gaseous hydrocarbon species.

3.1.1 Sample preparation

In order to test different size fractions it was necessary to carry out some preparation on the fuels prior to testing. From the literature it is known that the most reactive mixture for most dusts is in the range of 500- 1500g/m^3 (Wilén, 1999). This is further defined as around 750 g/m^3 and a flammable range from around 30 to >4000 g/m^3 (Eckhoff (2003), (Cashdollar, 1996) however recent literature has now expanded the flammable range to >5000 g/m^3 (Wong, 2013).

As each sample (wood type and size fraction) needed approximately 7-15kg of material in order to run a full concentration profile according to the ISO standard the number of size fractions tested depended on the mass available. With a large mass required for each test, a lot of sieving of as received dusts is also required as it is known (Eckhoff, 2003) that K_{st} and lean flammability limits are dependent on the particle size. This effectively increases the mass needs to run a full concentration range on the 1m^3 above 7kg for large particle size materials as they have a high MEC. For the as received “wood” sample 15kg was needed to run a complete ISO concentration test.

The woody biomass obtained from power stations was a coarse powder of elongated particles with length up to 1cm, as this is the size that is currently being burned in industry and hence work was carried out on these coarse size fractions.

Limited work was carried out on biomass particles <63µm as is proved nearly impossible to sieve woody, as received biomass in sufficient quantities below this size range. Even though this is the size at which a legal K_{st} measurement is supposed to be carried out. However, it was deemed critical to characterise dust explosion hazards on woody biomass at the size distribution actually used in power stations and therefore representative of actual risks. This was important as Hartman results showed that woody biomass will explode at particle sizes where more conventional dusts will not explode.

3.1.2 Milling

The samples were milled using a Retsch SM100 cutting mill located in the School of Geography, University of Leeds. A cutting mill is suitable for the grinding/cutting of soft, medium-hard, elastic and fibrous products, whereas ball or hammer mills only squash biomass samples due to its elastic, fibrous composition (section 2.1). The

cutting section of the miller was made of stainless steel. A 130mm diameter rotator with four fixed cutting blades in the cutting area of the mill is used to cut the sample.

Fig 3.1 Retsch SM100 cutting mill

The rotational speed of the rotor was 1500 rpm. For pellets a large mesh of 5mm was first used and then the resulting material was passed back through the mill using the smallest available 0.5mm sieve.

There was an issue with friction created by the mill heating the un-milled sample and releasing steam; this was overcome by using small amounts at a time and waiting between milling sessions for the apparatus to cool down.

Although this differs from the industrial method of breaking up the pellets (water absorption) this was used as the smaller particle size fractions could only be extracted from the limited samples in sufficient quantities if this was done.

3.1.3 Sieving

The samples were sieved using Retsch AS200 basic sieve shaker and sieves to get the required sample size. The diameter of the sieve pans was 20cm, each held 0.4kg per time and the pan used was described by the mesh size used and were stacked 500µm, 300µm, 150µm, 63µm and then a bottom pan with no mesh. The

sieve shaker filters the sample into the various size fractions; this is achieved through vibrational agitation of the sample that induces particles smaller than the mesh used to fall through.

However due to the size discrepancies between a cylindrical particles width and length a longer agitation time was needed than would have been the case for spherical particles (25min). Separation is useful as it enables dust explosions to be carried out for dust in a particular size range or below a specified size. However, as 7 -15kg of each size fraction was required for the $1m^3$ vessel ISO standard tests, this was very time consuming and limited the work on different size fractions that was carried out.

The same size fractions were used on the Hartman apparatus and that work is discussed in more detail later on.

3.2 Residue

After visual inspection of the residue left in the vessel post explosion; the material was observed to be made up of a mixture of both darker, (apparently burnt) and light (apparently unburnt) particles. To try and determine the ratio of these to one another it was decided to try and separate them, obviously this would be impractical to do by hand.

Therefore density separation using water as the medium was tried for all the materials tested so far, this was used to test the theory that if some of the dust in rich mixtures is burnt/pyrolyzed while other parts aren't, then this may create a density differential within the residue mixture. It was thought that the ash particles would sink (due to the lost volatile material) and the wood would float. It was theorised that this could then be used to separate the different fractions. However when preliminary teste were carried out on small samples of milled wood it was found that the raw unburnt material all sank and when the residue was tested the black (visually more burnt) particles were the ones that floated.

If this was to prove possible then it would allow for an accurate estimation of the mass and size range of the particles that burnt in the dust cloud suspension. After initial tests with small volumes for proof of concept a separator was purchased.

This led to the creation of 4 descriptions of material weight used during testing in the Leeds 1m^3 vessel.

1. Nominal mass – this is the mass weighed out at the beginning of the test procedure.

2. The injected mass - this is the mass that passed from the dust pot/hemispherical dust holder into the vessel.

3. Residue mass – this is the material that was dispersed within the vessel but did not burn.

4. Mass burnt – this is the mass that was burnt during the test.

3.2.1 Residue collection and separation procedures

While there have been many papers examining the residue/ash from burners and furnaces (Tortosa Masiá et al., 2007) none were found examining the residue from explosion vessels. This has many implications, not least of which is that all the tests carried out so far appear to be using the weighed nominal mass of dust loaded in to the vessel as the mass burnt. As has been published in Sattar (2012) Leeds University has developed a method of determining the actual mass burnt (this doesn't include the added mass of ash from combusted particles) when running explosion tests.

A Numatic MFQ-372 bagged vacuum cleaner was used to collect and measure the mass of dust that remained in the dust pot and in the test vessel (using separate bags) after the dust explosion tests. It has a 1100W/850W IEC vacuum motor producing 43.5 litres per second of airflow and 2450mmHg of vacuum pressure. The residue was collected in NVM-1CH dust bags. The bags were weighed before use and after to get the mass of the residue in the vessel. After collection and weighing the bags were mixed up by hand and a sample of 20g was taken for analysis and separation. It was later found that these bags are two layer vacuum bags, this fact results in size separation in the residue to some degree during the collection process, **Figure 3.2**.

Fig 3.2 Material trapped between the bag layers.

This material was collected and analysed separately, at the same time as the rest of the material.

So for each test run there were four samples to be analysed –

- the residue as extracted from inside the vacuum bag (r).
- the residue as extracted from between the layers of the vacuum bag (br).
- the residue after separation top fraction (t).
- the residue after separation bottom fraction (b).

The 12L separation funnel (**Fig. 3.2**) was filled with approximately 8L of water, the 20g of residue pre-mixed with a small amount of water to prevent floatation of the material when added to the separation funnel (due to the dust appearing mildly hydrophobic and floating without mixing first). The residue slurry was then added to the vessel and more water was added to mix them and ensure no reside was left stuck to the side of the vessel. Light was then used to detect the formation of layers by shining it through the suspension, when this was observed the tap at the bottom was released and the layer decanted into different containers for the top and bottom fractions.

Fig 3.3 12L separator

The separated fractions now sat in separate containers with approximately 10L of water used in the separation. To remove this within a reasonable time frame a suction rig (**Fig. 3.4**) was used to pull the water through a pad of filter paper.

Fig 3.4 Separation equipment used

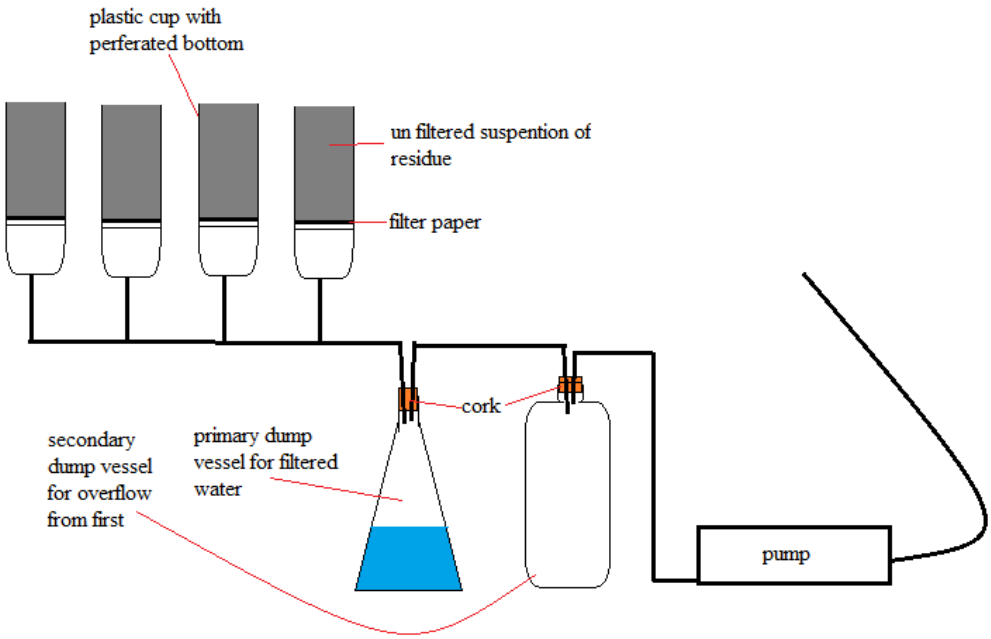

Fig 3.5 Separation equipment schematic

This apparatus was made at the University of Leeds and consists of a vacuum pump connected in series to a single dump vessel; this is in turn connected to two more dump vessels in parallel. The point of this being; that in order for the water that is being extracted to contaminate the pump it would have to fill up two vessels first.

These two dump vessels were connected in parallel to two cups each of which and a perforated bottom capable of holding/supporting filter paper and 1L of liquid below the rim of the filter paper.

After the tests had been carried out it was noticed that soot had become stuck in filter paper (**Fig. 3.5 and Fig. 3.6**). This was noted but unavoidable as the pump was already taking 2 hrs to completely pull the 10L of suspension water away from the particles, reducing the pump pressure would have made this wait too long given the time allocated to this task. If this was re-done in the future it would be advisable to use a lower powered pump and allow more time for the procedure.

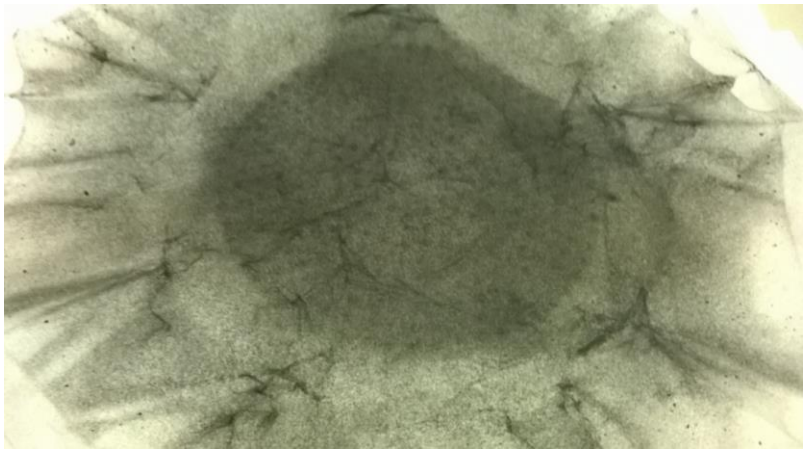

Fig 3.6 Top fraction filter paper

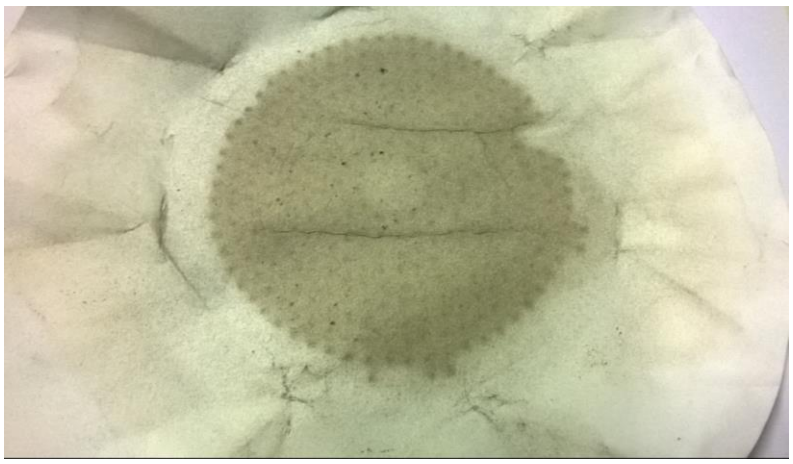

Fig 3.7 Bottom fraction filter paper

3.2.2 Residue separation equipment

The equipment used for this was a 12L Sigma-Aldrich large separator funnel as this had the 3 aspects needed to adequately fulfill the role of separator –

1. The hole at the bottom through the tap had to be large enough that it wouldn't get clogged by the particles (minimum 2cm diameter).

2. The shape of the separator had to be either spherical or inverse cone shaped in order to provide a large surface area for the residue –water interaction. Without a large enough area the particles that were light enough to float would have impeded the downward movement of the heavier ones, possibly forcing them to stay within the floating fraction.

3. The vessel must have a large enough volume that the mass of residue added to the water doesn't completely block out light from passing through.

The water separation equipment (**Fig 3.4**) is an in house "homemade" piece of apparatus that consists of a vacuum pump attached to two stages of dump vessels. The pump as shown is attached to the four cups holding the filter paper and unseparated residue suspension. When the pump is active the water is pulled through the filter paper, leaving the residue behind. The water is deposited in the primary dump vessels with a follow up dump vessel in series before the pump in case the water overflows the first stage. This is done as the pump (Edwards vacuum pump) is for air and would be damaged if water was run through it.

When the dump vessels are ¾ full of water they are emptied into the drain (there are no contaminants to prevent this). The filter paper is then removed from the cups and left to air dry, new filter paper is used to replace it and another test is run.

3.3 Material analysis

All the materials tested were analysed before and after combustion, to determine the original composition, what was left and therefore determine what was burnt during the dust combustion. Additionally any changes in the fuels condition (particle size/shape etc.) will be analysed and examined to try and determine how and why any such changes have come about.

3.3.1 Elemental analysis

The elemental analysis of materials was performed on a Flash 2000 Thermo Scientific Analyser with a single reactor for the determination of the elements carbon (C), hydrogen (H), nitrogen (N) and sulphur (S), the percentage of oxygen was calculated by difference from the original weight. The formula for calculating the as received oxygen is given in section 2.3.0.1 (Harker, 1981). The percentages of CHNS were given in as received form.

The typical amount of sample used was 3-4mg which was placed into a tin capsule and crushed shut. Coal, unlike biomass, contains high percentages of carbon and sulphur therefore vanadium pent oxide (V_2O_5) was also added along with the coal sample in the capsule (approximately the same weight as sample) to ensure

adequate burnout. To try to ensure a consistent sample area and to exclude atmospheric N_2 the samples were formed into cubes by folding and compressing the sample without breaking the tin foil.

To try and ensure that the sample is reprehensive when dealing with such small sample sizes, the containers were well shaken first then a spatula of material was taken from the top, middle and bottom of the bottle. These three scoops were mixed to create two samples for the analysis. The use of two samples enabled an average to be created; this is what is used in the elemental composition. If the variation for the carbon and sulphur was greater than 5%, the measurements were repeated to ensure accuracy (however there were some issues with the residue samples due to the small sample size and large particle weights making it hard to get reprehensive/consistent samples).

The samples were then placed into a circular auto sampler and dropped into the oxidation reactor tube kept at 900-1000^{o}C where they were combusted in the presence of injected oxygen (5-10 seconds of oxygen injection depending on sample) to ensure complete oxidation. The reaction of oxygen with the tin capsule is an exothermic reaction which raised the temperature to approximately 1800°C. The material was converted into elemental gases (CO_2, H_2O, NO_x, SO_2 and SO_3), these were then flowed over a reducer of copper in the presence of tungsten trioxide to convert NO_x into N_2 and SO_3 to SO_2. These were separated in a gas chromatographic column within the unit and detected by a thermal conductivity detector (TCD).

3.3.2 Thermo gravimetric analyser

Thermo gravimetric analysis was carried out using a Shimadzu TGA-50 thermo gravimetric analyser. This uses 4-6 mg of sample (depending on the reactive fraction) which was weighed into an alumina crucible. The small size of the samples made the risk of un-representative samples a real danger. To try to counter this 4-5 samples were taken for each test, these were then crushed with mortar and pestle into an approximately homogeneous mixture from which the test samples were taken. This ensured as far as possible when dealing with such small samples that they were accurate representation of the mean residue.

The alumina crucible along with the sample was placed on a taut band fulcrum balance mechanism. The method followed was to heat the sample under nitrogen

from room temperature to 110 ^{o}C at the rate of 10 ^{o}C /min and holding it for 10 minutes to obtain the weight loss associated with moisture content. The temperature was then again ramped to 910 ^{o}C under nitrogen at the rate of 25 ^{o}C /min and holding it for 10 min to get the weight associated with the volatile loss. After this, the temperature was increased slightly to 920 ^{o}C and air was introduced to burn off the fixed carbon content. The remaining weight after the complete oxidation of the sample was inert ash (the ash fraction dictated the initial mass used as this determines the mass loss which must be above the error margins of the detectors). The mass of the sample was measured continuously together with the temperature and this enabled the mass loss as a function of temperature to be determined (**Fig. 3.8**). The flow rates of nitrogen and air were fixed at 50 ml/min.

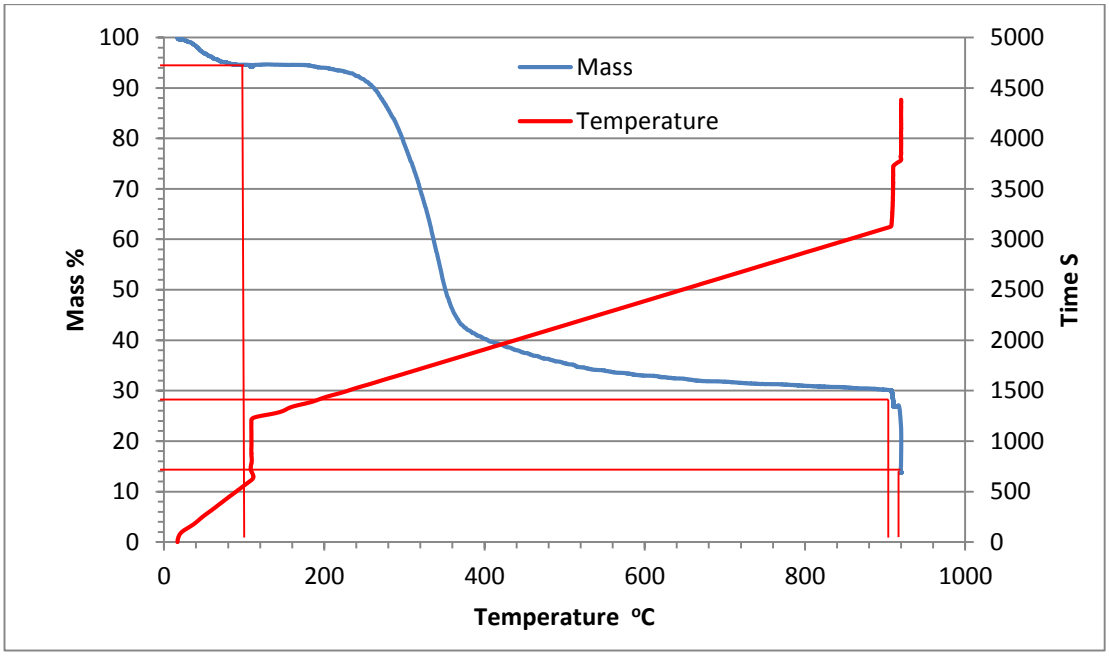

Fig 3.8 TGA percentage mass loss against temperature for EFB.

So for **Figure 3.8** the moisture content is 5.7%, volatile material is 67%, Fixed carbon is 13.5% and the ash is 13.8% of the sample by mass.

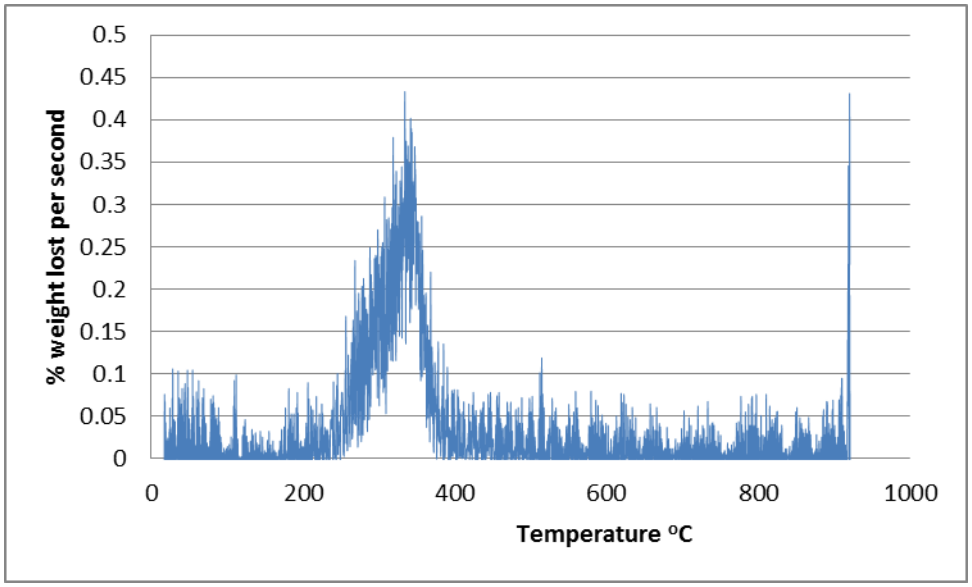

Fig 3.9 TGA mass loss per second against temperature.

A typical TGA curve of EFB pellets is shown above and its fractional weight loss as a function of temperature is shown below that.

The equipment uses 4-6 mg of sample, this results in <63µm samples forming a layer on the bottom of the pan while larger particles lie on top of each other with large empty spaces between the particles. This could be reducing the effective particle surface area to a bulk particle surface area as a result. However the heating rate was slow and hold times were used at the end of each successive temperature change to determine if the fractions (moisture, volatiles, ect) had been completely driven off at the end of each section.

3.3.3 Calorific values

Measurement of the gross calorific value for some materials was performed in a Parr 6200 Oxygen Bomb Calorimeter. Calorific values are measured by comparing the heat obtained from the sample to the heat obtained from a set material. A representative sample was burned in a high-pressure oxygen atmosphere (25 bar) within a metal pressure vessel or bomb. The energy released by the combustion was absorbed within the bomb calorimeter and the resulting temperature change was used to measure the heating value of sample.

Hammed Sattar carried out comparisons of the calculated CV to the measured CV for a number of materials and concluded -

“Coal sample showed the highest deviation from the measured values indicating that this relationship is not suitable for calculating the calorific values of coal whereas for the biomass the absolute error was within the specified range of the equation” (Sattar, 2012). Therefore this is the equation that will be used during this work.

3.3.4 Particle size distribution

The particle size analysis of the raw materials and of the explosion residue was measured by Malvern Mastersizer 2000, using the laser diffraction technique by assuming the shape of the particle as spherical. The sample is mixed with water into a paste and then added to a water pump that flows the particles through the analyses cell whilst suspended in the water. The particles in the cell are passed through a focused laser beam which scatters the light at an angle that is inversely proportional to the size of a particle, large particles scatter light at small angles relative to the laser beam and small particles scatter light at large angles. This angular intensity of the scattered light is measured by a series of photosensitive detectors. The map of scattering intensity versus angle is used to calculate the particle size. To ensure that this is accurate the refractive index of each material must be matched with that of a similar material within the database, if such a match is not found a new file that has parameters as that of the sample must be created.

Each result of particle size distribution is an average of 10 measurements, where there was no fall out or agglomeration of the particles in suspension.

This instrument measures the light diffracted from the actual particle and then gives it the size of a spherical particle that would diffract that amount of light, however biomass particles are not spherical, as has been shown. This spherical particle of the same refractive value as the cylindrical biomass particle will not have the same - mass, volume or surface area as the actual particle. Nevertheless, this method does enable the size distribution of two biomass dusts to be compared to each other.

Results come as D [3/2] (volume : surface area ratio), d_{10} (particle diameter at which cumulative 10% of sample by volume is reached), d_{50} (cumulative 50% of sample) and d_{90} (cumulative 90% of sample).

The results were given in volume terms as it allowed for a better idea of the distribution of the mass (even if it did not accurately represent the actual mass distribution) within the particle size distribution.

3.3.5 Surface morphology – SEM

The surface morphology of the materials and of the explosion residues was performed using a Scanning Electron Microscope (SEM), Leo 1530 Gemini (FEG-SEM). The sample materials were shaken/mixed well and 3 separate samples taken from the top, middle and bottom of each material, these 3 sub samples were mixed together and mounted on 12.5 mm diameter aluminium stubs using double-sided conductive tape. As coal and biomass are non-conductive, the sample was coated with a 10nm thick layer of gold in a sputtering coater to prevent charging of the material. Afterwards, the samples were placed in the sample holder of the SEM chamber and the pressure of the chamber was reduced to <10mbar. An electron gun produces an electron beam focused on the area of the sample, as small as 1nm in diameter. The electron beam on the sample is partially absorbed by the sample and partially reflected back as backscattered electrons (depending on the conductivity of the sample).

This was used to examine the samples pre and post combustion to try and notice any changes to the particles on an individual level such as partial burning, obvious devolatilization or distortion of the particle shape.

Fig 3.10 Leeds University Leo 1530 Gemini and attached computers.

3.4 Hartmann tube apparatus and its modifications

The Hartmann tube apparatus was manufactured by Chilworth Technology Ltd, the apparatus (**Fig. 3.12)** was originally used for the explosibility screening testing to determine whether a dust is explosible or not. This is used to test smaller volumes of material than the $1m^3$ making it more viable where a limited sample volume is available as less is destroyed in each test. Additionally due to easier operation than the $1m^3$ it is possible to do multiple (20-30) tests in a day as opposed to (4-6) in the $1m^3$. The apparatus consists of a vertical Perspex tube with 61mm internal diameter, 322mm long (volume of tube was 0.94L). The total volume of dust dispersion area was 1L which included the volume of tube plus the volume of the dispersion cup (~0.06L). The tube was mounted on a base that contains a 50mL air reservoir connected to a compressed air line. The other end of the reservoir was connected to an umbrella shaped disperser (**Fig. 3.11**), via a solenoid valve.

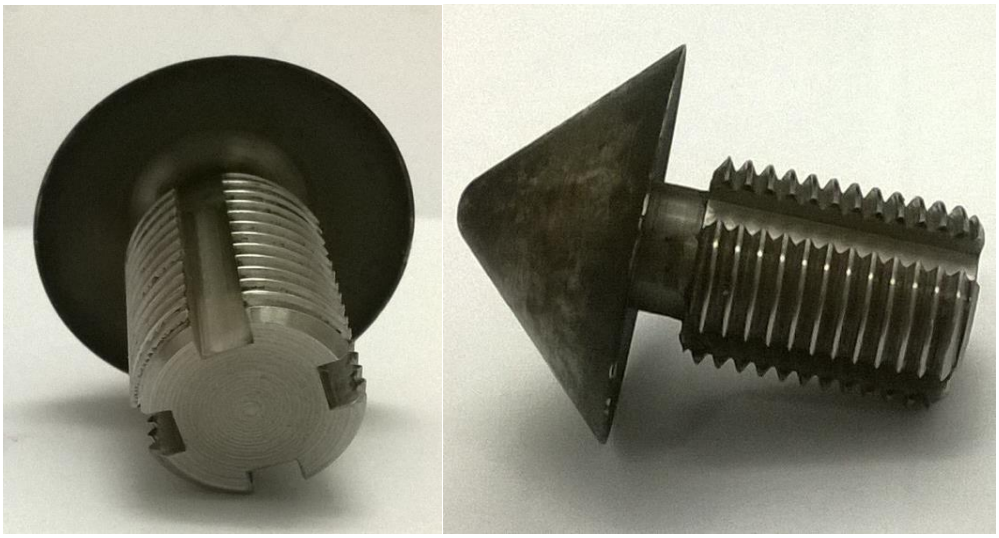

Fig 3.11 Hartmann dispersion device.

The device operates by dispersing the dust inside the tube with a deflected air blast that hits the bottom of the tube and entrains the dust, this is then ignited a third of the way up the tube using two electrodes to produce an arc of electricity to ignite the dust suspension. The apparatus has a timer that is used to alter the delay between the activation of the air reservoir and the spark, for these tests though this was kept at 0 seconds.

The pressure rise from combustion is then registered by the transducer up to the burst pressure of the tinfoil vent on the top.

Fig 3.12 Leeds University Hartman vessel.

The Hartman vessel used by Leeds University has some modifications from the original; it has a set of three insulated type-K thermocouples arranged vertically up the tube to measure flame arrival allowing for flame speed calculation and accurate determination of whether an explosion has taken place. A piezoelectric Keller PAA-11 pressure transducer has also been added to the top of the tube to determine explosive overpressure prior to the vent bursting. In the Hartman apparatus an explosion is deemed to have taken place when a pressure rise of 100 mbar above the air injection rise (350 mbar) is recorded and/or if the flame travelled to (and was recorded by) the second thermocouple 10cm from the spark location. The addition of a flame propagation distance criteria made the equipment similar to the standard EU gas LFL determination method (BSEN1839, 2003) with the additional advantage of the use of thermocouples to detect flame travel instead of the human eye.

The Hartman vessel is capable of measuring the – Minimum Explosive Concentration (MEC), the Leeds model can also measure – K_{st} (up to the vent bursting pressure) and flame arrival time at three points.

However, due to the tube design, quenching occurs and the parameters produced differ from larger and more spherical vessels. The difference in dispersion methods is probably also producing different turbulence levels and dust distribution patterns within the vessel.

The manufacturer of the Hartmann tube recommended an air injection pressure of 4 bar. However Clara Huescar carried out tests that showed that due to variance in the weight of dust loaded in to the vessel this pressure failed to disperse different concentrations equally. Higher injection pressure gave more repeatable MEC results and decreased the range of concentrations for which explosions occurred intermittently, therefore producing a more accurate determination of minimum explosible concentration. For this reason it was decided to use the highest air injection pressure allowed by the manufacturers, 7 bar.

The test procedure was to start with 1g of dust and repeat the test three times. If that mass was flammable (any of the 3 tests showing activation of the thermocouples or pressure trace) then the mass of dust was decreased by half and the test repeated. In the case of no flame propagation the mass of dust was increased by half (up to 4g where there was insufficient space for more dust). Once the minimum explosive concentration is found by this method the limit is further refined by halving the difference between the explosive and none-explosive concentrations. This was done until no ignition occurred in any of the three tests, this was carried out down to 0.01g using highly accurate scales.

3.4.1 MEC definition in Hartmann

To determine when an explosion had propagated it was defined as the activation of the second or third thermocouple AND/OR the rise of the pressure trace 100mb above the injection pressure. It should be noted that although no usable flame speeds were generated from the thermocouples, they were still used for determination of the MEC. How these are measured is covered in the preceding sub chapters.

Due to running three tests to generate one data point the chance of ignition was either 100%, 66.66%, 33.33% or 0% this was used when plotting MEC which is given as a percentage chance of ignition.

The MEC was measured as the leanest mixture that did propagate a flame, section 2.3.1 as specified in the European standard (BSi, 2012).

3.4.2 Thermocouple results

Actual readout of fine dusts from Hartman thermocouples show the thermocouples activation times, as the distance between the spark and the thermocouples is known the flame speed can be calculated as distance over time taken to reach the thermocouples.

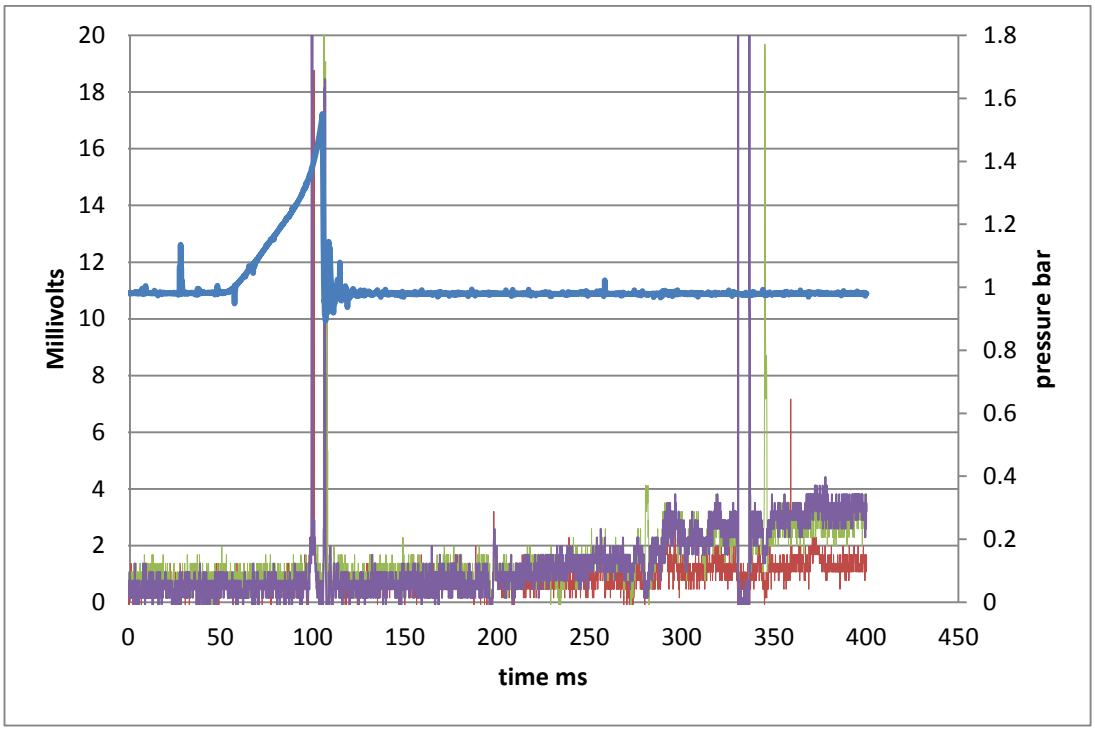

Fig 3.13 Pressure and thermocouple readouts from the hartmann apperatus for lycopodium powder

There appears to be an initial response from the thermocouples at 100ms that corresponds with the pressure rise, however, there are actually 2 rises (**Fig. 3.14**) the first of which activates all 3 thermocouples simultaneously. The second produces activation of thermocouples in the correct order; however the flame speeds are 250 and 500 m/s from the thermocouples which is clearly unreasonable.

Even when the responses begin to show sustained changes after 200ms the third thermocouple begins to respond first implying that this method of flame speed detection is flawed. Any flame speeds detected by the thermocouples were from the constant pressure stage of the flame propagation; therefore any tests that ignited but did not have a secondary propagation were unable to generate a thermocouple flame speed.

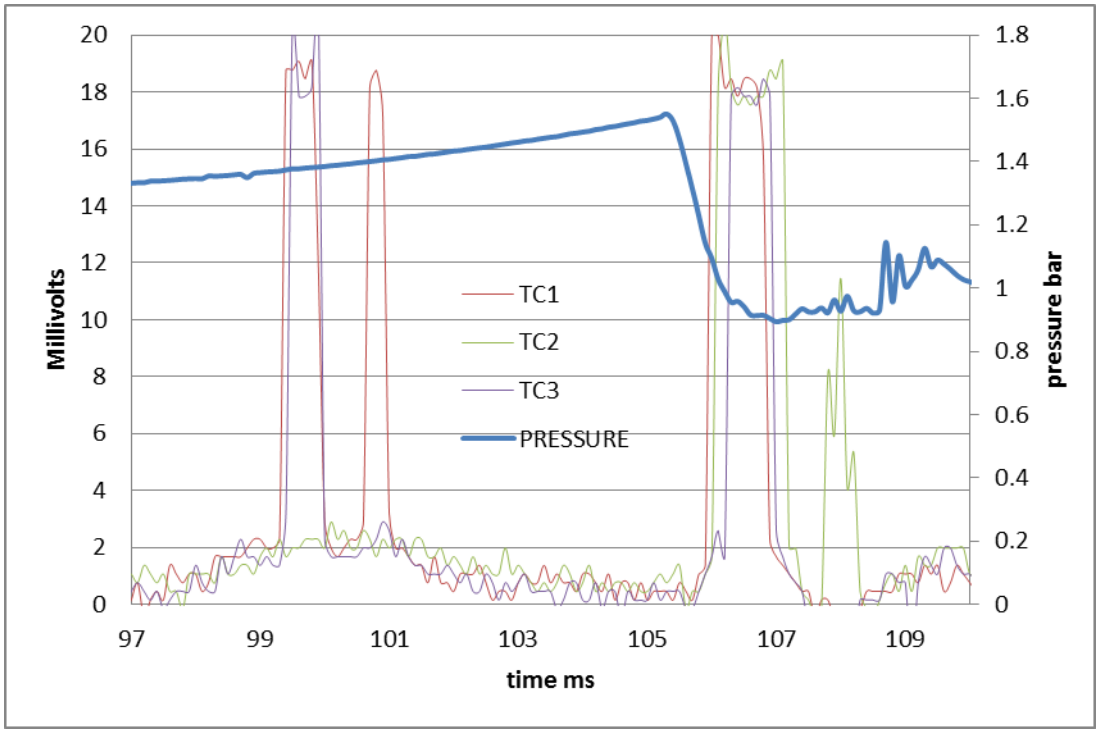

Fig 3.14 Thermocouple responces at and around the vent bursting

Although as has been shown (**Fig. 3.14**) the thermocouple responses are bad for lycopodium powder, large particles produce slower flame growth (section 3.3.4) therefore by the time vent bursts the flame is, in most cases, still below the second thermocouple. When the vent bursts it fires the first flame though the second and third thermocouples (**Fig. 3.19**) producing a simultaneous activation (**Fig. 3.14**) of the thermocouples, therefore preventing generation of usable data from them.

The flame speeds that were generated (from the thermocouples) were plotted against the pressure rise data from the same tests (**Fig. 3.15**), due to negetive or unrealisticaly high flame speeds, some tests did not produse usable flame speeds. Five materials were ploted in this way, as it has been demonstrated (section 2.3.3) that the flame speed should scale with rate of pressure rise or its derivitive K_{st} this was expected (especialy in this apperatus in which both measurments are taken during the constant pressuere period). This correlation is not obviously displayed by this data (**Fig. 3.15**).

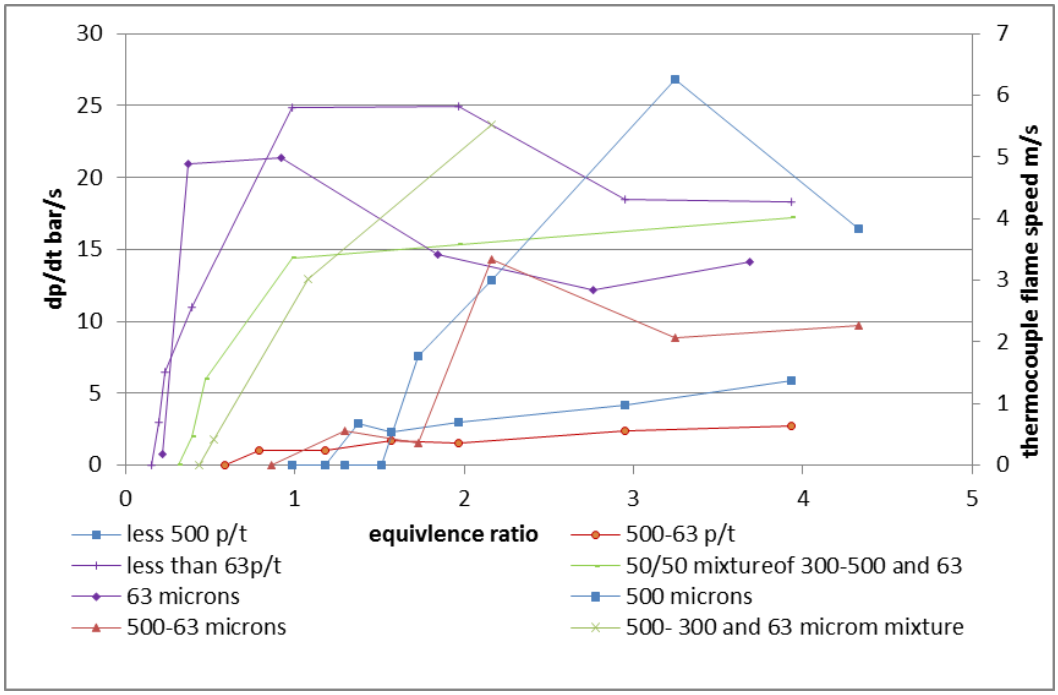

Fig 3.15 Rate of pressure rise against thermocouple flame speeds.

For this reason the high speed video was used to record tests from then on to generate flame speeds from the footage as will be explained in section 3.4.4.

3.4.3 Rate of pressure rise

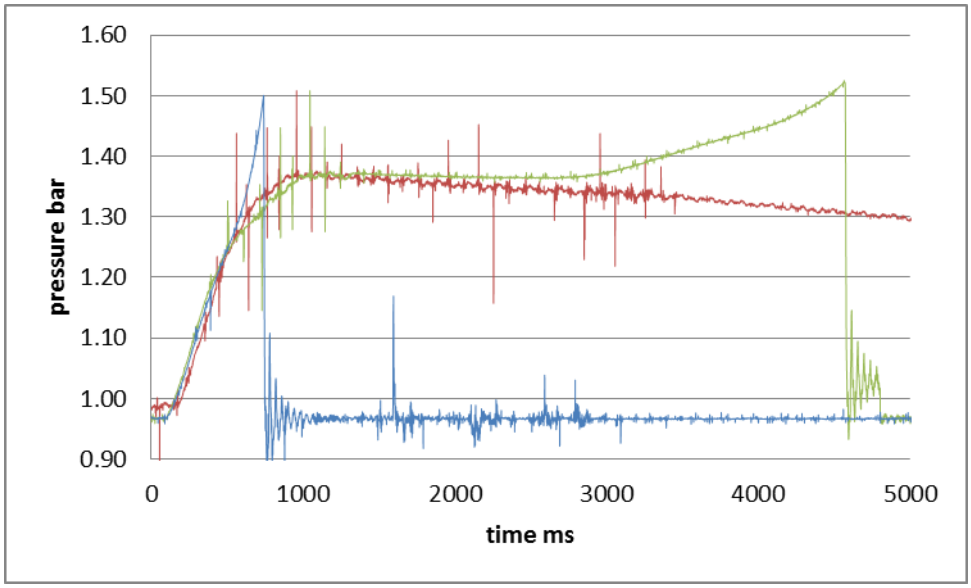

Fig 3.16 Without dust (red), With dust - coarse and ignition (green) and With dust - fine and ignition (blue).

The rate of pressure rise was measured over the last two milliseconds before the vent burst. This was chosen as, due to the physics of combustion (section 2.3.3), this is the point (in this apparatus) where the highest K_{st} is produced due to the slight pressure increase which is due to compression prior to the vent bursting.

However, due to inconsistencies in the tinfoil, scratches caused when handling or other unknown issues, some tinfoil vents were bursting before the injection pressure had been fully reached. If this happened the test was re-run.

3.4.4 High speed video

High speed videography was carried out on the Hartman explosions at 5000 fps to try to determine the flame speed, shape and how it interacts with the particles. This was done as full tube and close up footage, the first contains the whole propagation through the tube while the second is only focussed on the spark area to investigate the flame-particle interactions and was mainly used on near limit mixtures due to the small distances travelled by these flames.

This first method worked well allowing the propagation behaviour to be clearly observed, as it passed up the tube. These videos were then cut into single images and joined together to create a montage of the propagation that allowed for the determination of flame shape, structure and flame speed.

The Hartman vessel as described has three thermocouples inserted into the tube at 5cm intervals, this was utilised in conjunction with high speed video to generate a visual flame speed from the apparatus as these can be used to measure flame propagation distance. To do this the still images were combined into a single image allowing for determination of the thermocouple locations in all the images (as these are all the same size). From this the propagation of the flame up the tube with time can be determined by comparison to the known thermocouple locations. This is how the high speed video flame speeds were generated.

These thermocouples are designated with red lines (top 3) in the propagation montages produced while the spark is also shown in the same way. This was then compared to the thermocouple data from the same test run with the same material on the $1m^3$.

The Hartman equipment was operated on a 0ms ignition delay. At this setting the spark begins to discharge at the same time that the air blast is activated, therefore by the time the air blast has begun entraining the dust into the spark zone the spark is already active.

This results in a situation (generally for fine dust) where the whole of the dust (fuel load) is only distributed in the bottom 1/3rd of the vessel at the time of ignition (**Fig 3.17**), the red lines denote the dust cloud boundary. The picture also demonstrates that even below this there are different shades of colour present within the unburnt dust cloud indicating concentration gradients within the cloud.

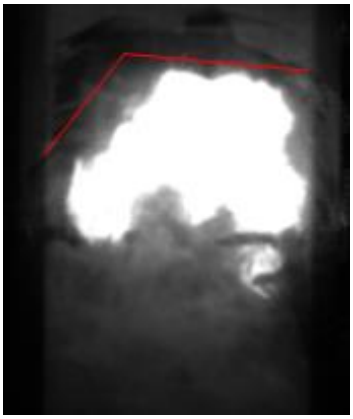

Fig 3.17 Image of dust distribution around the spark at ignition <63µm oak.

This will affect fine particle materials more than large ones due to the lower time to ignition of fine dust mixtures resulting in more stratification, hence an apparentaly lower than actual MEC for fine particles in this apperatus.

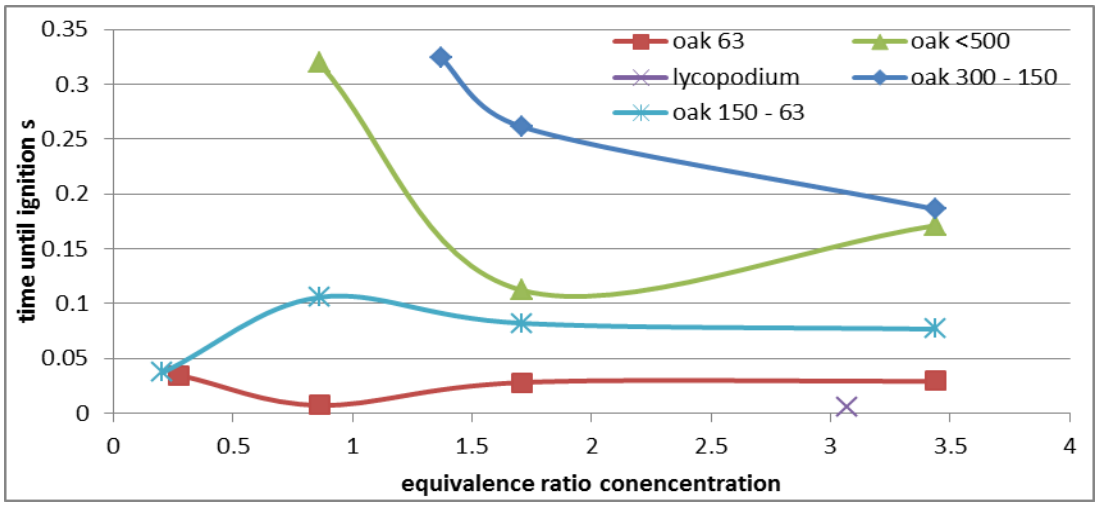

Fig 3.18 Ignition delay for different particle size materials in the hartmann apperatus as a function of equivlance ratio.

An MEC of 0.2Ø as found for oak <63µm or 0.17Ø for oak 63 – 150µm become's 0.6Ø and 0.51Ø respectivle as the full fuel load is only burning in 1/3rd of the avalible air. This makes sense as no HC gas (exept as H_2 or acetylene) will burn at stoichecemetric equvlence ratios bellow 0.4Ø.

Tests by Azam Saeed, showed that with no ignition the dust still only managed to distribute itself over 80% of tube, and for large particle materials this was even smaller. Therefore this equipment will always under predict the MEC values for a material even if the ignition delay is adjusted to occur at maximum dust distribution.

If bigger particles are burning behind the flame front then these would be in the products of the first combustion at elevated temperatures. It would therefore be reasonable to expect that these would devolatilise further to produce more volatiles. This appears to be demonstrated in oak <500µm (**Fig. 3.19 - 3.21**) where the initial combustion in rich mixtures has a secondary flame (**Fig. 3.19**) propagation that is not present in leaner mixtures (**Fig. 3.21**).

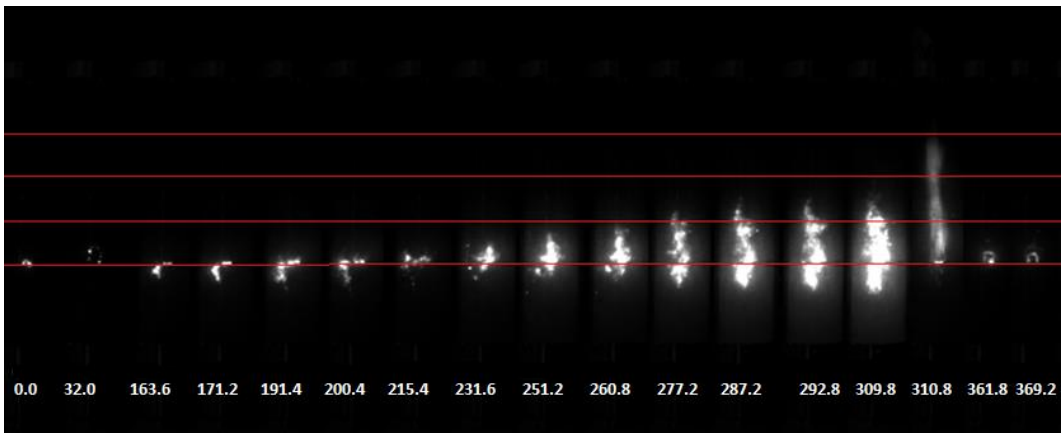

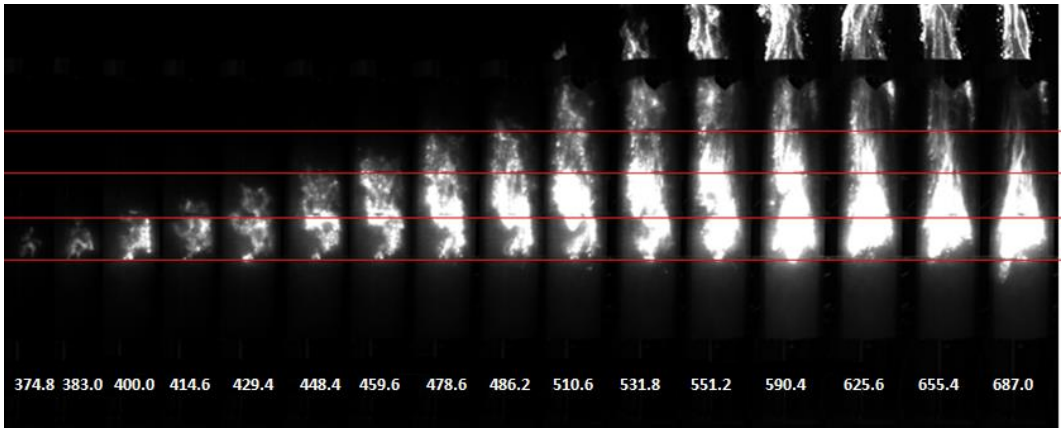

Fig 3.19 Oak <500µm (Ø=1= 218.9) 1 g, 750g/m^3, Ø=3.44

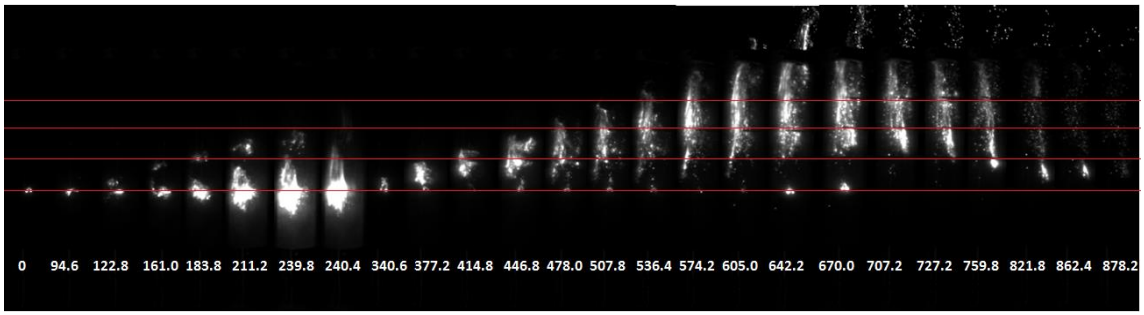

Fig 3.20 Oak <500 (Ø=1= 218.9) 0.5 g, 375g/m^3, Ø=1.71

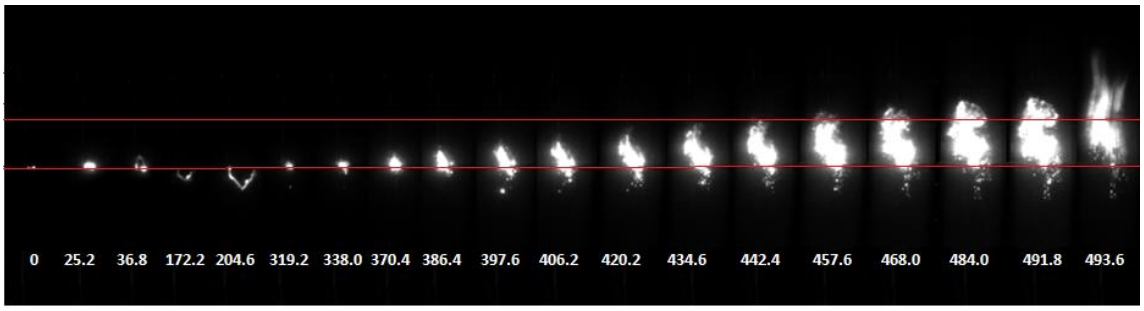

Fig 3.21 Oak <500 (Ø=1= 218.9) 0.25 g, 187.5g/m^3, Ø=.86

Additionally the <500µm oak, 375g/m^3 video shows far more localised independent flames in the secondary propagation than 750g/m^3, possibly due to the fines being burnt off in the first propagation therefore forcing the secondary flame front to propagate on the devolatilised volatiles and the particles still producing them. This idea is supported by the stabilised independent combustion at the top of the tube in **Figure 3.22** that could only be caused by unburnt volatile gasses from the second propagation mixing with air outside the tube to produce this external flame.

When the concentration is lowered, the distance between these leftover large particles increases to the point where propagation of a secondary flame becomes impossible. This would therefore suggest that it is a surface area dependence, as oak <63µm shows a smooth, uniform flame shape at all concentrations, **Figure 3.22 3.23** and **3.24**.

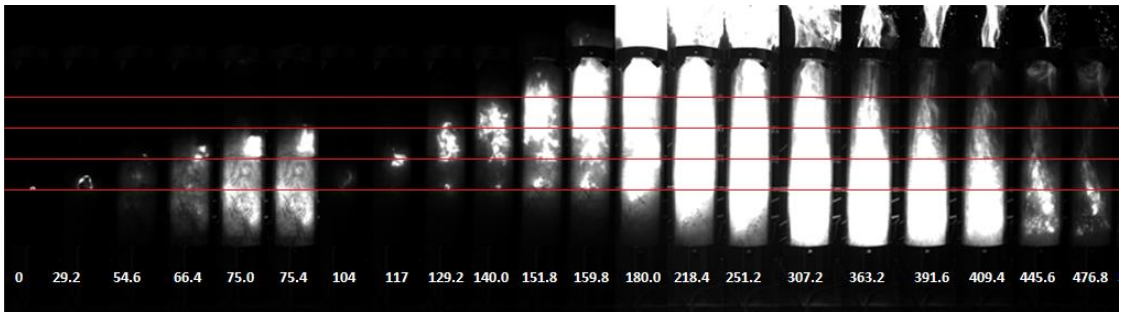

Fig 3.22 Oak <63µm (Ø=1= 218.9) 1 g, 750g/m^3, Ø=3.44

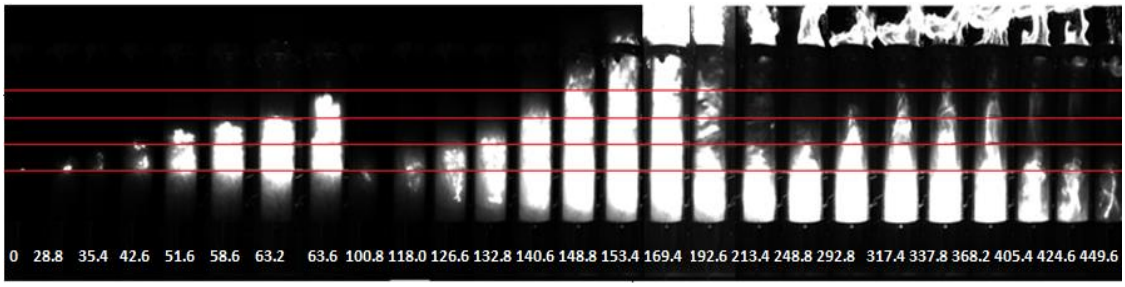

Fig 3.23 Oak <63µm (Ø=1= 218.9) 0.5 g, 375g/m^3, Ø=1.71

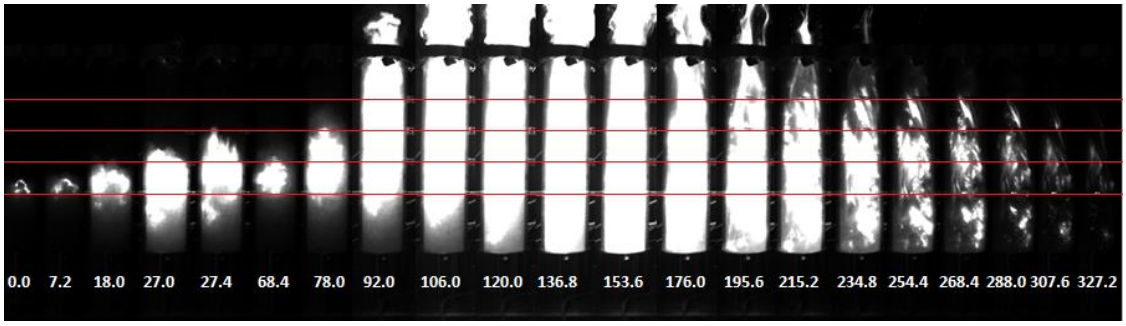

Fig 3.24 Oak <63µm (Ø=1= 218.9) 0.25 g, 187.5g/m^3, Ø=.86

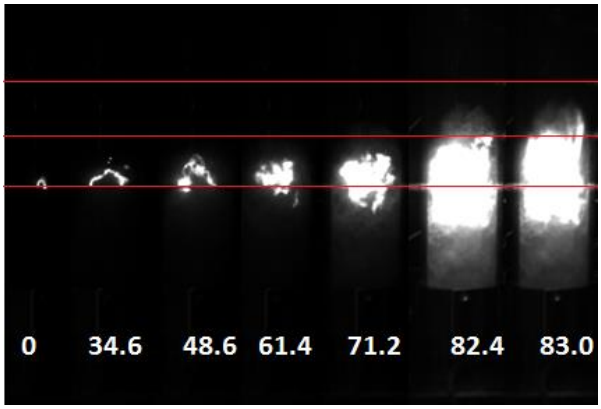

Fig 3.25 Oak <63µm (Ø=1= 218.9) 0.08 g, 60g/m^3, Ø=0.275

These flame propagation videos were used to plot the progress of the flame up the Hartmann tube (**Fig. 3.26**) using the leading edge of the flame as the reference point and comparing its progress visually to the height gauge given by the thermocouples. The gradient of these lines was taken as the flame speed.

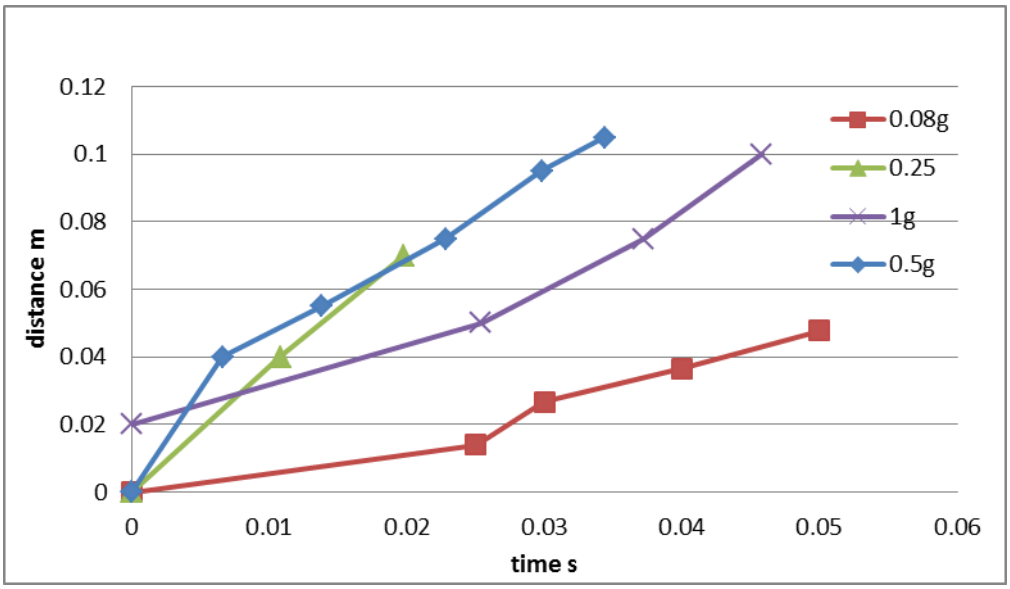

Fig 3.26 Flame speeds of oak <63µm at different concentrations.

When these flame speeds are plotted against concentration (**Fig. 3.26**) and rate of pressure (**Fig. 3.27**) rise (section 3.4.3), there is a much better correlation than was found for the thermocouple flame speeds (**Fig. 3.9**).

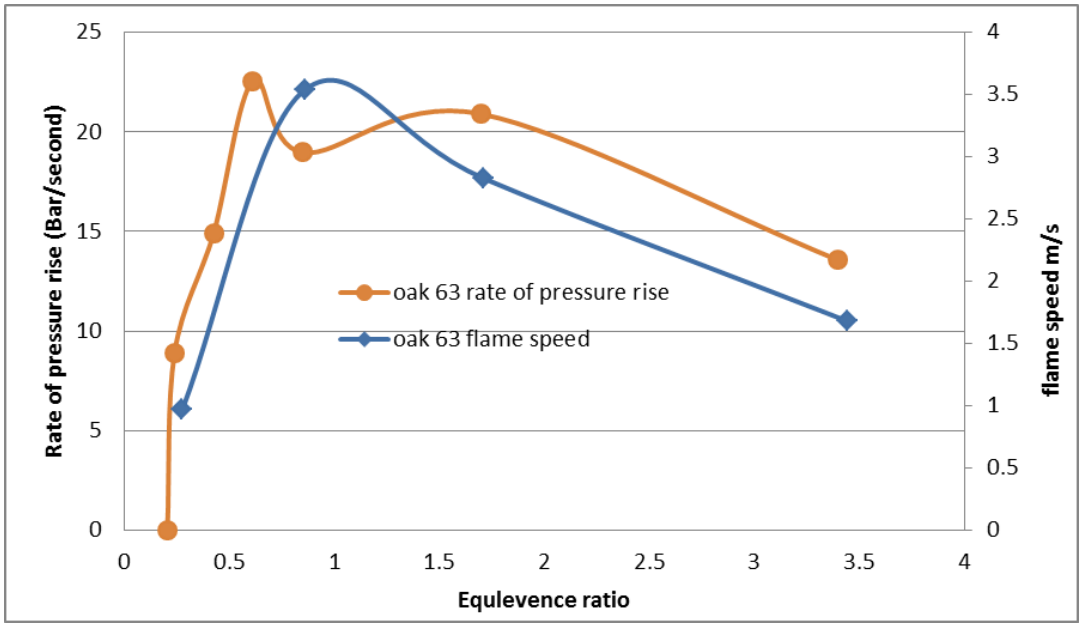

Fig 3.27 Flame speeds of oak <63µm compared to pressure results from same tests.

For this reason the only flame speed results that will be presented for the Hartman apparatus were from high speed video footage.

3.5 The 1m^3 dust explosion vessel set-up

The 1m^3 ISO standard vessel was originally developed by Bartknecht (1989) for his work on dust explosions. It is not spherical, but a 1.2m diameter cylinder with rounded ends and a length to diameter ratio of 1. This is considered to be the most reliable dust explosion test vessel and is the vessel specified to be used in the ISO dust explosion standard. Made of solid steel and rated to withstand up to 25 bar pressure rise from ambient. It consists of two interconnected chambers, the 1m^3 explosion vessel (actually 1.138 m^3 for the Leeds University vessel) (**Fig. 3.28**) and the dust container (**Fig. 3.29**) mounted above. As can be seen (**Fig 3.28**) for access to either dust pot or the main vessel a steel plate and gasket must be removed along with the fastening bolts that secure these.

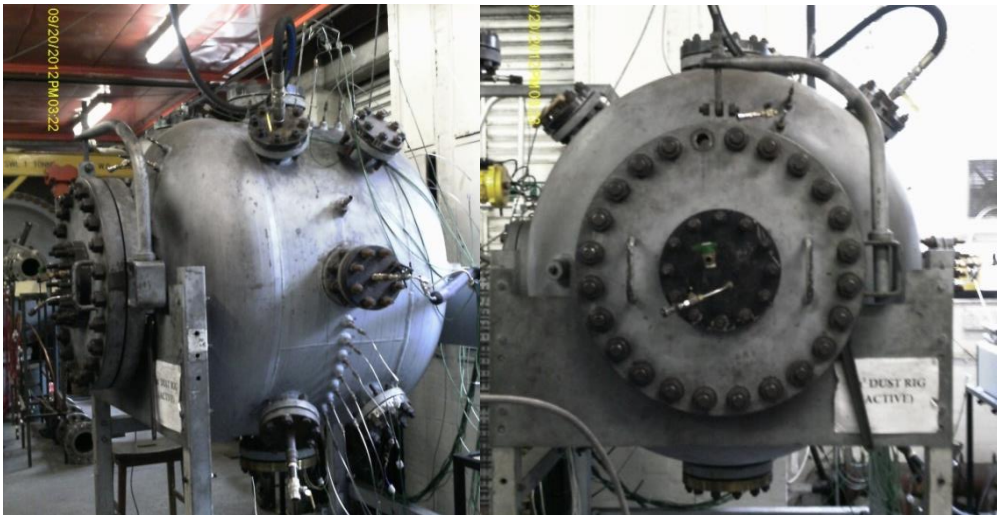

Fig 3.28 Leeds 1m3 vessel from front and side

The vessel was constructed to the specifications of the ISO 6184/1 (1985) ‘standard for the determination of explosion indices of dusts and gases’ (6184-1:1985, 1985) with the design code of 5500:1997 (BS-5500, 1997). The vessel was pressure rated to 25 barg, therefore it will withstand any high pressure produced during an explosion process as the maximum working overpressure for this vessel is 10barg.

Fig 3.29 Dust pot for Leeds 1m3 vessel

The dust pot (volume is 4.6L) dust vessel is pressurised up to 22 Bar in order to provide the injection pressure for the dust and therefore turbulence within the $1m^3$ vessel. This is connected to the $1m^3$ explosion vessel via a 19mm internal diameter pneumatic valve with a 10ms opening time and a 19mm internal diameter connecting pipe with a gradual 90^0 bend in it. The valve is actuated using compressed air from an external cylinder. The pipe is normally connected inside the vessel to a 19mm diameter C-ring with perforated holes at defined positions (**Fig. 3.30**) (BSEN, 2011), to give dispersion of the dust.

Although it should be noted “The apparatus described in this part of ISO 6184 has been chosen as the reference apparatus and is suitable for the evaluation of explosion indices of combustible dusts which have a particle size not exceeding 63 µm and a moisture content not exceeding 10%.” (6184-1:1985, 1985) This is due to particles larger than this (especially if fibrous) not flowing through this disperser.

The individual holes in the C-ring disperser have a diameter of 6mm (x2), 4.5mm (x13), and the total hole area is $263.3mm^2$. All these dimensions conformed to the requirements of the ISO standard as this allows a range of hole sizes from 4-6mm (ISO-6184/1, 1985). This can mean that different laboratories have similar but different equipment due to differing size and therefore number of holes; this will also affect the turbulence distribution, length scale and intensity created during injection.

Therefore the number of holes and their location/size affect the distribution and suspension of dust in the vessel and so influence the results it will generate. The variability in the equipment due to this lack of precision in the construction specifications leads to the vessels having to be forced empirically (discussed later) to agree with other vessels through manipulation of the ignition delay time which is also not fixed.

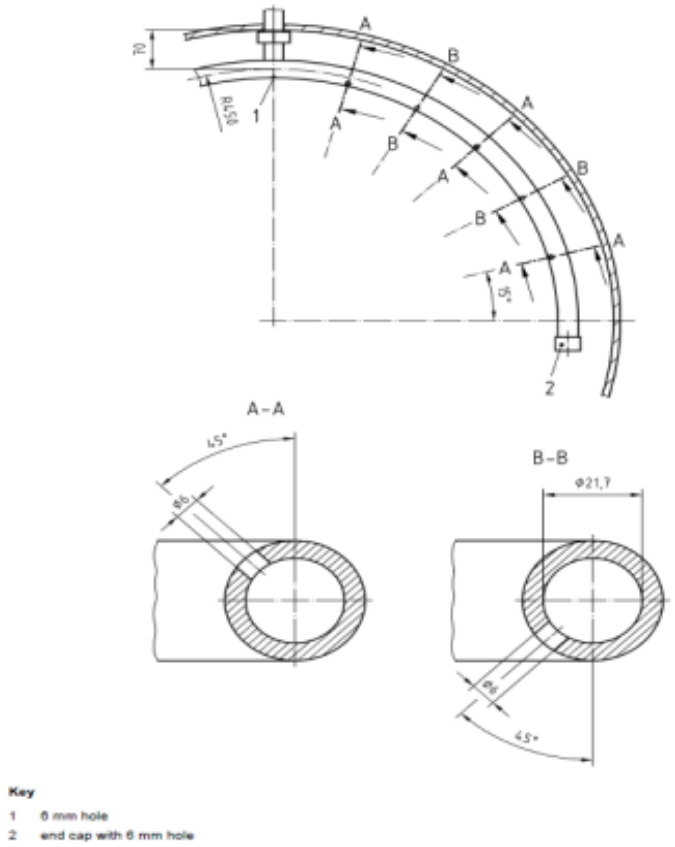

Fig 3.30 C-ring injector system.

During dust injection by the compressed air into the 1m^3 ISO vessel, the partially pressurised vessel (at 933 mBar) receives the extra air from the external pressure vessel, which brings the pressure in the test vessel to 1013.3 mBar and disperses dust placed in the external air vessel. The 4.6L external pot pressurised to 20 barg (21bar) expands to 95.3L at 1.0133 bar and thus the main vessel volume of 1.138 m^3 at 1.0133 bar (one atmosphere) has to be evacuated by 95.3L of air at 1.0133 bar, which is a pressure reduction of 95.3/1138 = 8.37% from the vessel which needs to be evacuated. This is a pressure reduction of 84.85mbar to a pressure of 928.4 mbar(a) of pressure.

This whole process, including valve opening and closing, pressure changes and ignition is shown well in **Figure 3.31** (BSEN, 2011).

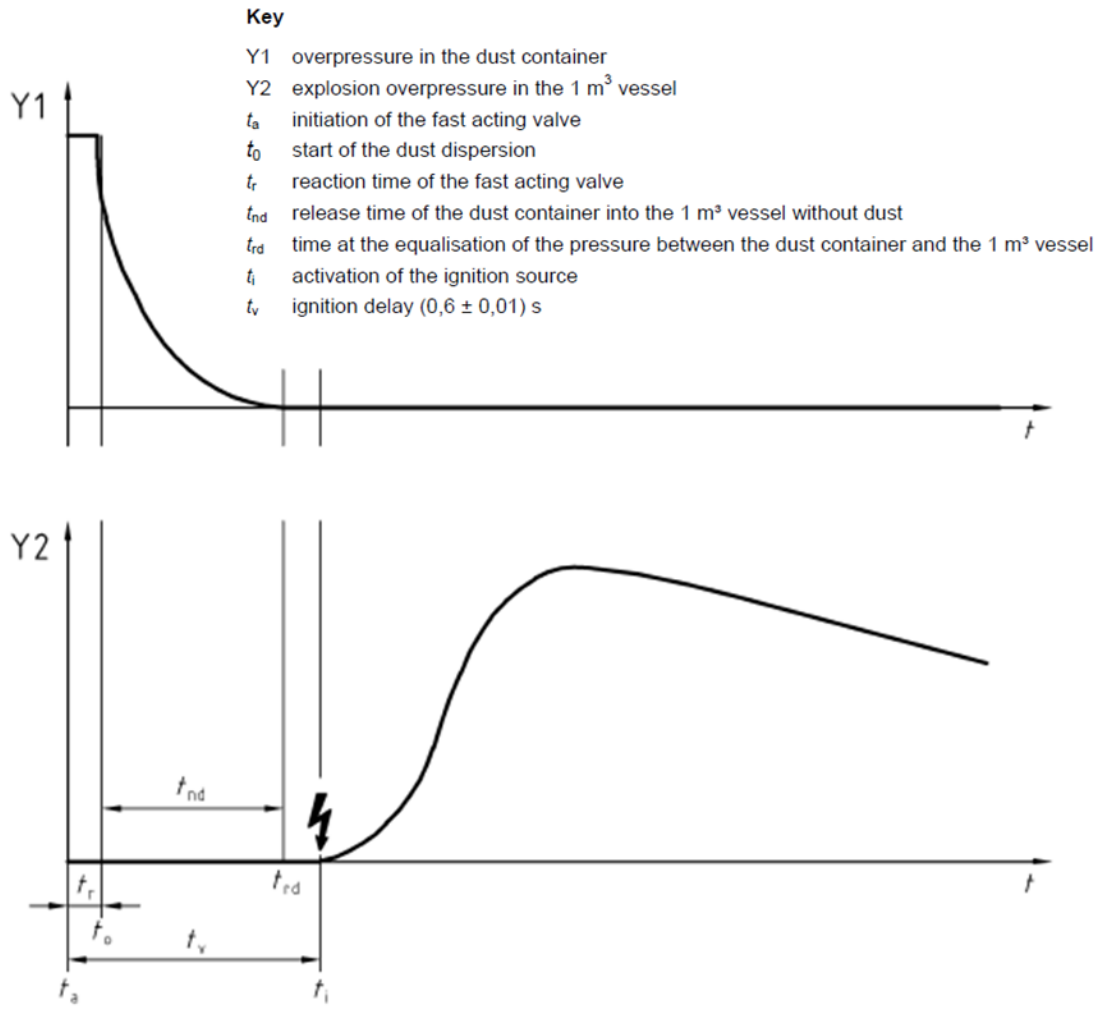

Fig 3.31 Pressure loss in injection pot and corresponding pressure rise in explosion vessel due to explosion (BSEN, 2011).

The compressed air blasts the dust and air through the 19mm diameter tube and into the C-ring. The air pressure ensures that there is sonic flow at the C-ring injection holes, resulting in dust dispersion and height turbulence levels within the $1m^3$ vessel.

The design of the injection system has a significant influence on the test results for K_{st}. Thus to achieve repeatable results between different laboratories the design of the C-ring injection system had to be standardised as this influences the dust dispersion and the turbulence levels. However the standard allows for various

different hole sizes and locations along with other parameters that are not rigorously stipulated and can influence the results from the vessel. These are -

1. The design of the C-ring injection system, tube size, total hole area, location of the holes and orientation.

2. The size of the dust vessel and its pressure. The pressure in the test vessel prior to injecting the air and dust.

3. The total injection time, which is dependent on 1 & 2 above.

4. The ignition energy (10kJ igniter) and the time delay between injection of the dust and igniting the mixture.

However, in the ISO standards it is considered to be the most reliable dust explosion test vessel and the one against which all the smaller 20 litre sphere must give comparable results.

The alternative 20L sphere is allowed by standard because it can be calibrated to give the same K_{st} values as the $1m^3$ equipment. However the 20L sphere is not a scaled down version of the $1m^3$ vessel as it has a different dust distribution system, different ignition delay and the vessel is spherical. As discussed in section 2.3.11, the results reviewed from for biomass dust that the 20L sphere does not produce the same MEC results as the $1m^3$ for the same dusts (Wilén, 1999).

3.5.1 Ignition system

The ignition source in the $1m^3$ vessel (for dust explosions) is two 5kJ pyrotechnic ignitrons (**Fig. 3.32**) producing a total ignition energy of 10kJ. The total mass of each igniter is 1.2g and consists by weight of 40% zirconium metal, 30% barium nitrate, and 30% barium peroxide. The igniters are fired by a spark box that sends current to the electrical fuse heads, igniting the chemicals which burn completely in about 10ms.

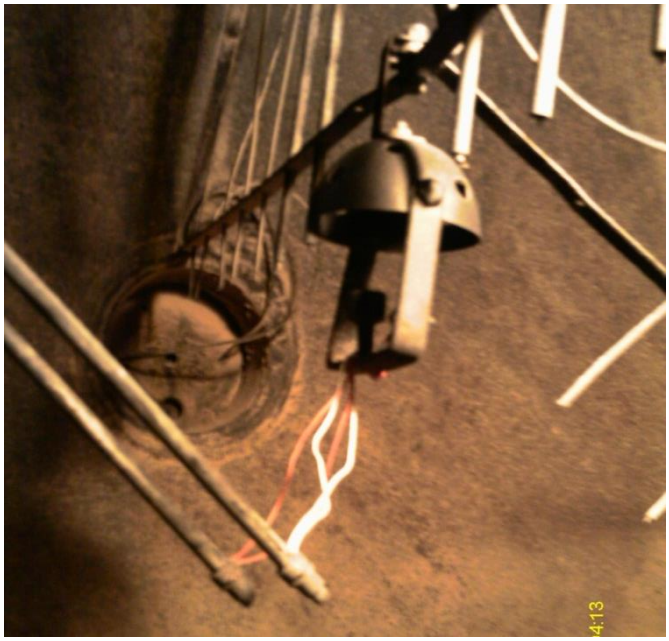

Fig 3.32 Two 5KJ igniters with blast cup.

These are located in the centre of the vessel to try to minimise quenching of the flame front by flame impingement on the walls before all the mixture is burnt. Additionally the cup that holds the igniters is designed to stop the igniters firing the flame across the vessel in a directional manner (as this would be expected from directionally restricted explosions) by containing it centrally. Without the hemisphere in place and using a single 10kJ ignitor (twice as big as normal) there was a long jet flame which impinges on the wall. The flame propagation would then start from a linier ignition source and the propagation cannot therefore be spherical. Thus, without the cap to contain and remove the directionality of the igniters the assumption of spherical flame propagation is not possible (Phylaktou et al., 2010).

3.5.2 Pressure transducers

Explosion pressures were monitored by two Keller type-PAA/11 piezo-resistive pressure transducers mounted on a flange plate in the back end of the test vessel (**Fig. 3.33**). The range for one of the pressure transducers was 0-25 bar(a) and other was 0-10 bar(a). Two transducers were used to check on the calibration of the other transducer and allow comparison between them on any single test. Another Keller type-PAA/11 piezoresistive pressure transducer (0-25barg) was installed in the dust pot to record the pressure loss from the dust pot as the dust is injected and to ensure the explosion is not re-entering the vessel.

An explosion is deemed to have taken place in this equipment if overpressure relative to the initial pressure Pi is raised by ≥ 0.3 bar (Pi is the pressure of the vessel before the ignition) (BSEN, 2011).

Three pressure traces form the 1m^3 vessel are shown below for a gaseous, finely milled solid and coarsely milled solid fuel.

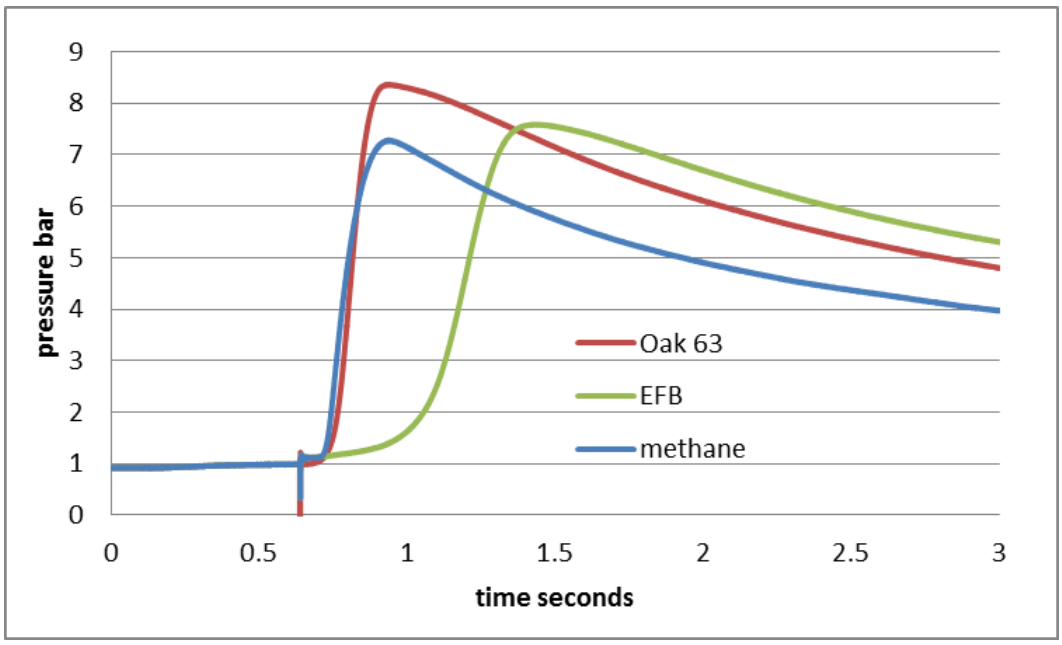

Fig 3.33 Curve from the experimental results for the pressure-time trace of an explosion test methane cornflour and EFB in the 1m^3 vessel.

The rate of pressure rise from the fine dust can be seen to be similar to that from methane while the coarse EFB dust takes a much longer time to start propagating and does so at a slower rate.

The rate of pressure rise was calculated by the differentiation of the explosion pressure signal after elimination of electronic noise, by a degree of smoothing. Two periods (A) and (B) marked in **Figure 3.34** are; constant pressure period and increasing pressure rise period respectively.

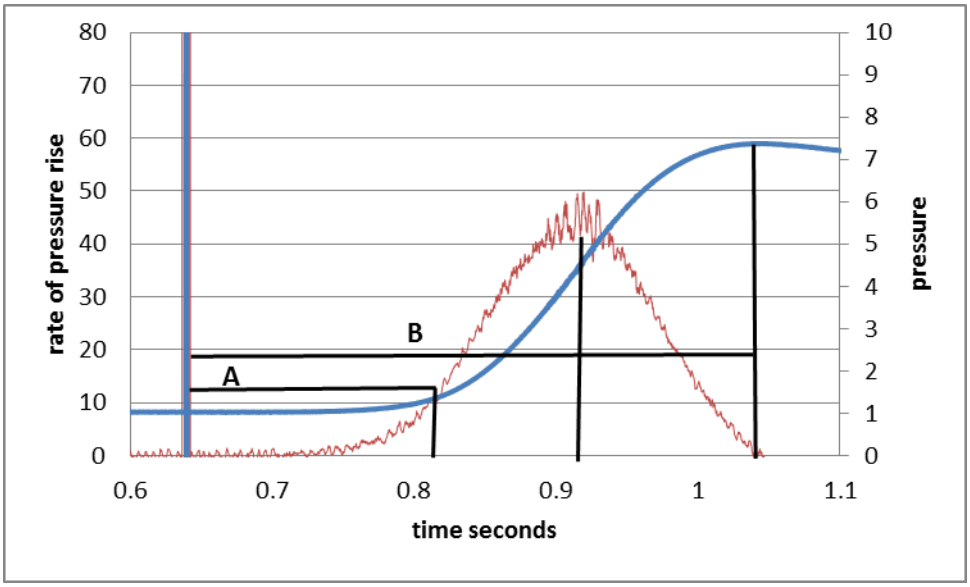

Fig 3.34 <63µm oak dp/dt and pressure traces from 1m^3 vessel.

The ISO vessel does not have the peak rate of pressure rise just before the peak pressure as should occur in a spherical vessel as it is not a sphere but a cylinder with rounded edges. If it was a sphere then the pressure would not start to rise until the flame was 50% across the diameter and there would be equal time in the constant pressure period and in the increasing pressure rise period (assuming the flame speed was constant, the flame thickness is negligible and if the vessel was spherical). This can be shown as 50% of a sphere filled with burned gases has only burnt 2% of the volume.

The volume of a sphere of diameter 1.2m, as in the ISO standard vessel, is 0.905m^3 so in the ISO vessel this leaves 0.233m^3 or 20.5% of the total volume in the non-spherical part of the flame propagation volume. This creates a problem as this non-spherical volume will be responsible for the last ~30% of the pressure rise.

Figure 3.34 demonstrates this well by the time difference between the peak rate of pressure rise (just before the flame contacts the wall) and the time of peak pressure when all the material within the vessel has been burnt. This last bit of burnt mixture is burnt with the product gases in contact with the wall which extracts heat and reduces the flame speed and the rate of pressure rise. The net effect is that this method should record a lower value for K_{st} and KG compared with values measured in a spherical vessel like the 20L sphere or the FIKE 1m^3 vessel.

A feature of biomass combustion which is difficult to understand is that for rich mixtures the peak pressure ratio did not occur at stoichiometric and did not decrease as more fuel was added. This is thought to be due to the dust in the vessel not displacing any air as this does not occur in gas explosions where the fuel displaces the air. An explanation for this is given by the fact that in a dust explosion the fuel occupies a negligible volume and there is a fixed mass of air that takes part in a constant volume explosion. For gases, the mass of air decreases as more gas is added in a constant pressure system. The heat release in combustion for all fuels is close to 3.0 MJ/kg of air and in constant volume dust combustion the air mass is fixed so the heat released is fixed and this controls the pressure rise. Additionally there is the state change of the fuel, when a solid fuel devolatilises to gaseous products the volume increases, this may be why the pressure did not decrease as more fuel was added.

3.5.3 Thermocouples

The Leeds 1m^3 vessel has been fitted with thermocouple arrays in order to track the flame development within the vessel over time. These arrays are orientated as a 2D cross through the centre of the vessel in order to track the flame speed through these different axis relative to each other. This allowed for the flame speeds in 4 directions to be calculated, therefore showing whether or not the flame propagation within the vessel is spherical.

Shown below is a picture of how the thermocouple arrays in the Leeds 1m^3 vessel are arranged (**Fig.3.35**).

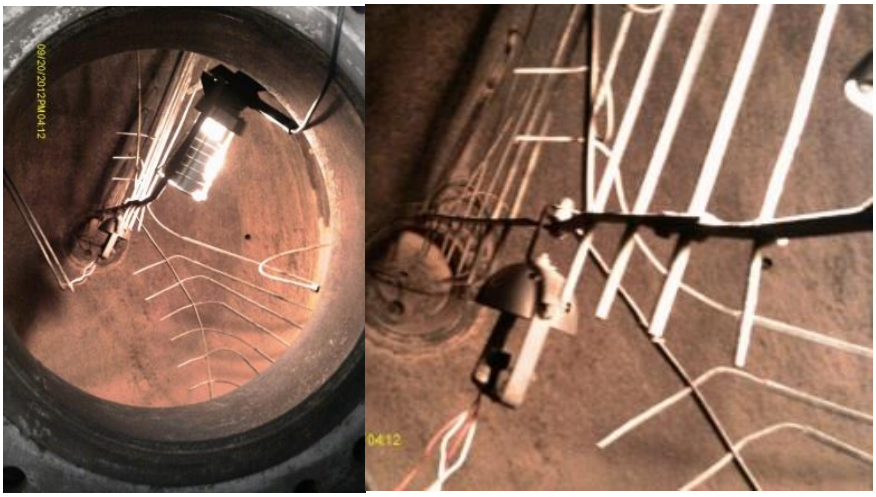

Fig 3.35 Vertical and horizontal thermocouple array.

Mineral insulated, type K thermocouples were used for flame arrival detection. A cross section of one is illustrated below, along with the fitting and method used to attach them to the vessel.

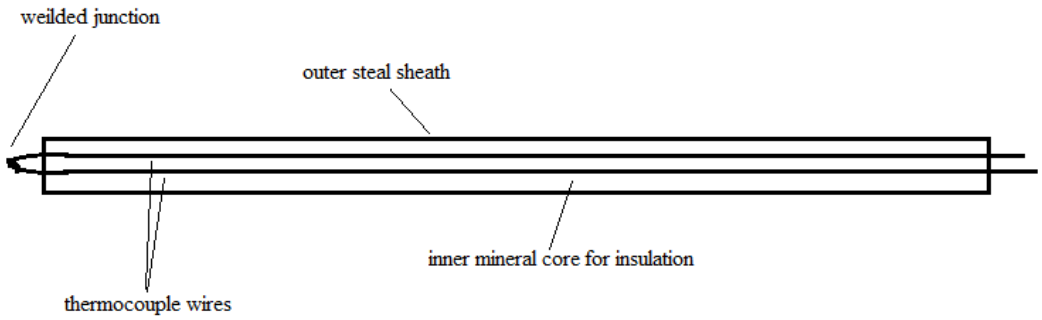

Fig 3.36 Cross section of a K-type thermocouple.

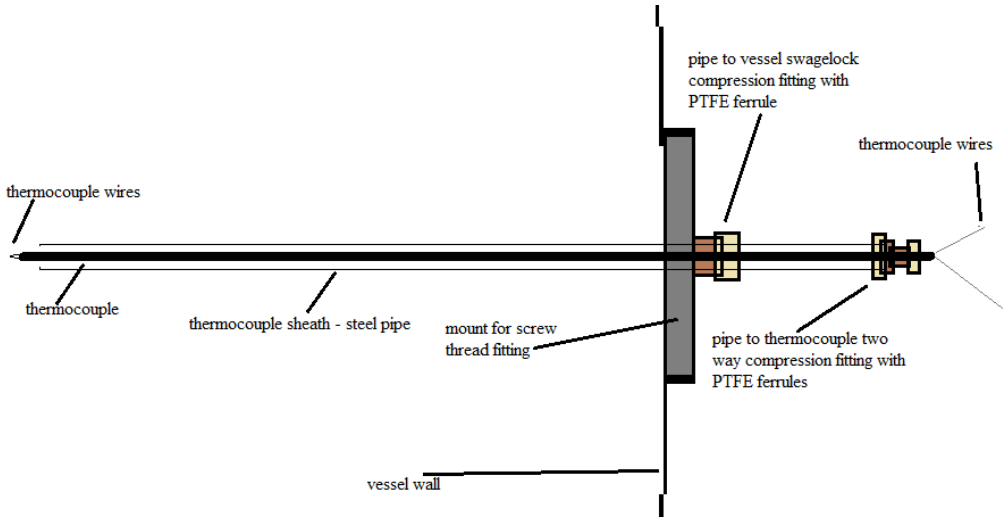

Fig 3.37 Mount used to secure thermocouple to 1m^3 vessel.

These are arranged as - An array of 4 thermocouples positioned along the horizontal radial centreline (side nearest the access hatch half of the vessel only). An array of 7 thermocouples positioned along the horizontal radial centreline (far side from access hatch half of the vessel only). An array of 9 thermocouples positioned along the vertical radial centreline (bottom half of the vessel only). An array of 3 thermocouples in the vertical upward direction is also present particularly to assist with lean flammability limit measurements, where buoyancy carries the flame vertically upward (Andrews and Bradley, 1973). The thermocouples are inserted through the wall of the vessel (**Fig. 3.37**).

As can be seen (**Fig. 3.35**) they are in a cross arrangement, horizontally and vertically within the $1m^3$ vessel with the intention of recording flame speed along all axis. This enables the spherical flame speed of a dust or gas/air mixture to be determined during the constant pressure period of the flame travel. This then enabled the burning velocity to be determined as the flame speed divided by the adiabatic expansion ratio (divided by the turbulence factor for laminar burning velocity's).

These thermocouples each have an individual data channel to transmit down therefore there is no transmission delay due to other thermocouples transmitting data simultaneously down the same channel. This ensures that the only delay present in this process is that of the time taken to transmit the data from the thermocouple to the data recorder and this is therefore the same for all the thermocouples to ensure repeatability and accuracy.

The thermocouples respond to temperature change incident upon them by changing their resistance and therefore output. Therefore by reviewing the readouts from the data logger it is possible to identify the point at which the flame front reaches each thermocouple (**Fig. 3.38**). As the distance between each thermocouple and the centre of the vessel is known, calculating the flame speed is a simple matter of how long it takes the flame front to cover a known distance.

Thermocouples respond to temperature change incident upon them, the variation in response's (**Fig. 3.38**) could be due to different tip shapes – different shapes will have different surface area to volume ratios therefore possibly explaining the different responses found. **Figure 3.38** shows two different responses from cornflour $1000g/m^3$, one has a very abrupt and distinct arrival time while the other increases gradually. Each has been marked with the chosen time of flame arrival, which was deemed the point when the signal rose above the average output for the first time.

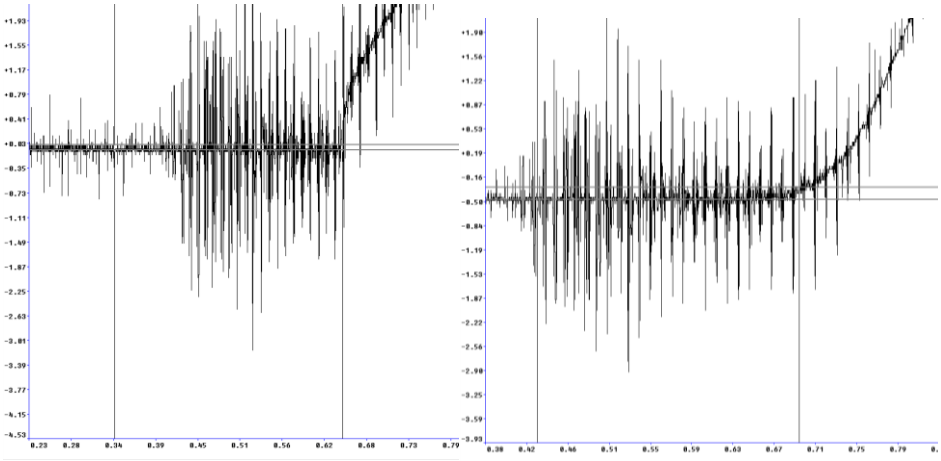

Fig 3.38 Different thermocouple responses from same test (cornflour).

The horizontal and vertical arrangement allows for determination of whether or not the deflagration is spherical in shape by determining the flame speed in either direction. This can be confirmed as if the deflagration is spherical the thermocouples will be activated in all directions at the same rate. If not, there is a problem, either the dust dispersion was not uniform throughout the vessel or there is a problem with the igniters.

An example of a response curve of a coarse dust (EFB) thermocouple response at position 17, left, an example of a response curve of a fine dust (cornflour) thermocouple response at position 17, right (**Fig 3.39**). As can be seen the fine dust combustion produces a far smoother response from the thermocouples. This is thought to be caused by a smoother flame front as seen in **Figure 3.23** as opposed to **Figure 3.20**.

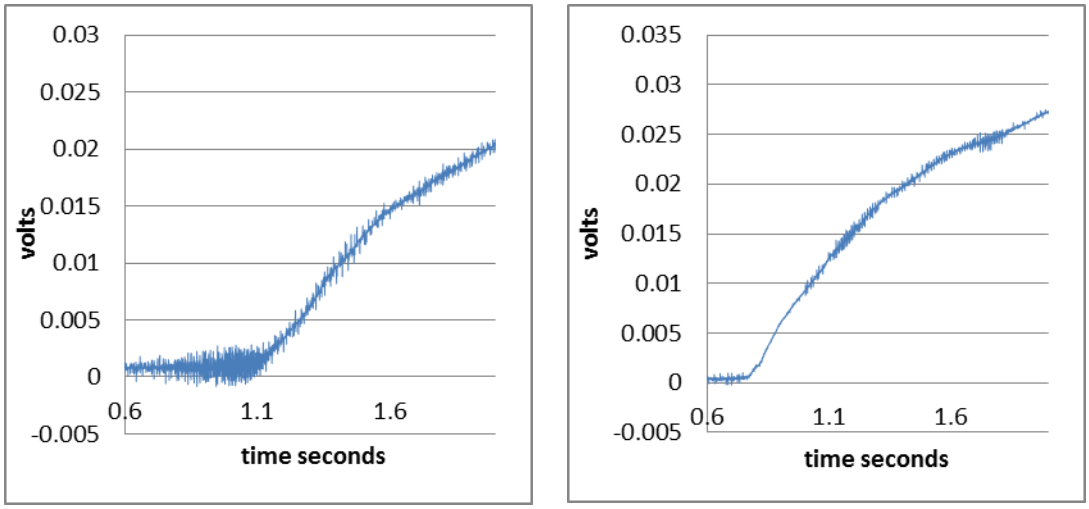

(A) (B)

Fig 3.39 Response of thermocouple against dust particle size (A) EFB (B) cornflour.

As can be seen the thermocouple responses from the different materials vary significantly, as is shown for cornflour there can even be different response rates to the same test by different thermocouples within the vessel (**Fig 3.38**). While the first trace in **Figure 3.38** displays a distinct point of rise it is far harder to discern this with the second graph where the line gradually rises. This makes deciding on the time of flame arrival very difficult. In situations such as is seen in **Figure 3.38**, the measuring sliders are used to determine the point at which the rise exceeds the background noise on the signal, this is then taken as the time of arrival. It was decided to take a rise above the background noise instead of a rise from the norm due to the large number of pre-curser rises experienced by the thermocouple. Therefore it was only once the readout has exceeded all previous fluctuations that it can be considered a definite flame arrival time.

The time of arrival was plotted against the thermocouple distance from the spark and a straight line indicated that the flame speed was uniform and constant. If the three line measurements were parallel but offset from each other, this indicated a spherical flame that did not propagate from the centre of the vessel and was offset at the ignition event.

3.5.4 Flame speed measurements 1m^3

For a spherical vessel a flame that has travelled half way across the radius of the vessel had only burnt 2% of the fuel, by mass. Thermocouples 2-6, 11-13 and 15-20 are in this part of the Leeds 1m^3 vessel under constant pressure conditions during the flame propagation (not using thermocouples 1, 9 and 14). Thus the flame speeds measured in this work were at the initial temperature and pressure. In the later stages of flame propagation, the P and T were rising by compression to the constant volume period.

For gases, the adiabatic expansion ratio is calculated by flame temperature calculations at constant pressure. However, this procedure is more difficult for dusts and instead the expansion ratio was taken as the measured ratio of peak pressure to initial pressure (this makes no allowance for the pressure increase related to the state change undergone by the dust but is the best available method). The gas explosion results for laminar and turbulent conditions (using air injection from the dust pot as in a dust test) were used to determine the turbulent enhancement of the flame and hence to deduce the laminar burning velocity of dusts from the turbulent burning velocity measurements.

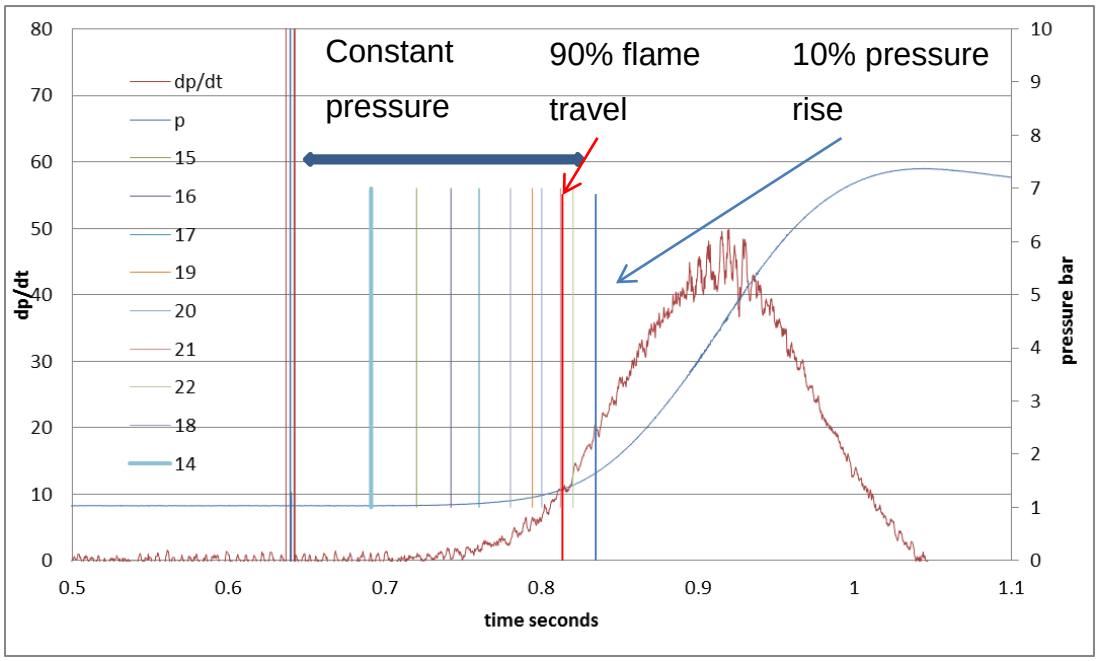

Fig 3.40 10% methane laminar test - pressure with thermocouple 15-22 activation times.

The flame speeds for gas and dust explosion tests were measured between 0.12-0.45m of the vessel radius from the spark which can be considered as a constant pressure period, (thermocouples 15-20, 2-6 and 11-13) **Figure 3.40**. In **Figure 3.40**, the time of flame arrival at the vertical downward thermocouples is indicated on the 10% methane explosion pressure-time trace, from this study. It can be seen that for the flame propagating 0.2-0.45m of the vessel radius (thermocouples 15-20), the actual pressure rise is only 3% of the total pressure. The rise in pressure (~8% of the total pressure) for the flame propagating 96% of the vessel radius means that the remaining 92% of the pressure rise happened in the last 4% of spherical flame travel (and the none spherical sections in the corners). It can be shown mathematically (for a spherical vessel) that for the first 50% of the flame travel, only 2% of the mass is burnt and for the 90% of the flame travel there is 10% of the mass that was burned therefore there is negligible pressure rise. Explosion pressure rise in a closed vessel is a linear function of initial mass of fuel and air that has burnt (Lewis, 1938). In spherical vessels consider the diameter of the flame is D_f and of the vessel is D.

Initial mass = $(\pi D^3 / 6) \rho_u$

ρ_u = unburnt material density

burnt mass= $(\pi D^3 / 6) \rho_b$

ρ_b = burnt material density

Percentage mass burnt = burnt mass / initial mass x 100

= $(D_f/D)^3 \times (\rho_b/ \rho_u) \times 100$

so D_f/D= 0.5 = 1.8% total mass burnt

D_f/D= 0.9 = 10.4% total mass burnt

However as the Leeds $1m^3$ vessel is not a sphere the values of mass burnt will be lower in actuality that those calculated. On **Figure 3.40** the line marked 10% pressure rise is the point at which this is reached while the red line shows the point in the flame propagation where this would be reached if the vessel was truly spherical. This is despite the fact that the last thermocouple (purple line) is located 96% of the way across the vessels radius and should, in a purely spherical vessel

have activated at 12.6% mass burnt. However at its activation time only 8% of the total mass had been burnt.

The reason for leaving out the initial 20% flame travel is to offset the ignitor and flame curvature effects in the early stages of flame development and the last 30% is where most of the combustion occurs with an increased pressure and temperature, which would affect the burning characteristics of the mixture (Andrews, 2010). **Figure 3.40** shows this as the steady rise in rate of pressure rise after the activation of thermocouple 20. **Figure 3.41** shows this as the steady rise in flame speed after the activation of thermocouple 20.

When running on fine dusts (<63µm) and gasses the activation of the thermocouples gives a very clear line, the gradient of the activation time against distance from the centre is the flame speed. Deviations of the flame speed from this straight line would indicate an influence of the increasing P and T on the flame speed measurement. Thus, once the time of arrival data deviated from the straight line plot, the data was not included in the determination of the slope of the line.

For hydrocarbons the burning velocity increases with T and reduces with P (Andrews and Bradley, 1973) so that the change in burning velocity is small and can be shown to be an increase of approximately 20% by the time of peak pressure is reached (Andrews, 2010).

Although the impact of P and T on burning velocity can be derived from the pressure time graph (Verakis, 1983) this was not done in the present work. However, this means that using the flame speed as a measure of the reactivity may not agree with the measurement of KG or K_{st} from the rate of pressure rise, as this is determined for flame propagation in the last half of the flame travel when the vessel is not spherical and spherical flame movement will cease once the spherical flame has touched the wall.

However, when large particle dusts were used in this equipment the results from the thermocouples deteriorated to the point that they were practically useless. This was first thought to be due to unequal distribution of the dust within the vessel. This was discounted after much consideration due to the consistent pressure results for repeat tests, near equal flame speeds in all directions (from calibration tests with cornflour) and a direct and repeatable correlation between the concentration of dust used and the pressure and K_{st} generated.

If the discrepancies in the thermocouple readouts had been due to none uniform flame propagation within the vessel it would have been expected to find discrepancies in the pressure results due to the quenching of the flame front.

The same materials were run in the Hartman apparatus with High speed video analysis to try and understand how this came about.

The turbulence factor (β) was determined by carrying out laminar and turbulent (under the same injection conditions as for dust explosions) 10% methane-air explosions and measuring the flame speeds and rates of pressure rise. The turbulence factor with the standard system (C-tube, 5L dust pot) was found to be equal to 4. Each alternative injection system had a turbulence factor evaluated in the same way and the ignition delay for each system was varied until the turbulence factor was 4 in agreement with the standard C-tube injection system where possible. Full details of this procedure are given in Chapter 6.1.2.

As the Leeds 1m^3 dust explosion vessel is not a spherical vessel but initial flame propagation will not be disturbed until it approaches the vessel walls. The flame speed was the average speed of the flame propagating in the horizontal right and downward thermocouples.

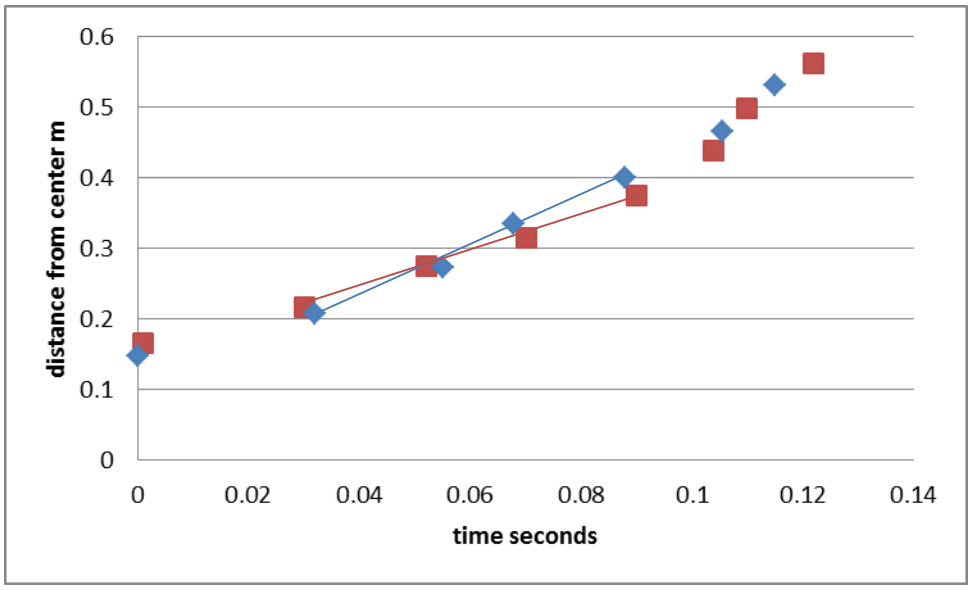

Fig 3.41 Flame speed 3.35m/s for 10% laminar methane test.

The distance of the thermocouples in each direction from the ignition source (flame position) was plotted against the time of flame arrival at the thermocouple. A linear

trend line was drawn for each set of the data, using a least squares plot. The final flame speed was the average slope of the trend lines in each direction. From the slope of each line, it can be observed that for the 10% methane laminar test, the flame is almost propagating spherically in all directions.

According to the current standard NFPA 68 (NFPA68, 2013), for gases the laminar burning velocity is a basic explosion protection parameter for the design of vents instead of the deflagration index (KG). However, for dusts the deflagration index (K_{st}) is still the basic parameter. The present work was designed to produce results that could make the burning velocity of dusts, the key reactivity parameter.

3.5.5 Thermocouples maintenance and separation

The thermocouple locations, numbers and their arrangement are shown below in **Figure 3.42**.

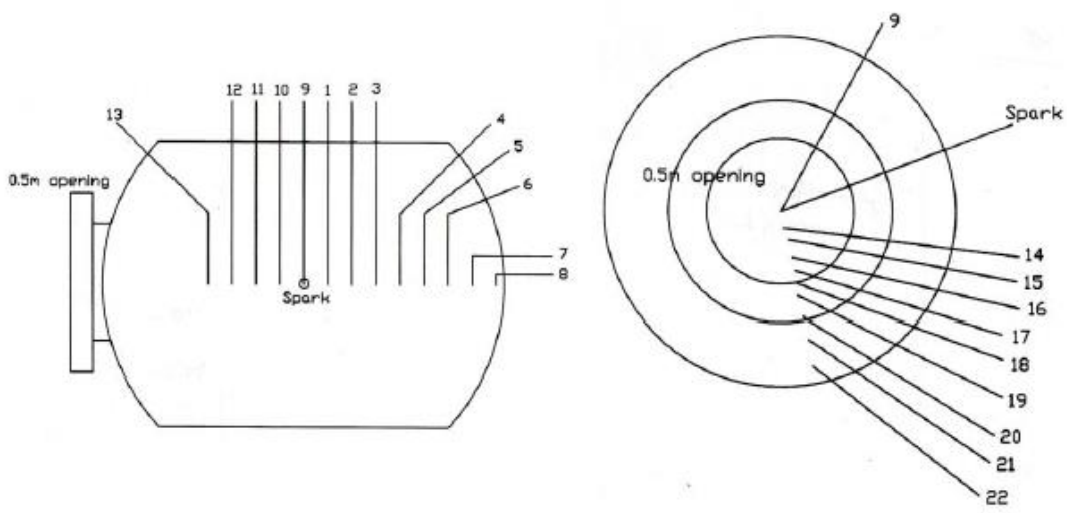

Fig 3.42 Thermocouple locations within vessel

Table 3.1 Thermocouple distences within vessel

thermocouple number	distance from centre m
2	0.148
3	0.207
4	0.272
5	0.334
6	0.399
7	0.465
8	0.53
11	0.143
12	0.205
13	0.265
15	0.166
16	0.216
17	0.274
18	0.315
19	0.374
20	0.437
21	0.498
22	0.562

These are the latest measured distance's, as the thermocouples had been replaced multiple times during the course of this PhD work. The thermocouples responded to temperature change and were measured in terms of their thermoelectric voltage output.

When the thermocouple junction broke after a time as they were liable to do in such an extreme environment they were repaired by cutting back 2cm of the cladding with a pipe cutter and then re-welding the undamaged wires. The repaired thermocouples were then tested with a voltmeter and a lighter flame was applied to the new junction to ensure a response change to temperature increase.

3.5.6 Vacuum pump

An Edwards two stage high vacuum pump model no. E2M 175 was connected to the Leeds 1m^3 dust explosion vessel.

Fig 3.43 Edwards two stage high vacuum pump

The purpose of the vacuum pump was to reduce the pressure in the test vessel prior to the test and to extract the combustion gases out of the test vessel after the test. This is done to ensure that the vessel has a breathable atmosphere present when opened. Additionally it is turned on during in vessel maintenance operations to ensure a clean air flow into the vessel.

It is an oil-sealed pump and had a nominal displacement rating of 2967 L/min. The vacuum pump was driven by a three phase motor and was water cooled. The flow of cooling water was controlled by an electronic isolation valve. The mechanism of pumping was a sliding vane type with high and low vacuum rotor and stator assemblies. A dust trap filter was assembled on the suction side of the pump to filter out any dust going into the pump. While an oil filter on the exit side prevents oil droplets from escaping the pump into the atmosphere.

3.5.7 Mixing control panel

This consisted of a trolley mounted gas cylinder with space for more cylinders on the back, the flow of air and gas to the test vessel was controlled by this mixing control panel. It consisted of one main 4-way rotary valve which was connected to three regulating valves. The fourth path of the 4-way valve was a male connection which was connected and used to fill the required amount of fuel gas inside the test vessel. Another line with a male connection was used to supply compressed air at 6bar to the test vessel.

The trolley also housed two pressure transducers (one for negative pressure and one for positive pressure) the negative one was used for measuring the desired vacuum in the vessel prior to the test and the positive one was used to measure the positive pressure in the vessel 5min after the test was carried out. Also mounted to this was a thermometer and a moisture meter. By taking a reading of the ambient conditions before each test it was possible to try to relate any unexpected results back to the conditions in which it was carried out. There by determining if the unexpected result was due to human error or simply a change in atmospheric conditions.

A diametric type 600 Barocel sensor and an absolute pressure gauge (connected in series) were used to monitor the test vessel pressure during mixture/test preparation. The principle working of the Barocel was to transform the absolute pressure into a DC output voltage. The Barocel sensor was connected to a Diametrics type 1500 digital pressure display.

3.5.8 Data acquiring and logging

All the instrumentation (ignition system, pressure transducers and thermocouples) in the Leeds $1m^3$ dust explosion vessel were attached to a 34-channel Microlink 4000 system. The sampling rate used by the data acquisition system was a sample interval of 0.2ms. Each channel contained its own programmable gain amplifier, 12 bit A-D (anolog-digital) converter, and on-board memory for the storage of instrument outputs. The voltage measurement range of the pressure transducer was 0 – 100 mvolts and for thermocouples was (-)100 – 100 mvolts. Each pressure transducer and thermocouple were connected to an individual channel in the data logger which meant that there was no delay in the transmission of data.

All of the timings for this (data logger activation, valve open/close time, ignition delay and the de-activation of the data logger) are controlled from a panel (**Fig. 3.44**) in the control room.

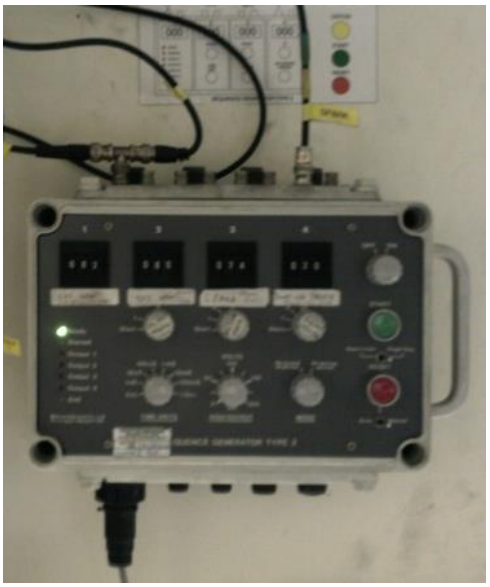

Fig 3.44 Sequence generator.

The Windmill Wavecap software was used for the initiation of the control signals (RUN and ARM actions) and the storing of captured data. This software allowed the parameters such as sampling frequency to be varied. After starting the program on Wavecap (RUN then ARM), the initiation of the test and data capturing process was started through a sequence generator.

The sequence generator had four time channels, only three of which were used after the specified time delays;

Channel 1: Time base (to trigger the data logger)

Channel 2: Electro pneumatic valve (to send signal to solid relay for activating the electro pneumatic valve)

Channel 3: nothing was connected.

Channel 4: Signal to spark box.

Channel 1 and 2 were activated at the same time (after pressing the start button on the sequence generator) whereas channel 4 was activated after the completion of

channel 2 timing. The purpose of using different time channels is to control the delay between each process.

Wavecap software stored the data of individual channels separately in FAMOS format. IMC FAMOS (Fast Analysis and Monitoring Of Signals) is a software program for the analysis and evaluation of measurement results. A typical response of pressure signal is shown in **Figure 3.34**. The rate of pressure rise (dp/dt) was calculated by differentiation of a section of the pressure signal after elimination of electronic noise, by smoothing of the raw signal **Figure 3.34**.

3.5.9 Reasons for injector modifications

As mentioned the original disperser in the $1m^3$ ISO vessel was the C-ring, due to flow problems with large particle size dusts this was changed to a side mounted spherical disperser, which in turn gave way to an in vessel spherical disperser.

When the first large particle tests were run on the C-ring injector the material failed to pass through the holes in the C-ring, this was assumed to be due to the particles agglomerating together due to the pressure forcing them through the holes. To try to alleviate this problem a wall mounted spherical disperser was made with larger holes in the hope that this would allow an unrestricted flow of material into the vessel. When this was tested, however, it was found to allow only particles slightly larger than for the C-ring to flow through. The hole size was increased again to no significant effect.

This indicated that the hole size at the injector opening was not the restricting factor in the particle size restriction we were finding. It was decided that the most likely problem was the flowing of the dust through the pipework connecting the dust pot with the $1m^3$ vessel. Therefore the way around this was to have the dust in the vessel to start with and then supply the compressed air through the pipework to provide the dispersion. This effectively removed any chance for the dust to block the system but did require a large number of disperser designs to be tested before a suitable one was found.

When the dust was moved from the dust pot to in vessel it was deemed necessary to ensure that no loss of capacity was suffered, therefore the hemisphere situated within the vessel was capable of holding 3.5kg of material, the same as the dust pot (without displacing any injection air from the pot).

3.6 Experimental procedures

Due to the safety considerations with the operation of the explosion vessel, a separate procedure and therefore tick sheet procedure was developed for laminar gas, turbulent gas explosions, C-ring dust explosions, hemispherical dust explosions and liquid + dust explosions. The aim of the tick sheets was to ensure a safe operation of the vessel, ensuring that no valve was left open to the explosion overpressure, which could then transmit the explosion flame/pressure into the laboratory. The operating area was behind a blast wall, to protect the operators in case any of the explosion vessel parts failed during a test.

3.7 Procedure for dusts explosions in the modified Hartmann tube apparatus

The dust was placed in the bottom of the Hartman apparatus containing the umbrella shaped disperser (connected to compressed air from reservoir). The tube is then attached over the top of this with the 20μm thick aluminium foil vent already secured in place on the tube with a locking ring. The tube was securely held vertically via a set of bayonet twist locks. A remote control handset operates the electrical arc and the opening of the solenoid valve. Once this is activated the dust in the tube is dispersed throughout the tube by the compressed air. The compressed air was supplied to the 50mL reservoir and pressurised at 7 barg. The electric arc is constant and generated from a high voltage power supply.

The vent cover had a burst pressure of 0.45 barg and the flame propagation was in a constant volume environment up to this pressure at which the vent ruptures therefore making it a constant pressure system. The volume of air prior to ignition inside the tube was 1L of air at atmospheric pressure, plus 50mL of compressed air at 7 barg giving 1.35L, at ambient conditions. The excess air from the compressed air cylinder in the reservoir was bled out via a bleed valve. The total volume of air inside the tube prior to explosion was increased under standard conditions, which was taken into account when calculating the dust concentration. This value is the one used to express the concentration of dust inside the vessel. Example, if 0.75g of dust is placed in the apparatus, the concentration would be 563 g/m^3.

3.8 Procedure for dust explosions in the Leeds 1m^3 explosion vessel - C-ring

The procedure used for dust explosion tests with standard system (C-tube and 5L dust holding pot) and standard ignition delay (0.65s) is described below; the calibration of new injection systems and their associated procedures are given later.

1. Check connections of the data transferring cables from the rig to the relevant channels in the data logger and from data logger to the PC.

2. Check the vessel, dust container and pipe work are clean. If not, then clean them using the vacuum cleaner.

3. Check the pressure sensors, actuators and sequence of operation by running the sequence without putting the dust in the dust holding pot and the chemical igniters in the vessel. The system should show a drop in pressure in the dust pot and a rise in the test vessel pressure (from the initial partial vacuum), confirming the proper working of the system and all pressure seals.

4. Chemical igniters were attached in the centre of the 1m^3 vessel and the wires were connected to the electrodes.

5. The front door was closed and bolted with 24 nut-bolts using a torsion wrench, an O-ring seal was placed between the flanges to ensure proper sealing. Check that all vent valves to the vessel are closed.

6. The valve at the top of the dust pot and the electro pneumatic valve were closed (by looking at the horizontal indicator on the side of the valve).

7. Add test dust to the 5L dust pot, top cover of the dust holding pot was closed tightly using a torsion wrench set at 150 kN/m^2. The mass of sample needed for the required concentration of dust was found by the following – [mass to be loaded into pot] = [mass in g/m^3 required] x[volume of vessel in g/m^3] (1.138)

8. Vacuum out the 1m^3 vessel to 0.928 bar. The pressure of the test vessel was initially reduced to about 0.9 bar(a) and then some ambient air

was allowed to flow into the test vessel to bring the vessel pressure to 0.928 bar. There is an access valve to the test vessel on the front door. This valve was used to allow ambient air into the vessel. The overall pressure in vessel before ignition but after injection was 1013.3 mbar, as 85 mbar will be added by the injection pressure from dust container. Thus all data in this work was obtained at a standard atmospheric pressure, irrespective of the ambient pressure on the day of the test.

9. The compressed air line from the bottled air used to pressurise the dust pot was connected.

10. Pressurise the dust pot to 20 barg. The 4.6L external pressure at 20 barg (21bara) expands to 95.3L at 1.0133 bara and thus the main vessel volume of 1.138 m^3 at 1.0133 bar (one atmosphere) has to be evacuated by 95.3L of volume at 1.0133 bar, which is a pressure reduction of 95.3/1138 = 8.37 % from the vessel which needs to be evacuated. This is a pressure reduction of 84.85mb to a pressure of 928.4 mbar(a) of pressure. (The pressure seal on the dust pot has some very minor leaks and is therefore pressurised last.)

11. The dust pot airline was detached and reattached to the electro pneumatic valve to drive the valve. The pressure on the compressed air cylinder regulator was set at 10- 11 bar(g) to drive the valve.

12. The igniter electrodes were connected to the spark box and the equipment was ready to be operated from the control room.

13. All the personnel left the test room and the doors were locked.

14. The desired programme was loaded onto the Wavecap software.

15. The RUN and ARM commands were sent to the data logger by the Wavecap program.

16. The ignition sequence was activated by the sequence generator.

17. The electro pneumatic valve was activated which dispersed the dust inside the vessel through a semi-circular C-tube. After a fixed delay time of 0.65s, the chemical igniters were activated. The 0.65s delay is made up of a

0.6s delay between the compressed air entering the vessel (determined by pressure rise on the pressure transducer) and the ignition and a 0.05s delay time for the air to flow from the dust pot valve to the end of the C-tube. This was the method used by Bartknecht (1989) to define the ignition delay.

18. The pressure–time history of the explosion, the thermocouples response and the pressure trace of the dust holding pot were recorded by the data logger and saved by Wavecap in FAMOS format.

19. The dust explosion properties were measured and calculated from the FAMOS outputs (in the form graphs).

20. After leaving the vessel for 5 minutes, the vessel pressure after the explosion was recorded. Water vapour condenses after the explosion and this reduces the pressure, but in all dust tests the pressure after the explosion was always greater than atmospheric. This was not the case for gas explosions where there was always a vacuum at the end of the test. This was mainly because for dusts, the fuel occupies negligible volume, so there is a greater mass of air in the tests then for gas explosions. The volume release from the products of combustion of solid fuel increases the pressure in the vessel after the mixture has cooled.

21. On the top right hand side of the vessel, there is a valve which is connected to a vacuum pump. The vacuum pump was used to extract the air and burnt gases out of the vessel before and after the explosion.

22. The pot and test vessel were opened using a torsion wrench and the mass of dust left in the pot and mass of residue in the vessel after the explosion process was also determined to find out the actual mass burned. A vacuum cleaner with a clean filter bag was used to remove the dust from the pot and the test vessel. A fresh filter bag was used each time and the bag was weighed before and after the sample was obtained so that the mass extracted was determined. After the in vessel residue had been collected and weighed, a sample of about 70 – 100g was taken.

3.8.1 Dust explosions in the Leeds 1m^3 explosion vessel – wall mounted

As mentioned dispersion/flow problems have been encountered with the standard C-ring set up regarding woody biomass, to allow for this a globe disperser (**Fig. 3.45**) along with the rebound nozzle (**Fig. 3.46**) design from the ISO standards (BSEN, 2011) were fabricated.

Fig 3.45 Globe disperser side

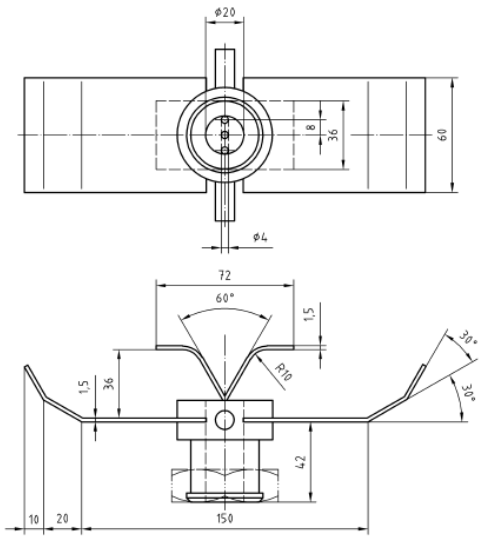

Figure B.2 — Rebound nozzle

Fig 3.46 Deflection plate disperser from ISO standard

This requires the removal of the C-ring T piece from inside the vessel and its replacement with one of the following – globe disperser or deflection plate.

Then the ignition delay needs to be altered to 0.55s for the globe disperser (the rebound nozzle ignition delay was not calibrated as the injector failed to disperse material of the desired particle size and so was rejected at that point).

The dust pot vessel needs to be extended using the 5L extension to house the low bulk density biomass in the volumes needed for rich explosion tests.

These ignition delays have been tested and calibrated to the C-ring using the methods used to standardise the C-ring. This allows for combustion and comparison of more fibrous materials than will flow through the C-ring, also this allows for comparison to materials tested on the C-ring.

However the globe disperser would not disperse/flow material with a maximum particle size of up to 500µm as was needed for this research.

3.8.2 Dust explosions in the Leeds 1m^3 explosion vessel – in vessel dust storage/dispersion

Having failed to make the rebound nozzle usable for material of the required size the last disperser recommended for this in the ISO standard was tested (**Fig. 3.47**). “For coarse, voluminous, fibrous or poorly flowing dust samples, it may not be possible to properly discharge the dust through the dust dispersers detailed ~It may, therefore, be necessary to use special dust dispersers, examples of which are given in Figures B.2 and B.3. In such cases, the dust disperser used shall be described in the test report.” (BSEN, 2011). However there were no technical drawings or schematics available to manufacture it from, only **Figure 3.47**.

Fig 3.47 dispersion cup

To get from that to a working dispersion unit (**Fig. 3.48**) took a large amount of trial and error, 5 intermediate dispersers were produced that did not evenly or adequately disperse the material placed within them. These will be covered in chapter 6.1 Disperser designs and testing.

Fig 3.48 Disperser made from dispersion cup design

This method of dust dispersion requires the removal of the C-ring T piece from inside the vessel and its replacement with pipework running from the vessel wall to the centre and a flange at the bottom to which the bottom half of the hemispherical dust holder attaches. Also the ignition delay needs to be moved to 0.55 seconds due to the change in injector setup. Hole area for drilled pipe hemispherical disperser = 254.4mm^2. The procedure is altered for these tests; replace section 1- 8 in the normal C-ring operating procedures with the following steps.

1. Check connections of the data transferring cables from the rig to the relevant channels in the data logger and from data logger to PC.

2. Check the vessel, injector and pipe work are clean. If not, then clean them using the vacuum cleaner.

3. Check the pressure sensors, actuators and sequence of operation by running the sequence without putting the dust in the dust holding pot and the chemical igniters. The system should show a drop in pressure in the dust pot and a rise in the test vessel pressure (from the initial partial

vacuum), confirming the proper working of the system and all pressure seals.

4. The disperser and attached pipework were fixed into the vessel.

5. The disperser was then loaded with dust and sealed (if spherical or lipped).

6. Chemical igniters were attached in the centre of the $1m^3$ vessel and the wires were connected to the spark electrodes.

7. The front door was closed and bolted with 24 nut-bolts using torsion wrench, an O-ring seal was in-placed to ensure proper sealing. Check that all vent valves to the vessel are closed.

8. The electro pneumatic valve was closed.

9. Vacuum out the $1m^3$ vessel to 0.928 bar. The pressure of the test vessel was initially reduced to about 0.9 bar(a) and then some ambient air was allowed to flow into the test vessel to bring the vessel pressure to 0.928 bar(a). There is an access valve to the test vessel on the front door. This valve was used to allow ambient air into the vessel. The overall pressure in vessel before ignition but after injection was 1013.3 mbar, as 85 mbar will be added by the injection pressure from dust container. Thus all data in this work were obtained at a standard atmospheric pressure, irrespective of the ambient pressure on the day of the test.

3.8.3 Repeatability of tests

The repeatability of dust explosions tests in the $1m^3$ were checked by testing several runs of wood at 1500 g/m^3 with the hemispherical disperser with drilled nozzle with the 5L dust pot pressurised to 20 barg and at 0.55s ignition delay. A good repeatability was obtained between the test results-

Table 3.2 repeat tests with the new disperser

K_{st} Bar/s	P max/pi Bar

19.41901	5.66
18.68818	5.6
18.42718	5.7

The percentage deviation with Pmax/Pi was 1.7%, with K_{st} was 5.1% the mass burned (%) was also relatively consistent in each test (variation = 12.3%) however this variation was believed to be more a feature of the complicated layout of the vessel trapping some residue material than actual differences in the mass burnt.

The hemispherical drilled pipe disperser was also compared against the standard C-ring disperser using cornflour where it achieved a percentage deviation of 0% Pmax/Pi and with 17% K_{st}.

While this is far from perfect (especially with regard to K_{st}) it is within the 20% deviation limit specified in the ISO standard (BSI, 2006). However a 17% deviation is worse than was hoped for therefore as will be explained in chapter 6 more work is being carried out to try and reduce this deviation.

3.9 Procedure for gas explosions in Leeds 1m^3 explosion vessel

The procedure to carry out laminar gas explosions was to make up the mixture in the vessel by vacuuming out the vessel and then adding the gas using partial pressure measurements, to determine the quantity. The mixture was then made up to a standard atmosphere by adding air. This mixture was allowed to stand for about 5 minutes for diffusion mixing before the explosion was carried out. The addition of the fuel into a vacuum would ensure fuel mixed throughout the volume. The vessel had to be prepared before the test with a central spark igniter. Recording of the data was as for dust explosions.

The procedure for turbulent gas explosion tests was the same as for the standard dust injection system but without the dust. Air was put into the external 5L pot at 20 bar and injected into the vessel using the dust injection C-tube and the standard ignition delay (0.65s) was used. The gaseous fuel was injected into the main vessel using pressure differentials as for the laminar gas explosion tests, but the air was

only added to the level necessary for a standard atmosphere to be achieved after injection of the air from the external 5L pot.

The turbulence levels for the standard system and for the new injection systems were quantified by doing the laminar gas explosion tests and turbulent gas explosions at different ignition delays for the different dispersion units evaluated.

First three steps (1 – 3) for dust and gas explosions were the same.

Due to safety reasons the gas mixtures were prepared in the main vessel rather than injecting the gas from external dust pot as in the case of dust explosions.

For example, for the preparation of 10% methane mixture in air in the test vessel for the test at standard atmospheric pressure (1.013bar),

The total pressure in the test vessel prior to ignition = 1013.3 mbar

Therefore, the pressure of methane in the test vessel for 10% methane – air mixture

= 1013.3 × 0.1 = 101.33 mbar.

1. The test vessel should be evacuated to less than 200 mbara, followed by the addition of the required volume of fuel gas (calculated as above) and then the rest of the mixture is made with compressed air. Thus all data in this work was obtained at a standard atmospheric pressure, irrespective of the ambient pressure on the day of the test.

2. The spark electrodes were connected to the spark box and the equipment was ready to be operated from the control room.

3. All the personnel left the test room and the doors were locked.

4. The RUN and ARM commands was sent to the data logger by the Wavecap.

5. The ignition sequence was activated by the sequence generator.

6. The pressure–time history of the explosion, the thermocouples response and the pressure trace of the dust holding pot were recorded by the data logger and saved by Wavecap in FAMOS format.

7. The gas explosion properties were measured and calculated from the FAMOS outputs (in the form graphs).

8. After leaving the vessel for a few minutes, the vessel pressure after the explosion was recorded. Water vapour condenses after the explosion and this reduces the pressure, therefore in all tests the pressure after the explosion was always lower than atmospheric.

9. On the top right hand side of the vessel, there is a valve which is connected to a vacuum pump. The vacuum pump was used to extract the air and burnt gases out of the vessel before and after the explosion.

10. The test vessel was opened using a torsion wrench and the water left in the vessel was removed.

3.9.1 Turbulent gas explosions tests

In order to study the turbulent gas explosions tests, the vessel pressure after the injection of fuel, was increased to 928 mbar by the addition of ambient air.

The external dust pot was pressurised to 20 barg and operation of the electro-pneumatic ball valve increased the vessel pressure by 85 mbar, so that the total pressure in the vessel prior to the explosion was 1013 mbara.

The ignition of the gas mixture occurred after a controlled delay, using a 16J capacitance spark (0.5m long electrode) extended to the centre of the vessel.

3.9.2 Laminar gas explosions tests

For laminar gas explosions, no air was injected from the external pot. After addition of the gasses the vessel was allowed to settle for about 5 minutes, the pressure in the vessel after the addition of fuel gas was and mixing air was 1013 mbara. The ignition of the gas mixture for the laminar tests was the same as described above for the turbulent gas tests.

3.10 Mass burned concentration

Due to the attaching flanges, electrostatic attraction and other obstructions it was not possible to collect 100% of the residue from the test vessel, on average between + or - 50–100g of the residue was not collected from each test. As was mentioned earlier the material added into the dust pot or internal dispersers does not all take part in the combustion, this is due to fractions of the dust being lost at various stages of the process. Therefore the injected concentration of dust was calculated using the following relationship;

Injected concentration = (nominal mass of dust – pot/disperser residue)/ vessel volume

Fraction of mass burned = (injected mass – residue) / Injected mass

pot/disperser residue = dust mass left in injection pot/disperser.

nominal dust concentration = the mass of dust placed in the pot/disperser / vessel volume

Injected mass = nominal dust mass – pot/disperser residue

As has been mentioned it is suspected that some of the material in dust combustion is pushed ahead of the flame front. This is important as near the flammability limits gas explosions do not burn all the fuel available due to the action of buoyancy on the flame (Andrews and Bradley, 1972). Therefore it stands to reason that a similar phenomenon must occur for dust flames (and may even be more acute due to cake formation excluding some of the mass from the flame propagation). There are now two sources for the unburned dust found in the vessel at the end of the explosion (for lean or near MEC mixtures), dust compressed against the outer wall and dust that is not burnt due to buoyancy.

For near MEC mixtures if all the unburned dust is counted then the flame propagated through an unrealistically low concentration, much lower than found in the Hartmann lean flammability tests (see Chapter 5). These problems mean that the ISO $1m^3$ vessel is completely unsuitable for the measurement on the lean flammability limit as the concentration of the mixture through which the flame propagates is not (and at this point cannot be) known – unless some form of optical

concentration measurement method is added. This is a problem as the legal definition of the lean flammability limit of a dust is that measured in the ISO $1m^3$ vessel using the nominal dust concentration and at this point it cannot be confirmed that this is the concentration the flame propagated through. This problem is a major part of the present research that is discussed later (see Chapter 6).

The nominal, injected and mass burned concentrations are also represented in terms of equivalence ratio either as received or dry ash free.

4 Biomass composition and characteristics

All the biomasses tested are listed in this chapter for easy access and referral.

Table 4.1 Particle size of as received and post combustion fuel samples with corresponding MEC's.

	µm	Nominal mass g/m^3	D [3, 2] - Surface weighted mean µm	d (0.1) µm	d (0.5) µm	d (0.9) µm	MEC Hartmann	1m^3 MEC
Oak	63	-	23.9	12.8	44.7	110.2	0.2	0.4
Oak	63 1	500	36.3	19.6	56.9	150.7		
Oak	63 2	250	49.7	28.4	72.9	198		
Oak	63 - 150	-	82.2	62.7	141.2	299	0.17	1.1
Oak	63 - 150 5	300	120.3	77.6	147.4	293.8		
Oak	64 - 150 6	1000	97.2	64	138.3	291.2		
Oak	150 - 300	-	302.9	180.7	357.2	712.7	1.4	4.3
Oak	150 - 300 3	2000	266.3	158.6	325.8	666.2		
Oak	150 - 300 4	1250	265.8	155.2	311.3	621.8		
Oak	500	-	109.3	62.8	381	845.4	0.6	2.3
Oak	500 3	750	167.6	86.7	292.5	696.1		
Oak	500 4	1000	136.7	69.5	270.8	674.2		
Pine	500-63	-	230.7	122	386.9	808.5	0.6	
Pine	63	-	41.3	23.6	66.4	162.4	0.2	
Pine	less 500 pine	-	172.0	84.7	358.3	793.9	1.3	1.8
Pine	500-300 milled	-	346.0	252.6	530.5	900.6	4.9	
Pine	500-300	-	402.4	282.3	547.1	909.9		
OPT	500	-	80.8	45.3	249.5	683.1	1.8	
EFB	500	-	55.0	30.3	257.7	755.5	1	2.3
CT	500	-	56.8	31.5	197.1	634.9	1.1	
RH	500	-	60.5	31.8	253.7	683.5	0.8	
DBD	500	-	26.0	18.7	64.4	196.3	0.19	0.42
cornflour	500	-	7.36	7.89	14.1	21.66	0.27	0.45
kellingley coal	500	-	12	5	25.5	65.29	0.44	0.74

Table 4.2 Materials analysied by TGA and Proximate analysis

Sample	GCV (MJ/kg)	ELEMENTAL[a]					TGA-Proximate					STOICHIOMETRY			
		C	H	O	N	S	H_2O	VM	FC	Ash	ASH[b]	H/C	O/C	A/F	Ø=1[a] (g/m^3)
Willow	19.2	49.1	6.1	44.7	0.2	0.0	5.3	84.5	9.0	1.2	1.2	1.5	0.7	5.8	206.2
Hardwood	18.3	46.7	5.9	47.3	0.1	0.0	6.7	84.7	14.6	0.7	0.7	1.5	0.8	5.4	223.2
Softwood	18.5	46.9	5.9	47.2	0.0	0.0	7.0	90.1	9.8	0.1	0.1	1.5	0.8	5.4	223.1
Wheat Straw	18.2	53.8	7.4	38.4	0.4	0.0	6.6	72.3	7.3	13.7	14.7	1.6	0.5	7.1	169.0
pine wood	21.0	54.8	6.2	37.1	1.9	0.0	4.3	80.2	11.1	4.4	4.6	1.4	0.5	7.0	172.0
efb pellets	18.1	53.0	7.0	38.4	1.6	0.0	5.7	67.1	13.5	13.8	14.6	1.6	0.5	7.0	172.5
coconut trunk pellets	18.3	52.4	6.7	40.0	0.8	0.0	5.1	68.2	15.3	11.3	12.0	1.5	0.6	6.7	179.7
rise husk pellets	17.3	53.3	6.9	38.7	1.0	0.0	5.1	64.4	13.6	17.4	18.4	1.6	0.5	6.9	173.3
opt pellets	18.6	52.4	6.8	39.6	1.2	0.0	5.1	72.5	11.9	10.5	11.1	1.6	0.6	6.8	177.7
lycopodium hammed	30.6	68.2	9.4	20.4	2.0	0.0	1.6	89.2	5.1	4.1	4.2	1.7	0.2	10.4	115.1
wood 1	19.2	49.2	6.3	44.2	0.3	0.0	6.3	71.3	20.9	1.5	1.6	1.5	0.7	5.9	202.4
Corn flour	18.5	44.7	7.4	47.8	0.1	0.0	11.6	77.8	6.8	3.8	4.3	2.0	0.8	5.7	179.6
Oak original	20.0	51.4	6.5	41.8	0.2	0.0	8.9	72.7	13.3	5.1	5.6	1.5	0.6	6.4	161.9
Coal original	28.2	51.6	4.4	15.0	2.0	2.0	2.4	33.2	41.8	22.6	23.2	1.0	0.2	9.6	93.9
Walnut original	20.7	52.9	6.8	39.6	0.6	0.1	5.0	74.6	14.2	6.3	6.6	1.5	0.6	6.8	157.7
Pine nut original	21.1	54.2	7.3	36.4	1.9	0.1	5.4	73.2	11.7	9.8	10.4	1.6	0.5	7.3	138.8
drax biomass fines DBD18	18.1	49.7	7.0	42.6	0.7	0.0	3.5	79.5	8.7	8.2	8.5	1.7	0.6	6.3	189.2

[a] dry, ash free (daf) [b] dry

Table 4.3 Residue materials analysied by TGA and Proximate analysis

Sample	GCV (MJ/kg)	ELEMENTAL[a]					TGA-Proximate					STOICHIOMETRY			
		C	H	O	N	S	H_2O	VM	FC	Ash	ASH[b]	H/C	O/C	A/F	Ø=1[a] (g/m^3)
oak 632 T1	17.7	64.6	5.8	29.3	0.3	0.0	4.4	36.0	32.6	28.9	30.2	1.1	0.3	8.2	146.8
oak 632 B1	18.4	65.6	7.3	26.0	1.0	0.2	5.0	56.0	24.9	20.0	28.9	1.3	0.3	9.0	132.9
oak 632 BR1	18.6	54.2	5.7	39.5	0.6	0.0	3.9	58.9	24.9	12.3	12.8	1.3	0.5	6.5	183.7
oak 632 R1	17.7	64.6	6.3	27.9	1.0	0.2	3.9	42.3	24.7	29.1	30.3	1.2	0.3	8.5	141.4
oak 631 T1	20.4	59.7	5.0	34.6	0.7	0.0	5.4	40.8	42.4	11.4	12.1	1.0	0.4	7.1	168.2
oak 631 B1	16.4	44.3	5.5	49.7	0.5	0.0	5.6	62.7	24.1	7.6	8.1	1.5	0.8	4.9	246.1
oak 631 BR1	21.9	59.5	6.0	33.9	0.5	0.0	4.3	57.0	31.1	7.7	8.0	1.2	0.4	7.5	160.0
oak 631 R1	20.1	57.1	5.8	36.6	0.6	0.0	4.5	56.5	29.1	9.9	10.4	1.2	0.5	7.0	171.0
oak 63155 T 1	19.1	49.4	5.9	44.7	0.0	0.0	6.2	73.0	18.8	2.1	2.2	1.4	0.7	5.8	207.1
oak 63155 B 1	17.2	44.7	6.0	49.3	0.0	0.0	6.1	76.4	15.0	2.5	2.7	1.6	0.8	5.1	236.5
oak 63155 BR 1	16.9	45.1	5.4	49.1	0.5	0.0	5.9	64.6	24.2	5.3	5.6	1.4	0.8	5.0	242.3
oak 63155 R 1	19.2	49.6	6.2	43.7	0.4	0.0	5.7	70.8	21.3	2.2	2.4	1.5	0.7	6.0	200.4
oak 63153 T 1	19.2	49.0	5.8	45.2	0.0	0.0	6.2	74.3	18.8	0.7	0.8	1.4	0.7	5.7	210.7
oak 63153 B 1	16.6	41.6	5.9	52.5	0.0	0.0	6.1	76.9	17.0	0.0	0.0	1.7	0.9	4.6	263.6
oak 63153 BR 1	19.2	51.7	6.2	42.2	0.0	0.0	6.5	61.9	26.3	5.3	5.7	1.4	0.6	6.2	192.1
oak 63153 R 2	19.0	54.9	6.8	37.7	0.5	0.0	5.3	63.1	19.6	12.0	12.7	1.5	0.5	7.1	169.4
oak 500 3 T1	21.0	54.8	5.9	39.3	0.0	0.0	5.2	68.7	22.9	3.2	3.4	1.3	0.5	6.6	180.8
oak 500 3 B1	18.3	47.7	5.9	46.4	0.0	0.0	5.9	74.0	17.5	2.6	2.8	1.5	0.7	5.5	217.5
500 oak 3 BR 1	21.0	57.0	5.8	36.7	0.5	0.0	4.9	55.3	33.1	6.7	7.0	1.2	0.5	7.0	171.5
500 oak 3 R 1	19.8	51.3	6.0	42.3	0.4	0.0	5.5	66.2	25.6	2.7	2.9	1.4	0.6	6.2	194.3
oak 500 4 T1	21.2	55.5	5.5	39.1	0.0	0.0	5.2	62.8	29.0	3.0	3.2	1.2	0.5	6.6	182.3
oak 500 4 B1	15.8	39.8	5.8	54.2	0.3	0.0	5.7	73.1	19.7	1.5	1.6	1.7	1.0	4.2	283.3
oak 500 4 BR1	21.7	58.2	5.5	35.9	0.4	0.0	4.8	54.1	35.6	5.5	5.8	1.1	0.5	7.1	169.9
oak 500 4 R 1	20.2	51.6	6.1	41.9	0.4	0.0	5.6	66.5	26.5	1.4	1.5	1.4	0.6	6.2	192.0
oak 1534 T1	21.1	54.2	6.3	39.5	0.0	0.0	6.3	73.0	18.0	2.7	2.9	1.4	0.5	6.7	179.4
oak 1534 B1	19.0	49.5	6.2	44.3	0.0	0.0	9.2	72.2	15.8	2.8	3.1	1.5	0.7	5.9	202.8
oak 1534 BR1	16.8	56.3	5.9	37.7	0.1	0.0	3.4	47.5	25.1	24.0	24.8	1.3	0.5	6.9	173.8
oak 1534 R1	19.3	50.6	6.2	43.1	0.0	0.0	7.8	69.8	19.0	3.4	3.7	1.5	0.6	6.1	196.3

[a] dry, ash free (daf) [b] dry

Table 4.4 Residue materials analysied by TGA and Proximate analysis

Sample	GCV (MJ/kg)	ELEMENTAL[a]					TGA-Proximate					STOICHIOMETRY			
		C	H	O	N	S	H_2O	VM	FC	Ash	ASH[b]	H/C	O/C	A/F	Ø=1[a] (g/m^3)
oak 1533 T1	21.3	52.0	6.2	39.5	0.0	0.0	7.0	71.0	18.0	4.0	2.9	1.4	0.5	6.9	185.2
oak 1533 B1	19.4	46.8	6.2	48.3	0.0	0.0	6.0	72.8	16.2	3.3	3.1	1.5	0.7	5.7	187.8
oak 1533 BR1	19.5	54.6	6.2	39.7	0.1	0.0	5.1	45.7	36.6	12.3	24.8	1.3	0.5	6.6	189.8
oak 1533 R1	19.8	50.1	6.1	41.1	0.0	0.0	4.4	69.8	20.6	5.0	3.7	1.5	0.6	5.9	196.5
Coal original	28.2	51.6	4.4	15.0	2.0	2.0	2.4	33.2	41.8	22.6	23.2	1.0	0.2	9.6	93.9
Coal residue	26.2	81.9	4.5	9.0	2.8	1.8	1.6	25.1	50.5	19.5	19.9	0.7	0.1	11.1	85.4
Coal residue top layer	26.8	90.6	3.6	0.5	2.2	3.0	1.3	15.4	49.0	24.0	24.3	0.5	0.0	12.3	73.0
Coal residue bottom layer	26.7	83.2	6.0	5.7	2.3	2.7	2.1	30.0	44.6	23.4	23.9	0.9	0.1	12.0	74.6
Walnut original	20.7	52.9	6.8	39.6	0.6	0.1	5.0	74.6	14.2	6.3	6.6	1.5	0.6	6.8	157.7
Walnut residue	19.6	53.3	5.7	39.8	1.1	0.2	3.2	76.0	14.2	6.6	6.8	1.3	0.6	6.4	168.0
Walnut residue top layer	22.5	63.1	5.8	29.3	1.8	0.0	3.8	61.0	24.0	11.2	11.6	1.1	0.3	8.1	125.3
Walnut residue bottom layer	20.3	54.9	6.2	37.9	1.0	0.0	5.9	74.1	11.5	8.5	9.0	1.4	0.5	6.9	149.4
Pine nut original	21.1	54.2	7.3	36.4	1.9	0.1	5.4	73.2	11.7	9.8	10.4	1.6	0.5	7.3	138.8
Pine nut residue	22.1	55.1	8.3	34.8	1.7	0.0	3.8	60.3	24.4	11.5	12.0	1.8	0.5	7.8	129.8
Pine nut residue top layer	22.5	62.6	6.5	28.8	2.1	0.0	5.2	54.5	27.1	13.2	13.9	1.2	0.3	8.4	117.1
Pine nut residue bottom layer	20.6	51.1	7.0	40.9	0.9	0.0	8.0	66.4	16.2	4.7	5.1	1.6	0.6	6.6	159.1
Pine wood original	19.2	49.7	7.0	42.6	0.7	0.0	3.5	79.5	8.7	8.2	8.5	1.7	0.6	6.3	167.0
Pine wood residue	20.6	56.7	6.6	36.2	0.4	0.0	3.3	66.2	18.2	12.3	12.7	1.4	0.5	7.3	139.2
Pine wood residue top layer	21.9	58.7	7.0	33.9	0.4	0.0	4.8	62.6	21.1	11.5	12.1	1.4	0.4	7.7	130.1
Pine wood residue bottom layer	20.2	56.0	6.8	37.2	0.0	0.0	5.5	65.8	15.7	13.0	13.8	1.5	0.5	7.2	136.0
Corn flour	18.5	44.7	7.4	47.8	0.1	0.0	11.6	77.8	6.8	3.8	4.3	2.0	0.8	5.7	179.6
Corn flour residue	14.7	45.0	6.1	47.7	1.0	0.1	8.3	67.6	9.2	14.9	16.3	1.6	0.8	5.3	174.0
Corn flour residue top layer	15.3	50.2	7.2	35.4	6.6	0.5	8.6	59.3	5.8	26.4	28.9	1.7	0.5	7.3	107.6
Corn flour residue bottom layer	13.5	45.2	7.2	46.7	0.5	0.5	8.8	62.0	4.2	25.0	27.4	1.9	0.8	5.7	139.3

[a] dry, ash free (daf) [b] dry

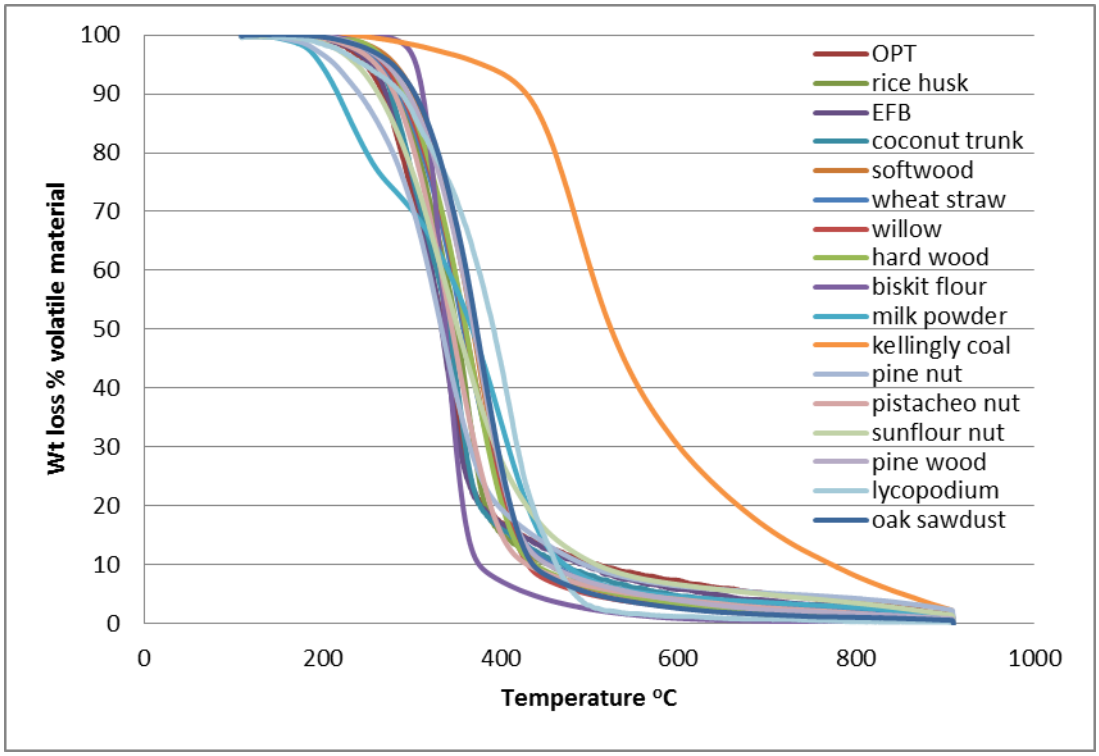

Fig 4.1 TGA volatile release rates against temperature for all biomasses and coal tested by this group.

SEM, raw particle shape- oak (<63µm, 63-150µm, 150-300µm and <500µm) and "wood".

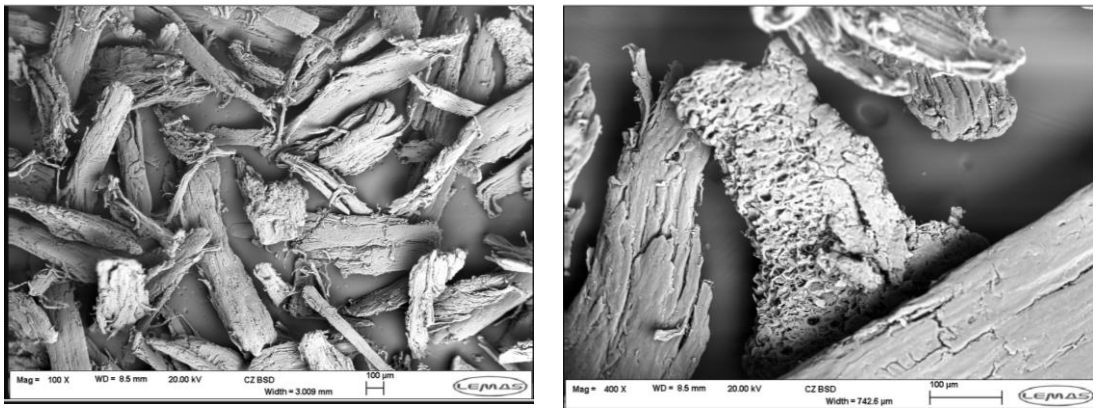

Fig 4.2 Oak 150-300µm

The images show cylindrical particles with fibrous protrusions as would be expected for material passed through a cutting mill. Of special note was the porous particle on the right hand side. This is believed to be the layer of wood that was still alive at the time the tree was harvested and therefore the Xylem and Phloem were still in

use and open. As a tree grows these close up to become the woody structure of the tree and are grown over by the new Xylem and Phloem structures.

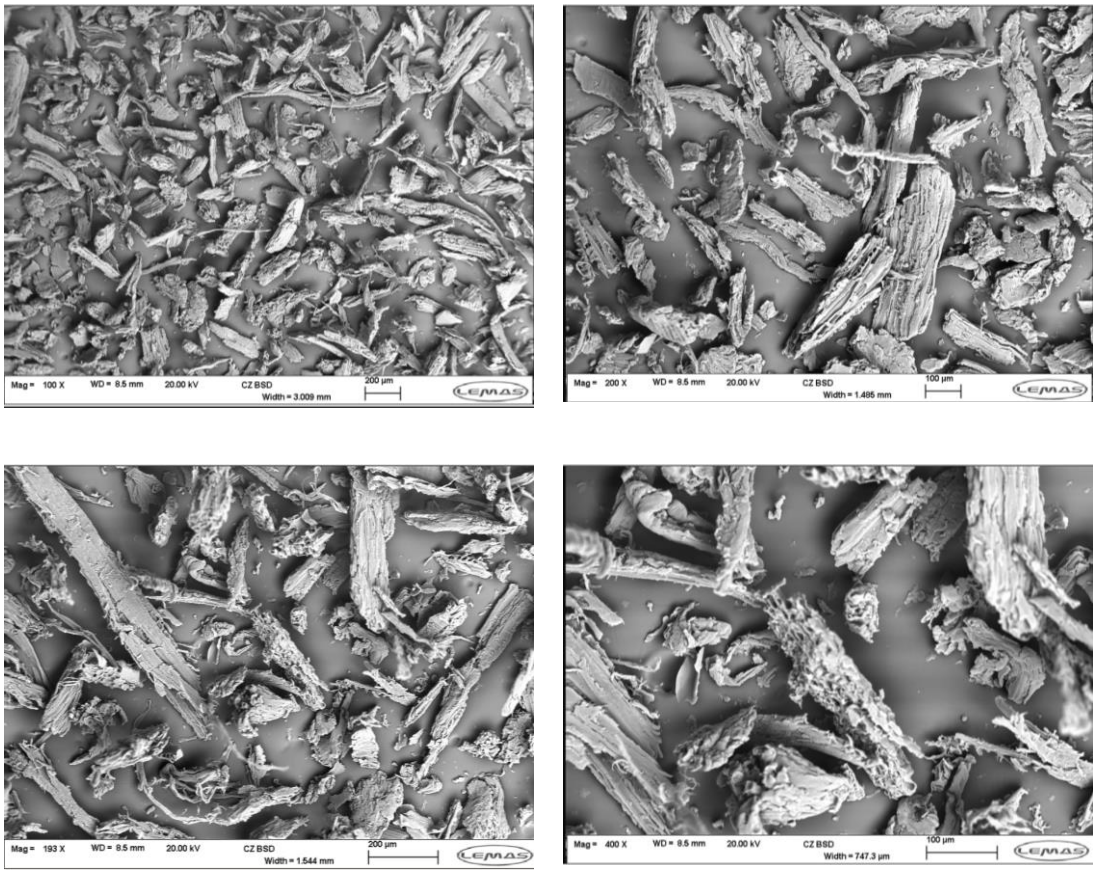

Fig 4.3 Oak 63-150µm

The particles created in this size range are almost identical to those in the 150-300µm range but appear thinner and more elongated, porous particles are again in evidence pre combustion. The particle radius is far closer to the separation mesh size used than the height, this indicates that the particles were size separated based on their radii not their height.

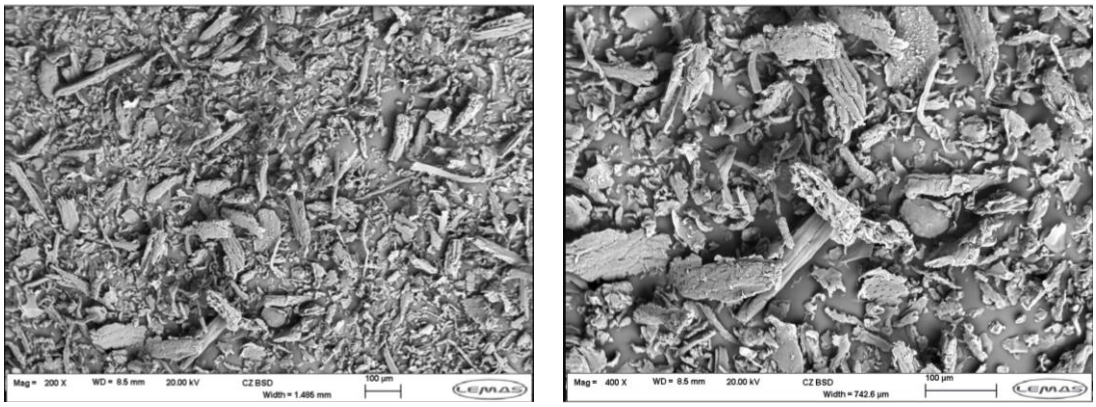

Fig 4.4 Oak <63µm

The particles created in this size range are the most spherical seen for materials tested.

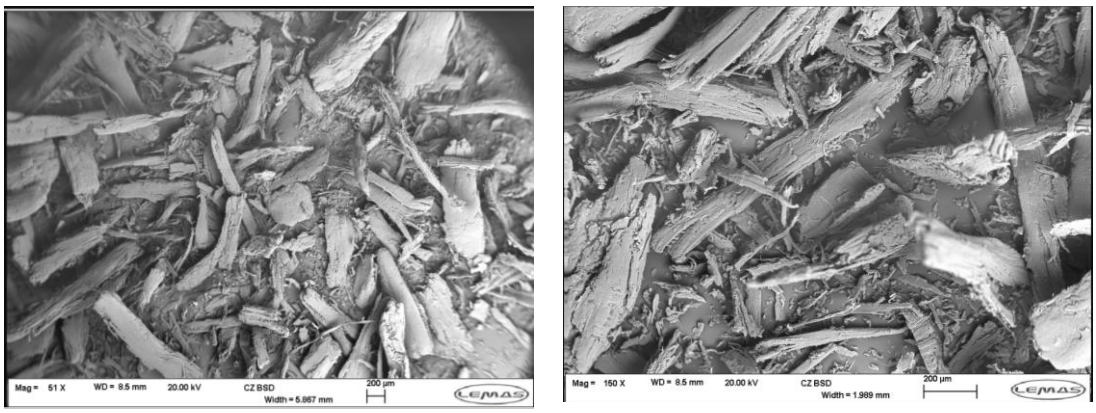

Fig 4.5 Oak <500µm

The particles here are a mixture of all the previous samples seen so far; however the largest component by volume appears to be the large particles.

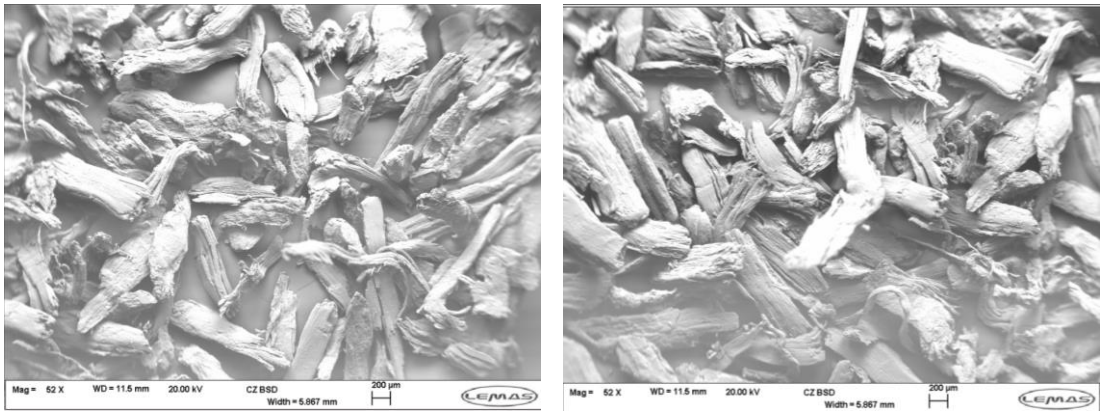

Fig 4.6 Pine 300 - 500µm

The particles created in this size range are almost identical to those in the 150-300µm range but appear more elongated, pre combustion. The particle radius is far closer to the separation mesh size used than the height, this indicates that the particles were size separated based on their radii not their height. Although some smaller particles were found.

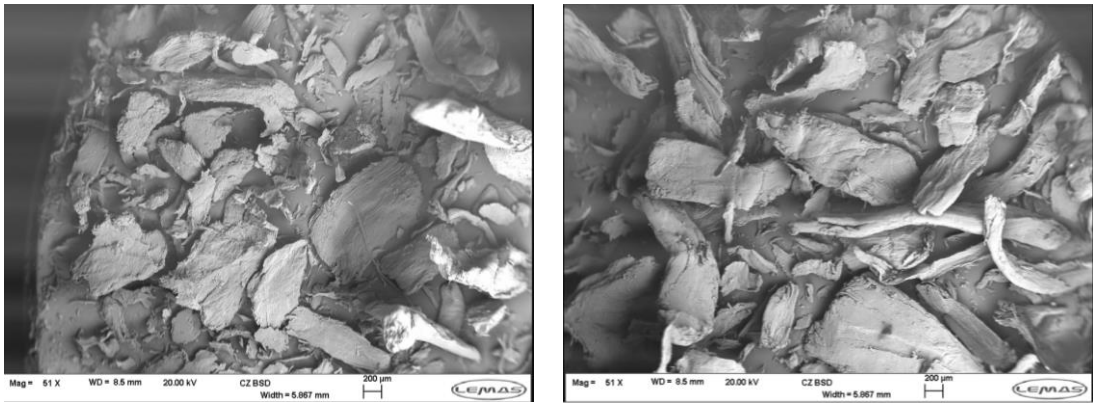

Fig 4.7 Wood as received

This was the only sample that was not milled for which there is SEM analysis, the material was palletised and then broken up again (unspecified method) and shows the smooth edges characteristic of particles that have been compressed. They also show a far smaller height : radius ratio than the other biomass particles.

5 Influence of particle size on MEC and mixture reactivity using the Hartmann equipment.

5.1 Introduction

The Hartmann apparatus was used for investigating particle size and concentration effects on combustion as the 1m^3 explosion vessel requires about 1kg of sample per test and it was not possible to generate this quantity of milled biomass for a range of particle sizes and biomass types. The Hartmann equipment requires 1/1000 of the mass of the 1m^3 vessel and was thus a practical vessel to use for this work. The Hartmann equipment enables the MEC and the approximate mixture with the highest reactivity to be determined. This then reduces the testing carried out on the 1m^3 as the most reactive mixture is known from this work and hopefully only 3 or 4 tests on the 1m^3 are required to determine the peak K_{st}.

A large part of the work done in this thesis examined the effect of particle size on the combustion behaviour of biomass, the reason for this emphasis was that feedback from the industrial committee connected with this work suggested that pulverised biomass used in power stations was of a relatively coarse size. It was the aim of this work to determine whether in mixed particle sizes only the fines burnt or whether large particles could burn without fines being present. Milled particles were separated into size fraction by sieving for this purpose.

Fines were defined as particles <63µm (BSEN, 2011) but also some work was done for fines <75µm. In addition some work was undertaken on ultra-fine particles <38µm. This was to investigate whether variability in size <63µm was significant in variation of MEC and K_{st} and in relation to this some samples were tested with the size fraction 38-75µm to see if the presence of ultra-fines was important. It should be emphasised that in the dust explosion regulations (BSEN, 2011) it is only required to test fine dusts ,<63µm and the explosibility of coarse dust is not required. However, if in industry particles are not used at <63µm then the explosion risk of the actual plant is not being investigated. Also this work was relevant to understanding the mechanism of flames propagation in biomass dusts. As coarse dusts are used in the power generation industry there is interest in knowing the flame propagation characteristics of coarse biomass dusts.

To investigate a full range of sizes, particles sieved to <500um were investigated and these would have fines and coarse particles present. Then different coarse fractions only were investigated – 63/75-150µm, 150-300µm and 300-500µm. These sizes are written in the figures and referred to in the text as – a material-pine, oak etc. followed by a size range in microns. So pine 38-75µm is – pine wood with particles sized between mesh sizes of 38µm and 75µm.

The size fraction 63-500µm allowed for the examination of how a material was burning without any fine particles present. The 63/75 - 150µm fraction was investigated to limit the maximum size of the largest particles present, whilst still eliminating fines and 150 - 300µm and 300 - 500µm continued this theme. 50/50, 300-500µm and <63µm was a mixture of half (by mass) 300-500µm particles and half <63µm. This allowed the examination of the effect of large particles on the combustion of the fine particles.

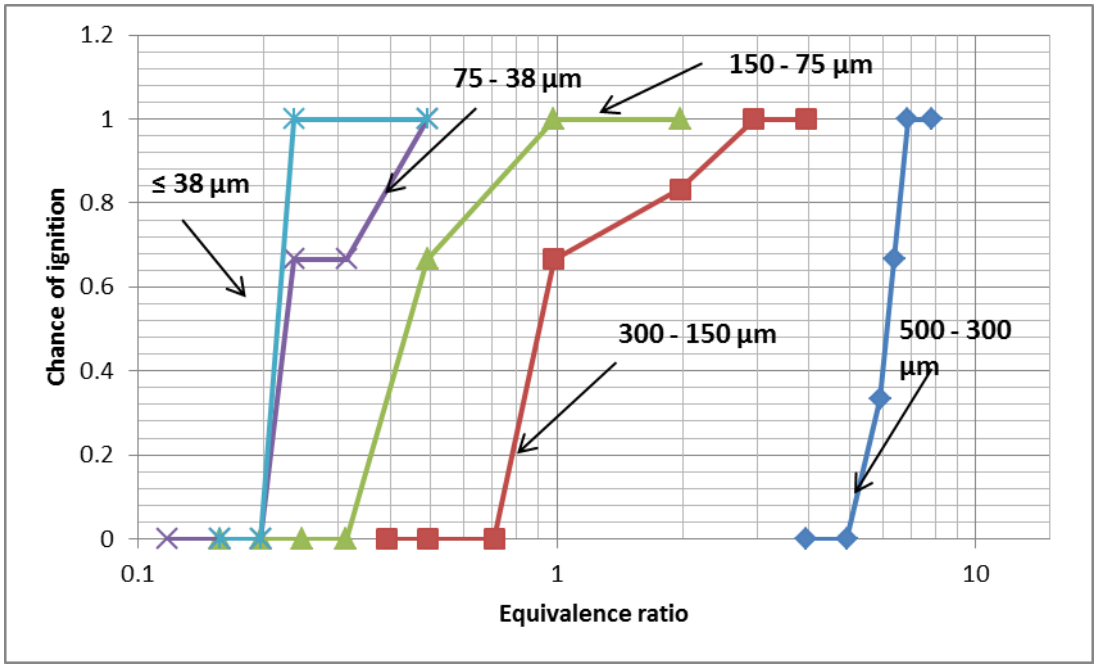

Fig 5.1 Milled pine sieved into different size fractions

The influence of particle size on MEC for pine is shown in **Figure 5.1**. For fine dusts (<75µm) the MEC for pine wood was 0.19Ø for no explosion and 0.23Ø for a propagating flame. Sieving to a finer fraction (<38µm) had no influence on the MEC. This was an unexpected result as this is leaner than a pure hydrocarbon gas MEC which is normally Ø~0.45 at ambient conditions (Andrews, 2010). The reasons for this are discussed later, but are thought to be due to stratification of the mixture with

more dust in the spark region than for the mean composition. This <0.45 Ø MEC is a found for most of the fine biomass dust explosion MEC's in this work for this apparatus.

Figure 5.1 also shows that coarser particle sizes with no fines would explode but the MEC was much richer than for <75µm. The influence of mean particle size on the MEC for pine is shown in **Figure 5.2**. The MEC for as received (no milling) pine is also shown in **Figure 5.2** this shows that the particle size range of 300-500µm ignited with a 4J continuous spark and propagated a flame. Up to now this point has not been covered in the literature, neither coal particles nor kerosene droplets of this size range will ignite (Polymeropoulos, 1984, Cook, 1977, Man and Harris, 2014).

Sattar (2012) have shown using the ISO 1m^3 dust explosion vessel that very coarse particles of >150µm could explode and Huescar et al.(Huescar et al., 2012a, Huescar et al., 2012b) has shown that particle size for fibrous biomass and for torrefied biomass influences the MEC with fine particles exhibiting a very lean flammability limit at around 0.2 Ø, with coarser particles having an MEC closer to Ø = 1. The present work extended this earlier work into mixtures with wide and narrow size distributions. The aim was to determine if the presence of finer particles was necessary for coarse particles to burn or whether coarse particles were flammable without the presence of fine particles. For coal particles it is known that coarse particles >~150µm will not explode (Bartknecht, 1989, Cashdollar, 1996, Eckhoff, 2003) and so the ability of coarse biomass to explode would constitute an additional explosion hazard above and beyond that of coal.

The MEC results for the raw sieved pine wood samples are shown in **Figure 5.2** as a function of equivalence ratio, these were sized to the new size ranges. **Figure 5.2** shows that as expected the finer particles had the leanest limit with an MEC of 0.17Ø (~30 g/m^3). However, 100% explosion probability did not occur until 0.35Ø (70 g/m^3). The particles sieved to 300-500µm did not explode, yet particles sieved to include all particles <500µm did explode with an MEC of 1.1Ø (220 g/m^3) for 100% explosion probability a 1.8Ø was required (360 g/m^3). It is clear that very rich mixtures are required for large particle sizes to form an explosive mixture, and their behaviour is quite different to fine particles which have an MEC of about 0.2Ø.

When this fine <63µm fraction was mixed with the non-flammable 300-500µm to make a 50/50 mixture (by mass) that had a MEC value of 0.35Ø, twice the value of

the <63µm fraction. This suggests that it was this fraction alone that was burning in this material. This therefore indicates that in a mixture of fine and coarse particles not only are the fine particles controlling the MEC and rate of pressure rise but this is un-affected by the inert mass of the larger particles. These would have been expected to cool the flame but did not, at least not sufficiently to alter the MEC.

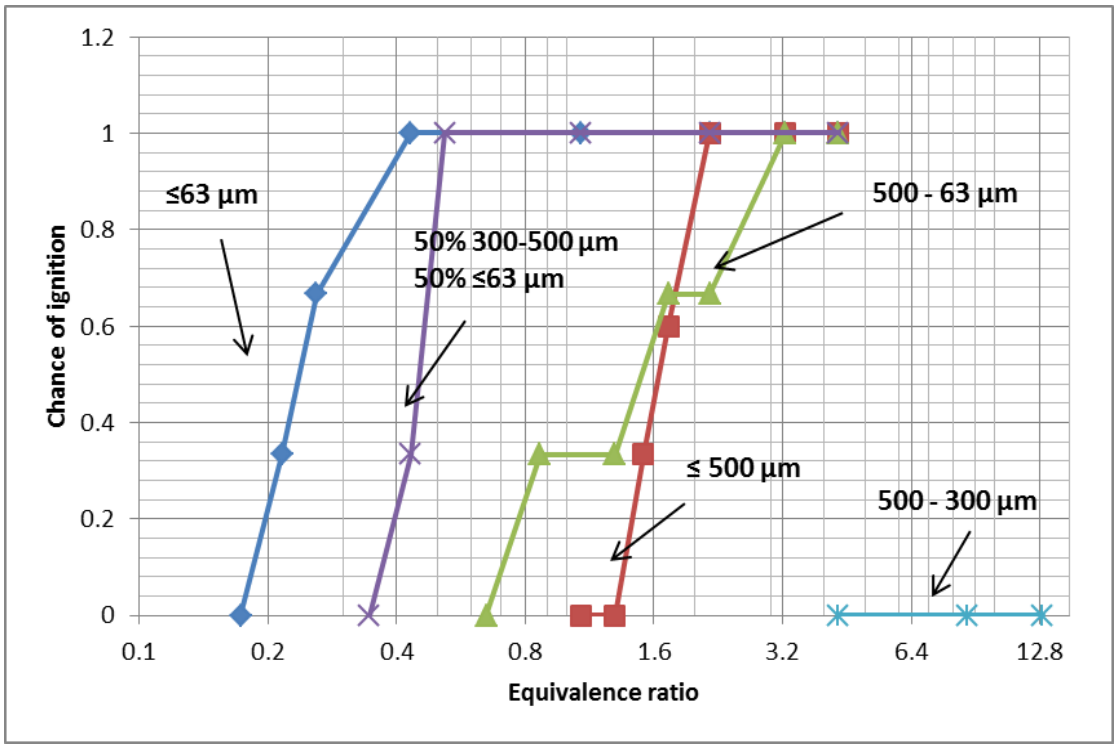

Fig 5.2 Un-milled pine sieved into different size fractions

When different materials of the same fine (<63µm) particle size were tested the MEC was found to be nearly identical (**Fig. 5.3**) even though as was shown in chapter 4 there are elemental differences in the composition between pine and oak (**Table 4.1**).

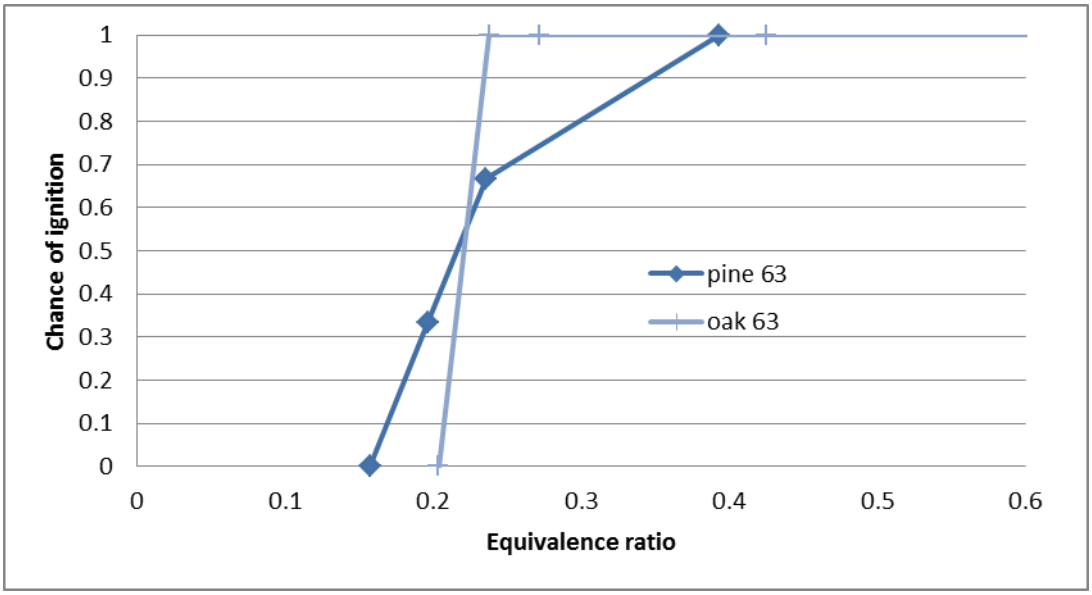

Fig 5.3 Comparason of oak and pine MEC at size distrubution <63µm.

When these same materials were tested at <500µm this was not the case. This is investigated further in section 5.3.

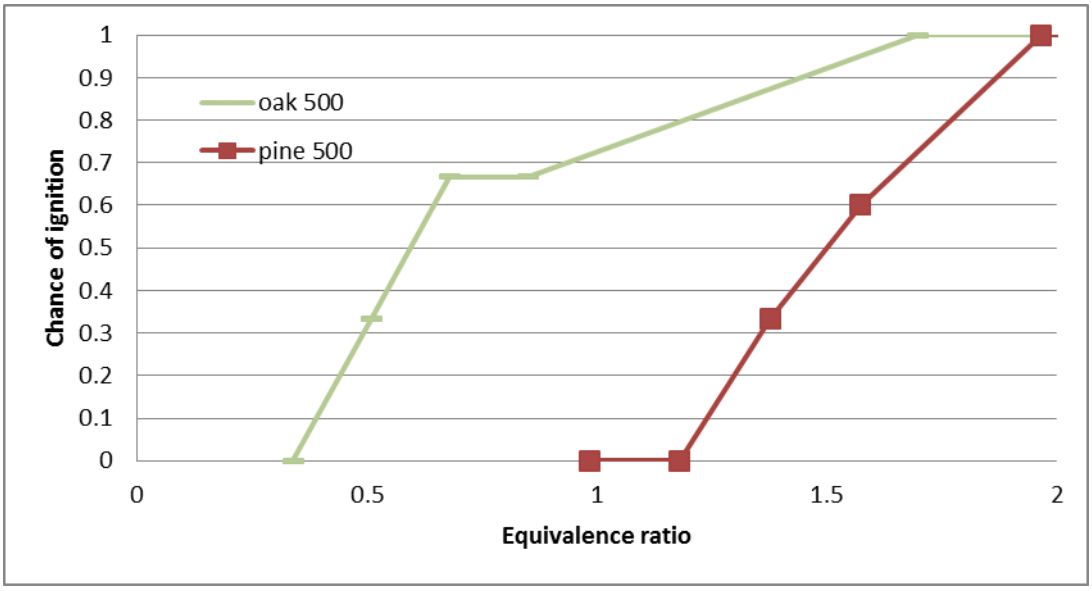

Fig 5.4 Comparason of oak and pine MEC at same size size distrubution <500µm.

When the size segregated oak was tested in the same way it showed the same dependence of MEC on particle size (**Fig. 5.5**) as was seen for pine wood (**Fig. 5.1** and **Fig. 5.2**). Mixtures with fine fractions showed higher reactivity than those without, however the 63-150µm size range for unknown reasons displayed a lower

MEC than the <63µm fraction. Also just like the un-milled pine 300 - 500µm fraction did not ignite in these tests while the milled pine 300 - 500µm did.

Additionally there appear to be to be two distinct areas that the MEC's fall into 0.1-0.35 Ø and 0.5-1.25 Ø ranges. The only outlier in this trend is oak <500µm and this is understood from **Table 4.1** to have an average particle surface area: volume ratio nearer to the 63 - 150µm size fractions than the pine <500 µm size fractions. The pellets that were milled and tested at <500µm had average particle surface area : volume ratios well below both of the aforementioned woods in the same size fraction (<500µm) however it is thought that the added inert material collected with these crop residues (see increased ash content for theses samples in **Table 4.1**) is the reason for the higher than expected (based on average particle surface area: volume ratio) MEC results. Although differences in the particle structure that arise through the pelletizing process could also be the reason for this.

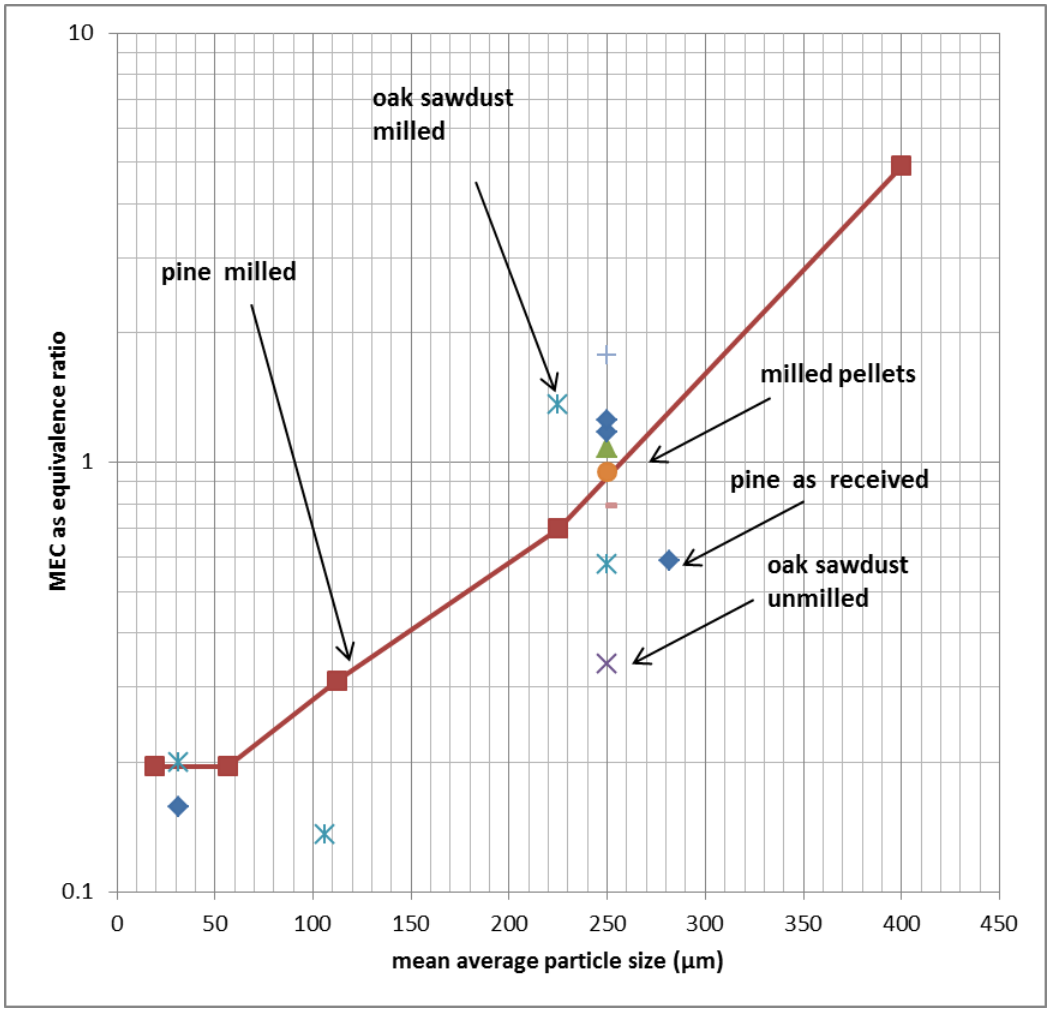

Fig 5.5 Comparason of all MEC's based on average size distrubution.

Figure 5.5 did not produce a very good correlation, this is believed to have been caused by using a mean average particle size over a large size range (0 -500µm = 250 µm, 63 - 500µm = 282µm, ect.). Therefore these tests were plotted as actual size against MEC equivalence ratio for d 0.1, d 0.5 and d 0.9.

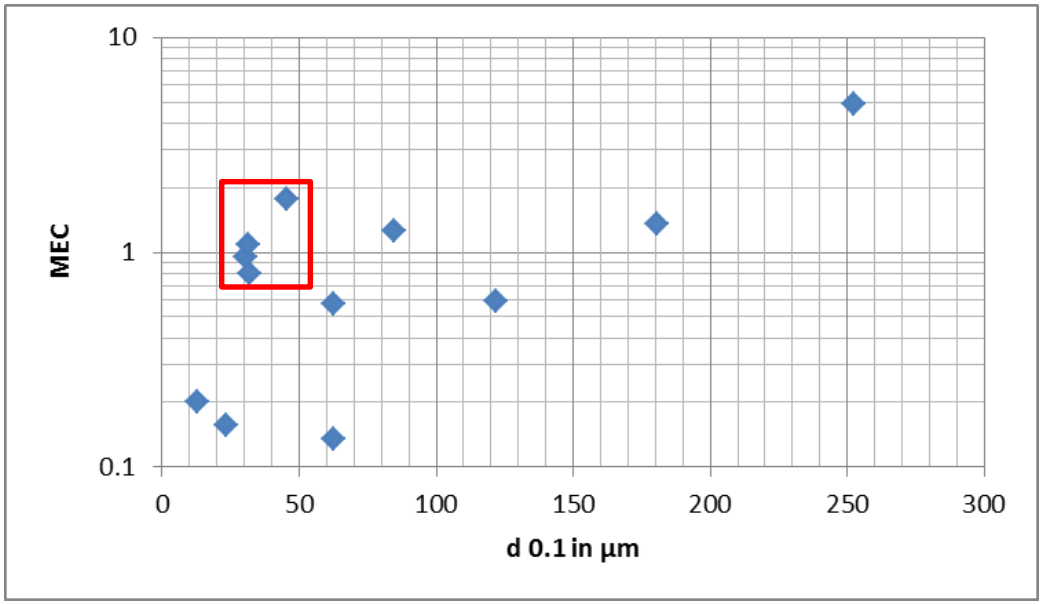

Fig 5.6 MEC (equivalence ratio) of materials tested against d_{10}

The palletised crop residues have be highlighted as the graphs displays better correlation between MEC and particle size without them.

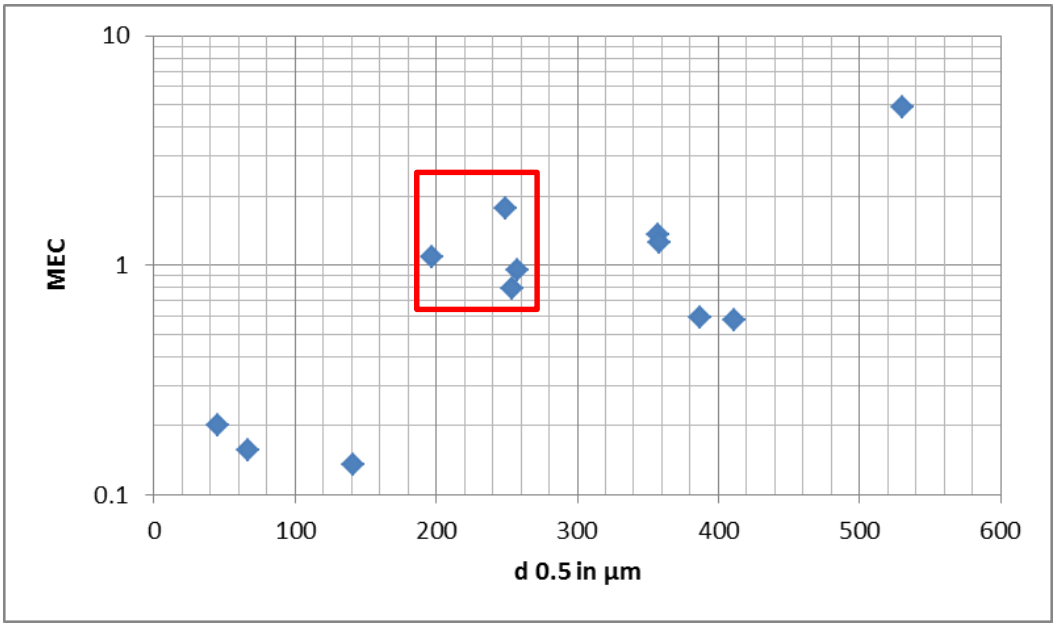

Fig 5.7 MEC (equivalence ratio) of materials tested against d_{50}

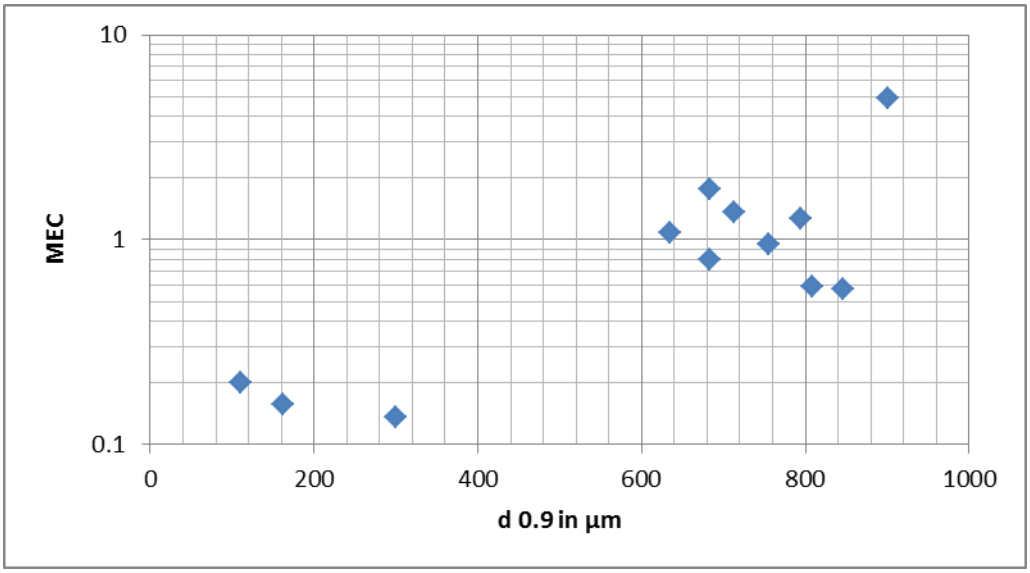

Fig 5.8 MEC (equivalence ratio) of materials tested against d_{90}

Significantly this appears to indicate that the fine component of the mixture (**Fig. 5.6**) is not the dominant effect on MEC (when all the materials are selected) as there is no trend between the size finest 10% or 90% of particles (by volume) and the MEC. The best agreement between particle size and MEC comes from **Figure 5.7** which is the particle size at which 50% of the material is reached. This suggests that the MEC, while influenced by the size distribution of the material is most effected by the average or mean particle size that dictates the MEC for a given mixture of particle sizes as Man and Harris (2014) suggested. Therefore it would appear that the larger particles in a mixture do not affect its MEC when they are in the minority by volume as the flame front that is propagating from the fine particles is sufficient to devolatilise and burn them.

However when the palletised materials are removed there is a far better correlation between the MEC and the volume of particles below 10% and 50% of the total particle volume (covered further in section 5.3). This indicates that pelletized and un-pelletized materials appear to behave differently. This could be due to the increased ash content or possibly due to the compressed nature of the material that happens during pelletizing.

5.1.2 Hartman flame speed and rate of pressure rise

The thermocouples mounted in the tube were used to detect flame speeds, however these did not corrolate well with the rare of pressure rise results from the

same tests and therfore as explained (section 3.4.2) were discarded in favour of the HSV flame speeds.

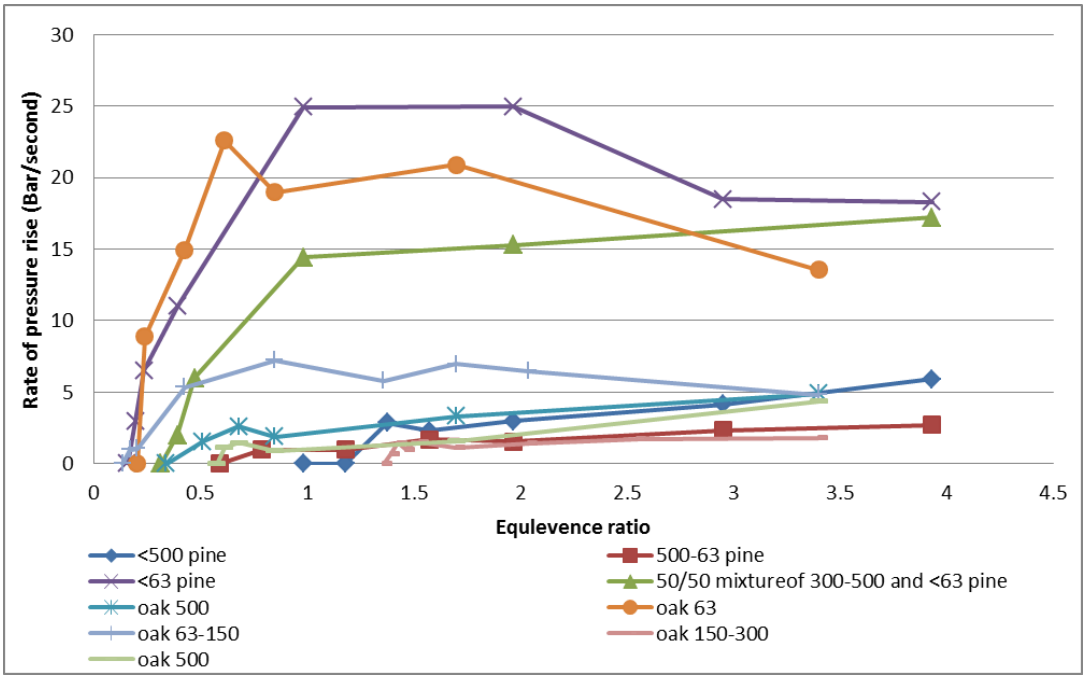

Fig 5.9 Rate of pressure rise and MEC for oak and pine size ranges tested

The results from the as received <500µm pine showed lower MEC's than the 63 - 500µm mixture (**Fig. 5.9**), this was unexpected as the particles <500µm would include fines <63µm, which were excluded for the 63 - 500µm sample. The rate of pressure rise was greater for the <500µm sample as expected from the inclusion of fines, but the MEC results were unexpected. This is possibly due to the small amounts of dust used in the Hartmann equipment which may not have been representative of the mean size distribution in this case. Alternatively in this case, the strong compressed air dispersion could have caused break up of conglomerated fine particles resulting in fines being present in the material that were not expected in the 63 - 500µm sample.

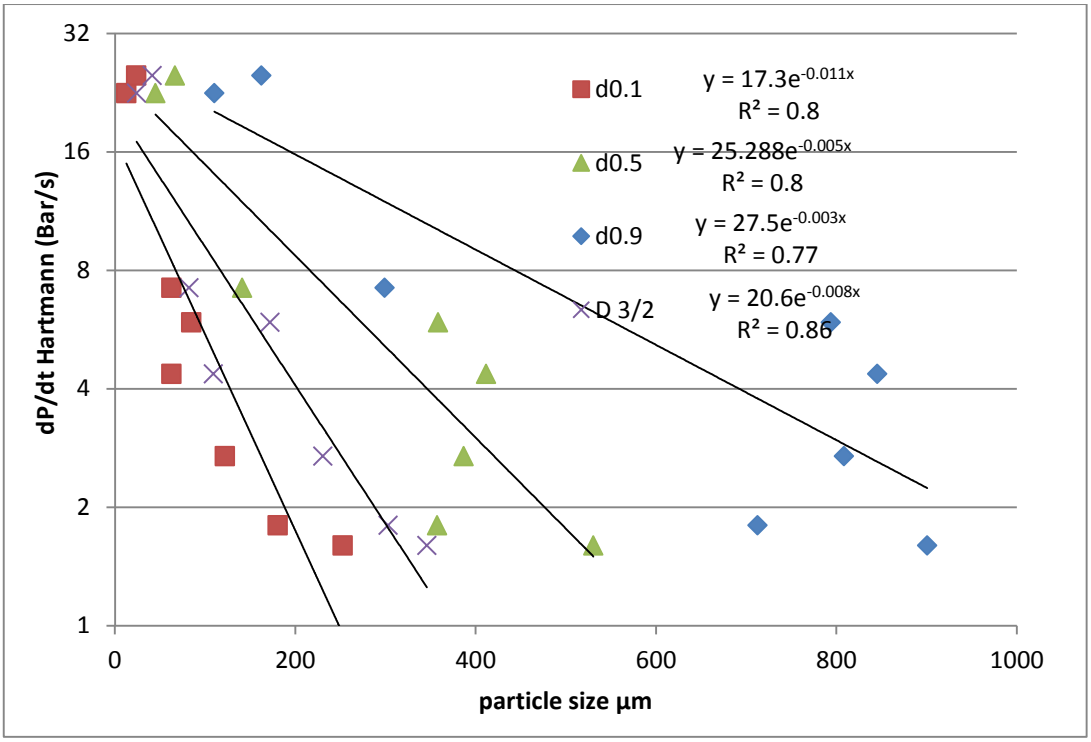

Fig 5.10 rate of pressure rise against particle size.

When the rate of pressure rise is plotted against the size analysis results (d_{10}, d_{50}, d_{90} and d3/2 which is the average volume : surface area ratio) they correlate very well. Most notably the best correlation is for the average volume : surface area ratio and the correlation gets worse for larger particles. The explosion pressure generation rate (K_{st} equivalent) appears to be controlled by the fine particles (**Fig. 5.10**), the lowest rates of pressure rise were generated from the largest particles. The pine wood 63 - 500µm size fraction produced a higher rate of pressure rise than the pine wood 150-300µm but only just, indicating that the <63µm particles are the dominant factor in rate of pressure rise generation. This is supported by the data in **Figure 5.9** where once the <63µm particles are removed (or as with the <500µm samples sparsely present) there is a step change in the rate of pressure rise produced. It is worth mentioning that the MEC of the 50/50 mixture is the same as the MEC of the fine particle mass alone, suggesting that this is what is dictating the combustion properties of this mixture.

The other samples appear to show the same trend of a gradual rising of the rate of pressure rise, with 63-150µm having values between these two groupings suggesting that this size range may be the point at which biomass samples deviate with the larger particles giving similarly low pressures and the smaller particles producing similarly high values (**Fig. 5.9**).

The material (oak or pine) appears to have virtually no effect on the rate of pressure rise as this is practically identical for pine and oak that have been size segregated the same way (<63µm and <500µm size fractions).

<63µm and 63-150µm materials both show a lessening of the rate of pressure rise (after a peak) over a concentration range of 0 – 4 in equivalence ratio while all other materials (excluding 150 - 300µm oak) are still producing higher rates of pressure rise with richer mixtures. This would make sense if the rate of pressure rise is driven by the concentration of material <150µm in size as this would still be rising in these mixtures.

This is supported by the fact that the 150 - 300µm oak which has no material <150µm in size shows no increase in rate of pressure rise with concentration. Additionally the rate of increasing dp/dt with concentration is lowest for 63 - 500µm pine indicating that while the largest effect on rate of pressure rise is from the <63µm material the 63-150µm component also plays a role if to a lesser extent.

It is proposed that the reason for the lessening of the rate of pressure rise (after a peak) in the <63µm and 63-150µm materials is due to material of this size devolatilising a much bigger percentage of its total mass than the larger particles either ahead of or in the flame front. This therefore leads to the same phenomenon found in gas explosions where the O_2 molecules become so diluted by the fuel that combustion efficiency is reduced.

A possible reason why the rate of pressure rise is affected by the finest particles in the mixture yet the MEC is not so dependent is that while the larger particles will still devolatilise and therefore propagate a flame for MEC measurements the rate at which they do so will be less that for fine materials therefore having a larger effect on the rate of pressure rise measurements than the MEC ones.

5.2 Hartman tests with high speed video

There is, as mentioned, little information on flame propagation in clouds of coarse pulverised biomass and this work was carried out to show that coarse biomass could burn in a similar way to fine biomass but with slower flame speeds. There is little in the open literature on flame propagation and explosion risk for fine or coarse biomass particles and this work presents some results using the Hartmann dust explosion tube with high speed photography to do so. All the materials and size

fractions run on the $1m^3$ were also run on the Hartman with high speed video recording as this allowed both observation of the flame structure as well as comparison to the thermocouple flame speed results from the $1m^3$.

High speed videography was carried out on Hartman explosions at 5000 fps to try to determine the flame speed, shape and how it interacts with particles. This was done as full tube and close up footage, the first contains the whole propagation through the tube while the second is only focussed on the spark area to investigate the flame/particle interactions. The first method worked best allowing the propagation and behaviour to be clearly observed, as it passed up the tube.

The thermocouples failed to record accurate results as thermocouple 2 and 3 activate simultaneously due to the bursting of the vent forcing the fireball up into the second and third thermocouple. As the high speed footage shows, by the time the flame front has reached the second thermocouple and in the majority of cases before, the vent bursts taking it from a constant volume to constant pressure environment. This change forces the flame to accelerate out of the tube. This is the reason for the unreliable thermocouple flame speeds from the Hartmann apparatus in section 3.4.2.

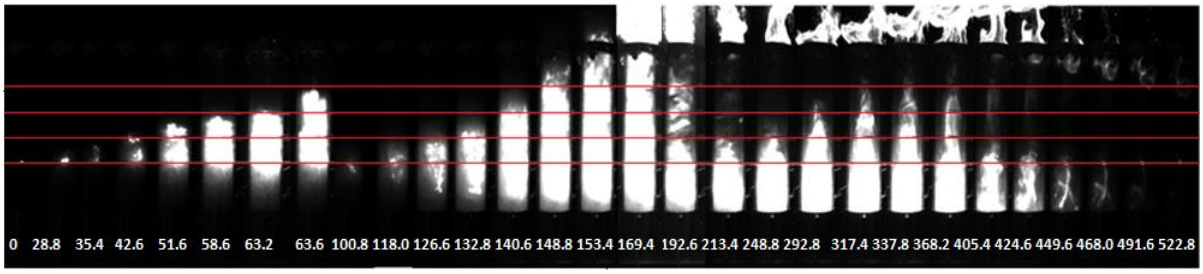

Fig 5.11 Oak less than 63µm (Ø=1= 218.9) 0.5 g, 375g/m³, Ø=1.71

Issues with determining the explosion concentration arose due to the fact that each single test resulted in 3 -4 separate flame propagations (**Fig. 5.11**). There was the initial propagation, a second one follows straight after, followed by a final upwards propagation and then a downwards propagation. This downwards propagation is particularly interesting as it originates from the independent flame that develops at the top of the tube approximately 154ms after ignition and remains there for 275 ms before re-entering the tube. The only feasible reason for this external flame to have arisen is that the combustion in the tube below it has produced more volatile products than could be burnt in the oxygen available. Therefore these remained

unreacted until they exited the tube and mixed (through diffusion) with the external air where enough oxygen is present to allow combustion to take place.

This indicates that the combustion taking place in the tube is very rich, with most of the devolatilised gasses unable to react within the tube. It is unknown at what rate the particles are exposed to the flame temperature or the rate of gaseous devolatilization of the solid; this makes it nigh on impossible to determine the gaseous product concentration that the flame is propagating through. Although these images do not allow for the determination of the flame thickness, they do suggest that the flame thickness is greater than the 20mm proposed by Han et al. (2000) as the luminosity does not decrease as the flame progresses up the tube.

The Hartman tube and high speed camera were set up in a fume cupboard to stop the escape of the combustion gasses and provide extra containment in the event of any unforeseen problem's arising during the experiments.

5.2.1 Hartman flame propagation

For each test 3 concentrations were made into montarges. These concentrations were very rich (1g = 750g/m^3), the MEC and a value between these. These were decided upon based on the fact that different materials or material of different particle sizes have different MEC's and stoichiometric values. Therefore concentrations were needed that were independent of these variations. These were selected as 1g as this concentration is very rich for all the materials tested, the MEC value for each material as this is a repeatable point for all the materials tested. The final value was chosen as either 0.5g or half way between the other values as this was observed to be the value at which most materials began to exhibit two propagations, for more reactive mixtures 0.25g was also added if that was after the MEC had been encountered.

The initial flame front propagation before the vent has burst was the only flame that propagated through the injected concentration (theoretically); therefore it is the only flame speed for that test. Once the vent burst the flame exited the top of the Hartmann tube and then air entered the tube as the products of the first flame propagation cool and this caused a reduction in pressure, which created a vacuum that drew air into the tube. As the initial mixture was rich there was fuel left in the tube that caused a second flame propagation in the tube. For coarser oak dusts the

flame was more fragmented and propagated more slowly, but there was still a clear explosion risk.

Although initially high speed photography was run on both full tube and half tube shots it was rapidly discovered that the half tube shots were of little use in this study. Mainly due to the low levels of luminosity preventing observation of the thermocouples for flame speed generation. However they did provide good images of the flame structure of near limit dust combustion (**Fig. 5.12**).

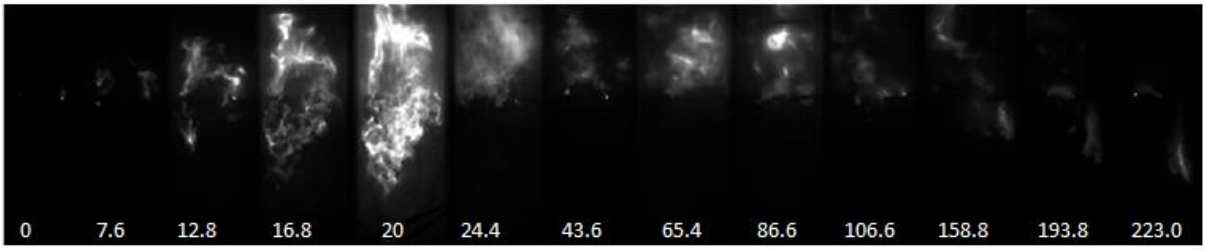

Fig 5.12 Lycopodium 37.5g/m^3, Ø= 0.307 close up

The photographic images show that apparently the combustion behaviour of the materials tested are dictated by the finest and average particle size's as was suggested from the dp/dt results (**Fig. 5.10**) in section 5.1.2. <500µm oak tests displayed the same flame elongation tendency's as 150 - 300µm when these were burnt on their own indicating that the large particles here are burning which would explain the dp/dt and flame speed results (**Fig. 5.9** and **5.13**).

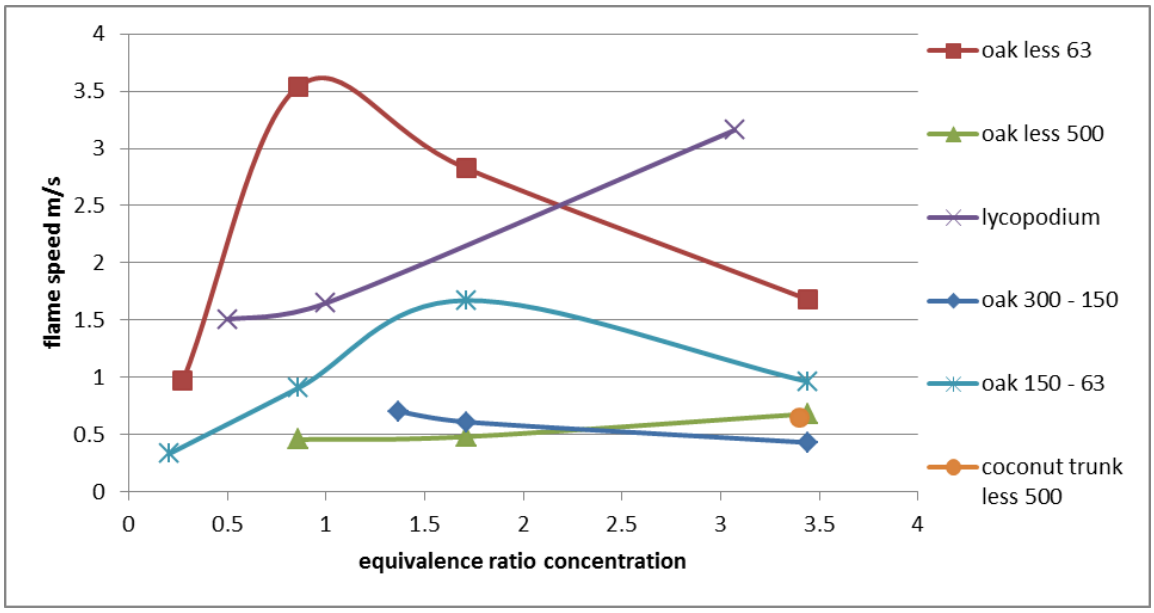

Fig 5.13 High speed video flame speeds for oak and lycopodium

For <40µm material the whole particle appears to devolatilise ahead of the flame front resulting in a flame propagation similar to that of gas combustion (faster flame speeds that particle to particle propagation) Burgoyne and Cohen (1954). While for larger particles the flame front devolatilises a part of its mass ahead of the flame front and the remaining particle mass burns in an envelope flame behind this flame front with the remaining oxygen. The equivalence ratio of the initial flame front is determined by the particle size, the closer the particles are to <40µm the closer the devolatilised fuel concentration will be to the dust concentration it passed through. Therefore the gas equivalence ratio will be closer to 1 (the concentration where the fastest flame speeds are found for gaseous mixtures) the finer the particles are and the closer the concentration of fine particles are to Ø = 1. That appears to be what is being shown here with oak dust <63µm showing its fastest flame speed just lean of stoichiometric while 63-150µm having it at an equivalence ratio of 1.71. This supports the theory that the reactivity of dust explosions is intrinsically linked to the surface area : volume ratio of the dust tested.

For all the materials tested the flame shape has a strong dependence on the particle size- with fine particles the flame develops as a uniformly luminous ball with a slightly irregular but not elongated flame front (**Fig. 5.11**). It is proposed (Gao, 2015) that this elongation tendency in flames for large particle tests (**Fig. 5.14**) is due to lean fuel mixtures around the devolatilising particles making buoyancy a significant factor in propagation. This mixture is (as the dust was) of an un-uniform mixture resulting in directional differences in the flame propagation depending on the overlap of these devolatilised gas pockets with each other and unburnt particles. This results in irregular, elongated flames for the larger particle explosions (>63µm) (**Fig. 5.14**) and smoother more spherical propagation in finer particle sizes (<63µm) (**Fig. 5.15**). This was suggested by the Biot number calculations done in section 2.3.8 where the larger the particle and the larger the velocity difference between the particle and the gas flow the more thermally thick the particle becomes therefore devolatilising less of its mass ahead of the flame front. This results in a leaner (less luminous) flame front that's propagation is linked to the particle distribution. As the particles become more thermally thin the particle devolatilises more of its mass ahead of the flame front and its propagation becomes more uniform.

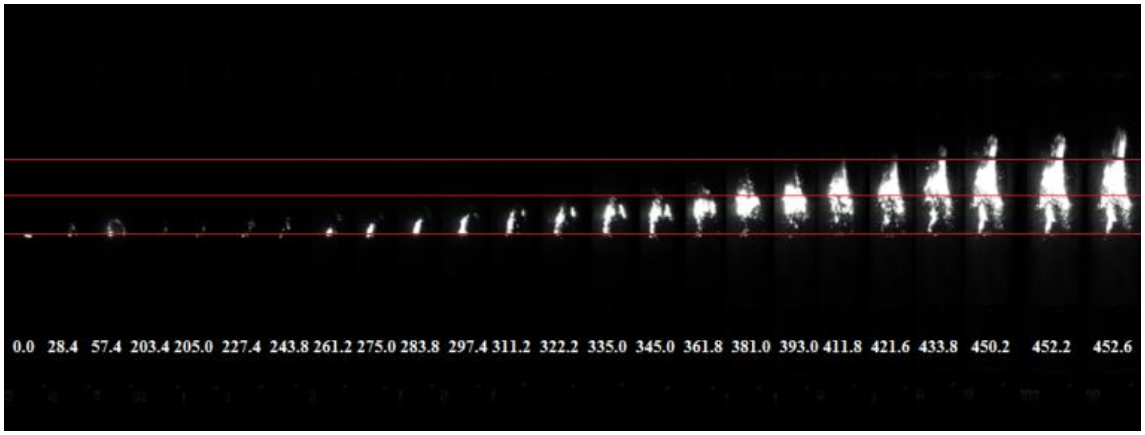

Fig 5.14 Oak 300 -150µm (Ø=1= 218.9) 0.5 g, 375g/m^3, Ø=1.71

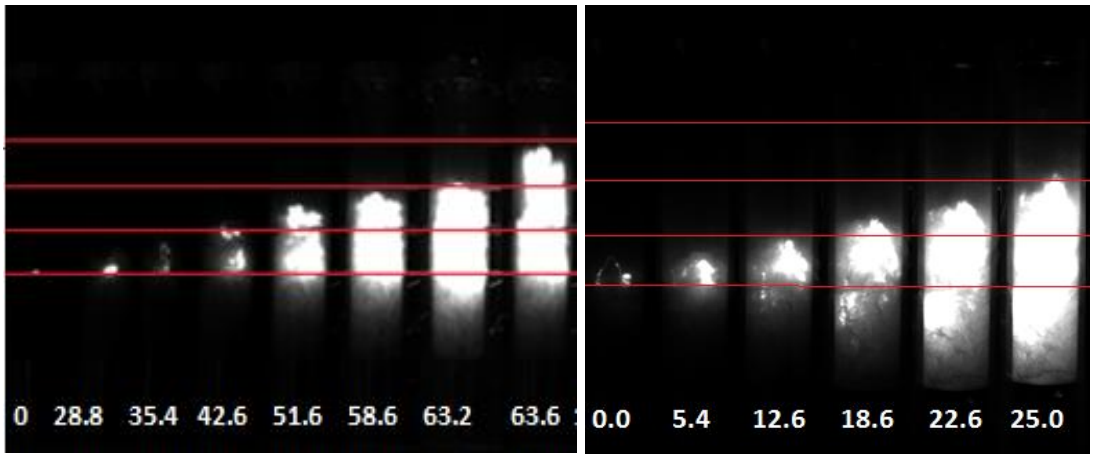

Fig 5.15 Oak <63µm 375g/m^3, Ø=1.71 Lycopodium powder 375g/m^3, Ø= 3.07

The observation that bigger particles produce less luminosity in the initial flame front is believed to be due to a combination of factors, firstly as they release their volatiles slower than small particles (Bidabadi and Rahbari, 2009), there is therefore more oxygen present in the gas mixture leading to less soot production. This is exasperated by the ease of entrainment of small particles compared to larger ones (**Fig. 5.22**). Second due to the higher flame speeds found in smaller particle tests it is suspected that the fine particle combustion is burning material at a faster rate and therefore putting out more luminosity.

It was also observed that for bigger particles at low concentrations there was less likely hood of the flame moving off the spark, appearing to need the constant spark energy input to maintain the combustion (**Fig. 5.16**). This implies that the larger particles need the spark to be constantly partial devolatilising the particles prior to entering the stabilised combustion zone. Those devolatilised gasses would then

propagate/sustain the pre-existing, stabilised combustion that would then consume the remaining particle mass behind the flame front (Han et al., 2000, Proust, 2006, Yao B. Yang and Jenny M. Jones, 2008, Bidabadi and Rahbari, 2009).

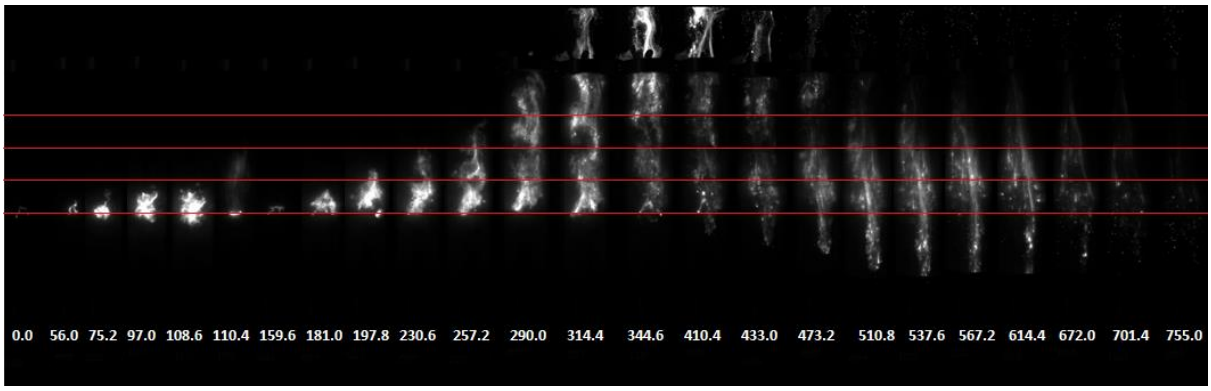

Fig 5.16 Coconut trunk <500µm 0.5g 375 g/m^3, 1.75 Ø

While reviewing the footage of the combustions it was noted that all of the videos showed a larger amount of obscuration (caused by dust), this was mostly seen below the flame (**Fig. 5.17**). This indicates that the dust is not uniformly dispersed within the vessel at the time of ignition. Therefore the MEC data generated was for a richer concentration than the nominal dust loading would indicate, this would help a lot in explaining the MEC values for fine dusts that were well below the 0.5 equivalence ratio that is the MEC for most HC gasses (**Fig. 2.14**).

The spark is located 37% of the way up the tube and the 1st thermocouple 50%, therefore as **Figure 5.17** shows the actual MEC is between 2-2.7 times the nominal MEC (actual measured mass is only occupying 37%– 50% of the volume, therefore actual concentration is 100/37 – 100/50 = 2-2.7 times the nominal MEC).

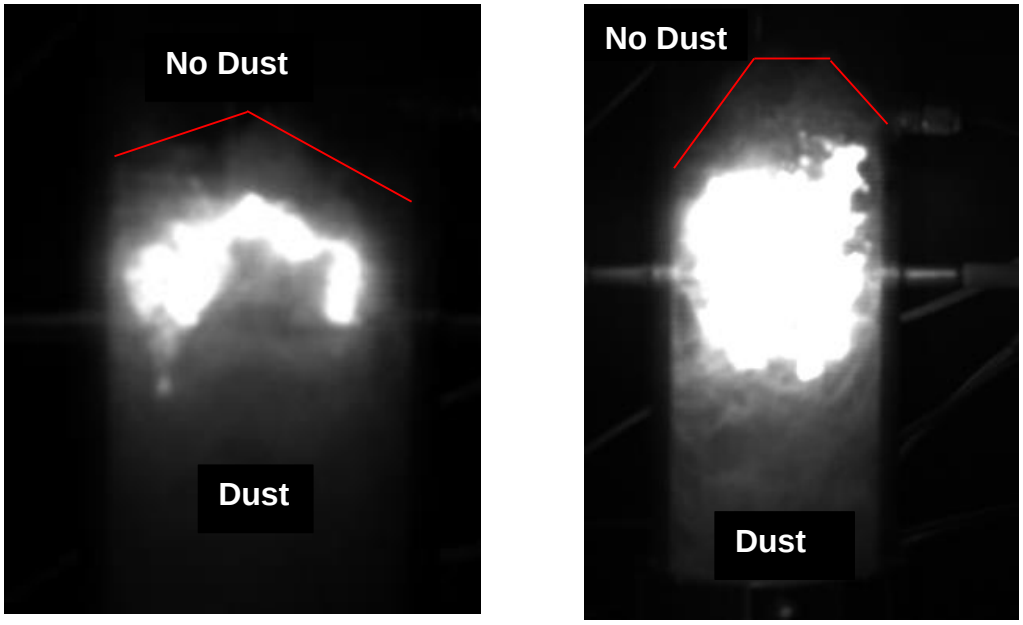

A B

Fig 5.17 A - Oak <63µm 0.25g and B - Oak 63µm 0.08g

However this is not a fixed conversion factor and will be affected by the particle size used due to the ease of entraining smaller particles into the air flow. Another issue is that finer particles ignite faster (**Fig. 5.22**) after the dust has reached the spark region due to more material being in the spark path at a given time. This makes determining the MEC using this equipment difficult.

A phenomenon that was observed in all the tests was that for rich tests after the vent bursts there is a second and sometimes a third flame propagation (**Fig. 5.18**), this can also be accompanied by an independent flame located at the top of the tube. This flame indicates that the second flame propagation is burning so rich that the unburnt devolatilised gasses are setting up a stabilised diffusion flame at the top of the tube where the air mixes with these unburnt gasses.

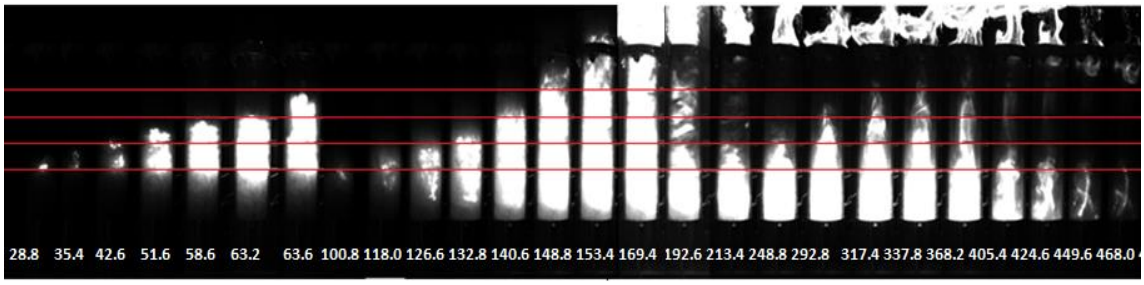

Fig 5.18 Oak less than 63µm (Ø=1= 218.9) 0.5 g, 375g/m^3, Ø=1.71

This shows that there is still sufficient dust in the tube, in suspension after the first propagation to sustain combustion (the bursting of the vent may also be helping to keep dust in suspension). This therefore raises the question that if this is combined with the uneven distribution – how can these tests be reliable when there is at present no sure method of knowing the mass that took part in the combustion. By adjusting for the unequal distribution using the high speed video footage to estimate the distribution of the dust at the time of ignition.

5.2.2 Hartman single particle combustion/spread

It was realised that the video footage showing single particles burning (for larger size, high concentration mixtures mostly) could be used to determine the burnout time of particles and hopefully gain some insight into the propagation mechanism and whether heterogeneous, homogeneous or a mixture of both combustion methods in the form of a double flame structure (Gao, 2015) is taking place as was suggested in the literature.

Assumptions - were made in the analysis of the videos for this section - it was assumed that the particles were spherical, equal in size and uniform chemically. The particle sizes were determined by sieve separation in to - ≤63µm, 63 – 150µm, 150 – 300µm, 300 – 500µm and ≤ 500µm, as these were ranges it was assumed that all particles had median size (150 – 300µm = 225µm Diameter particles). Both concentration and density are in g/m^3, the volume is standardised to 1 as this is constant throughout the calculations and will in no way effect the particle separation calculations as the separation distance between particles in a 50g/m^3 mixture is the same whether the mixture is made in a 1m^3 vessel or a 1,000,000m^3 vessel.

Volume of space taken up by each particle

The bulk density of oak sawdust of various sizes was found, from these and the previous assumptions it was possible to estimate the number of particles in each concentration by rearranging

$concentration = \frac{\frac{4}{3}\pi r^3 \rho N}{V}$ to $N = \frac{\frac{concentration}{\frac{4}{3}\pi R^3}}{bulk\ \text{density}} \times V$ for different particle sizes.

Then to generate a spatial distribution for these particles they were assumed to be evenly distributed around the vessel by

$$distance\ between\ particles\ (edge\ to\ edge) = \left(\sqrt[3]{\frac{1}{N}}\right) - 2R$$

Where R is the particle radius and V = 1 as the volume is constant.

This was combined with the MEC data from the Hartman tests to generate a critical separation distance between particles at their MEC (**Fig. 5.19**). This shows an increase in separation at MEC up to around 200µm particle diameter at which point it levels off at around 1500-2000µm. It could be interpreted that at this point the volume of the particle ceased to matter as the initially devolatilised material at the edge of the particle is sufficient to reach the MEC. One interpretation of this is that the particles transitioned from thermally thin too thermally thick and there was insufficient time to devolatilise any more material no matter how much more material was available.

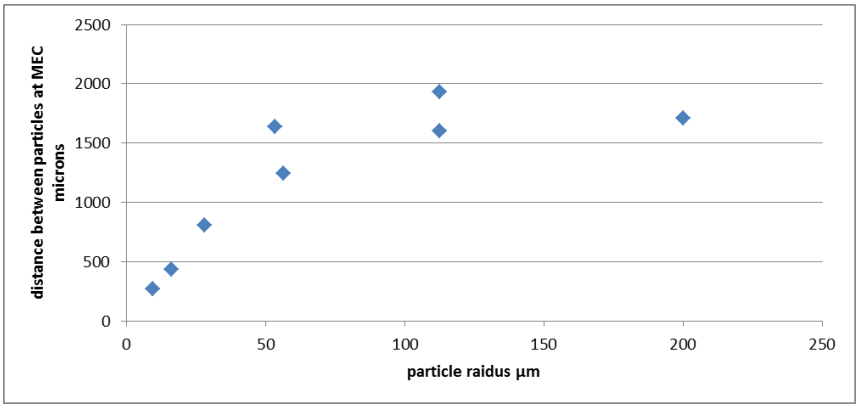

Fig 5.19 Seperation distences against MEC for oak and pine tests

Interestingly this phenomenon occurs at the particle size Yao B. Yang and Jenny M. Jones (2008) estimated biomass particles would make the transition from thermally thin too thermally thick (150-200µm in cylindrical particles) even though it was assumed that the particles were spherical for these calculations.

The separation distance against concentration was also plotted to show how it varied as the concentration was altered.

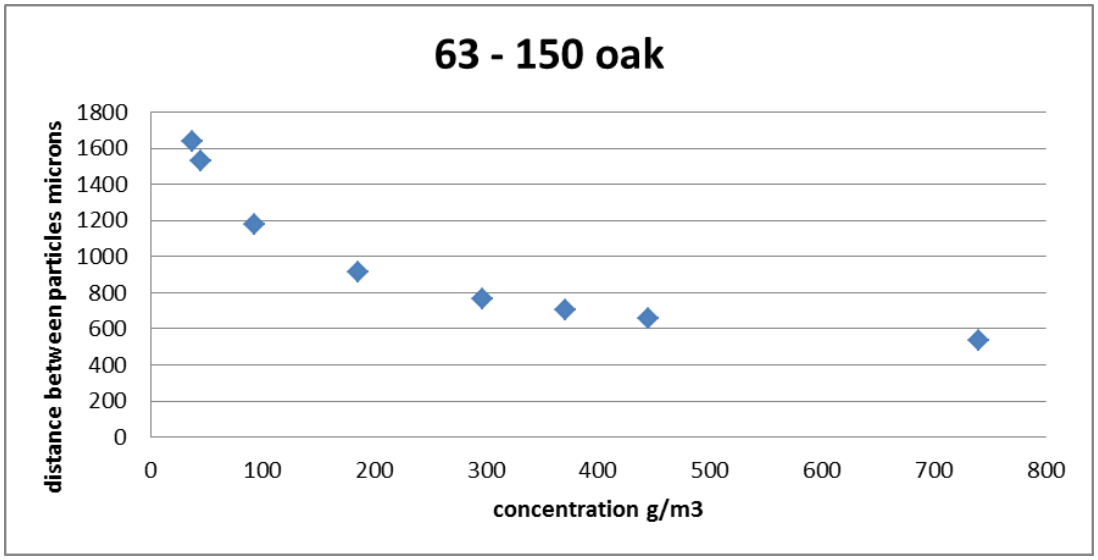

Fig 5.20 Seperation distences oak 63-150µm fraction.

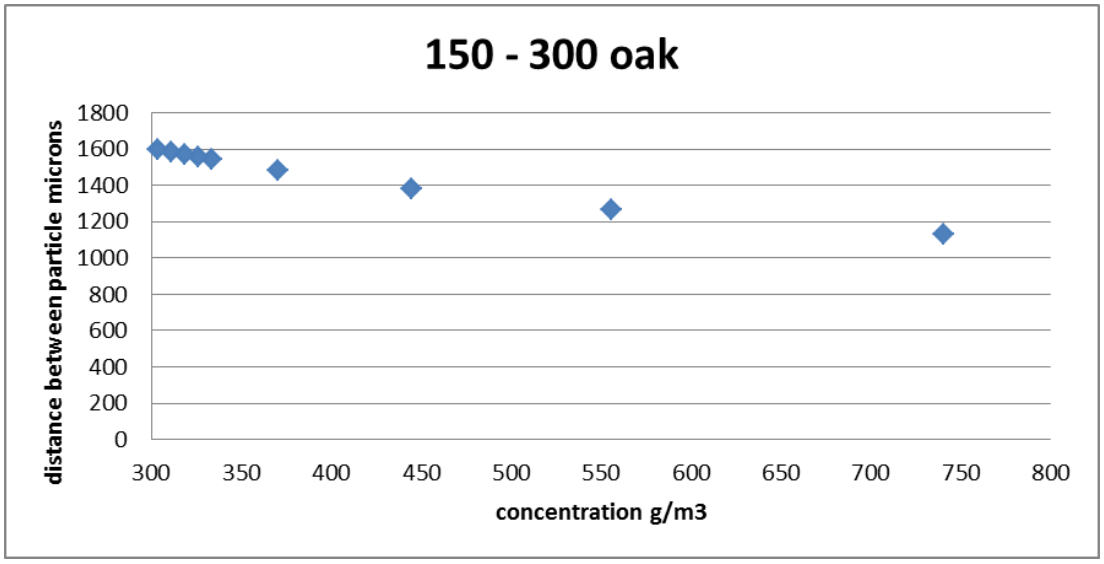

Fig 5.21 Seperation distences oak 150-300µm fraction.

It was also attempted to relate the surface area to the MEC (**Fig. 5.22**) however this did not produce any meaningful results, this may have been due to the wide range of particle sizes used in some mixtures, i.e. <500µm.

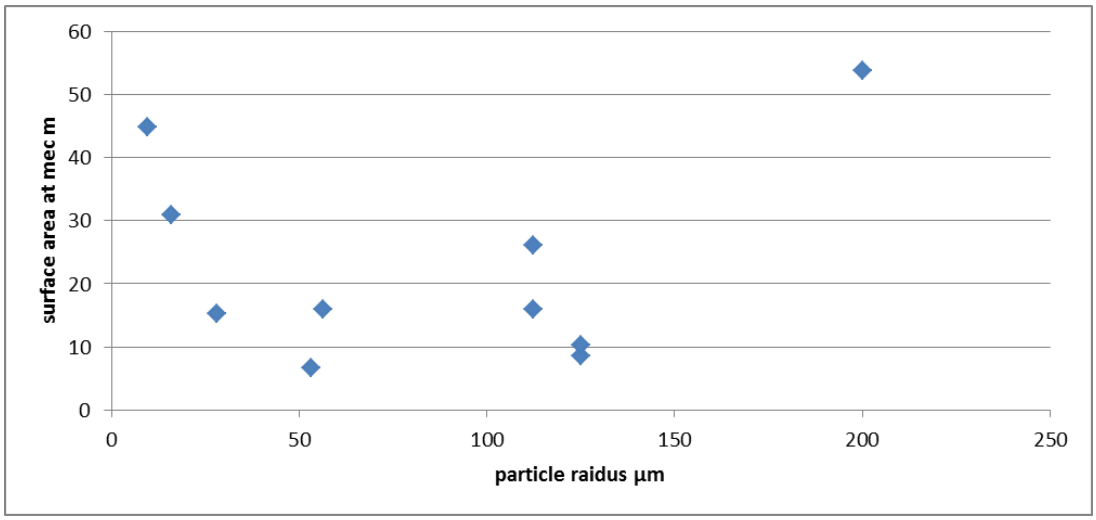

Fig 5.22 Surface area plotted against MEC.

5.2.3 Single particle combustion and propagation video

With the critical separation calculated it was speculated that this could be confirmed with the HSV footage that had been captured, especially in the early stages of propagation of larger particles. This is because larger particles have a longer delay between the injection of air and the vent bursting (**Fig. 5.23**).

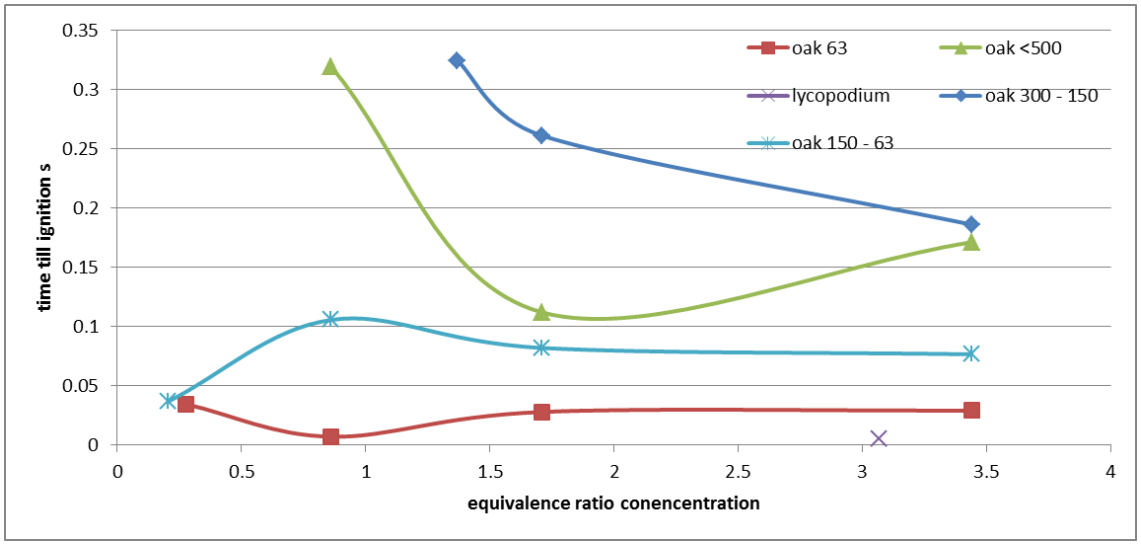

Fig 5.23 Delay between injection of air and the vent bursting.

This is believed to be due to –

- Less particles per given volume and therefore less probability of a particle in the spark zone at any point in time to begin propagation.

- The volume : surface area ratio increases with particle size, therefore there is less likely hood of said particle releasing sufficient volatiles to allow propagation.

- The increased resistance to dispersion caused by a larger particles inertia makes it likely that the time taken to get too the spark is larger for big particles than for small ones.

It was found that the best times to observe particle to particle propagation in the HSV was ahead of the main flame development due to the flame luminosity preventing the identification and tracking of single particles after this due to it creating too much background luminosity or entraining the particle into the main flame.

These 10 still images were taken by a high speed camera for Oak 150 - 300µm, 0.75g, recording at 5000 fps. The images were enlarged from the original video to provide more detail at such a large magnification without ruining the images.

HSV timings- 1186.2 1188.0 1184.4 1189.0 1189.6 1189.8 1190.0 1190.2 1190.4 1190.6 Total time elapsed = 4.4ms

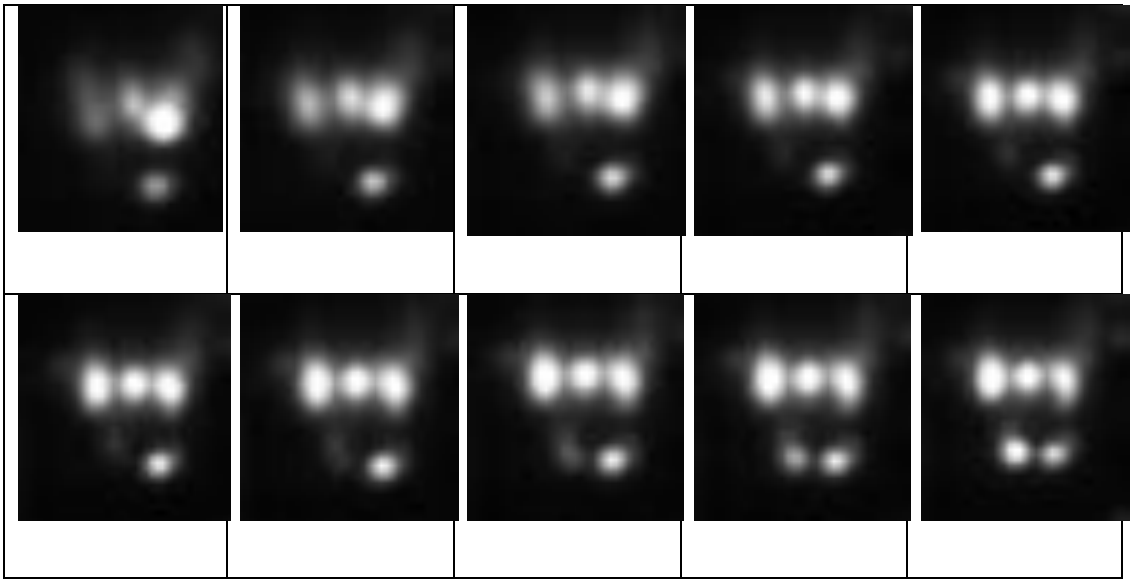

Fig 5.24 Particle to particle propagation in 150-300µm oak.

The fact that this is a 2D view of a 3D situation is appreciated, however no software/technology was found that could provide a 3D view from the images.

The images appear to show a right to left propagation from the far right particle to far left particles. Of more interest however is the very faintly luminous protrusion that develops below the top left hand particle. In the first images, this begins to detach itself from the bottom of the particle and begin to travel downwards. In the 8th image this protrusion increases in luminosity and size significantly before becoming a spherical, luminous ball exactly like the 4 others in the frame. As this luminous protrusion travelled through the space that existed between the particle/location of origin and the secondary particle in a transient manner, this would appear to show that the protrusion was a gaseous flame. This is deduced as the particles appear to burn with a more intense light and display a distinct spherical shape.

The flame development shown in **Figure 5.24** matches closely with what (Gao, 2015) report as devolatilization-controlled regime double flame structure flame propagation. The still images show it is clear that the particles do not fully devolatilise (at least at this particle size) ahead of the flame front and are therefore possibly acting as radiating bodies behind the flame front (Proust, 2006). Therefore the assumption that radiation plays no part in heating the particles ahead of the flame front (Proust, 2006) may need to re-examined for large particle combustion.

5.2.4 Single particle combustion – separation distance

After the particle to particle footage had been analysed it was decided to try and calculate the size of the flame and if possible the duration it lasted for. Although this has been done many time for individual particles (Yao B. Yang and Jenny M. Jones, 2008, Zanzi et al., 1996, Biagini et al., 2006, Commandré, 2011) this is (to the authors knowledge) the first time it has been done for an explosion situation involving multiple particles.

As the videos showed both the apparatus and the combustions in each video this was used as a scale to judge the size of other objects by. The stills of the tube of known size formed the starting point for an effort to calculate the distance between burning particles.

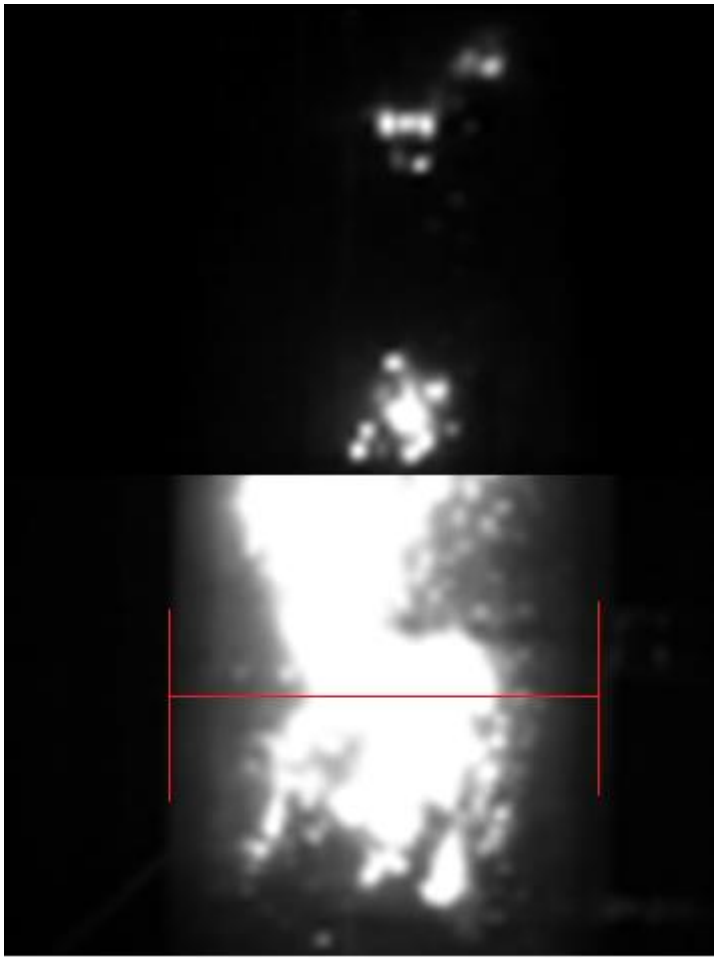

Fig 5.25 Images used to scale the magnified particle to particle propagation images.

Error margin for measured values is 0.5mm either way

Pic of tube is 6cm (*measured*) (from outer lit point to outer lit point), actual diameter 7.5cm

3 point flames total size edge to edge *measured* = .7cm

6/7.5 = 0.8 so 0.7 x .8 = **0.56 cm or 5600 µm**

Error is therefore 4764 - 6450 µm

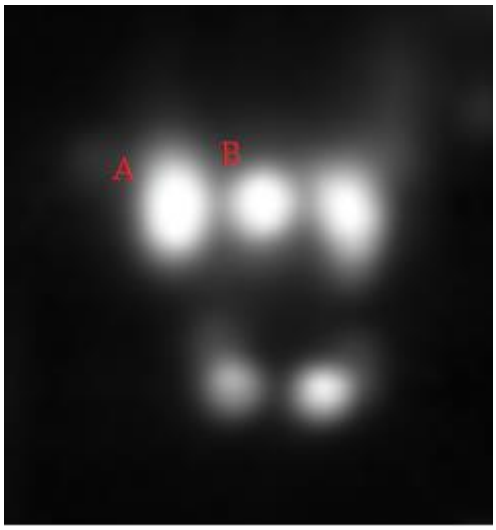

Fig 5.26 Particle to particle propagation A-B.

150 – 300µm particle separation up to **1600µm from calcs** at MEC, particle diameter average 225µm.

New expanded image – 32000µm (*measured*) while calculated at 5600µm

Therefore ratio measured to actual = 0.175

Error is therefore = 0.149 - 0.23

Distance *measured* between centrelines of particles A and B – 1.1cm = 0.175 x 11000 = **1925µm**

Therefore distance between particles = 1925 – 225 = 1700µm

Error is therefore 1564 - 2334µm

Distance *measured* between luminous areas of particles A and B – 0.3cm = 0.175 x 3000 = **525µm - flame separation**

Error is therefore 372 - 710µm

Assuming particles were and still are 225µm diameter

Distance *calculated* between edges of particle and flame front (flame thickness) = **(1925 - 525 – 225)/2 = 588µm flame thickness**

Distance *calculated* between centre of particle and flame edge (flame thickness) = **588µm flame thickness + 112.5 particle radius = 700.5µm**

Error is therefore 314 – 868.5µm

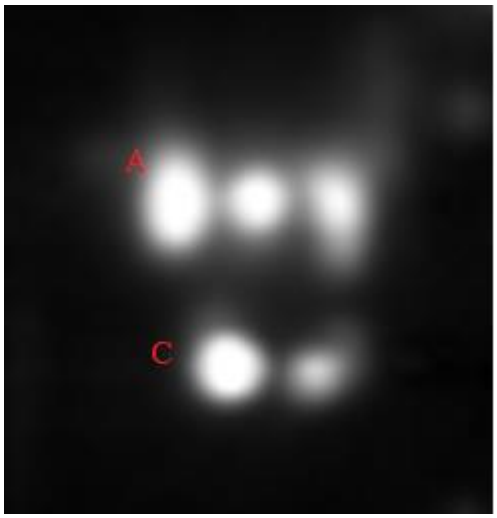

Fig 5.27 Particle to particle propagation A-C.

Distance measured between centrelines of particles A and C – 2.4cm = 0.175 x 24000 = **4200µm**

Therefore distance between particles = 4200 – 225 = 3975µm

Error is therefore 3500 - 5000µm

Distance measured between luminous areas of particles A and C – 1.5cm = 0.175 x 15000 = **2625µm**

Error is therefore 2160 - 3150µm

Assuming particles were and still are 225µm diameter

Distance calculated between edges of particle and flame front = (**4200 - 2655 – 225)/2 = 660µm**

Therefore distance between centreline of particle and edge of flame = 660 + 112.5 **= 772.5µm**

Error is therefore 62.5 - 1307µm

2625 µm greater than 1600µm so not within the critical separation calculated from MEC.

However the video stills show a faintly luminous flame propagating from particle A to particle C. As there is no continuous burning in the path this flame takes it has to be assumed that this flame (prior to reaching particle C) was propagating on gasses (volatile gasses released prior to this point). This indicates that particle C was under thermal stress prior to the flame reaching it resulting in the release of volatile gasses (Gao, 2015) that the flame propagated on to reach the particle. However due to not being able to see the particle prior to ignition it is impossible to tell how this thermal energy was delivered to the particle or how far it had been devolatilised prior to the images. This previous release of volatiles may help explain how this particle can be ignited even though it is just over twice the calculated critical separation distance from its ignition source. It may be that due to un-equal distribution within the tube at ignition (0s ignition delay) as shown **Fig. 5.17** the calculated separation distance may be out if the fuel is unevenly distributed, although that would reduce the separation distance needed even further. A more likely explanation is that this particle was only able to ignite due to the previously released volatiles providing a pathway for the established flame on particle A to travel down. It would be useful to assess the degree of unequal distribution within the Hartman at the time of ignition to re-calculate the separation distances based on the actual volume of the tube they occupy at the time of ignition.

Calculated separation (MEC) = 1600µm

Calculated separation from A – B (HSV) = 1700µm

Calculated separation from A – C (HSV) = 3975µm

It was hoped that that the measured values could be used to back calculate the burnout time of the particles to validate the calculations done so far. However due to a number of factors this proved impossible. These were -

- Going from particle mass to devolatilised gas volume was impossible as the A/F ratio for the devolatilised gasses varies massively, from 15-17 for CH gasses (methane, ethylene, butane….) and 2.4 for CO and H_2. That meant that depending on the volatile species used the gas volume could vary by a factor of 7.

- The above values assume that it was a stoichiometric concentration of the aforementioned gasses that burnt which is not known.

- The expansion ratio varies for 5–8 depending on the flame temperature, this is affected by both the gas species and the concentration it burnt at.

The combination of these factors made it so that any values generated would most likely be wrong by a large margin.

From the footage it was possible to record 8 instances of single particle burnout, an example of which is shown below.

Oak 150-300µm 0.75g 1177.6 1182.6 - 1207.4 total burnout time = **<u>29.4 ms</u>**

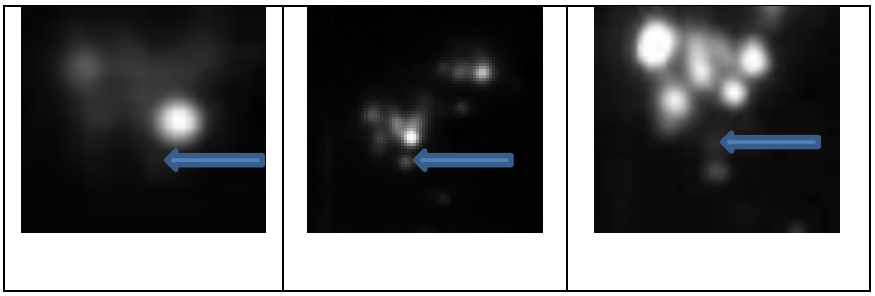

Fig 5.28 Single particle burnout time from video.

The average burnout time was 22.5 ms over 8 particles that were observed.

Using an equation for biomass particle burnout time *(Mason, 2015)* it is possible to calculate the time taken to burn the volatiles within the particle completely (visual combustion).

volatile flame duration = am^b

m=mass in mg

a=1.33

b=0.59

$=1.33 \times (0.00185)^{0.59}$ = **32.4ms**

If the volatile mass (from TGA) is used

$=1.33 \times ((0.8*0.00185))^{0.59}$ = **28.5ms**

This is very good agreement with the observed values. The mass of 0.00185mg was found by the average particle size (225µm) volume multiplied by the material density, 310 kg/m^3 the agreement suggests this assumption is no too inaccurate.

Assumptions that need testing/altering

Spherical particles – SEM and size analysis would be the best method of doing this, the SEM could be used to measure the actual particles dimensions. Although the size analysis is incorrect (section 3.3.4) it allows comparison of the size distribution within a sample of similarly shaped particles to be compared to each other as was the case with these samples.

5.3 MEC

Having failed to relate the MEC of fine materials to the particle surface area: volume ratio (**Fig. 5.22**) it was attempted to link it to the inert components of the mixture. This was done as it was thought that with the volatile mass of most biomasses being nearly identical and Kobayashi et al. (1977) and Lewellen (1977) research indicating that any differences in volatile yield in TGA tests would be negligible to non-existent in real explosion conditions. It was thought that the percentage of inert material in the fuels composition may be dictating the MEC as this would not only displace combustible material in a fuel controlled environment but also extract energy from the flame front to heat the inert material and vaporise the water.

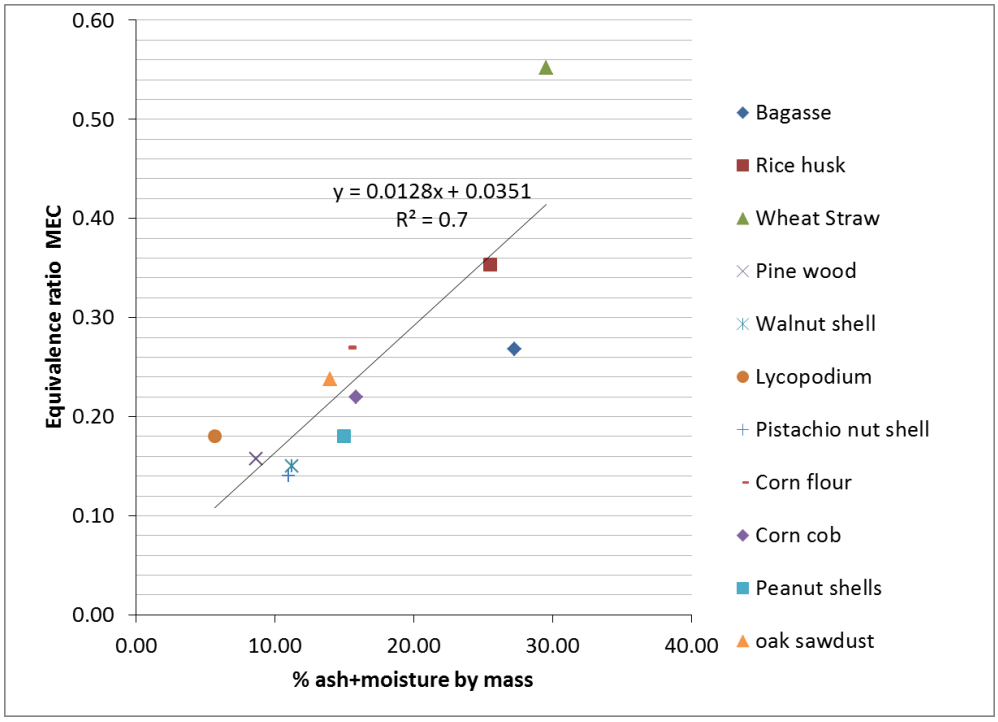

Fig 5.29 Inert material content against MEC from the Hartmann.

This produced a good correlation as would be expected, however this is only for <63µm materials and therefore has no influence of particle size outside of the variation up to 63µm. However as has been shown in **Figure 5.1 and 5.3** there is very little variation in the MEC generated by material and particle size variation below this point anyway.

When fibrous biomass particles over a large range of particle sizes were examined however there was a correlation with particle size.

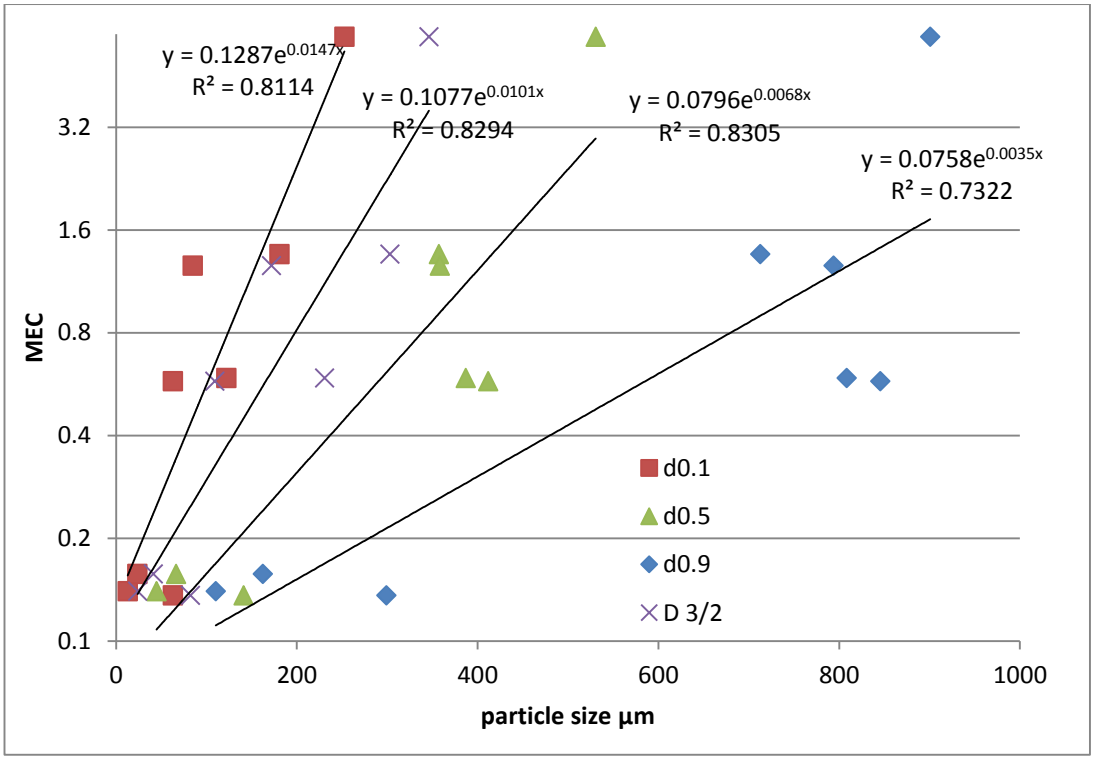

Fig 5.30 MEC of materials tested against d_{10}, d_{50}, d_{90} and D3/2.

The correlation between the MEC and the volume of particles below 10%, 50% and 90% of the total particle volume is good, although 10% and 50% have a better fit than 90%. More importantly it does not seem to show a preferential dependence on any size fraction, although the effect of altering the finer size fractions has a more pronounced effect on the MEC than the d_{90}.

When the Surface weighted mean (D 3/2) is plotted for only fibrous biomass samples there is good agreement (**Fig. 5.31**). This suggests that the MEC depends on the finer particle size distributions (d_{10} and d_{50}) not on any particular size fraction. However as was shown in **Figure 5.19** the particle separation at MEC appears to be constant after 200µm diameter, and that will be affected by the largest particles in a mixture.

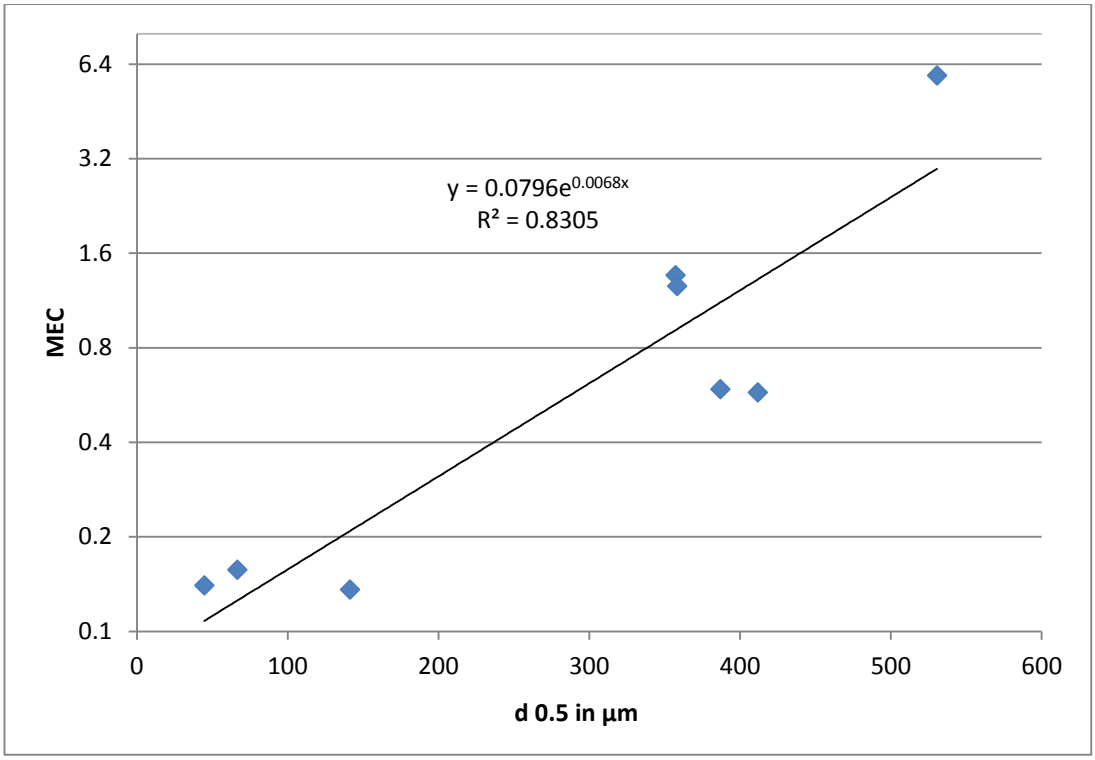

Fig 5.31 MEC of materials tested against D 3/2.

The fact that the palletised fuels did not fit the fibrous biomass trend indicates that surface texture, density, surface morphology, ash content, particle shape or any of the other areas affected by the palletisation process are important in the combustion process of biomass particles. Particles (pine and oak) with the same surface texture, density, surface morphology, ash content and particle shape behaved similarly to each other when varying particle size.

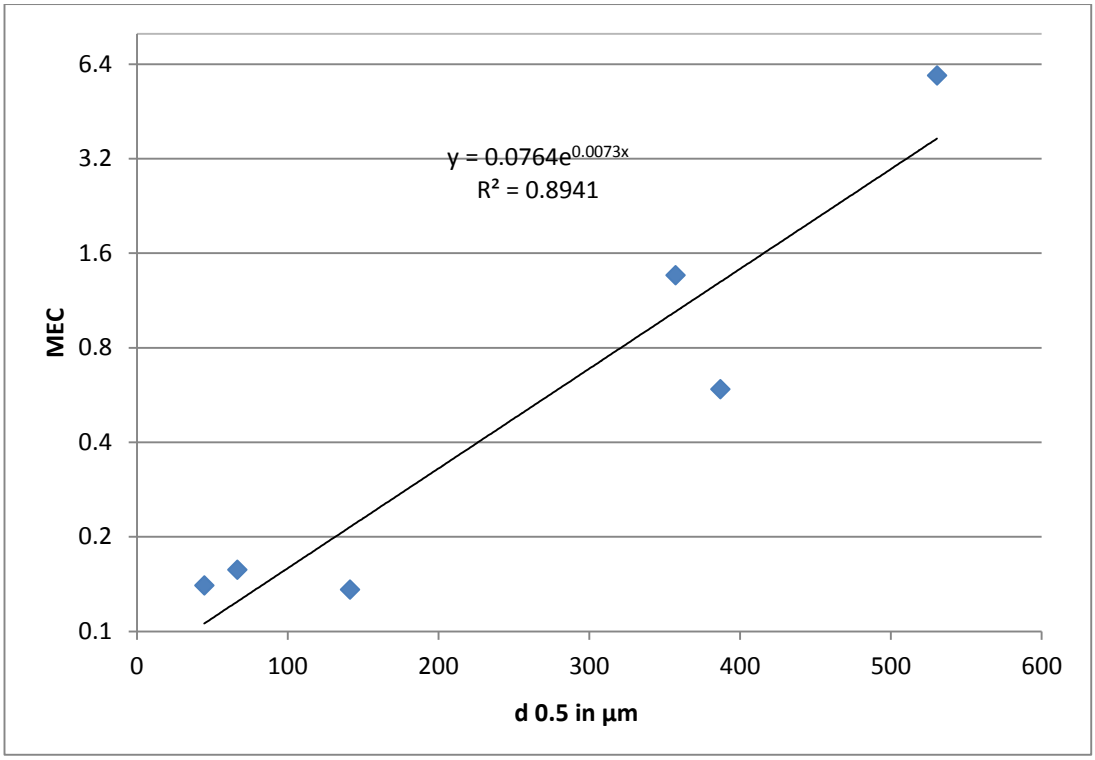

Fig 5.32 MEC of materials tested against D3/2 without <500µm.

Removing the <500µm fractions improved the correlation suggesting it works best for narrow size ranges. Importantly however both <500µm fraction points were above the predicted MEC value, suggesting that the large particles may be having the effect of preventing a large percentage of the mass at MEC from interacting with the air as well as increasing the separation distance between particles therefore pushing the MEC up in wide size range samples.

5.4 Discussions

In the Hartman equipment different woods of the same size fraction give almost identical rates of pressure rise with concentration. Although the MEC's for the <500µm fractions of pine and oak are different it is believed that this is due to the oak mixture having more fines and a higher surface area : volume ratio compared to the pine.

Table 5.1 <500µm fractions pine and oak particle size compared

	D [3, 2] - Surface weighted mean µm	d (0.1) µm	d (0.5) µm	d (0.9) µm

500 oak	109.2	62.7	381.7	845.4
500 pine	172.0	84.7	358.2	793.8

The finer particles are believed to play the dominant role in the rate of pressure rise and MEC values for any given material. The equivalence ratio MEC's was very rich for the large particles, for fine particles <63µm the MEC was Ø ~ 0.2 (uncorrected) and the presence of coarser particles in mixed particle size tests acted as heat sinks and deteriorated the rate of pressure rise. As was shown in the 50/50 mixture of <63µm and 300-500µm the MEC and rate of pressure rise appear to be dictated by this finer fraction of the mixture as the MEC is twice that of <63µm pine and the rate of pressure rise most closely matches that of <63µm pine. If this is the case it suggests that the presence of large particles within the mixture does affect the MEC and rate of pressure rise by acting as a heat sink, but not significantly, especially in the presence of fine particles. Furthermore the presence of large particles appears to have a more influential effect on the rate of pressure rise than the MEC.

The lowest rate of pressure rise was shown by the largest particles to ignite, 150-300µm oak although this rate of pressure rise was only slightly lower than for the 63-500µm pine fraction. This further supports the idea that while the largest effect on rate of pressure rise is from the <63µm material the 63-150µm component also plays a role if to a much lesser extent.

The size fraction 63–150µm stands out as the only fraction to produce intermediate rates of pressure rise suggesting as (Yao B. Yang and Jenny M. Jones, 2008, Proust, 2006) suggested it is in this size range (100-200 µm) that cylindrical biomass particles turn from thermally thin to thermally thick.

As commercial biomass millers produce a wide range of particle sizes, the presence of large particles with fines is a reality. However, ISO measurements of dust explosion properties are for fine dusts <63µm and hence the present measurements of MEC of Ø <0.2 for this size range are significant. In our research this is believed to have been caused by the uneven distribution of the dust in the vessel when run on 0 seconds ignition delay on the Hartmann apparatus.

The results in **Table 2.9** appear to show that pulverized biomass and HCO dust lean limits are different to those of HC dusts including coal. For pure hydrocarbon

dusts a model that the flame propagates as a gaseous hydrocarbon appears valid as the MEC's are the same as that for a hydrocarbon gas. However, for biomass (Pine and Spruce) and pure CHO chemicals (PMA, PMMA, Polyethylene terephthalate, Polyvinyl acetate) show an MEC = 0.14 - 0.25Ø, which is supported by the present results for fine dusts MEC = 0.136, 0.196 and 0.204Ø. This MEC is 2 - 3.5 times as lean as HC dust's or gases will burn. However later work carried out using the high speed video appears to indicate that these exceptionally lean MEC results may be the result of unequal distribution of the fuel within the vessel (**Fig. 5.17**). The present work on particle size effects agrees with the work on MEC for biomass with fine particle sizes shown in **Table 2.12** and the $1m^3$ values in **Table 2.13**. However if the MEC values are adjusted for the proportion of the tube that the dust was distributed over (approximately $1/3^{rd}$) then the values become far more like those found in **Table 2.13** for the 20L sphere which is far closer to the 0.4 -0.5Ø values found for gaseous materials in **Figure 2.15**. It is thought that this may be due to the 20L sphere having the dust at the bottom of the vessel and dispersing it much like the Hartmann apparatus (but in a spherical vessel) while the $1m^3$ uses the rebound nozzle or other directional injection systems.

A feature of pulverized biomass combustion and general dust combustion that is rarely mentioned is that there appears to be no rich flammability limits, and this was found in this work as well. It has been postulated (Sattar, 2012) that H_2 may be being created by gasification within the particles, as this is the only gas that will burn as lean and as rich as both biomass and CHO materials have been observed to. However at this time there is no evidence to suggest this once the corrections to the recorded MEC values are made (Ø of 0.17 x 3 = 0.51). This would suggest that there is a problem in the distribution systems used in the literature, especially the LOM $1m^3$ vessel used by Wilén (1999).

It should be noted that liquid alcohol (HCO) vapours have a very similar flammability limit in equivalence ratio terms to hydrocarbon gases (**Fig. 2.15**). Thus, it is only solid HCO compounds that show very lean MEC's and hence it is likely that this is associated with the decomposition of the particles under rapid heating that occurs in a flame front, producing predominantly CO volatiles (Commandré, 2011). Coal clearly behaves differently to biomass dusts with a maximum flammable particle size of 150-212µm compared to 300-500µm for pine biomass (this study) and mixtures of an average particle size of 1227µm (Wong, 2013).

The MEC differences between HCO and CH compounds, 80-90 g/m^3 for Pittsburgh coal = 0.74-0.83 Ø (Jensen, 1994) can, potentially be explained by the release of hydrocarbon volatiles, 60% (Kobayashi et al., 1977) and a hydrocarbon flame propagation, as the MEC is close to that for hydrocarbon gasses (0.7 x .6 = 0.42). Possibly due to the large difference between the volatile percentage of the two different materials combined with the ease with which biomass releases its volatiles compared to coal, **Figure 4.1**.

Large particle and wide particle size distribution tests showed fluctuations in the ignition probability near the MEC (**Fig. 5.33**) that was not shown in any of the fine particle tests. This suggests that this was caused by an uneven distribution of dust or a none uniform sample of material, both of which are far harder to achieve with fine particles. The proportional mass of larger particles to smaller ones means that a slight shift in the distribution of the particles will make a large numerical shift in the number of particle in the mixture and therefor their separation from each other.

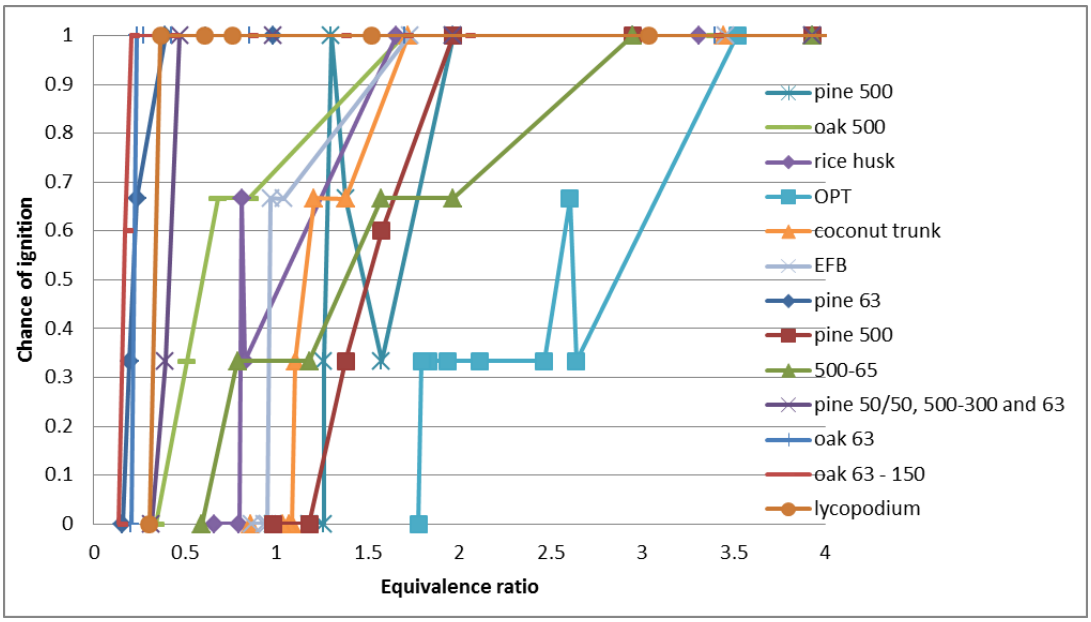

Fig 5.33 Ignition proberbility of all hartmann tests

The 300-500µm pine did ignite after milling but would not before, it was suspected that milling lowered the size distribution with the result that the milling increased the reactivity of the biomass as seen in **Fig. 5.1 and Fig. 5.2** and this was confirmed with particle size analysis.

Table 5.2 Effect of milling on oak <500 µm

pine 300-500		
	milled	Un-milled
D [3, 2] - Surface weighted mean µm	346.0015	402.387
d (0.1) µm	252.566	282.343
d (0.5) µm	530.544	547.0525
d (0.9) µm	900.6475	909.8555

When the dp/dt and 1/MEC are plotted against the average volume : surface area ratio there is good agreement. However the dp/dt follows a power function while the 1/MEC follows an exponential one. This infers that the dp/dt is more strongly influenced by the loss of fine particles from the mixture than the MEC, this is logical as the MEC is a fuel controlled environment while dp/dt is controlled by the rate of devolatilization of the particle.

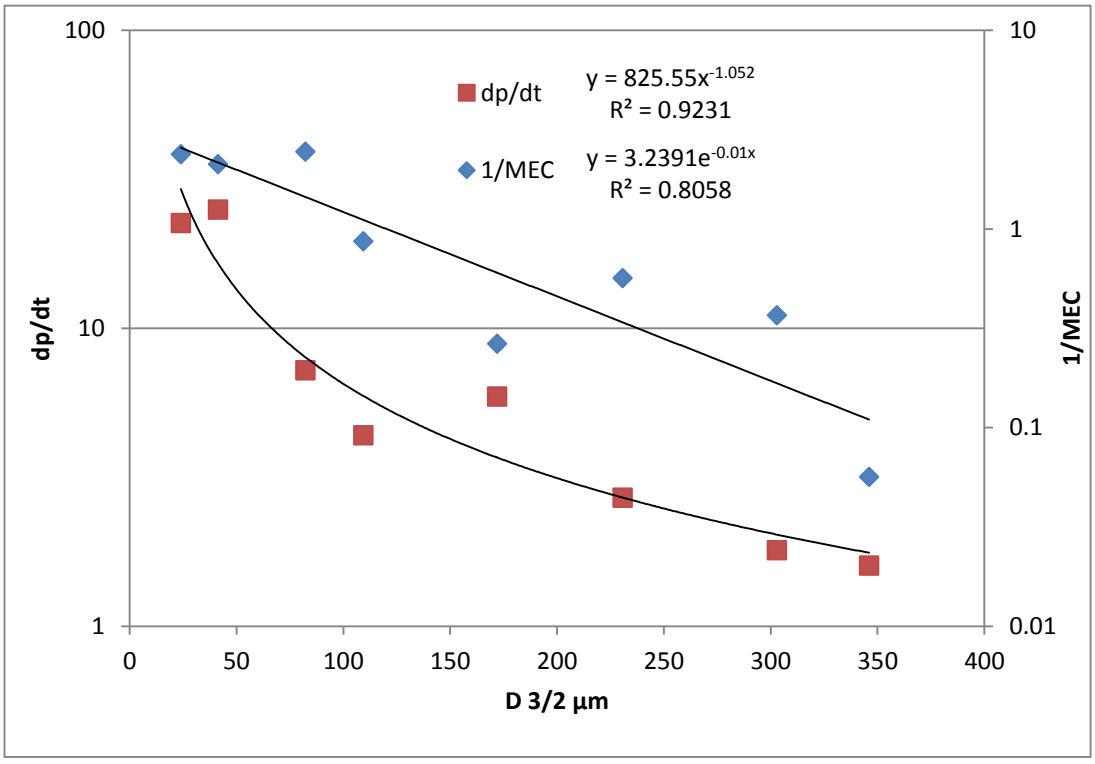

Fig 5.34 MEC and dp/dt againse D 3/2.

As predicted from Proust (2006) once the particles reach a specific size the dp/dt appear to become insensitive to particle size, this would be expected if after a specific particle size the flame front is no longer propagating as a discontinuous particle to particle propagation but as a gas combustion on the devolatilised material.

5.5 Conclusions

1. The results show that although the finer particles present in the mixture appear to dictate the rate of pressure rise, coarse particles without the presence of fine particles were flammable at rich mixtures even up to a particle size of 300-500µm. These rich conditions occur in pulverizing mills and pneumatic dust conveyers and the explosion of particles in the 300-500µm range is a reflection of the high reactivity of pulverized woody biomass. Although these particles produce low K_{st} values they still generate sufficient pressure rise to cause damage to instillations and structures. It should be noted that the maximum combustible particle sizes were larger for biomass than coal which had a maximum flammable particle size of 150 - 212µm (Man and Harris, 2014) and similar to kerosene mist 300µm (Cook, 1977).
2. The high speed video showed that the dust was only distributed over 1/3 to 1/2 of the tube at the time of ignition depending on the particle size. Therefore the concentration at the MEC is actually 2-3 times the nominal concentration; the high speed video footage from each test was used to determine whether it is 2 or 3.
3. The Hartman dust dispersion at 0 seconds ignition delay is non-uniform at the time of ignition of the dust (**Fig. 5.17**) and as such needs to be re-calibrated. Murillo et al. (2013) puts the Hartman ignition delay at 60ms. However the degree of this un-uniformity corresponds to the particle size of the dust used (**Fig. 5.23**). This then leads to a further conclusion that in wide size fraction tests (<500µm sample) there may be some size segregation of the material taking place during injection.
4. In mixtures of fine and coarse particles the MEC and rate of pressure rise appear to be determined by the proportion of fine particles, (as shown by the 50/50 mixture) but there was evidence that the large particles contributed to the heat release and did not just act as a thermal sink as the large particles would ignite on their own. In reference to the MEC of a mixture this is significant as it means that the material in these particles can contribute to the available fuel in a fuel controlled environment. However as this release will take place slowly it is believed that these large particles will not contribute significantly to the K_{st} for coarse and fine mixtures. This was shown by the fact that the dp/dt of the tests corresponded to the D 3/2 best with the closest particle size fit

being d 0.1, while the MEC D 3/2 was the second best fit, with the closest particle size fit being d 0.5. This implies that for dp/dt the finest fraction is the most important while it is the average particle size that is most influential in dictating the MEC this is also shown in **Figure 5.34**.

5. The material (oak or pine) appears to have virtually no effect on the rate of pressure rise or MEC as this is practically identical for pine and oak that have been size segregated to the same narrow size (<63µm). However the coarse fibrous biomass particles had a completely different trend to the pelletized materials.
6. In **Figure 5.19** the separation distance between particles at the MEC (assuming spherical particles) indicates that after an average particle diameter of about 200µm the separation distance between particles at the MEC stops rising. This could be interpreted as the point at which the particle ceases to yield a larger envelope of devolatilised gas with increasing particle size. This occurs at the particle size Yao B. Yang and Jenny M. Jones (2008) estimated biomass particles would make the transition from thermally thin too thermally thick (150-200µm in cylindrical particles). This may explain why particles with very high average particle size (1227µm) have such high MEC values.
7. The Hartman apparatus used in this work appears to give similar MEC results to the Hartman apparatus used by Maisey (1965) for similar materials.
8. The results show that biomass was very reactive with an MEC of down to 0.17Ø and these results for pulverised biomass are in agreement with other measurements using the $1m^3$, 20L sphere and Hartman apparatus carried out by other groups (**Table 2.14** and **2.15**). It should be noted though that the 20L sphere gave on average higher MEC results that the other two vessels. This is believed to be a distribution issue.
9. At a preheat zone thickness of 6-7mm (Han et al., 2000) the turbulent burning velocity is around 0.44m/s, the residence time is 13.6ms, the temperature rise is then of the order of 2000K which produces a heating rate of 147,000k/s. Turbulent burning velocity of 0.625m/s were reported by Sattar (2012) and this gave a residence time of 9.6ms and a particle heating rate of 208,000 K/s, which is very hard to reproduce in any laboratory test. However high heating rate tests carried out on biomass indicate that the volatile yield is predominantly CO and H_2 (when carried out in an inert atmosphere) with a maximum achieved ratio of H_2/CO of

0.4 producing a gaseous MEC = 0.258Ø. This could be used to explain the low MEC values of biomass relative to coal. However the lowest MEC results found during this work with the Hartman apparatus were 0.41Ø (when corrected).

10. The high speed video showed a less luminous flame front ahead of more luminous combustion zone- it is thought to show lean gas flames from devolatilised material ahead of oxygen diffusion flames around particles undergoing very rich combustion, this therefore creates soot leading to high luminosity flames. Fine particles <63µm do not show this as they instantaneous devolatilization (Proust, 2006) of the particles yields a rich gaseous mixture that produced a uniformly highly luminous flame.

11. It had been speculated that the biomass particles may be releasing H_2 and therefore this may have allowed biomass to have an MEC of Ø 0.14. However this is impossible as for oak, at 5.6% H this is therefore = 212 x .14 x .056 = 1.66g/m^3 H_2. For H_2 the stoichiometric concentration is 34.96g/m^3 and the recorded MEC for H_2 is 4.76 g/m^3 which is > 1.66g/m^3. If the other volatile species (CO and CH_4) (Commandré, 2011) that have been found to be released are added in to this it will raise the MEC of the devolatilised gasses higher. This calculation was preformed to prove that NO volatile species can explain these exceptionally low MEC results. If no gaseous volatile species can explain these results the logical conclusion is that the cause is unequal distribution of the dust.

12. <63µm and 63-150µm materials both show a lessening of the rate of pressure rise (after the maximum) over the concentration range of 0–4Ø while all other materials are still producing higher rates of pressure rise with richer nominal mixtures. This would make sense if the rate of pressure rise is driven by the concentration of material <150µm in size as this would still be rising in these mixtures. This appears to be what is being shown in **Figure 5.34** where once a D 3/2 of 250 is reached the dp/dt flattens off. The D 3/2 for 150 -300µm is 300 suggesting that the D 3/2 for 150µm is around 200-250. Which means there appears to be a surface area dependence on the rate of pressure rise. However there was insufficient time to go into this in more depth.

13. It is proposed that the reason for the lessening of the rate of pressure rise in the <63µm and 63-150µm sized materials is due to material of this size devolatilising a much bigger percentage of its total mass than the larger particles either ahead of or in the flame front. This therefore

leads to the same phenomenon found in gas explosions where the O_2 molecules become so diluted by the fuel that combustion efficiency is reduced.

14. A possible reason why the rate of pressure rise is affected by the finest particles in the mixture yet the MEC is not so dependent is that while the larger particles will still devolatilise and therefore propagate a flame for MEC measurements the rate at which they do so will be less that for fine materials therefore having a larger effect on the rate of pressure rise measurements than the MEC ones.

6 1m^3 Explosion vessel tests and disperser calibration

In order to use the 1m^3 vessel for testing of coarse dust samples a disperser capable of doing so must first be fabricated. Once this was achieved the disperser would then be calibrated – ensuring the turbulence factor is recorded using methane gas explosions both turbulent and none turbulent through both the standard C-ring and the new disperser. Then the flame development will be measured to ensure the flame propagation resulting from this distribution is spherical in nature, which will indicate even distribution of the dust around the vessel.

6.1 Disperser designs and testing

The reasons for the need to develop an alternative disperser were covered in Chapter 3.5, 3.8.1 and 3.8.2. These can be summed up as three main points.

- The dust holding pot (**Fig. 3.29**) was not capable of holding sufficient dust to reach the required dust concentration to test the MEC and/or the most reactive concentration for large particle biomass.

- Large particle biomass (larger than 100µm) would not flow through the external and internal pipe work needed to inject it into the vessel in suspension using either the C-ring or wall mounted spherical injector.

- Previously when the dust was placed in the dust dispersion pot this would displace some of the injection air, therefore if a series of increasing concentrations were tested the last (richest) test would have less injection air and therefore turbulence than the leanest test.

Therefore based off **Figure 3.47** from the ISO standards a new dispersion mechanism was designed. The aim was to create a disperser that would evenly and effectively disperse both larger and fine material, either as a mixture or independently.

Each disperser was calibrated using 750g/m^3 cornflour, purchased from Morrisons supermarket. This was chosen as it is readily available and cheap to buy; it has the additional advantage of being of relatively uniform particle size. 750g/m^3 was chosen as the concentration as it was the most reactive mixture for this dust and

therefore the flame propagation was unlikely to be affected by buoyancy that may have produced different values of K_{st} and maximum pressure.

6.1.1 Disperser designs

Firstly the disperser from **Figure 3.47** from the ISO standards was fabricated to the best possible degree of accuracy given that there were no technical drawings. To do this a 19mm diameter pipe was run from the wall of the vessel where the pipe to the dust pot attaches into the centre of the vessel. It then makes two 45^{o} bends to end up facing directly downwards into the hemispherical bowl. This was of a diameter of 35cm and capable of holding a maximum load of 3.4kg of biomass at the standard density.

Then the disperser was placed in the 1m^3 vessel (**Fig. 6.3(A)**), secured to the bottom with a bolt and run using 750g/m^3 cornflour. However this produced neither the K_{st} or Pressure that was generated from the C-ring with the same test conditions, (**Fig. 6.1 and Fig. 6.2**).

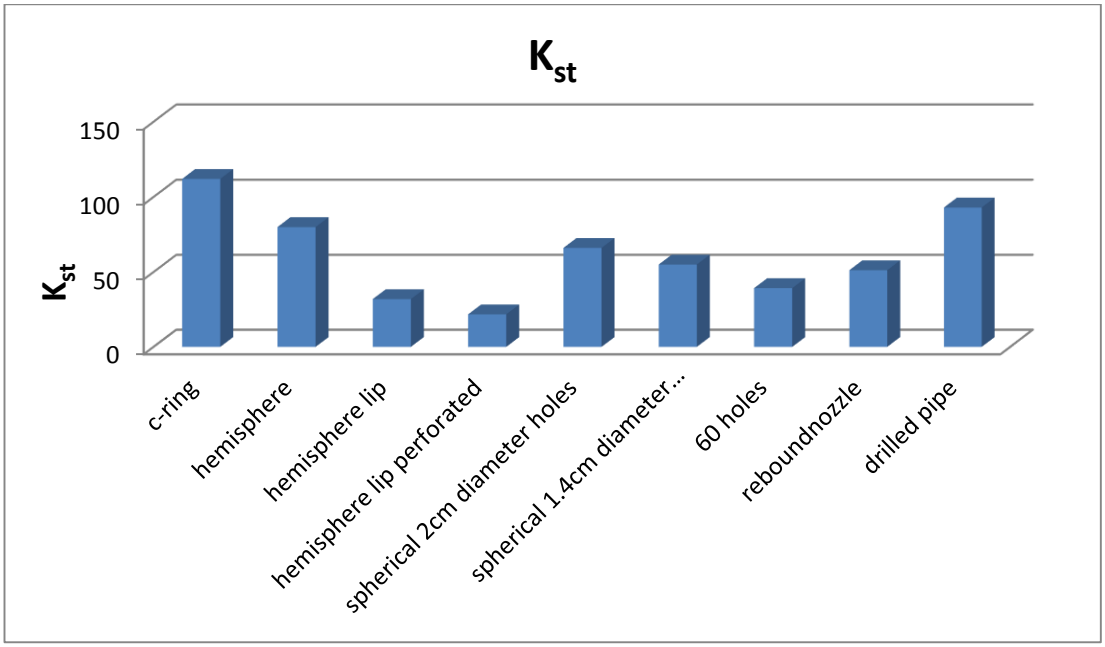

Fig 6.1 K_{st} produced from various disperser designs with 750 g/m^3 cornflour.

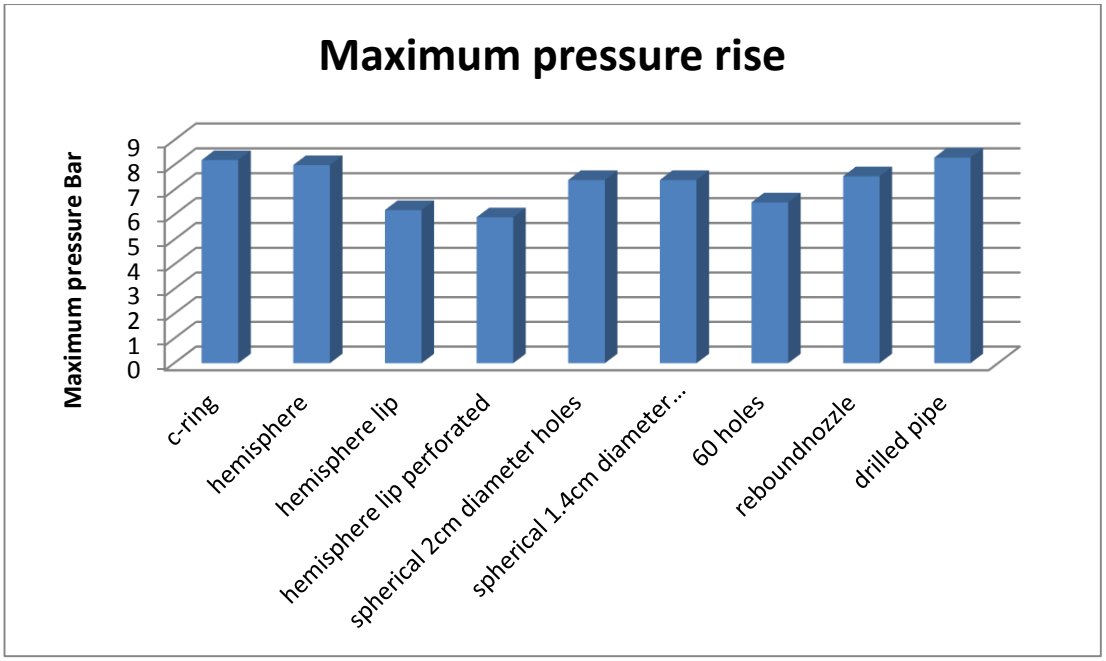

Fig 6.2 Maximum pressure produced from various disperser designs with 750 g/m^3 cornflour.

Through discussion it was thought that the issue was the air dispersion from the pipe re-directing around the curved bottom of the bowl and then coming up in a very directional manner. To try to break up this directionality and create more turbulence it was proposed to add a baffle around the edge of the hemisphere (**Fig. 6.3(B)**) to try and break up the deflected injection air. To attach this to the hemisphere 4 protrusions were welded onto the hemisphere and 4 right angled holes were lathed into the metal of the lip's rim. The rim could then be lowered onto the protrusions then locked in place by turning it in the same manner as a bayonet fitting on a light bulb.

However this actually proved to make the situation worse (**Fig. 6.1 and Fig. 6.2**) as a large amount of the dust load was now getting trapped under the baffle after it had been entrained by the dispersion air, resulting in a lower maximum pressure. Additionally it appeared that the baffle was reducing the turbulence in the vessel and therefore reducing the K_{st}.

To try to alleviate this 50% of the area of the baffle was removed in alternating panels (**Fig. 6.3(C)**) to see if this would improve the results. However this produced the worst results so far (**Fig. 6.1 and Fig. 6.2**). The lip was therefore abandoned as a design as there had been no successful improvement in the original hemispherical results (**Fig. 6.1 and Fig. 6.2**).

(A) **(B)** **(C)**

Fig 6.3 (A) hemispherical disperser, (B) hemispherical lip disperser, (C) hemispherical lip perforated disperser.

After this a new approach was attempted, if the right angle of the baffle was too intrusive to the flow of dispersion air then perhaps another hemisphere placed on to it and perforated with holes would allow the dust to disperse while breaking up the directionality that had been observed in the original hemispherical disperser (**Fig. 6.3(A)**). Therefore the spherical disperser with thirty 2cm diameter holes (**Fig. 6.4(A)**) was produced, however it again produced lower K_{st} and pressure rise values than the original hemisphere (**Fig. 6.1** and **Fig. 6.2**).

However as it had the highest K_{st} and pressure generated from any disperser (apart from the original) yet tried, it was proposed that perhaps altering the hole size would improve this result by achieving faster flow through the holes and therefore producing turbulent jets with more reach and power than had been the case previously.

Therefore 2 different variations were created, one with the same number of holes but at 1.4 cm diameter instead of 2cm (**Fig. 6.4(B)**) and the other with twice as many (60) 2cm holes. Unfortunately both dispersers failed to produce an improvement on the original design (**Fig. 6.1** and **Fig. 6.2**).

(A) **(B)**

Fig 6.4 (A) spherical disperser 30 holes 2cm, (B) spherical disperser 30 1.4cm holes

Subsequently, it was decided to try the rebound nozzle (**Fig. 3.46**) that had previously been mounted on the wall in the same location as the wall mounted spherical disperser, (**Fig. 3.45**) attached to the end of the pipe in the hemispherical disperser (**Fig. 6.3(A)**). It was thought that this might break up the air jet from the 19mm diameter pipe better, therefore creating a more even dispersion of the dust throughout the vessel. While this was the best alteration of the hemispherical disperser so far in maximum pressure generation, it only produced 50% of desired K_{st}.

Then it was noticed that there appeared to be a brass fitting on the end of the pipe in **Figure 3.47**, closer examination of the image located a single visible hole on the side of this brass fitting. From this it was summarised that there must be 3 other holes not shown, at equal distance around the fitting to ensure equal distribution. Although there was no way of confirming (there were no technical drawings just the image) it was suspected that there was also a hole on the bottom of the pipe of the same size. To try and get the hole area as close to that of the standard C-ring as possible (263.3mm^2) five 4mm radius holes were created in a sealed pipe of the same 19mm internal diameter as used previously for a total area of 251.3mm^2. The pipe was then suspended 2.2cm from the bottom of the hemispherical dust holder so that the holes would be covered by the dust load. This disperser (**Fig. 3.48**) known as the “drilled pipe hemispherical disperser” was then run in the same manner to all previous dispersers and compared (**Fig. 6.1** and **Fig. 6.2**).

This was found to be the best disperser design, as it produced identical pressure rise to the C-ring disperser and 83% of the K_{st}. Although this 17% error in K_{st} is within the 20% error margin for K_{st}'s 50-100 (BSI, 2006) it is still higher than would be desired and will be discussed more in the future work.

As the K_{st} and pressure rise were within the acceptable limit set out in the ISO standards this disperser was chosen to run all future large particle biomass tests. To ensure that the propagation was even the flame speeds were plotted (**Fig. 6.5**) and showed a spherical, even propagation in both the horizontal and vertical axis.

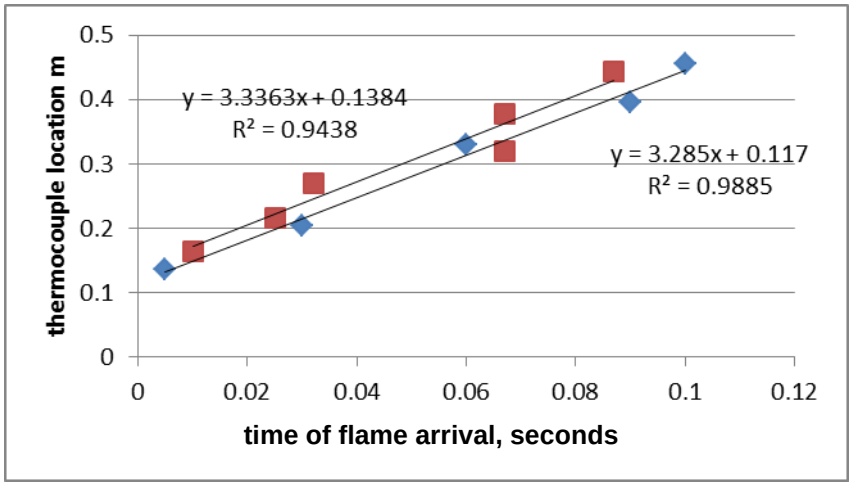

Fig 6.5 750g/m^3 cornflour flame propagation in drilled pipe hemispherical disperser.

6.1.2 Calibration and timing alterations

As each different disperser would have different turbulent flow patterns, dispersion air velocity's and dust dispersion each disperser needed to be calibrated using alteration of the ignition delay for optimum pressure and dp/dt generation (**Fig. 6.6** and **Fig. 6.7**).

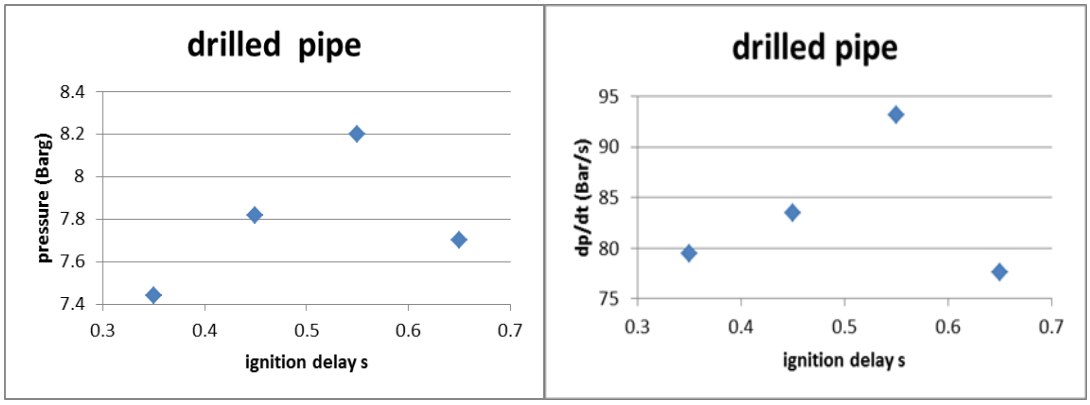

Fig 6.6 Ignition delay changes for drilled pipe hemispherical disperser

The drilled pipe disperser was found to have both its maximum K_{st} and Pressure generation for an ignition delay of 0.55 seconds. Before this the dust has not yet had time to fully distribute itself around the vessel therefore lowering the maximum pressure value (**Fig. 6.6**).

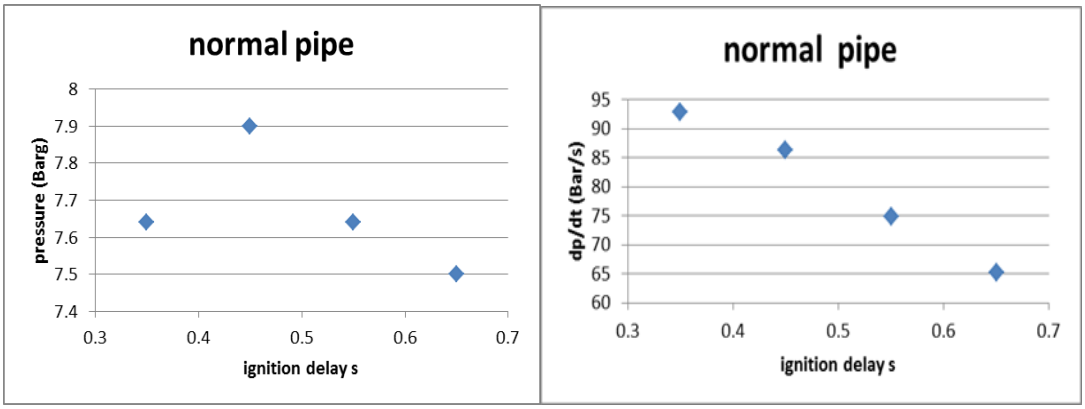

Fig 6.7 ignition delay changes for hemispherical disperser

For some dispersers (**Fig. 6.7**) the maximum turbulence and therefore K_{st} was found for an earlier ignition delay than the maximum pressure generation. This was due to the larger air flow through the unaltered 19mm diameter pipe, 1134.11 mm^2 vs 263.3mm^2. The ignition delay was altered by pushing forward the time at which the chemical igniters were fired, t_i in **Figure 3.31**.

The turbulence factor, β was found to be 3.92 for the drilled pipe disperser compared to 4.03 with the C-ring disperser. This was done by running turbulent and laminar methane tests with 10% methane and comparing the differences in K_{st} between the two.

6.2 Fibrous biomass tests

Now that a dispersion method capable of handling biomass particles larger than 100µm had been developed and calibrated to produce the best results possible the testing of the material began.

6.2.1 Biomass explosibility

Initially (at this point the drilled pipe disperser was not ready for testing) biomass explosion tests were run on cornflour and very fine pine dust collected from the dust filters in Drax power plant. These were chosen as the only available biomasses that would flow through the dispersers available at that time.

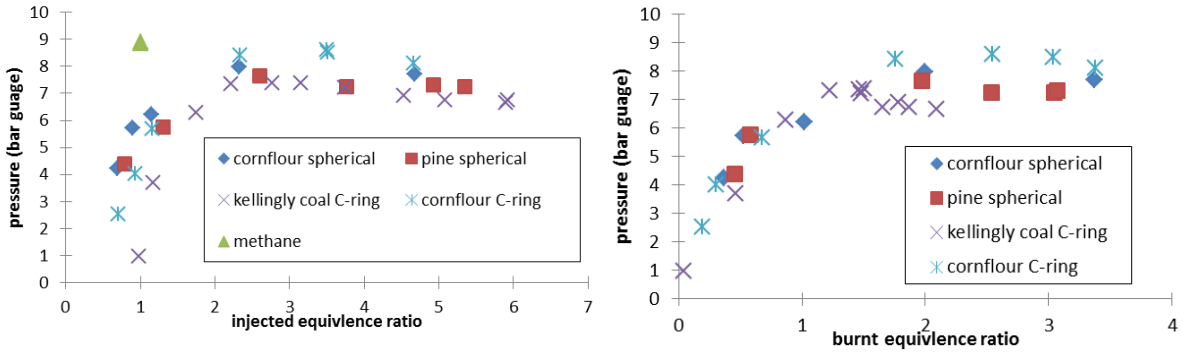

(A) (B)

Fig 6.8 Maximum pressure as a function of the (A) injected and (B) burned equivalence ratio

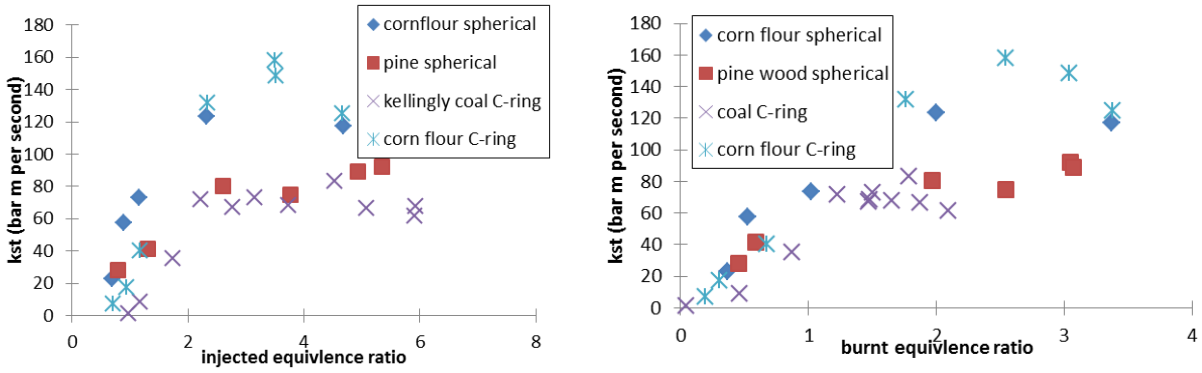

(A) (B)

Fig 6.9 K_{st} as a function of the (A) injected and (B) burned equivalence ratio.

A significant feature of **Figs. 6.8** and **6.9** is that biomass K_{st} and P_{max} increases with burned mass Ø in the lean region and continues to increase in the rich region with the peak reactivity and P_{max} occurring for Ø of 2 or richer. In terms of injected Ø (which is a more practically relevant parameter) it is evident that combustion still takes place and that strong and significant pressures are generated for both coal and biomass for equivalence ratios of 6 and beyond, with the reactivity of biomass being higher than coal for the two types of biomass investigated. This clearly shows that the risk of explosion with significant overpressures remains at 100% in very rich environments with little indication that a rich combustion limit is "near" and this was determined in standard testing equipment that had been modified and calibrated to handle larger quantities of powder than normal. This challenges the general industry assumption that operating in very rich conditions is safe. This demonstrates that if there is indeed a rich limit for dusts the present standard testing equipment (1m^3 vessel and external dust pot) is not capable of measuring it (maximum capacity 1250g/m^3).

Once the drilled pipe disperser was fabricated and run this maximum capacity increased to 3000g/m^3, a significant improvement on the original design. Oak of various particle sizes, *Empty Fruit Bunches* (EFB), milled pine and "Wood" were tested in this injector (**Figs. 6.10** and **6.11**).

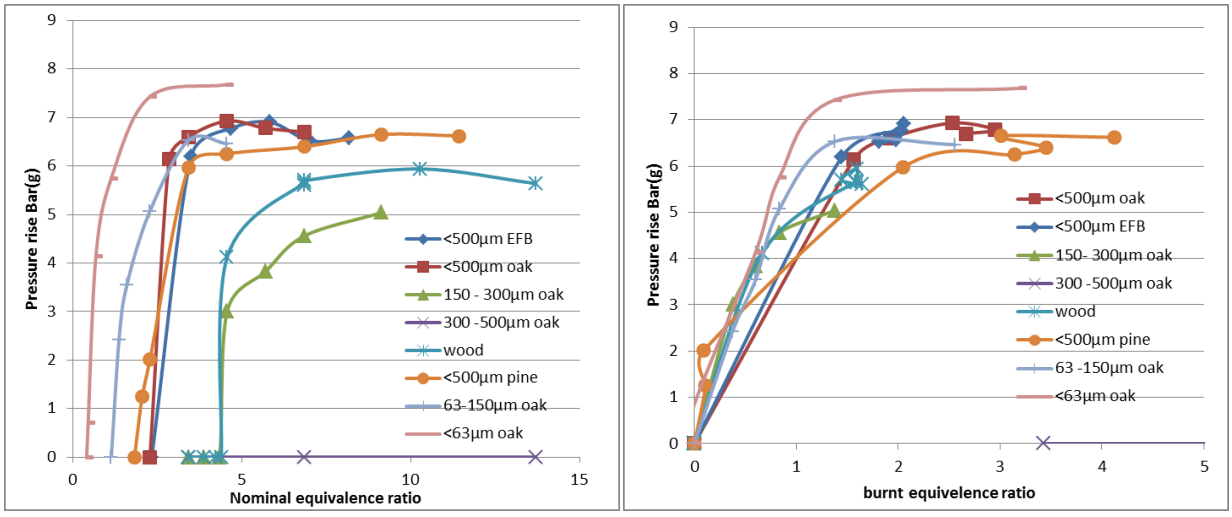

(A) (B)

Fig 6.10 Maximum pressure as a function of the (A) injected and (B) burned equivalence ratio

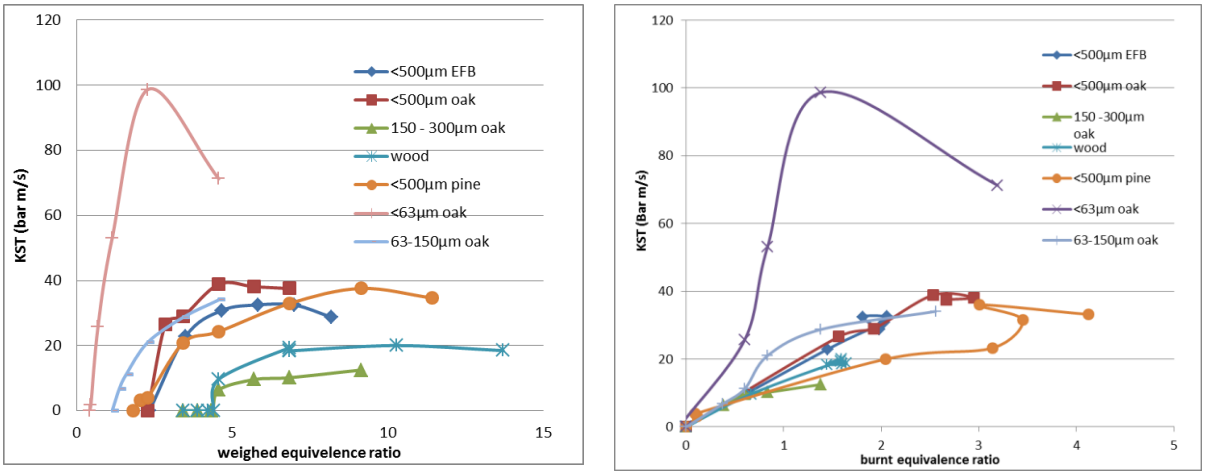

(A) (B)

Fig 6.11 K_{st} as a function of the (A) injected and (B) burned equivalence ratio.

These test showed the same trend as the previous fine biomass tests (**Figs. 6.8** and **6.9**) with the peak reactivity and P_{max} occurring for Ø of 2 or richer, additionally the same dependence of reactivity on particle size as was seen in **Figure 5.9** is observed here (**Figs. 6.10** and **6.11**). The pressure and K_{st} generated for <500µm size fractions is nearly identical irrespective of the material used. Interestingly the K_{st} for <500µm is nearly identical to the 63 - 150µm oak sample tested and these size fractions have very similar d_{10} and D 3/2 values which the Hartmann tests indicated should be the best indicator of the K_{st} for a material.

The finest fraction tested, oak <63µm had comparable results to the materials tested in (**Figs. 6.8** and **6.9**) with the maximum reactivity around Ø 2-3 nominal concentration. Particle sizes larger than this had progressively larger MEC's and K_{st}'s that corresponded to increasing particle size. Similarly to **Figures 6.8** and **6.9** these tests show no decrease in the reactivity of biomass up to the maximum nominal concentration of almost Ø = 14 (3000g/m^3). This behaviour of rich dust/air mixtures is dissimilar to gas/air mixtures (**Fig. 1.4**), which have a rich limit at much lower equivalence ratios. Some potential reasons for this are:

- In a closed vessel explosion there is a fixed mass of air and the dust is injected into this and does not displace any air. There is a fixed heat release of 3MJ per kg of air (Drysdale, 1992) irrespective of the fuel. For gases, rich mixtures have higher volume concentration and more air is displaced as the gas concentration is increased. So in a fixed volume system for rich dust/air

mixtures the energy available to be released is greater than the equivalent rich gas/air mixture because of the relative mass of available air (which is the controlling reactant in rich mixtures).

- Another possible contribution to these phenomena is that although the initial mixture pressure is 1 atm, before the powder can burn it has to turn into pyrolysis gases and when these gases are added to the fixed system volume the initial mixture pressure effectively goes up. So as the hot flame kernel develops from the ignition point progressively more volatiles are driven off the dust cloud ahead of the flame and this would have the effect that each combustion step would take place in comparatively higher pressures than the equivalent gas/air mixture. This will have a compounding effect on the final explosion pressure Pmax for dusts resulting in higher overpressures than the equivalent gas air mixtures (equivalent temperature gas air mixtures burning same volume of oxygen and fuel). This effect could be partially or totally counter balanced by the excess dust particles acting as a heat sink.

- It is more difficult to explain why the mixture reactivity, K_{st}, is so high for rich mixtures and why the maximum reactivity is not close to Ø = 1 as it is for gases. Part of the reason is that reactivity is related to flame temperature, but this comes back to the reason why the flame temperature does not peak until about Ø = 2-3 nominal concentration. Another possible explanation is that the definition of the equivalence ratio for dusts is based on the chemical composition of the solid particle rather than the actual combustion chemistry which is defined by the composition of the pyrolysis gases (which is not known). However this should be similar to the dust equivalence ratio as no fixed carbon and little ash is created to trap material, therefore what is vaporised (90 -95% of the material should be combusting in the gas phase). However only the percentage of material that is devolatilised during combustion will actually participate in the energy release.

The MEC results (**Figs. 6.10** and **6.11**) show three distinct groupings – 0.4-1.14 where the fine materials have their MEC's, 1.8 - 2.3 where all the <500µm materials have their MEC's and 4.4 where all the material without any particles smaller than 300µm have their MEC's.

However when this is plotted as the actual mass burnt in each test instead of the nominal concentration these lines converge (**Fig. 6.11**) with only the <63µm material producing significantly higher K_{st} per unit mass burnt and 63 - 150µm having a slight rise. This supports the idea that the <63µm material is the only size that is mostly devolatilising ahead of the flame front to produce a mixture of gaseous fuel upon which the flame propagates. 63 - 150µm oak has a much lower rise per unit mass suggesting it has a much more discontinuous flame propagation than <63µm, however this is still higher that for the other materials tested.

There are some exceedingly low values of mass burnt caused by incomplete residue collection; this was discussed in section 3.10.

There exists a problem that in the $1m^3$ dust explosion apparatus there is no way of determining what dust concentration the flame front propagated through at the MEC, although it is possible to infer this from the flame propagation in calibrations with fine particles which indicated uniform distribution.

6.2.2 Effect of elemental composition

There appears to be little to no difference (**Figs. 6.10** and **6.11**) at comparable particle size's (<500µm) between EFB, pine and oak despite these materials having significantly different calorific values, moisture content, volatile content and ash content (**Table 4.2**).

It can be seen that the burnt equivalence ratio for EFB, oak <500µm, wood and Pine <500µm all stop consuming more fuel once the maximum K_{st} and Pressure rise are reached (**Figs. 6.10** and **6.11**).

- Wood –Ø 1.6
- EFB – Ø 1.85
- Oak less 500 µm – Ø 2.66
- Pine less 500 µm – Ø 3.4

This could be related to the materials composition but the reason is not yet understood. It is thought to be that once the maximum possible flame temperature and therefore the maximum K_{st} and pressure rise are reached there is only the time

taken for the flame front to cross the vessel in which material can be devolatilised. This could therefore be the maximum mass of material that can be devolatilised in that time.

6.2.3 Particle size effect

For 150-300µm oak particles the pressure and K_{st} generation is still rising at nominal equivalence ratio 9 while oak <500µm has K_{st} and maximum pressure beginning to fall off at an equivalence ratio above 5. This indicates that as Cashdollar (1996) suggested the solid dust needs time to devolatilise, however while he states that “As soon as sufficient volatiles are generated to form a stoichiometric concentration in air, the flame front propagates ~ before excess fuel volatiles can be generated ” it is thought that a lean mixture is burnt instead of a stoichiometric concentration. This is based on the observations in section 5.2 (**Figs. 5.14** and **5.16**) that large particles produce an initial, low luminosity flame front (Gao, 2015) then upon flame arrival the heat release takes place in the gaseous phase. (Gao, 2015, Han et al., 2000) observed a double flame structure in biomass and liquid mist combustion where the initial flame front propagated on the devolatilised material while the remaining droplets/particles burn in an envelope diffusion flame around the droplets/particles. This would explain the increasing rise in pressure and K_{st} with concentration for 150-300µm oak (**Figs. 6.10** and **6.11**) as there is not sufficiently available fuel to reach maximum reactivity yet as such a large percentage of the fuel load is trapped in the large particles and unable to be devolatilised in time to take part in the combustion and release the energy fro the available air.

Therefore the pressure generation rate for a single material at a set particle size would appear to be fixed; however altering the surface area to volume ratio effectively stretches the limits as a percentage of the mass is effectively trapped as the surface area to volume ratio decreases when the particles get larger. However as was shown in chapter 5 once a flame front is established the larger particles will burn behind the initial flame front producing a pressure increase but not contributing significantly to K_{st} generation as this is predominantly generated by the initial flame front. This is illustrated by **Figures 6.12** and **6.13** where the maximum rate of pressure rise for oak <63µm is 0.1062 seconds before the maximum pressure is reached while it occurs 0.3198 seconds before for <500µm oak. This indicates that

the <63µm oak sample is producing its pressure rise from the initial flame front propagation faster than for the <500µm oak.

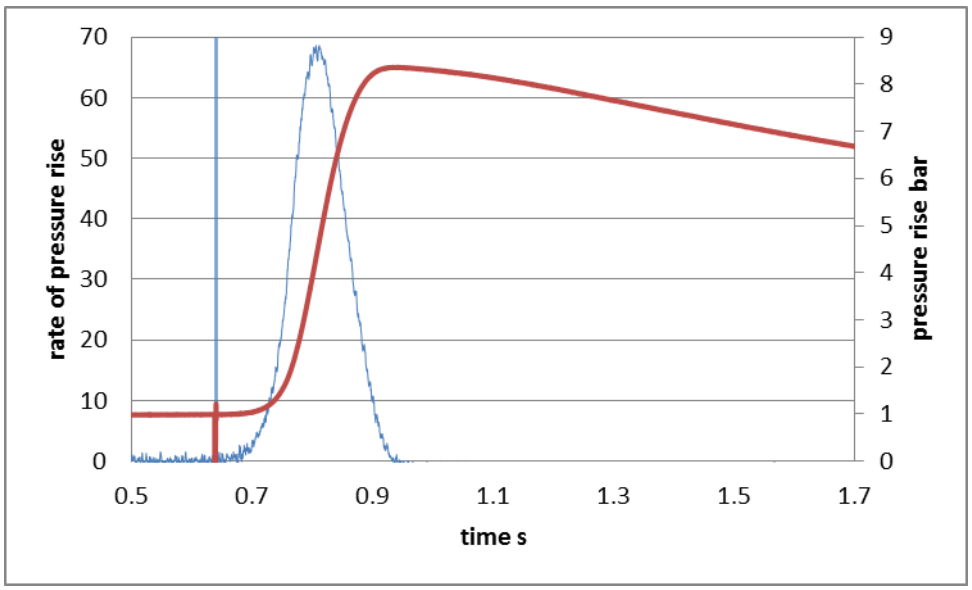

Fig 6.12 <63µm oak dp/dt and pressure trace

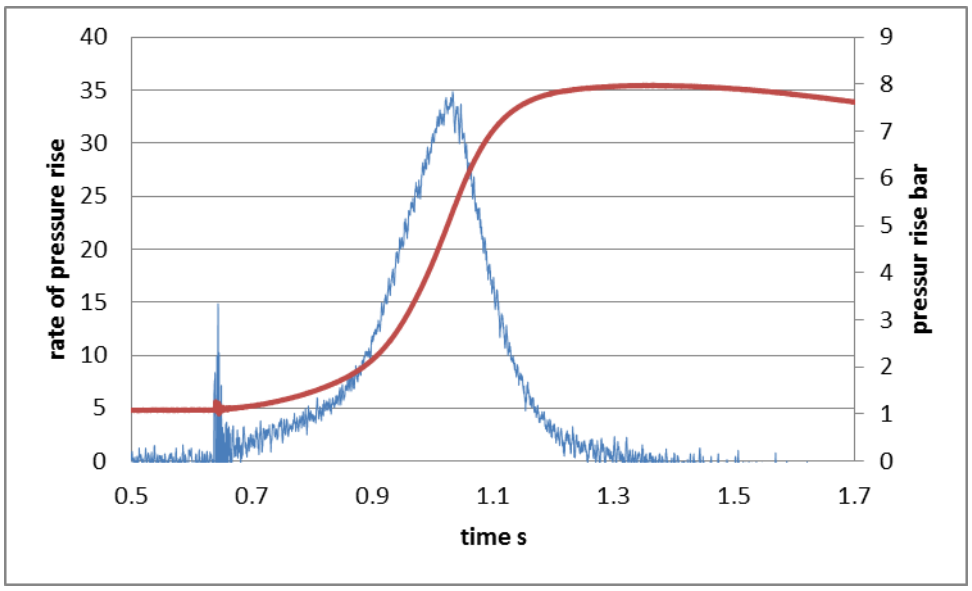

Fig 6.13 <500µm oak dp/dt and pressure trace

Furthermore when these pressure traces are plotted together (**Fig. 6.14**) it can be seen that the <63µm oak has a sharper peak than the <500µm oak, this is interpreted as indicating a larger flame thickness in the <500µm oak. Additionally the corresponding pressure difference between them is attributed to the corresponding energy loss from the <500µm oak flame front spending a longer time in contact with the wall as both are from the same concentration of material (although the <63µm oak burnt slightly more mass).

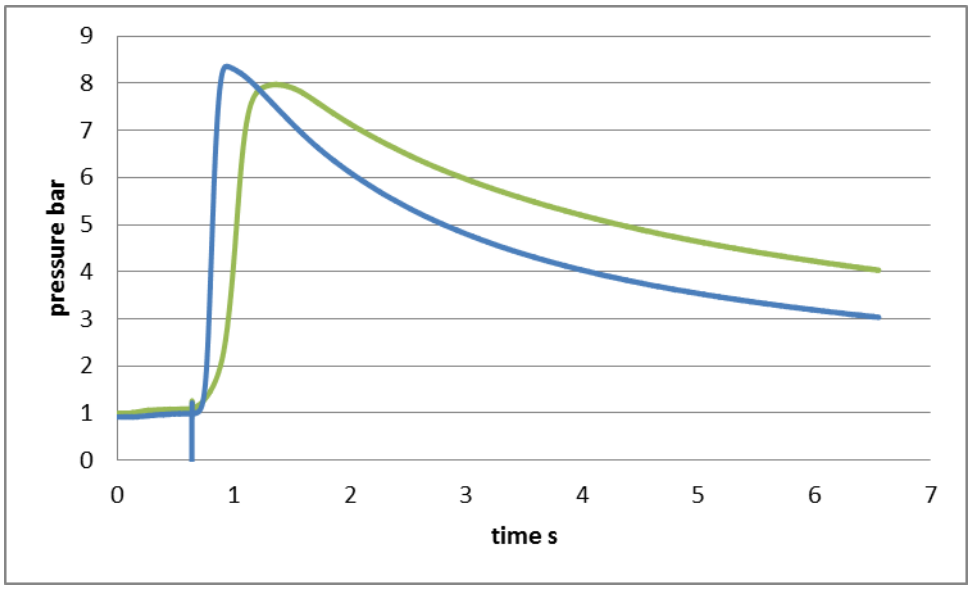

Fig 6.14 Pressure trace from <63µm (blue) and <500µm oak (green).

It was proposed that the larger particles in a mixture do not affect its MEC when they are in the minority by volume (apart from separation distance between particles) as the flame front that is propagating from the fine particles is sufficient to devolatilise and burn them. However this suggests that larger particles increase the flame thickness in propagations where they are present. This explanation fits with the observation that particle size distribution affects K_{st} more than MEC, made in section 5.1. This was also theorised by Proust (2006) in his work on lycopodium flame propagation where he proposed an increased influence of radiation on flame propagation in large particle mixtures.

As was found in section 5.1 the average volume : surface area ratio was the best fit to the K_{st} and MEC data (**Fig. 6.15** and **6.16**), although this time the K_{st} and MEC were both closest to the d 0.1. This may indicate that the best indicator of the K_{st} and MEC is actually the finest fraction of the dust out of the d_{10}, d_{50}, and d_{90}.

Although K_{st} (dp/dt in the Hartmann) has a better correlation with the d_{10} for both vessels than the MEC.

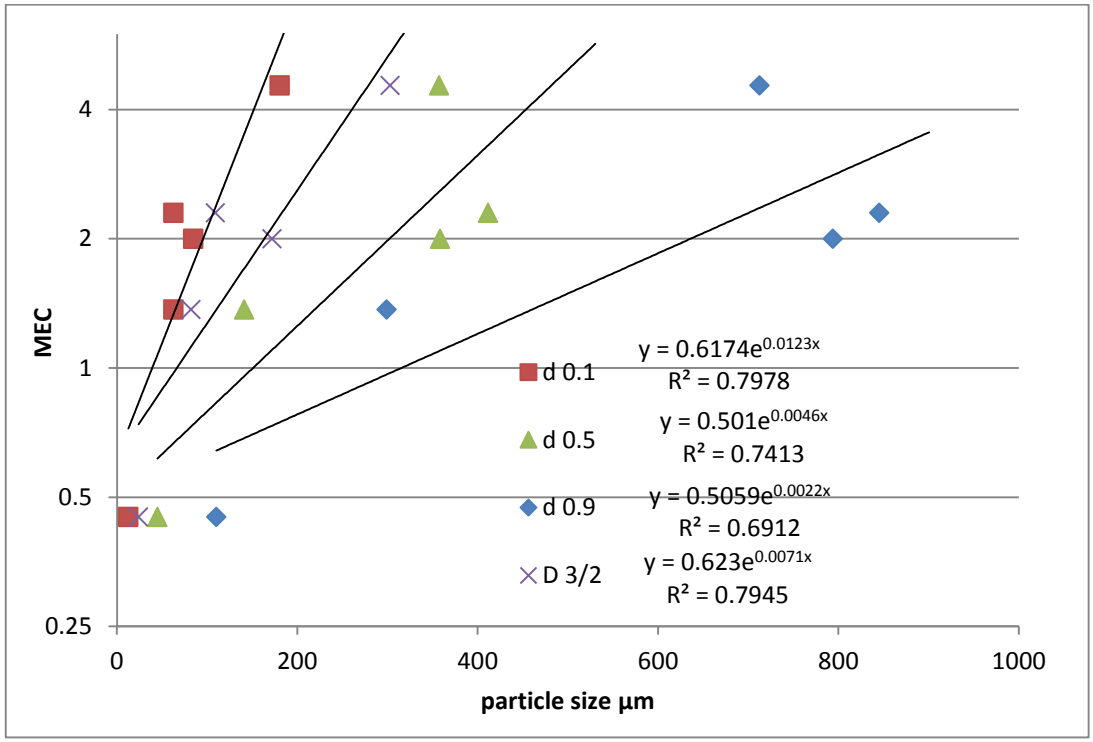

Fig 6.15 MEC against d_{10}, d_{50}, and d_{90} and D 3/2

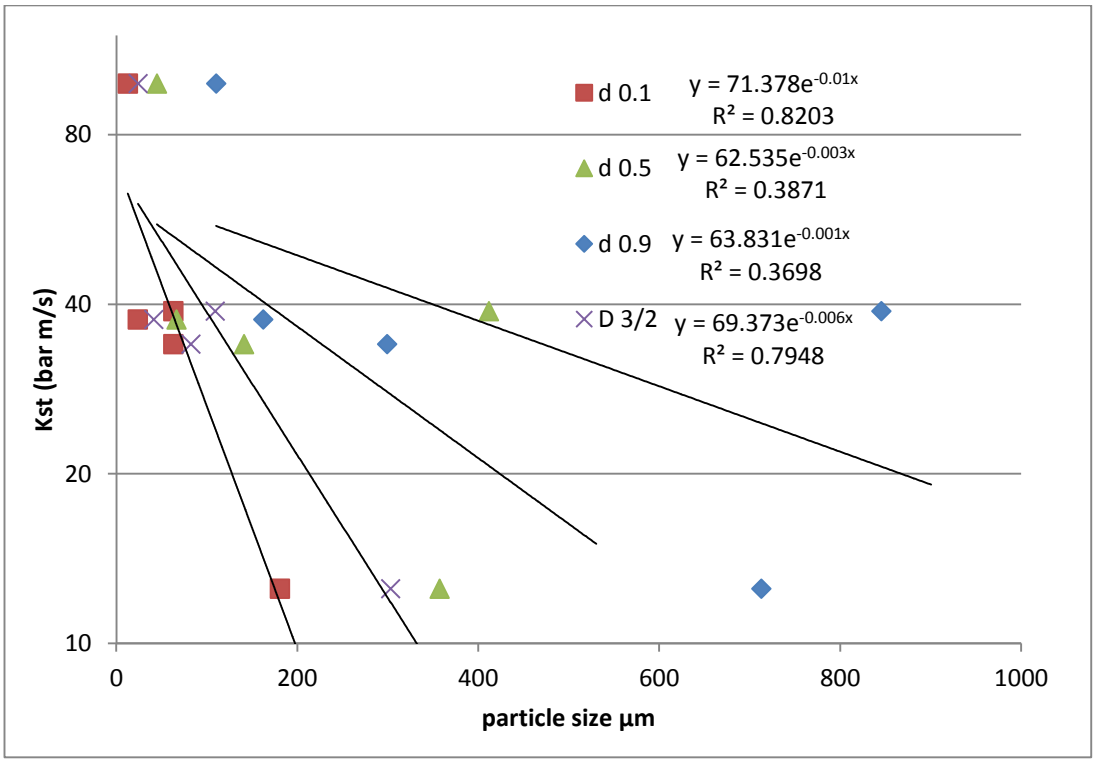

Fig 6.16 K_{st} against d_{10}, d_{50}, and d_{90} and D 3/2

As the D 3/2 provided the best indicator of K_{st} and MEC it was used to plot these against increasing average particle size as was done in **Figure 5.34**. Again, as in section 5.1, K_{st} (dp/dt) decreased faster than MEC with reducing D 3/2.

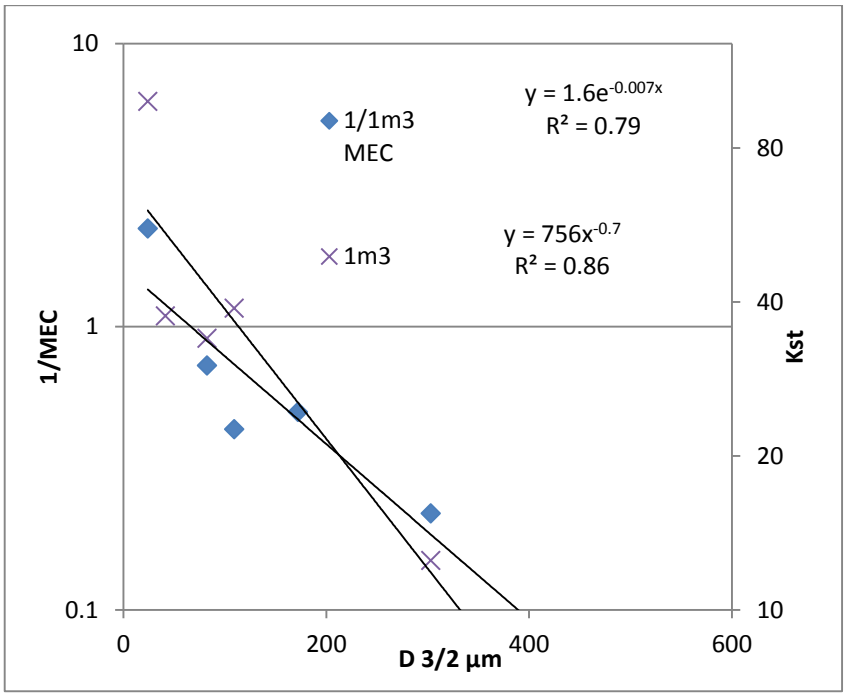

Fig 6.17 1/MEC and K_{st} against D3/2

This supports the work in section 5.1 that indicated that the K_{st} or dp/dt value for a mixture is more sensitive to the increase in the D 3/2 than the MEC is.

6.2.4 Flame speeds

Flame speeds from the $1m^3$ vessel varied wildly depending on the particle size of the dust used in the test. Tests on <63µm material generally produced symmetrical flame speed readouts (**Fig. 6.18**), where the flame propagated in all directions at the same rate. The graphs are plotted as the distance from the centre of the vessel against the time of thermocouple activation.

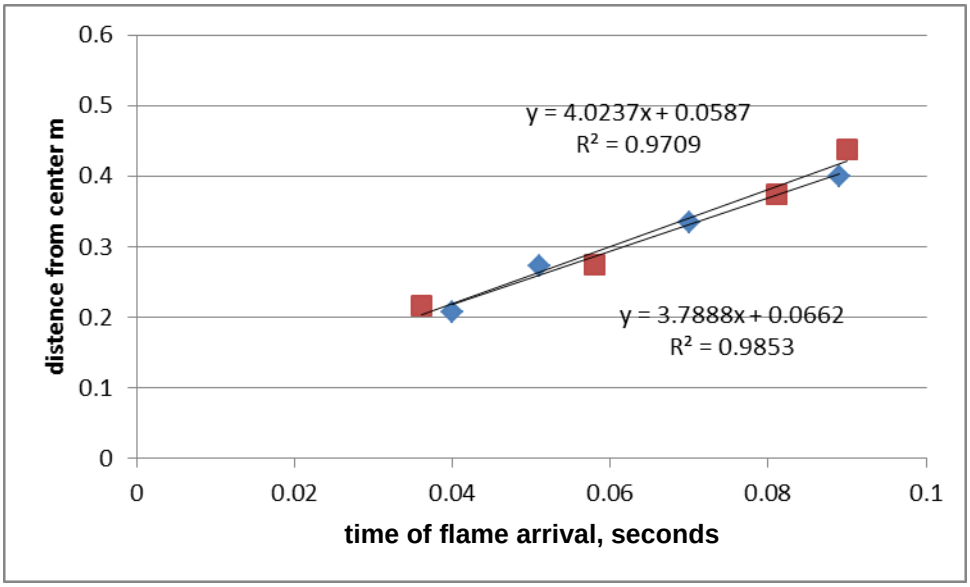

Fig 6.18 Oak <63 µm 500g/m³

A number of the tests however displayed off centred propagation, where, although the flame propagated at the same speed in both directions it was not centred in the middle of the vessel (**Fig. 6.19**).

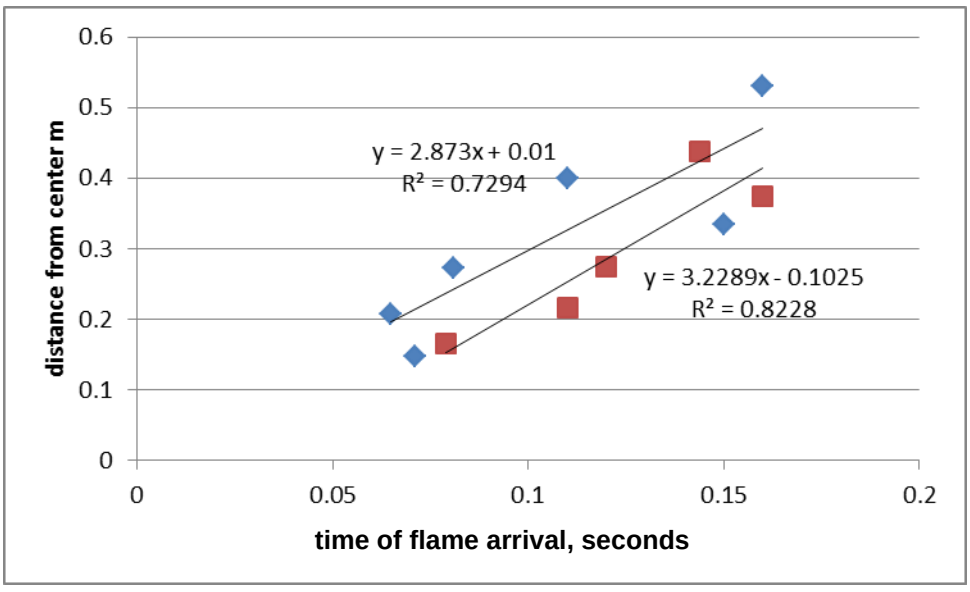

Fig 6.19 Oak <63 µm 1000g/m³

This was believed to be caused by the igniters producing directionality by breaking the plastic casing holding the chemical igniters (**Fig. 6.32**).

However while the flame speeds were good for fine particle dust explosion tests the thermocouple responses became more erratic as the size of the dust used increased (**Figs. 6.18** and **6.21**).

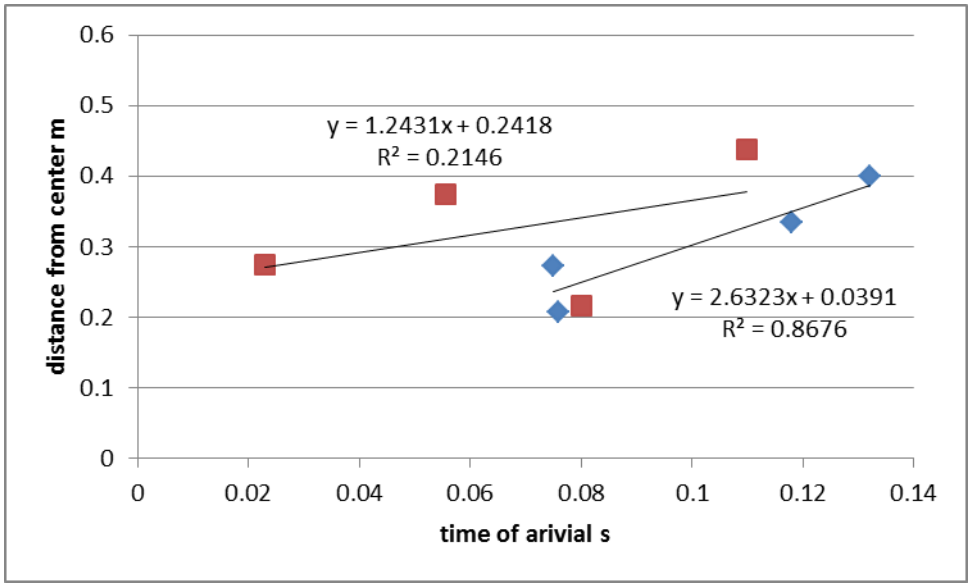

Fig 6.20 Pine <500µm -1500 g/m^3

As the size of the particles used becomes bigger so the flame speed derived from the thermocouples becomes worse. This is thought to be caused by the flame propagation becoming much more discontinuous and the propagation un-uniform/random, as was shown in chapter 5 with the high speed video.

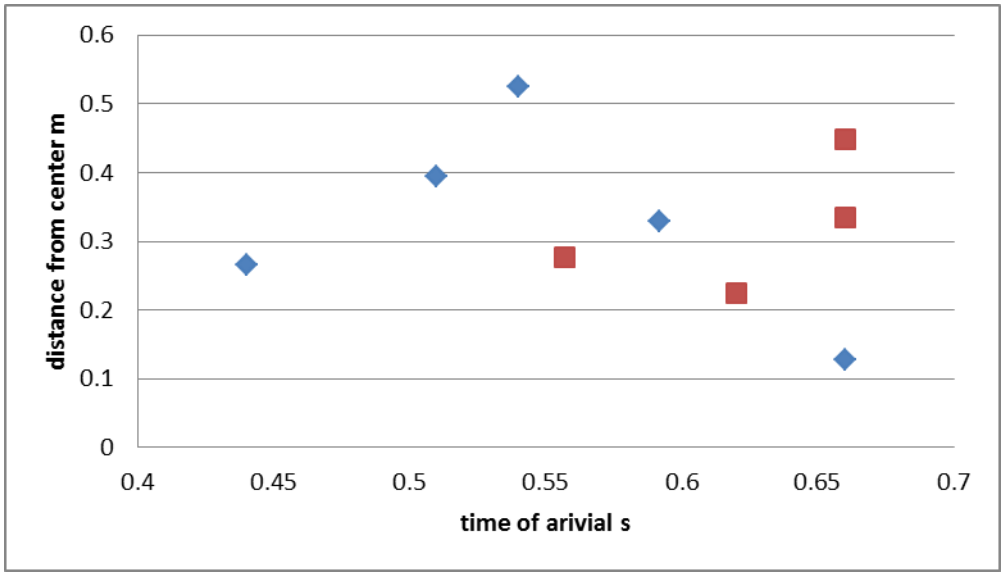

Fig 6.21 Oak 150 - 300µm - 1500 g/m^3

The largest particle sizes tested had the worst results with, as seen in **Figure 6.21**, the thermocouples nearest to the centre activating last for one test. This is thought to be due the fragmentation of the flame front for large particles that was observed in **Figure 5.16**. This is where the particles become so large that only sufficient

volatiles for a very lean flame front are produced ahead of the flame front. The flame front then propagates in the direction where there is sufficient localised gas concentration to sustain it, this is determined by the local particle distribution. This results in a completely random flame propagation based of the local distribution of particles around the ignition source that is heavily influenced by buoyancy.

The flame speeds from the <63µm oak at its most reactive concentration (500 g/m^3) was between 3.8-4m/s in a turbulent environment with a turbulence factor of 3.92. Therefore the laminar flame speed is 0.96-1.02m/s.

The same dust when run through the Hartmann apparatus gave a maximum flame speed of 3.54m/s at a nominal concentration of 187 g/m^3. This would be 561 g/m^3 when corrected for the uneven distribution which is in good agreement with the 1m^3, however that agreement was only possible with that particle size of fuel as will be shown in chapter 8. The Hartmann β would need to be known to calculate the burning velocity from this piece of equipment which at this time is unknown.

6.2.5 Mass burnt

The mass burnt stops increasing for large particle biomass (**Figs. 6.9** and **6.22**) once or just after the maximum pressure was reached. This means that the proposed increases in pressure from the mass of devolatilised fuel equalling out the pressure loss to the inert mass of the extra fuel load as this increases is not possible. Therefore there has to be another reason for the constant pressure once peak pressure is reached in dust explosions.

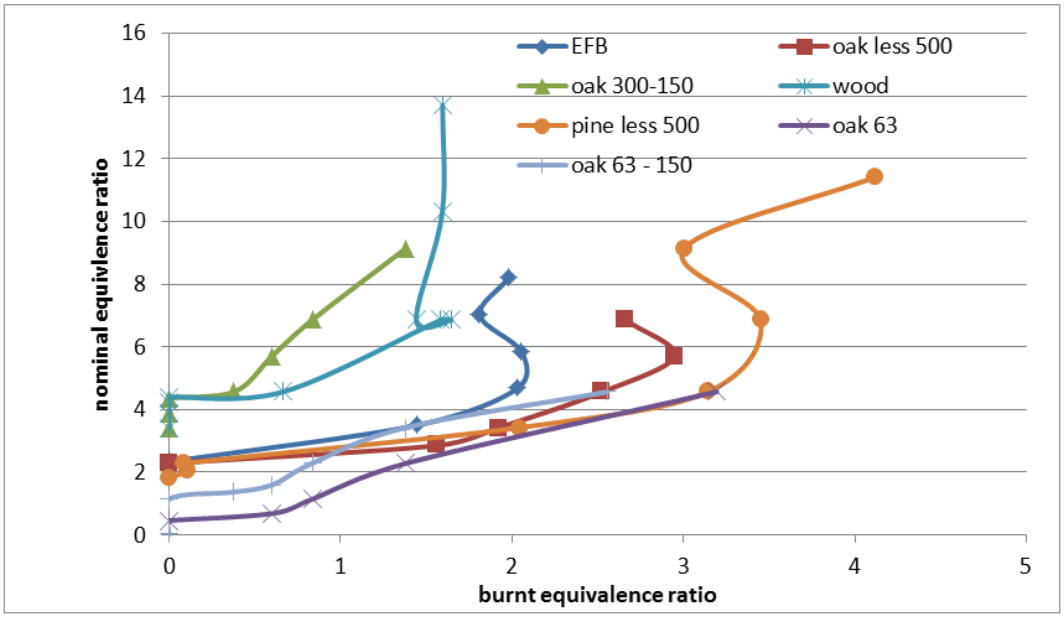

Fig 6.22 Mass burnt against nominal mass.

As the fine particle oak appears to be behaving differently to the large particle oak, the fine biomass from the wall mounted dispersers was also plotted, (**Fig. 6.23**).

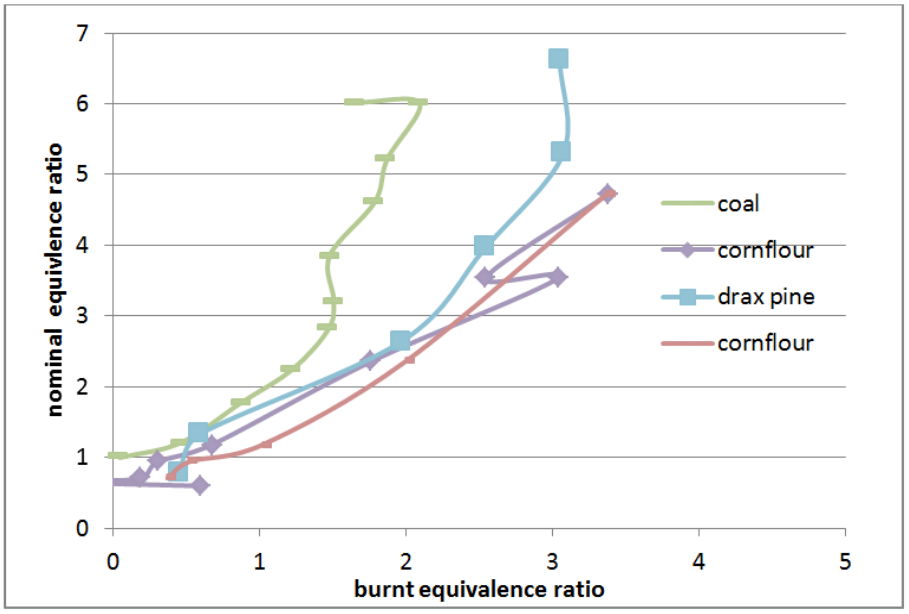

Fig 6.23 Mass of powder burned as a function of mass injected in equivalence ratio.

Figures 6.22 and **6.23** show that the mass of material burned had a non-linear relationship with the mass injected and that coal behaved differently than biomass. For coal there was a very sharp increase in the unburned proportion of mass after a nominal equivalence ratio of 3, as at 3.8Ø only 1.47Ø burned and at 6Ø injected this was increased to 2.1Ø that burned. This indicates that the amount of fuel that will be vaporised during an explosion is directly related to its particle size, with finer materials displaying higher mass loss with nominal dust loading. This may be why in **Figures 6.9** and **6.11** only the finest particle sized material had a fall in K_{st}. This is believed to indicate that the fineness of a material affects its behaviour, with the finest material's behaving more like gas explosions with a steep rise and fall in the K_{st} around the most reactive concentration. However with a fixed mass of air that is not displaced as it is in gas explosions there appears to be no corresponding fall in the pressure generation (**Figs. 6.8, 6.9, 6.10** and **6.11**). This suggests that the particle size of the dust would dictate the percentage of fuel in a particle that could interact with the flame front to release its energy in the available time. Therefore at very fine (<10 - 40µm) particle sizes it is expected the MEC of a dust will be the same as the gaseous volatile products (Burgoyne and Cohen, 1954), however due to the lack of any displaced air as is found in gas explosions there is no expectation of encountering a rich limit where these same gasses wound encounter one.

It is clear that for rich burning mixtures coal and biomass behaved quite differently in terms of the proportion of the injected dust that burned. This is important in pulverising mills and pneumatic conveyor systems as dust concentrations are maintained in the rich zone by design in the anticipation that combustion, if initiated, will be weak. In the present results the directly comparable concentration to the industrial applications is the injected powder concentration or injected equivalence ratio. The present results clearly show that biomass will burn more readily at a much higher concentrations than coal and consume more of the material in doing so. This is particularly important as the highest overpressures and reactivity rates were encountered in the rich mixtures for large particle biomass.

Prior to this work on residue mass the method used at Leeds University was to measure the percentage of the material left as residue after combustion for the most reactive mixture and then apply that percentage to all tests. **Figure 6.22** demonstrates that this method is not correct and should no longer be utilised. Instead using the procedure detailed in section 3.2 and 3.2.1.

6.3 Cake formation

As mentioned in the previous sections, in the ISO 1m^3 vessel a large fraction of the mass of dust injected does not burn and is left as a residue in the vessel at the end of the explosion (**Fig. 6.22**). Most of the literature on dust explosions does not mention that a large fraction of the dust injected into the ISO 1m^3 vessel does not burn and hence the concentrations reported are not the dust concentrations that the flame propagates through but a nominal “intended” concentration. Pilão et al. (2006), in a wide ranging work on cork dust explosion hazards also detailed the large proportion of the cork dust that was left as debris at the end of the explosion but gave no explanation for it.

For some dusts, such as milk powder, the residue was left adhered to the vessel walls after the explosion. Photographs of the wall “cake” from milk powder explosions are shown in **Figure 6.24 (A** and **B)**. They clearly show that the side against the metal wall was not burned or pyrolysed, but the side exposed to the flame was pyrolysed by the flame. Very few dusts we have tested had such a clear residue and in most cases and in all the dust explosions in this work, the residue was left as a powder on the bottom of the ISO 1m^3 dust explosion vessel.

In the near wall region, particle combustion may be different from combustion across the rest of the vessel due to particle behaviour. As the flame approaches the wall the gas velocity ahead of the flame must be reduced to zero as the fixed volume restricts the expansion. The flame speed must therefore be drastically reduced to the burning velocity in the near wall region. The effect of this flame deceleration for dust mixtures will be for the inertial of the particles to leave them travelling towards the wall. With 90% of the original mass of air compresses into the last 10% of flame travel (50mm for a 1m diameter sphere) this effectively will compress the particles onto the wall and prevent them from burning. This is why around half or more of the particles injected survive the explosion and are found as residue. For some dusts, such as milk powder, this compressed layer is still attached to the wall after the explosion.

(A) (B)

Fig 6.24 (A) Milk powder "cake", wall-touching side (B) Milk powder "cake" flame-touching side

The rate of pressure decay from the 1m^3 vessel following the explosions was recorded as shown in **Figure 6.25**. The pressure decay was due to heat loss; not leakage, as the vessel is hermetically sealed. The decay rate was measured for the period immediately after the peak explosion pressure, until the pressure was reduced to 90% of its peak value, as shown in **Figure 6.25**. A faster decay indicated greater heat losses and **Figure 6.28** shows that for a gas explosion the heat loss was much faster than for a dust explosion for similar peak pressure and hence similar peak temperatures. It is considered that the rate of pressure loss is related to the thickness of dust that is deposited transiently on the wall at the end of the explosion. The dust then acts as an insulation layer at the moment the flame hits the wall. The rate of pressure loss should then be a function of the thickness of the dust on the wall.

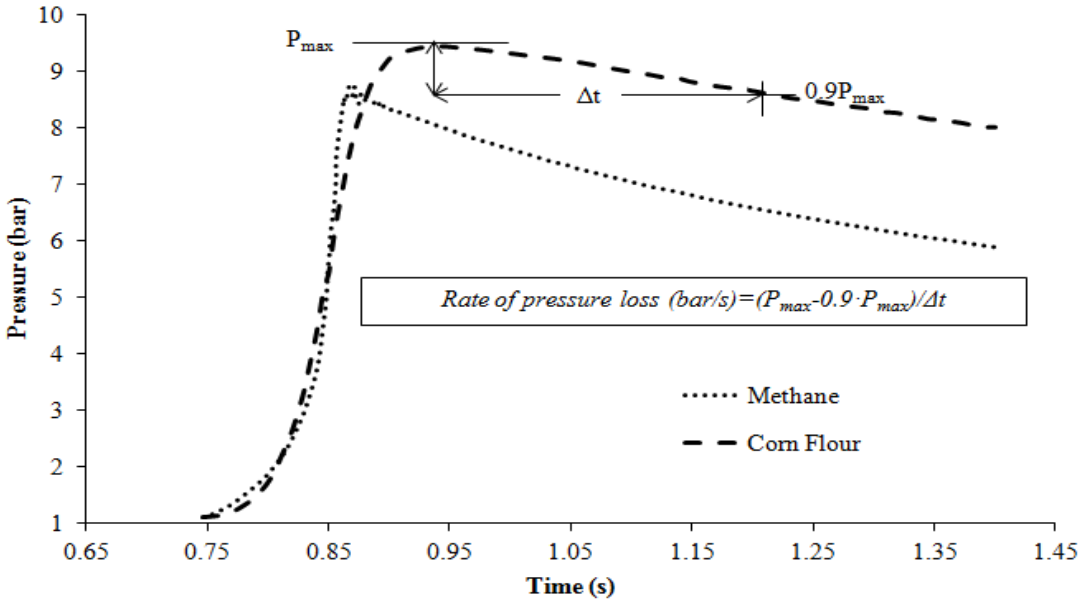

Fig 6.25 Rate of pressure loss for methane and corn flour

The residue recovered from the vessel was subtracted from the mass loaded into the dust pot to give the “mass burnt” value as described in section 3.10. The measured rate of pressure loss is plotted as a function of the calculated compressed dust wall layer thickness, assuming uniform thickness throughout, in **Fig. 6.26**. There are two trends in the pressure loss rate: firstly, there is a maximum pressure loss rate which corresponds with the peak flame temperature; secondly, the dust layer thickness increases as more dust is used in the explosion and the mass of unburned dust increases. This increased thickness reduces the rate of pressure loss even though for rich mixtures the peak pressure and therefore temperature remain high.

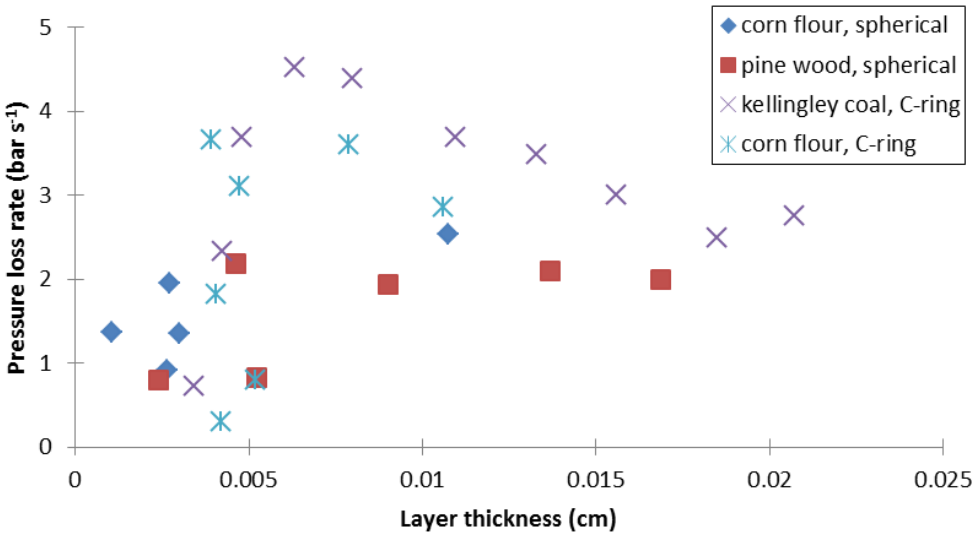

Fig 6.26 Pressure loss rate, after the peak pressure as a function of the calculated dust wall layer thickness.

The pressure loss rate was higher for coal than for biomass, as expected due to the higher flame temperature for coal, this could also be the result of woods higher specific heat capacity. The pressure loss rate decreases after peak pressure as the insulation of the flame front from the wall increases with increasing layer thickness.

The temperature difference between the flame and the wall would drive the conductive heat transfer and any dust layer would act as an insulating layer which would reduce the rate of heat loss to the metal walls. The flame temperatures were calculated using in-house FLAME software, from the equivalence ratio, Ø, based on the mass burned. The flame temperatures were computed at constant pressure and are not strictly valid for the constant volume conditions of the closed vessel explosion.

The differential form of Fourier's Law of thermal conduction shows that the local heat flux, $\vec{q}$, is equal to the product of thermal conductivity, k, and the negative local temperature gradient, $-\nabla T$. The heat flux is the amount of energy that flows through a unit area per unit time.

$$\vec{q} = -k\nabla T$$

Therefore if the temperature difference between combustion products and the vessel wall is constant (as is implied by the constant maximum pressure in tests after the maximum pressure is reached **Figure 6.10**) it is the thermal conductivity of

the gas/vessel boundary that dictates the rate of pressure loss. Changes in the peak flame temperature due to the dust composition and concentration will influence the pressure decay. However as no significant drop in pressure (which is intrinsically related to temperature) is observed (**Fig. 6.8**) after the maximum is achieved, this would appear not to be happening.

Figure 6.27 shows that the rate of pressure decay after the peak pressure in the explosion as a function of the flame temperature. This shows, as expected, the fastest decay was for methane-air explosions with no insulating deposits on the wall. Comparison with coal and cornflour at the same temperature gave over 50% lower pressure decay rate, indicating the presence of an insulating deposit. The peak pressure decay rate for dusts was 30% lower than for gas. This shows that the deposit thicknesses in **Figure 6.26**, which were between 0.08 and 0.2 mm were sufficient to reduce the heat losses.

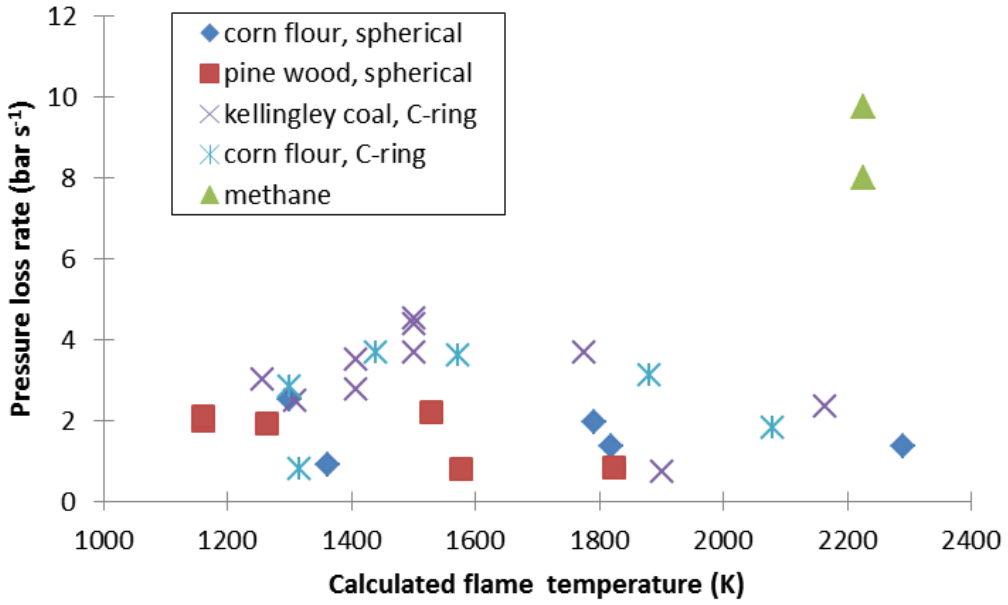

Fig 6.27 Rate of pressure decay as a function of the adiabatic flame temperature at constant pressure.

Figure 6.28 shows the rate of pressure decay as a function of the burned dust equivalence ratio. This shows unexpected results when compared with **Figure 6.27**. The peak pressure decay does not occur at the peak flame temperature. FLAME predicts that the peak temperature should occur just richer than Ø=1, as for gases. It is not known why, in dust explosions, the highest pressure and the peak reactivity occur for rich mixtures, but this is a feature of dust explosions generally and is not specific to biomass. Thus the reason the peak pressure decay occurs for rich

mixtures in **Figure 6.26** is that experimentally this is where the peak temperature occurs, which gives the peak pressure. At this mixture FLAME predicts a low temperature, as would occur for a gaseous mixture, which accounts for the peak in the rate of pressure loss in **Figure 6.27** at 1500K, which is the predicted adiabatic temperature for Ø~2.

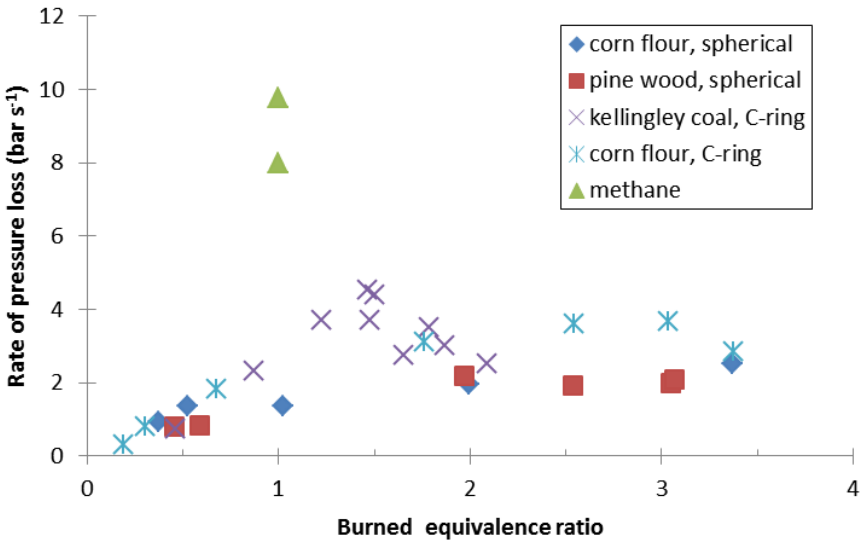

Fig 6.28 Rate of pressure loss as a function of the burned dust Ø

This cake formation has three major influences on an explosion test –

- It reduces the energy losses to the wall of the vessel when the flame contacts the wall, this is especially important for large particle biomass combustion as the flame front will be thicker than for fine particle dusts.

- It reduces the energy losses to the unburnt material by reducing its surface area prior to interaction with the flame front.

- Based on particle drag it should be the larger particles from the mixture that lag behind the carrier gas velocity. Therefore theoretically if a large particle size range is exposed to an explosion wind in a constant volume system it should be the larger particles that fall behind the flame front.

6.4 Disperser limitations

It was noted that when larger quantities of material were used in the disperser that the amount left in the hemispherical dust holder increased (**Fig. 6.29**).

Fig 6.29 3000g/m^3 wood after explosion.

This was plotted for a number of different particle sized samples and found to be constant regardless of the size of material used. **Figure 6.30** shows that up to 1000g/m^3 around 90-95% of the material in the vessel is dispersed, after this the percentage of material placed in the vessel that is dispersed falls dramatically.

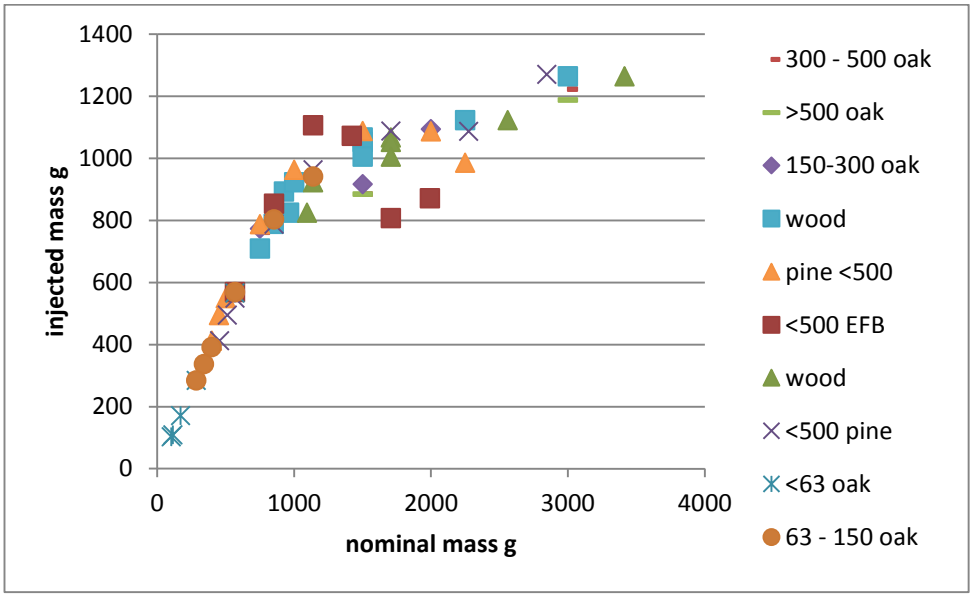

Fig 6.30 Mass injected vs mass placed in hemispherical drilled pipe injector.

After 1000g/m^3 the mass injected falls off very sharply, 3000g/m^3 nominal fuel load only dispersed a maximum of 1264g/m^3, or 42%. As the mass injected was independent of the particle size or material used it was deduced that this was an issue with the energy available in the injection air to disperse the mass of material placed in the hemisphere.

When **Figures 6.22** and **6.23** are re-plotted as mass burnt against mass injected the graph alters to reflect the large amount (42-50%) of material that never left the dust container in large nominal mass loading tests. However coal, Drax pine, pine wood and wood still display vertical deflection from a 1:1 ratio of injected mass/ burnt mass. Therefore the observations made in **Figures 6.22** and **6.23** were not incorrect even if the nominal mass was not the best indicator of the concentration.

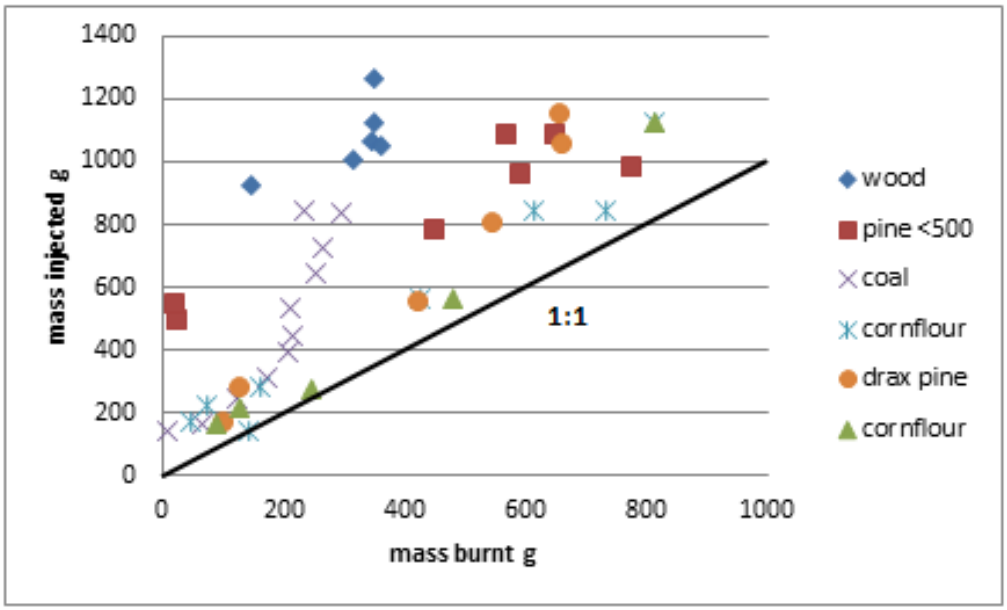

Fig 6.31 Mass injected against mass burnt

To solve the issue of the dust mass remaining in the hemisphere with the drilled pipe disperser there were two options –

- Increase the pressure that the injection air was delivered at – this would both increase the mass of air in the dispersion pot and increase the energy each unit mass of air would possess.

- Keep the pressure the same and increase the volume of air used for injection.

The second option was chosen and will be explained in section 6.5.

6.5 Future work on dispersers and 1m^3 vessel

The Leeds vessel with the drilled pipe hemispherical disperser can only inject up to 1300g/m^3, this is well below the MEC of <5000g/m^3 reported by Wong (2013) for

some large particle size biomass materials. It is also bellow the nominal 1300g/m^3 found to be the lean flammability limit in the Hartmann for 300-500µm particles, 2600-3900 g/m^3 when considering the un-equal distribution found in the Hartmann apparatus.

Therefore for these reasons –

- The 300-500µm material run on this disperser in the 1m^3 vessel cannot be considered non-flammable as it is very likely that the disperser was not able to disperse enough material to reach the flammable range for this material. If this concentration could be achieved it is considered very likely that this material would ignite as it did in the Hartmann apparatus.

- The external pot (**Fig. 3.29**) needs to be extended using the 5L (and possibly more) extension to increase its volume to disperse more material at higher dust loads. This will involve re-calibration of the ignition delay. This is the only viable method to increases the dispersion energy as the external pot is only rated to 25 Bar and is currently being used at 20 Bar therefore leaving no room for tests at a higher injection pressures.

It was noticed that while running tests in the 1m^3 vessel that the igniters would, on many occasions come out broken or cracked from the vessel (**Fig. 6.32**). The igniter cup was originally created for the purpose of preventing a directional ignition source from being created by the directional igniters. The jet flame from the igniters would hit the cup and be held in the centre of the vessel. However when the igniter shell cracks or disintegrates during ignition this would allow for the igniter flame to escape in un-planed directions, **Figure 6.32 (A)** is especially directional.

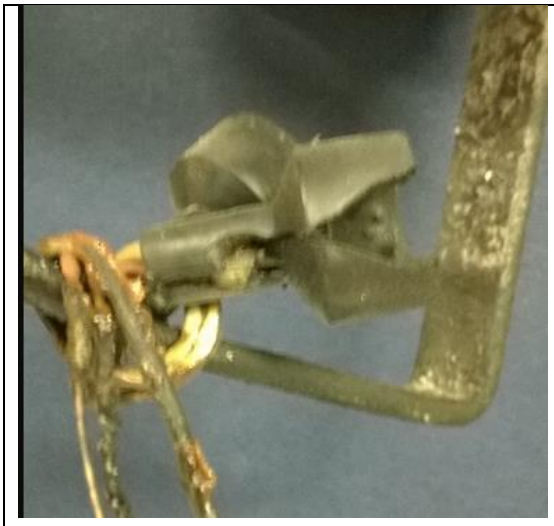

(A)

(B)

Fig 6.32 Igniters post ignition (A) partial failure of igniter shell (B) complete failure of igniter shell

To prevent this happening again the igniter cup should be re designed to both hold the igniters and prevent this (breakage of igniter casings) from being possible in the future. The simplest method would be to create 2 small metal igniter holders on the bottom of the cup to hold the igniters. Then any breach of the plastic igniter casing would have to also penetrate the metal igniter holder before making contact with the suspended dust.

6.6 Conclusions

1. Only about half of the dust injected is burnt, at the end of the explosion there is unburnt dust on the floor of the vessel. This has not been burned and it has been observed in some dust explosions (for example with milk powder) that this unburnt dust is compressed against the wall of the explosion vessel with an outer layer slightly charred. In other explosions and more commonly, the dust compressed on the wall falls off onto the floor of the chamber after the explosion. Thus the actual mixture that the flame propagated through is not the nominal mixture injected into the vessel but is leaner than this. Thus the combustion equivalence ratio is leaner than the nominal equivalence ratio over all. However if the distribution of the material is even then the concentration of material passed through is the injected

concentration, but a percentage of the material in suspension does not burn as it is compressed against the wall.

2. The disperser fabricated in this work is the only one known for the $1m^3$ that will allow dispersion of material with a particle size larger than 100µm. Other work with large particles, Wong (2013), used the 20 L sphere with internal dust storage and dispersion. Wilén (1999) reported dispersion of particles with a mean size of 318µm using the rebound nozzle with external dust pot in the $1m^3$ vessel, however this could not be repeated here and the disperser jammed when this was tried.

3. All the evidence relating to the above observation is that the injection process does NOT result in dust depositing on the floor before it participates in the explosion. Thus the concentration of dust through which a flame propagates is very rich, however the action of the explosion induced wind and the reduction in this wind to zero at the wall may change the effective size distribution at the flame front, when large particles are present. This takes 2 forms, the large particles being overtaken by the flame front during propagation across the vessel and then the large particles being preferentially moved to the wall in the last stage of propagation.

4. There is an issue that in the $1m^3$ dust explosion apparatus there is no way of determining what dust concentration the flame front propagated through at the MEC. Additionally at MEC buoyancy will play a large part in the propagation mechanism therefore leaving a proportion of the material unburnt. However as flame speed measurements were constant in vertical and horizontal directions in disperser calibration tests it is believed that the distribution of the dust was close to uniform. This has important consequences for MEC determination in the ISO Im^3 dust explosion vessel – the MEC flame front can propagate through the initial part of the mixture where the concentration is as injected but will not reach maximum pressure as the cake material will trap a percentage of the material. This is seen in the drop off of the pressure as the MEC is approached. Therefore the nominal measured MEC should be what the flame front passed through although there is no way to confirm this at present. This is further complicated by the + or – 50-100g of reside that is collected from each test

in the vessel due to attachment pipes and crevices. This especially bad at MEC mixtures where the concentration is around 100g/m^3 making the error in residue mass at the MEC too high to be reliable.

5. As was covered in section 2.3.1 the MEC results in the literature are the result of the extremely crude method of MEC determination in the ISO standards. As such, reported measurements are not real MEC determinations, but are the last mixture that did explode in 50% increments. An MEC in the literature of 30 g/m^3 could mean that the real MEC lies between 15 and 60 g/m^3 depending on the definition of MEC, as this is different in different standards.

6. The MEC and K_{st} in the 1m^3 vessel displayed a similar dependence on particle size (observed in section 5.1 for the Hartmann vessel), with the K_{st} being more affected by increasing D 3/2 than the MEC. Furthermore the K_{st} was found to more closely correspond to the d 0.1 of a material while the MEC more closely corresponds to the d 0.5, this is thought to be due to the K_{st} being dependent on the rate of volatile release while the MEC is dependent on the ability to propagate a flame in a fuel controlled environment.

7. A further feature of dust explosions that is difficult to explain and was seen in the present work is that the explosion peak pressure decreases very slowly for mixtures richer than that for the peak pressure. This is considered to be a feature of dust explosions as the presence of the dust does not displace air, whereas gas mixtures at the same pressure have less air mass and the air mass decreases as the proportion of fuel is increased. This is worst for hydrogen and is the reason why hydrogen/air mixtures have lower peak pressures even though the flame temperature is higher than hydrocarbons. As the mass of air in a dust explosion is independent of the amount of dust we can use the fact from fire research that the heat release per unit mass of air is constant irrespective of the amount of fuel. As heat release in a closed volume gives rise to pressure rise, this is a reason why the peak pressure does not decrease for rich mixtures. The small decrease is likely to be due to combustion inefficiency with all the carbon in the flame front not converted into CO_2 (soot production) and the reporting of nominal concentrations instead of mass burnt.

8. The most reactive mixture (highest K_{st}) is still very rich for large particle biomass even after the unburnt biomass has been taken into account. For coal the most reactive mixture was close to stoichiometric and similar to the mixture for gas peak reactivity (after correction of the stoichiometry for unburnt coal).

9. If larger particles get left behind the flame front and are then burnt in the high temperature burnt gases this should result in some particle size shift in the dusts at the end of the explosion. However, in the fast deceleration of the flame as it approaches the wall, larger particles should be preferentially thrown onto the wall due to inertia and finer particles take part in combustion (if they have not already all fallen behind the flame front and burnt). This could then leave the two particle size effects roughly cancelling out, leaving the debris with little apparent change in particle size. A more careful examination of the changes in particle size distribution between the starting and final dusts is required (chapter 7). Also it could be possible to capture some wall deposited particles before they fall off by adding a small side tube that the flame could push the particles ahead of the flame into, so their size distribution could be measured after the explosion. In the above qualitative model it was postulated that the action of the explosion induced wind on the biomass particles with a large distribution of size fractions is to result in large particles lagging the flame front. This will result, assuming a uniformly mixed dust and air mixture at the start, that the flame propagation produces a stratification of the mixture with large high mass particles lagging behind the flame front. These particles are then heated by the burnt gases in the presence of excess oxygen in the lean mixtures left by the fuel lean first flame front. The heat release from these particles then makes the effective mixture richer behind the flame front and leaner in the initial flame zone.

10. A feature of the combustion just before the flame front reaches the wall was thought to be that the air may have been heated by compression to a temperature higher than the devolatilization temperature of the biomass. Thus it might be expected that the last flame travel could be purely gas phase leaving mainly biomass without volatiles compressed on the wall. However, the analysis of the residue biomass after the explosion shows that this has not occurred (no consistent loss volatiles or fine particles). The

explanation may be that there is insufficient residence time to devolatilise the biomass large or small particles; alternatively the outer layer of the cake could be absorbing most of this energy as was seen for milk powder where the outer surface was charred. Fine particles could be being preferentially burnt in this part of the combustion as the explosion wind reduces, as theoretically this should preferentially push the larger particles onto the wall if there are any left after the propagation across the vessel where they were lagging behind the flame front and being burnt.

11. The feature of biomass dust explosions that is most difficult to explain is why their lean flammability limit is lower than that of gaseous hydrocarbons. Large numbers of such values were found in the literature review. The devolatilization of biomass and a flame propagating in the hydrocarbons released is a viable model with volatile yields of near 100% expected (Ubhayakar et al., 1977, Cetin, 2004, Kobayashi et al., 1977, Mohan et al., 2006) for fine particles. This work found a minimum MEC of 0.45Ø in the Leeds 1m^3 vessel and the Hartmann MECs were down at 0.17Ø. However these have been shown to be unevenly distributed over only 1/3 of the vessel, when this is corrected for it becomes 0.51Ø. This suggests that the volatiles released during combustion may have a lower H_2 composition than was suggested by Commandré (2011) which predicted volatile gasses with an of MEC of 0.258 Ø (tests performed in inert atmospheres). It is thought to be far more likely that the volatiles released in the flame front were predominantly CO and some other CH gasses.

12. Calculations have shown that the minimum weight of oak sawdust required to produce sufficient H_2 to reach the MEC of H_2 (4% volume or 3.83 g/m^3) is 67.12 g/m^3. This is assuming that all the material is vaporised and that no other gaseous products (CO, CO_2, CH_4 ect.) are produced. However the measured MEC from this work is 100g/m^3 which is an elemental MEC of 0.45Ø.

13. Literature MEC values of 30 - 60g/m^3 are, when transferred into equivalence ration (0.14 – 0.24) are leaner than most gaseous hydrocarbons will ignite. Therefore it is thought likely that this is due to unequal distribution of the dust in the vessel as these extremely low values

cannot be repeated (now that the un-equal Hartmann dust distribution is known about).

14. The results also show that the risk of an explosion with significant overpressures occurring remains at 100% in very rich environments with little indication that a rich combustion limit is “near” and this was determined in standard testing equipment that have been modified and calibrated to handle larger quantities of powder than normal. This challenges the general industry assumption that operating in very rich conditions (for example in mills and pneumatic conveying ducts) is safe and demonstrates that if there is indeed a rich limit for dusts, the present standard testing equipment are not capable of measuring it.

15. 300-500µm pine ignited at 1300g/m^3 in the Hartmann apparatus; however this injected concentration could not be reached for 1m^3 vessel therefore this mixture/particle size is (from the Hartmann apparatus) flammable, however the MEC just wasn’t reached in this equipment.

16. The lack of reliable flame speed measurements from coarse materials (>63µm) in the 1m^3 vessel is believed to be due to the un-uniformity of the flame propagation in large particles that was observed in the Hartmann vessel in chapter 5.

7 Residue separation and analysis

In this chapter the residue from the explosion tests was separated using density differentials in water and these separated fractions were then studied using SEM, TGA, CNHS and size analysis. This allowed for physical and elemental characteristics to be determined for each fuel at each stage (raw fuel, un-separated residue and the separated residue fractions). This showed the combustion residue was almost identical in composition to the raw fuel, indicating that the residue took no part in the combustion process. This indicates that previous experiments in the literature have overestimated the amount of material burnt at the rich concentrations (as was shown in section 6.2.5) and that the residue is in no way made up of ash and/or char.

Comparison of the residue (**Fig. 7.5 – 7.9**) indicates that the method of combustion taking place is homogeneous with char particles showing blowout holes from volatile release but no evidence of combustion on the particle surface as seen in **Figure 7.3**. However there is less char present than would be expected in the woody biomass residue, indicating complete combustion of the particles. Lewellen (1977) suggested that at high heating rates cellulose undergoes a complete conversion to volatiles which may explain some of these findings. The separation of the residue was first proposed after the raw residue from tests was visually observed to be made up of particles of different colours while still having almost the same composition as the raw material. Black specs of dust were found in the debris but the analysis after separation showed that they were not char but rather partially pyrolyzed biomass, similar to torrefied biomass.

This was supported by the finding of a cake formation within the vessel after explosions (**Fig. 6.24**). This led to speculations that there were different particles mixed together within the residue, it was attempted to separate these using density separation in water.

This was carried out to try and determine what material was lost from the fuel during combustion, if it was preferential loss of hydrogen, preferential loss of volatile material or if the lost material was constant across the elemental composition. To try to ensure that the residues selected were significant in terms of results generated it was decided to separate 2 samples from each particle size – the most

reactive concentration (highest K_{st}) and a near MEC mixture that generated significant K_{st}. The K_{st} qualifier was added to the MEC test as the actual MEC test would have very little burnt mass due to buoyancy.

7.1 Separated samples

As stated in section 3.2.1, for each test run there were four samples to be analysed –

- the residue as extracted from inside the vacuum bag (r).
- the residue as extracted from between the layers of the vacuum bag (br).
- the residue after separation top fraction (t).
- the residue after separation bottom fraction (b).

The separated samples are listed in **Tables 4.3 and 4.4**; this includes separations preformed on a previous PhD student's tests/materials to confirm that the process worked.

Table 7.1 Seperated residue samples

sample	bag res g	res g	Nominal g/m3	K_{st}	Top %	Bottom %
oak631	36.9	182.1	500	93.86679	18.26733	81.73267
oak632	47.8	36.3	250	53	24.02315	75.97685
oak63156	9.5	362.7	1000	33.33229	18.25013	81.74987
oak63155	19.4	233.6	300	11.27	6.315789	93.68421
oak1533	12.8	771.4	2000	11.97281	7.969639	92.03036
oak1534	20.6	763.2	1250	9.6	20.91359	79.08641
5004 oak	25.8	492.5	1000	37.25937	21.09912	78.90088
5003 oak	24.9	319.5	750	29	23.78641	76.21359

The bottom separated fraction averages 75 -93% by mass of the sample in every case. This indicates that this is a consistent trend, over 2/3 of the material from the combustion tests consistently sinks.

The bag residue is largest in <63µm samples but then increases again for the largest particle size fractions. This could be interpreted as the partial burnt material with reduced particle size being selectively trapped by the bag as they now have a particle size lower than the original material and so will preferentially pass through. This is supported by the fact that for <500µm, 150-300µm and 63-150µm samples the material trapped in the bag had the lowest percentage volatile material and highest fixed carbon and ash content of any of the fractions separated from that test. This indicates that the partially burnt material for larger particle size fractions is being preferentially trapped in the vacuum bags. It is postulated that the reason that this does not happen in the <63µm material is that the material itself is has sufficiently small particles to fit through the vacuum bag without size reduction unlike the other samples.

Unfortunately during the separation process soot and ash became trapped in the filter paper used (**Figs. 3.6** and **3.7**). Therefore the levels of ash found in the separated residue top and bottom fractions varied by only small amounts. Visibly however it was always noted that far more ash was trapped in the filter paper used for the top fraction than was found on the filter paper from the bottom (**Figs. 3.6** and **3.7**). The creation of ultra-fine soot particles (**Fig. 7.19**) indicates that the combustion taking place was rich, likely formed in the back of the flame front where all the available O_2 had already been consumed by the combustion of the devolatilised gasses.

7.1.1 Differences between layers

The separated samples analysis is listed in **Tables 4.3** and **4.4**. In every case the top layer has more fixed carbon than the bottom layer or the original material. In every case but one, the top layer has less volatile content than the bottom layer or the original, these two facts suggest that the volatiles are being driven off by the flame front, however this loss is generally only a few % (apart from the <63µm samples that will be covered later). However the top layer of the separation is only between 6-25% of the material recovered from the vessel by mass. This suggests that only a small percentage of the material injected was subjected to this

environment, while the majority of material, 75 -93% by mass was subject to less/no thermal stress. This would be consistent with the formation of a cake of material against the wall where it was protected from severe thermal stress by the quenching of the flame front on the wall and outer surface of the cake.

The hydrogen content in the residue is nearly the same for both top and bottom separations and has no set preference for the highest value in top or bottom separations. Therefore no apparent hydrogen loss from top layer in preference to bottom is taking place. The lack of any elemental difference between the top and bottom layers indicates that the volatile material loss appears to be uniform across the chemical composition of the material. This indicates that the volatiles could be H_2 and CO, however due to the ratios of hydrogen, carbon and oxygen in the biomass fuel CO and CH_4 would appear more likely. This would also produce MEC values in the same region (0.42 - 0.45Ø) as was found in this work, while H_2 and CO production, would, as has been covered produce lower MEC values than was found in this work.

In order to establish what fully combusted biomass should look like under SEM analysis ash from a biomass burner was analysed by SEM.

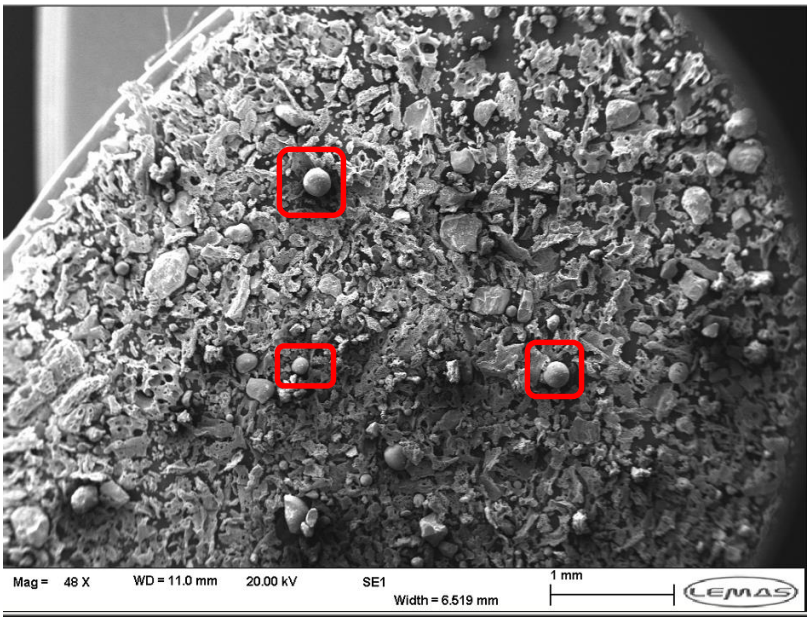

Fig 7.1 Cenosphere's in residue.

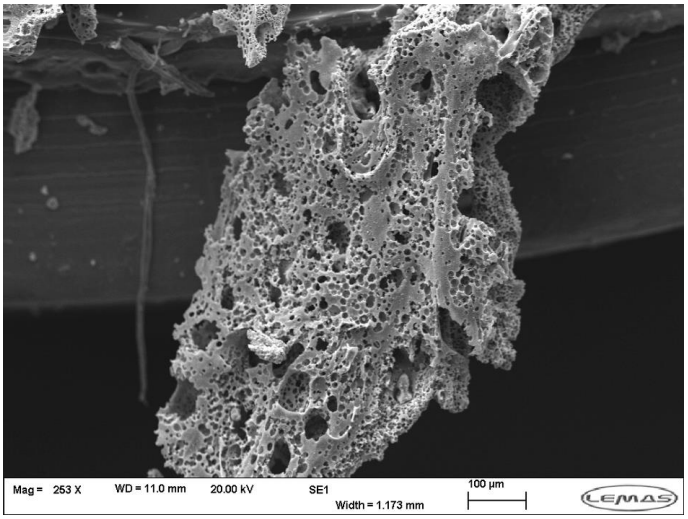

Fig 7.2 Fully combusted particle.

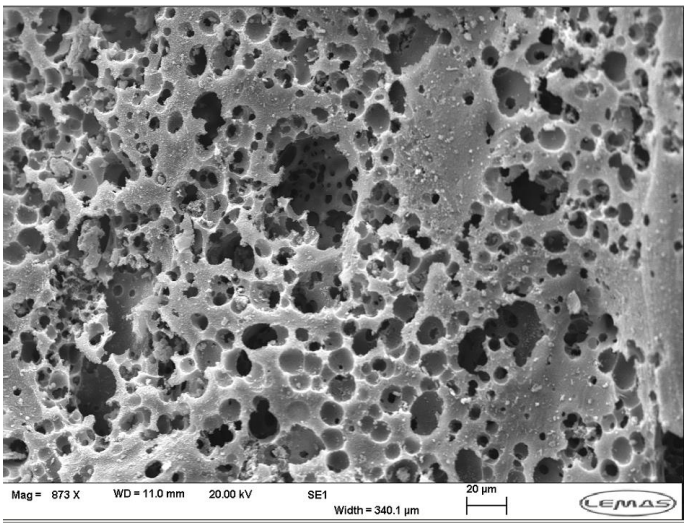

Fig 7.3 Secondary material loss.

The particles display far more small scale pores than was found by (Cetin, 2004) on Radiata pine sawdust at a heating rate of 1×10^5 °C/s, indicating that due to the particle going through a flame front more of the material was lost, possibly due to the longer residence time found in burners. This indicates that for biomass, as for coal there appears to be a residence time to burn out the fixed carbon content (for particles of this size). However unlike coal ash this secondary loss of fixed carbon (small pores) has deformed the original particles shape far less than the volatile loss (large pores), as would be expected for such a high volatile content material.

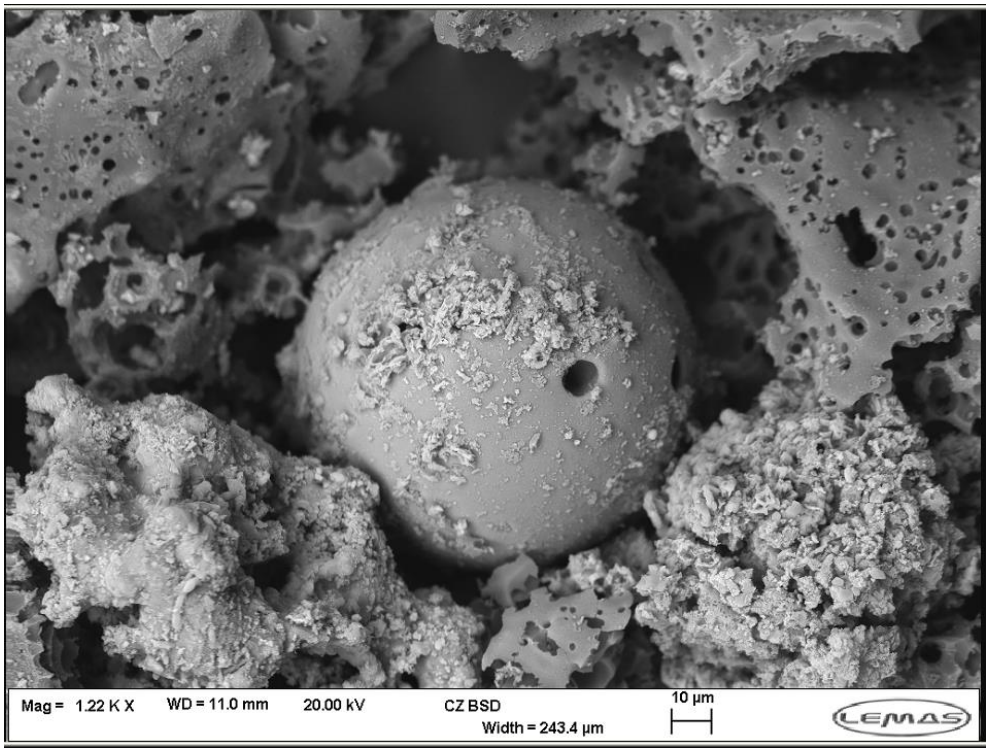

Fig 7.4 Cenosphere

During the analysis cenosphere's were noticed throughout the residue, these it was realised could be used as an indication of the temperature experienced by the particles as they are only formed in a specific temperature range 1400 -1700^{o}C (Fenelonov, 2010).

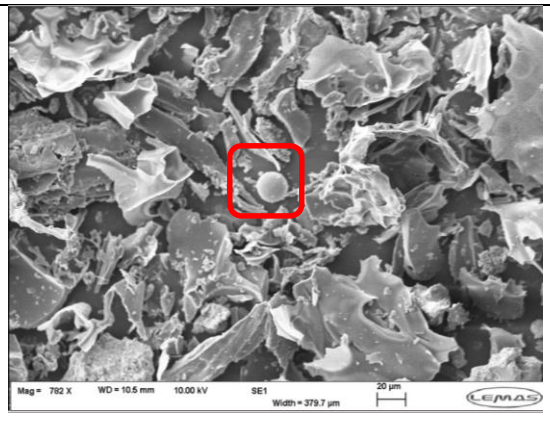

A

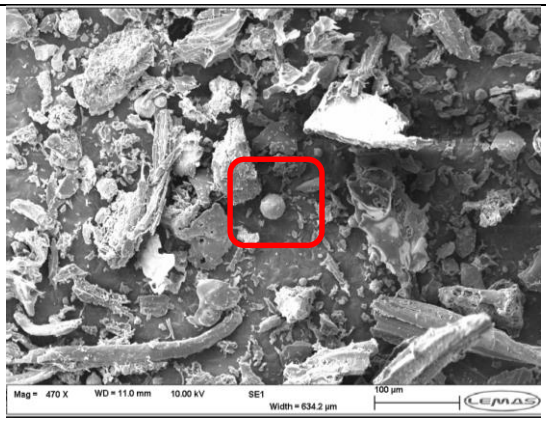

B

Fig 7.5 150 – 300 3 (A) and 4 (B) Image of cenosphere's in the residue

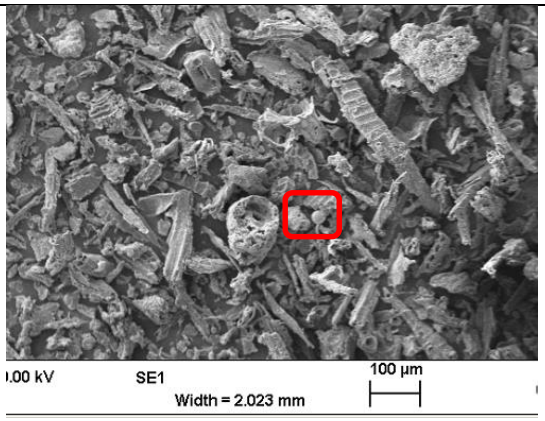

A

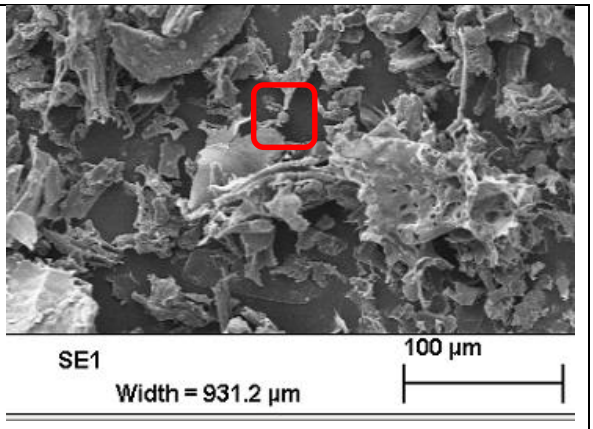

B

Fig 7.6 632 (A) and 631 (B) Image of cenosphere's in the residue

This suggests that the combustion reached temperatures of 1400 -1700^{o}C, this is higher than Proust (2006) who had 1300^{o}C for starch and the 1200^{o}C found by Han et al. (2000).

The images of the material before combustion are in chapter 4, **Figures 4.2 - 4.5**. When the residue was separated the finer material (<63µm) was found to visually contain more ash that the larger particle sizes in the top layer, this was also confirmed from the proximate analysis in **Tables 4.3** and **4.4**. However it should be noted that the <63µm tests and especially 632 were the lowest nominal mass tests run. For other size fractions 250-790g or reside was extracted from the vessel, for 632 <90g of reside was collected. This is thought to be the reason for the high ash content in these tests. The bottom layer of all <63µm tests consisted of visually partially burnt material (of a grey colour rather than black or light brown), the elemental and proximate analysis showed it to be lacking in volatiles (10-30% volatile loss) and to have an increase in fixed carbon content (10%). However this material was far from ash, with half the volatile material of the original fuel still present. Additionally the ash that is observed appears to be lacking the small scale pores associated with a residence time to burn out the fixed carbon content as seen in **Figures 7.2**, it is possible that under rapid heating the fixed carbon is converted to CO as was suggested by Lewellen (1977) and so would react in the gas phase. The ash observed in these tests was more distorted, with thinner walls than was found in the furnace residue, this is thought to be due to higher temperatures and higher rates of heating producing more distortion of the particles original shape.

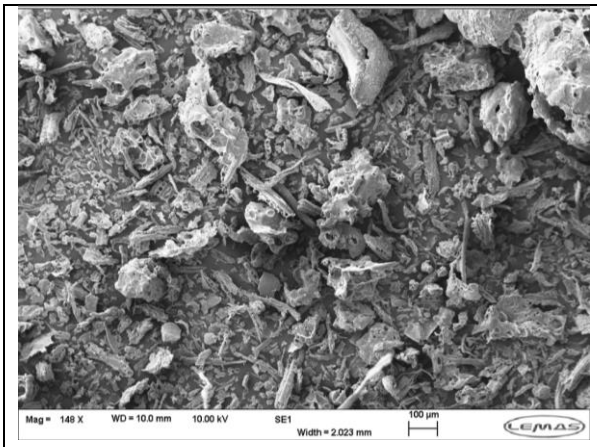

A

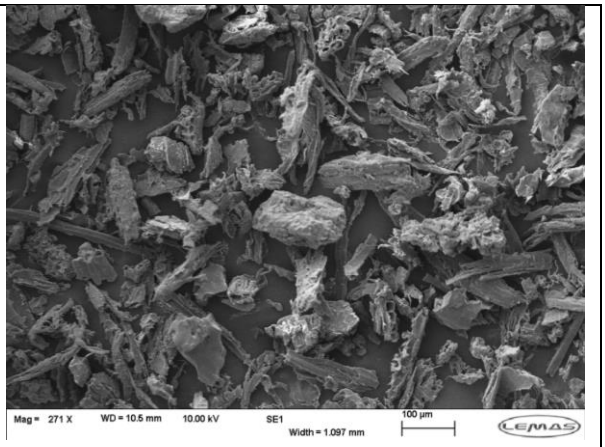

B

Fig 7.7 Residue 632 top (A) bottom (B)

For the 150 -300µm tests large numbers of the protrusions and fine elongated particles (**Fig. 4.2**) are missing from the large biomass particles post combustion. The particles themselves however show no evidence of devolatilization or charring, (top or bottom layer) the structure is identical to the original material. This is supported by the elemental and proximate analysis, **Table 4.3** and **4.4**, which shows that the 150-300µm top and bottom residues were almost identical to the raw material in both volatile and fixed carbon content.

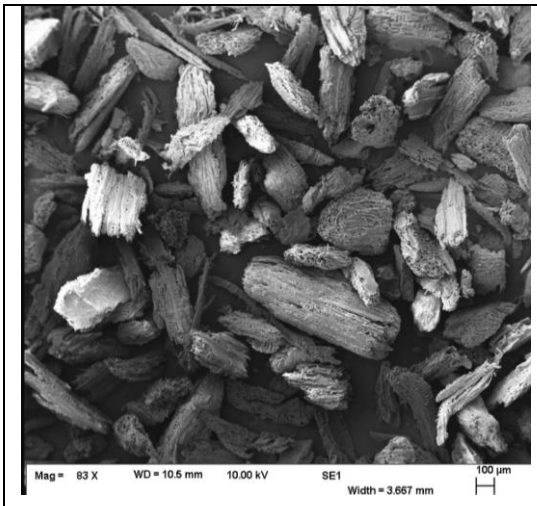

A

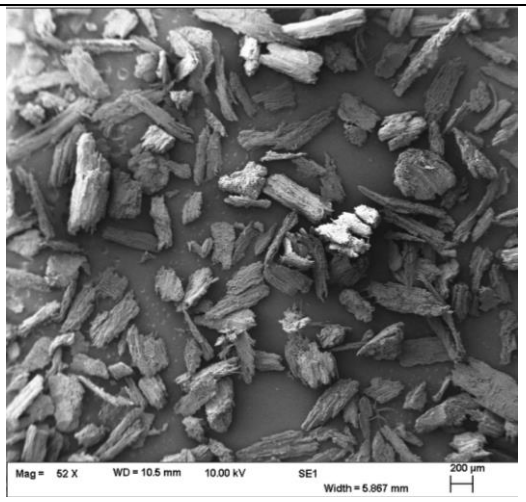

B

Fig 7.8 1533 top (A) bottom (B)

Other non-fibrous dust residues were put through the same process and displayed the same trend of high porosity char in the top layer and apparently unburnt material in the bottom layer that was observed in fine biomass (**Fig. 7.9**).

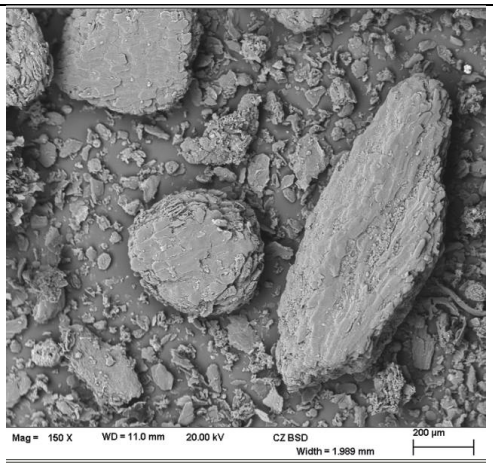

A

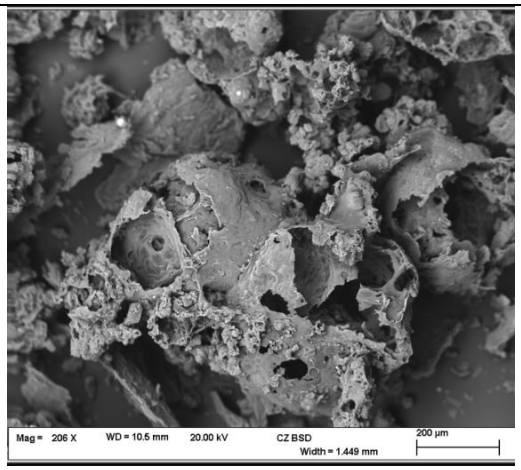

B

Fig 7.9 Pine nut top (A) bottom (B)

The SEM images show that while both the top and bottom separated fractions contained apparently unburnt particles the top fractions had more burnt out particles on average than the bottom. However as the particle size of the material tested was increased the number of burnt particles visible in the separated fractions decreased.

As has been stated in section 7.1 the mass of material trapped in the vacuum bag varied between size fractions, to try to determine the reason SEM analysis was performed on it.

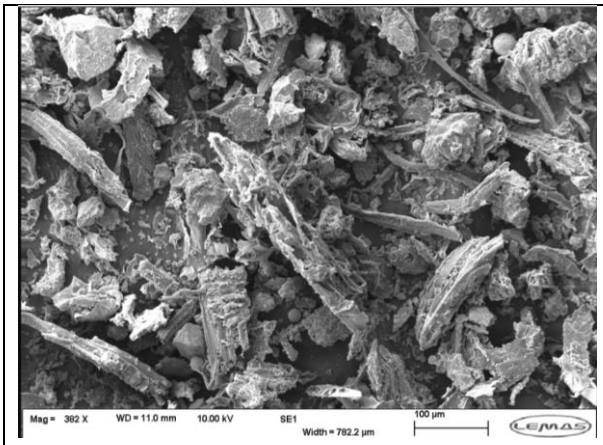	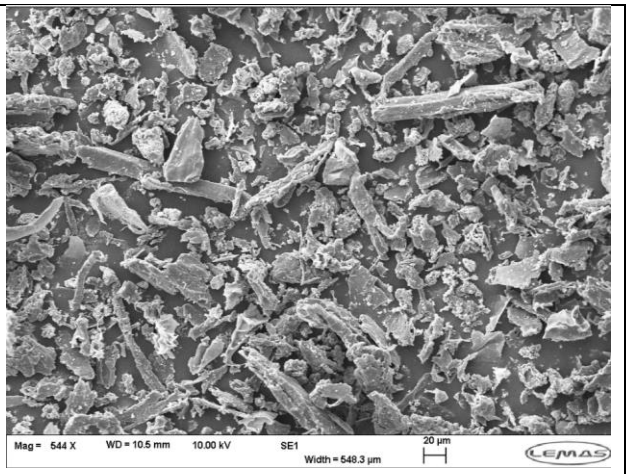
1533	**632**

Fig 7.10 Trapped material from vacuum bag.

This showed that the material trapped in the vacuum bag for <63µm oak was composed of far more unburnt material that for the 150-300µm oak as was proposed in section 7.1.

From the separated layer percentages in **Table 7.1**, analysis in **Table 4.3** and **4.4** and the SEM analysis, the vast majority of the debris in the vessel after an explosion had not been burnt. These SEM images show that the reason the top layer floats in the water separation is that the density of the particles are reduced by the porosity generated by the release of volatiles from the material.

It is speculated that the difference in the reside composition (volatile material, fixed carbon and ash) between the 150-300µm and <63µm oak may be due to three factors-

- The <63µm oak was only run at low concentrations (200 – 500g/m^3) compared to the larger (150-300µm and <500µm oak) particles (750 – 2000g/m^3) due to a limited supply of the material. Therefore there was less mass of residue in the cake to absorb the energy from the flame front, therefore the material was subjected to more thermal stress and lost more volatile matter than other size fractions.

- The material was of a smaller particle size; therefore it may have reacted differently to the final stage propagation, just before the flame reaches the

wall due to aerodynamic properties, possibly forming a less dense/stable cake.

- The difference in particle size will result in different thermal capacitance; it may be that biomass particles bigger than 63µm have a larger thermal capacity and therefore while exposed to the same thermal stress do not undergo the same loss of material.

A feature of the flame propagation in gasses is that in the last period of flame travel the air and fuel are both compressed so there cannot be any change in concentration. However, in dust explosions the air is compressed but what is the effect of pressure on a biomass particle? It cannot change its concentration due to compression as the particle is not a gas. But it was proposed that pressure could compress the porous structure of the biomass so that the material on the wall may have the original biomass chemical composition but not its open cellular structure. However from these images this does not appear to be happening. The structure of the material post combustion appears to have the same shape and texture as before.

It is thought that the small change in composition of the debris from the original biomass was due to its heating at the wall due to compression and flame quenching as the loss of volatile material and increase in fixed carbon content is so low. However, there was no evidence for the large increase in char or ash that would occur if the debris was partially burned biomass due to the flame propagating but not burning all the biomass dust particles in its path. The evidence suggests that all the particles, irrespective of size, are burned in the propagating flame (if there is sufficient oxygen) and what remains has not participated in the flame propagation. A consequence of this is that the concentration given in dust explosion work as the dust loaded into the injection pot divided by the volume of air in the vessel is not the actual concentration that the flame propagates through.

7.1.2 Size analysis of burnt material

Size analysis was carried out on the residue post combustion to identify what if any particle size material had been preferential removed from the fuel post combustion.

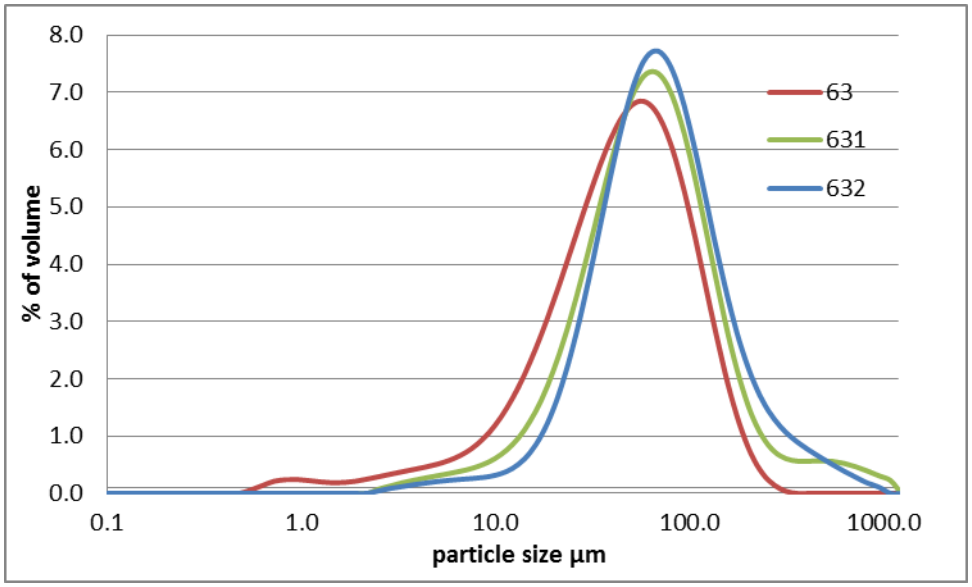

Fig 7.11 <63µm size analysis, logarithmic scale, particle distribution

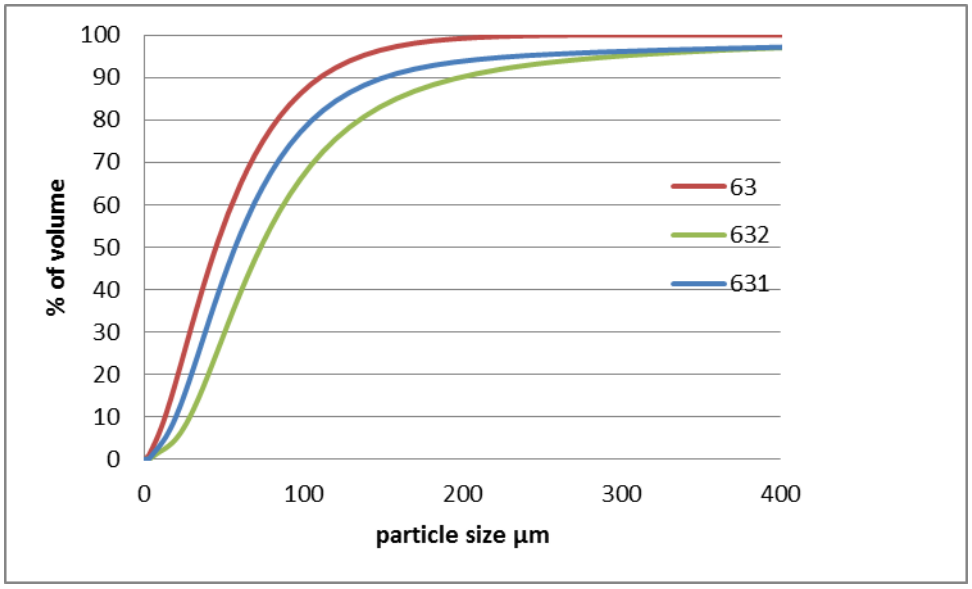

Fig 7.12 <63µm size analysis, cumulative distribution

Less than <63µm oak residue had an increase in size after combustion, this shift in particle size could represent the particles of char and ash that were found in the residue as these had increased in size. This is due to the swelling of the particle during melting of the structure and the gaseous release of material forming bubbles in the molten material (Cetin, 2004). The loss of fine particles could indicate preferential burning of the fine material; however the loss of the fine material could also have happened in the cake, either due to the energy transferred to the material by the flame front or due to the increased temperature/pressure at this point in the explosion. This could also have taken place during collection of the residue as the

pre-combustion material was not put through this and unreacted fine material was found in the vacuum bag of these tests.

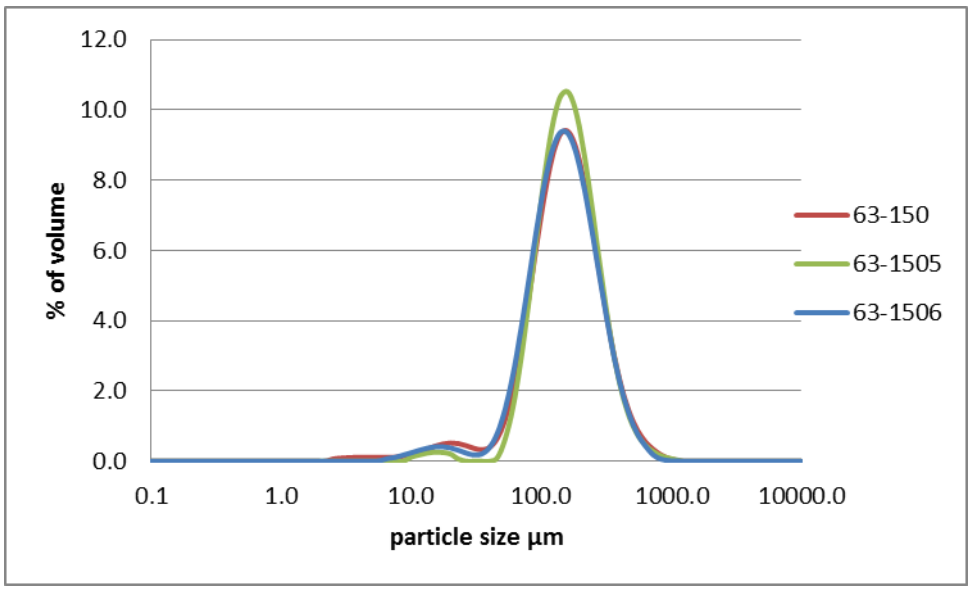

Fig 7.13 63 – 150µm size analysis, logarithmic scale, particle distribution.

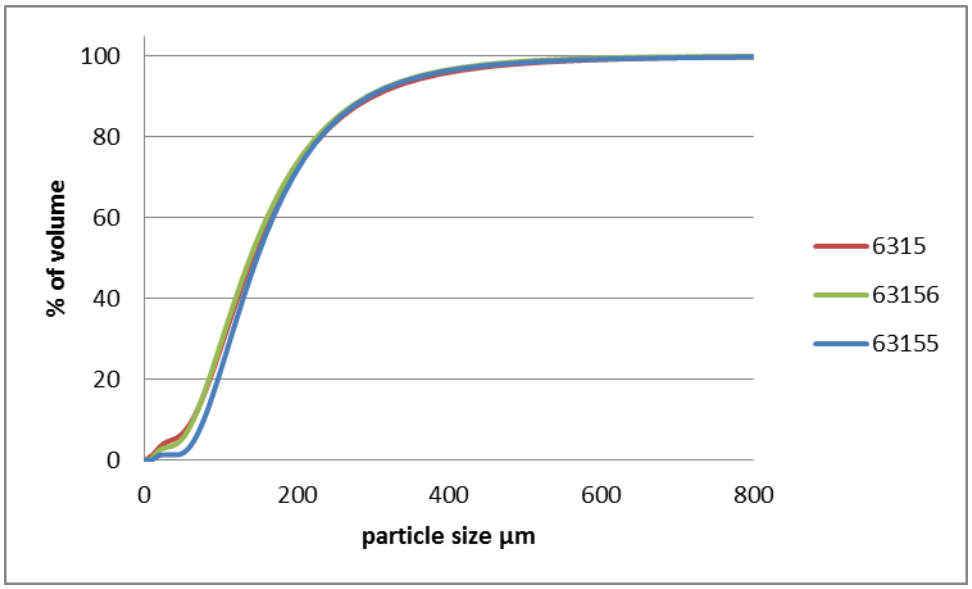

Fig 7.14 63 - 150µm size analysis, cumulative distribution.

The 63-150µm oak residue showed no significant alteration in size after combustion, this could be caused by the equal contribution of all the particle sizes present to the flame front. This would therefore suggest that there was no preferential burning of the fine particles and no size segregation during the propagation/injection. However this explanation would also require the ash particles formed to have the exact same size as the particles lost which seems unlikely. It is

possible that 63156 has an unaltered size distribution as it only burnt 82g of material out of 341g however this would still be expected to produce some variation in the size distribution. 63155 however burnt over 50% of the injected concentration therefore would be expected to show more alteration in the particle size from the creation of char particles. Therefore at this point the reason for this lack of change in the particle distribution is unknown, more samples of residue could be tested to see if this was a sampling error.

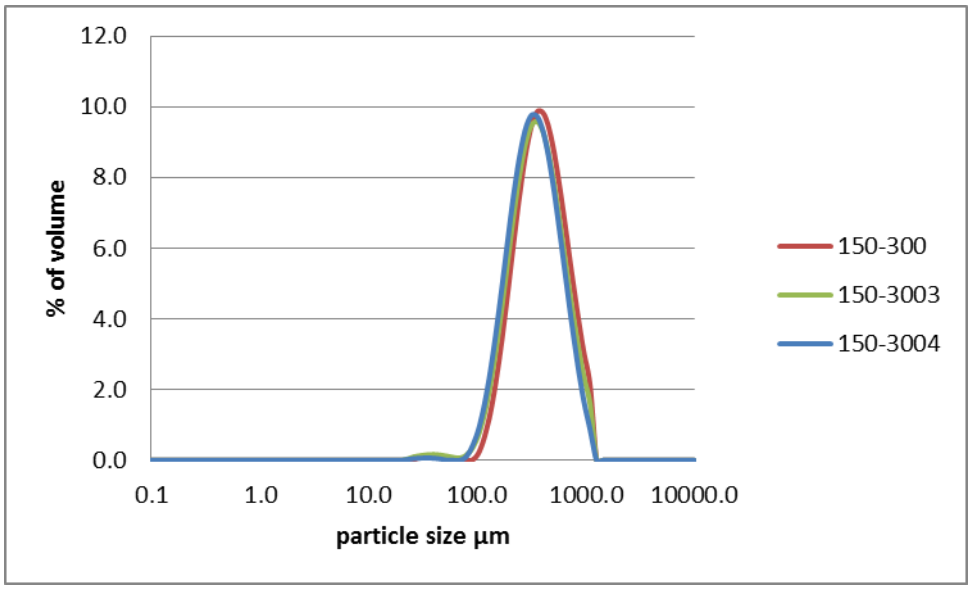

Fig 7.15 150 - 300µm size analysis logarithmic scale particle distribution.

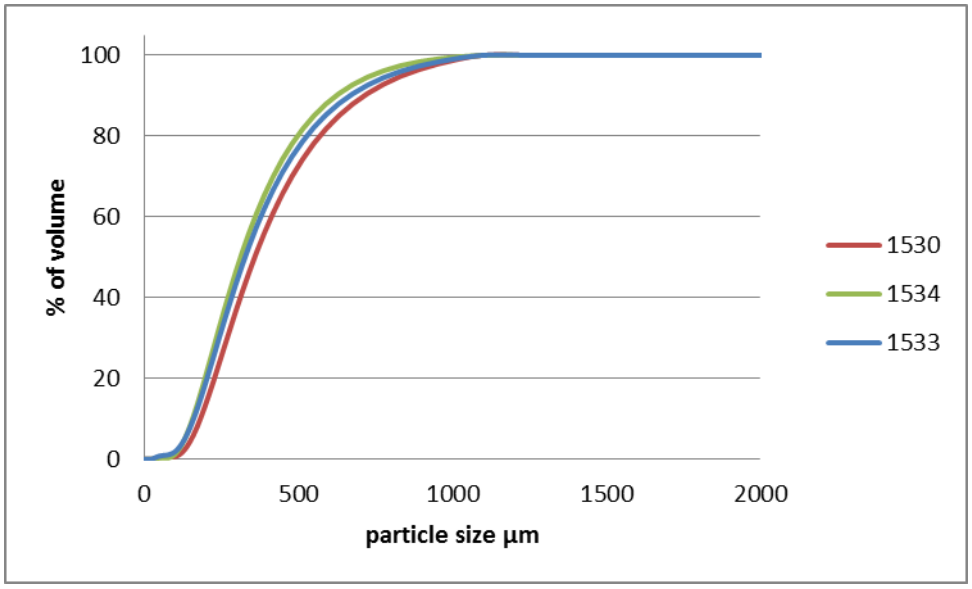

Fig 7.16 150 - 300µm size analysis cumulative distribution.

In this case it is thought that the reason why 150 - 300µm oak decreased slightly in particle size after combustion is that the ash particles formed during the combustion of the material could have broken up during the residue collection and become trapped in the vacuum bag. The reason that these particles would break up but not those in the <63µm oak residue is that they are larger, therefore giving them more inertia during collisions in the residue collection process. Furthermore from the SEM images it appears that the particles (**Fig. 7.8**) in the residue have lost their fine protrusions (**Fig. 4.2**), there is no corresponding devolatilization of the particles, represented by swelling or devolatilization of the particle. This is shown in the TGA analysis of the reside (**Table 4.4**) compared to the unburnt material (**Table 4.2**) where there is no loss of volatile material or increase in fixed carbon content that would indicate that the particles have interacted with the flame front. This suggests that the loss of the fine protrusions happened in the cake, either due to the energy transferred to the material by the flame front or due to the increased temperature/pressure at this point in the explosion.

It is postulated that the reason this temperature/pressure did not devolatilised the larger particles is due the thermal inertia of the particles being far larger than that of the protrusions coming off them.

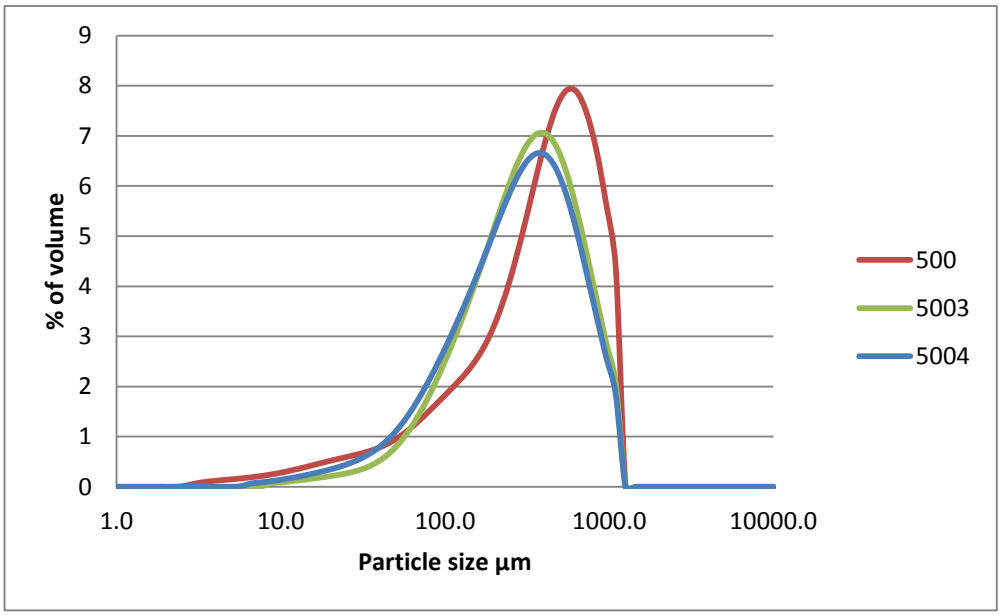

Fig 7.17 <500µm size analysis, logarithmic scale, particle distribution.

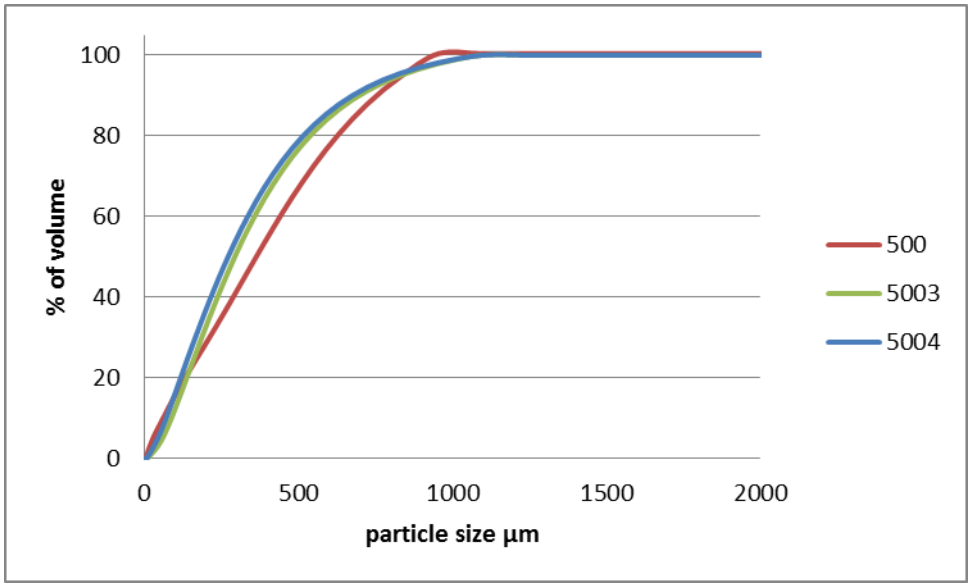

Fig 7.18 <500µm size analysis, cumulative distribution.

For <500µm oak the reason particle size decreased so dramatically after combustion is believed to be that the material (the only one with a wide size range) was size segregated during combustion with the larger particles preferentially falling behind the flame front during combustion. This led to these particles undergoing size reduction due to combustion, this is supported by the fact that <500µm oak is the only size of oak (not including the <63µm oak) where the top residue separation layer had decreased volatile content and increased fixed carbon. Indicating partial devolatilization of the material as not all the large particles behind the flame front had sufficient time to burn out completely. This burn out of the large particles is significantly improved by the presence of fine particles which provide the initial flame front. The larger particles then fall behind the flame front and burn in the hot gasses; this is backed up by the results from **Figure 7.13** where in the absence of fine material, with no significant size variation between the particles in the mixture there is no shift in the size distribution of the post combustion residue. This is supported by the K_{st} generated in the $1m^3$ vessel where, similarly to the Hartmann test results the K_{st} appears to be dictated by the finer particles present in the mixture. This is shown by <500µm oak producing nearly identical K_{st} to the 63-150µm oak (**Fig. 6.11**), the size fraction that has nearly identical values of d 0.1 (**Table 4.1**) and D 3/2.

It is again thought that the ash particles in the residue for this size fraction are breaking up during residue collection; this is supported by the large fixed carbon and ash content of this material in reference to the other separated fractions from

the same source. This indicates that only for this size range was material being partially burnt, all other smaller size material is completely devolatilised/burnt. This may be due to the flame front generated from the fine material using up a large amount of the available O_2 which doesn't happen with the 150-300µm oak as there are no fines to consume this.

The evidence is that all the particles, irrespective of size, are burned in the propagating flame front (if there is sufficient O_2) and what remains has not participated in the flame propagation. A consequence of this is that the concentration given in dust explosion work, as the dust loaded into the injection pot divided by the volume of air in the vessel, is not the actual concentration that the flame propagates through, the flame is much leaner than the nominal concentration.

To further determine if the combustion process affected the size distribution of the residues one way ANOVA tests were carried out on all the samples for pre and post combustion using D [3/2] average particle size. This showed that in all cases (<63. 63-150, 150-300 and <500) the F value was > than the F_{crit} and the P value was lower than the set Alpha, indicating that the null hypothesis of no statistically significant variation between the sample means is not valid. Therefore the combustion did alter the size distribution in the 63-150 and 150-300 micron size ranges.

7.1.3 Future work on equipment

To address the issue of filter paper trapping ash in the future the filter paper could be weighed prior to the separation, dried after and the mass of ash analysed through mass gained. Although the total mass of material trapped in the filter paper is only thought to amount to 1-2g of material when the total mass lost results in 20 – 40g of ash this can become significant.

To try to ensure that the assumption that this material was ash was correct; SEM analysis was carried out, Figure 7.19. This clearly shows thin shattered ash particles as were seen in **Figure 7.6 (B)** and **Figure 7.7 (A)** embedded into the filter paper, this indicates that it is ash particles and not soot.

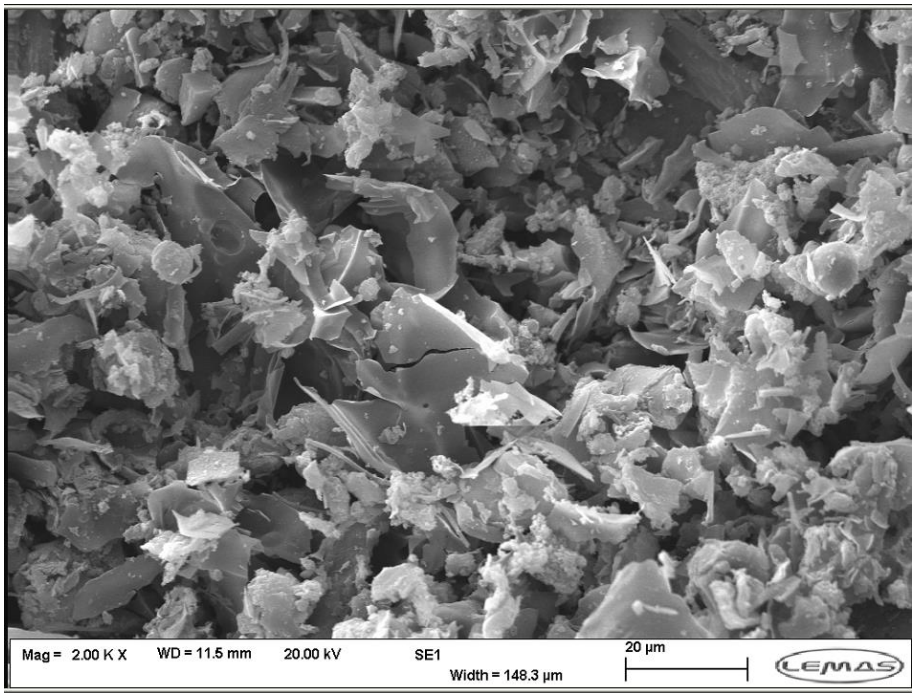

Fig 7.19 1533 top separation filter paper

To avoid the issue of trapping fine material in the vacuum bag finer mesh vacuum bags should be used in future tests. It is hoped that this will prevent the finer fractions of material from being separated from the residue samples during collection from the vessel. This would also help alleviate the issue that the bags trap different percentages of material and this material can have different compositions based on the particle size of the original material and that of the residue.

7.2 Conclusions

1. A key feature of explosions in the ISO 1m^3 vessel is that a large fraction of the mass of dust injected does not burn and is left as a residue in the bottom of the vessel at the end of the explosion. Most of the literature on dust explosions does not mention that a large fraction of the dust injected into the ISO 1m^3 vessel does not burn and hence the nominal concentrations recorded are not the dust concentrations that the flame propagates through overall. Furthermore the residue recovered from the vessel is (for most tests that are not near the MEC and for <63µm particle size), closer to the raw material than ash or char.

2. Overall this debris and raw biomass analysis shows that the model of the unburned dust being blown ahead of the flame by the explosion induced wind and depositing particles on the wall ahead of the flame is a reasonable explanation for the presence of about 50% on average (can be 10 -72% of injected mass depending on concentration) of the dust remaining at the end of the explosion.

3. The small change in composition of the debris from the original biomass was believed to be due to its heating at the wall due to compression and flame quenching. There was no evidence for the large increase in char or ash that would occur if the debris was partially burned biomass due to the flame propagating but not burning all the biomass dust particles in its path. It appears that at no stage do these particles participate in the heat release of the explosion, but neither do they take heat out of the system to any significant degree. As the flame impinges on the wall with the residue layer compressed on to it the outer surface of the residue is heated and undergoes pyrolysis.

4. It should be noted that if there is no significant heat release from these deposits then it is expected that overall the deposits left as a dust after the explosion will not to be greatly different from the raw biomass dust, as shown by Sattar (2012). SEM imaging showed that this was the case with both pulverized nut dust and woody biomass; however the nut dust, when separated showed more ash particles in the residue than the woody biomass. It has be hypothesized that this was due to a higher cellulose composition in the woody biomass that decomposed directly to volatiles with no char/ash formation while lower cellulose content in the nut dust led to more ash formation. However it is more likely that the ash formed from the nut dust was less friable that that from the woody biomass and therefore didn’t break up as easily during collection in the vacuum cleaner and end up trapped in the bag. This is due to SEM images showing a thicker more durable looking ash for the nut dust than for the fibrous biomass.

5. The results show that the risk of an explosion with significant overpressures (in that they will still destroy buildings and process vessels) remains at 100% in very rich environments with little indication that a rich combustion

limit is “near”. This was determined in standard testing equipment that have been modified and calibrated to handle larger quantities and particle sizes of powder than normal. This challenges the general industry assumption that operating in very rich conditions (for example in mills and pneumatic conveying ducts to burners) is safe and demonstrates that if there is indeed a rich limit for dusts, the present standard testing equipment are not capable of measuring it.

6. The particle size distribution of the dust not burnt is nearly the same as that injected for 63-150µm and 150-300µm size fractions, so for these size fractions combustion does NOT appear to be preferentially burning the finer particles. However it is also not showing the predicted loss of the larger particles due to aerodynamic drag induced particle size segregation either. For <500µm the large particles appear to have been lost from the residue, this is thought be due to the larger particles being left behind the flame front to burn in the higher temperatures there. It is postulated that the char particles formed from this are less stable that those formed from <63µm material and as such break up during residue collection. 500g of oak material completely combusted turns into only 25g of ash, therefore in 500 - 700g of residue this becomes very difficult to accurately represent. Additionally an amount of ultra-fine ash was lost from each separated sample to the filter paper.

7. The TGA analysis of the debris shows that it is NOT char and has a very similar volatile content and composition to that of the original mixture. Thus any theory based on flame propagation in gaseous hydrocarbons from devolatilised particles, leaving carbon char behind cannot explain the observed results (unburnt particles) unless this unreacted material comes from the cake formation and has therefore not been exposed to the flame front. This is also supported by the lean limit measurements which would have to be richer than hydrocarbon lean limits due to the mass of the char if only volatiles were burning, whereas the observed lean limits are very near those for gaseous hydrocarbons. Under rapid heating the fixed carbon is thought to convert to CO (Lewellen, 1977) and so would react in the gas phase indicating that in real heating rates biomass is almost 100% volatiles. One explanation proposed for this was that hydrogen is released as part of the combustion of biomass, as only hydrogen has a significantly leaner limit

than hydrocarbons. However with no proof of preferential loss of hydrogen from the reside this appears unlikely.

8. The hydrogen content in the residue is nearly the same for both top and bottom separations and has no set preference for the highest value in top or bottom separations. Therefore no apparent hydrogen loss from top layer in preference to bottom. The lack of any elemental difference between the top and bottom layers indicates that the volatile material loss appears to be uniform across the chemical composition of the material. This indicates that the volatiles could be H_2 and CO, however from the MEC results various CH gasses and CO appears more likely as this would have the required Ø MEC of around 0.42 – 0.45 found in this work. This would also fit better with the chemical composition of biomass $CH_{1.4\text{-}2}O_{0.5\text{-}0.8}$.

9. For <500µm oak it is thought that the reason particle size decreased so dramatically after combustion is that the material (the only one tested with a wide particle size range) was size segregated during combustion with the larger particles falling behind the flame front during combustion. This led to these particles undergoing size reduction, this is supported by the fact that <500µm oak is the only size of oak (not including the <63µm oak) where the top residue separation layer had decreased volatile content and increased fixed carbon. Indicating partial devolatilization of the material as not all the large particles behind the flame front had sufficient time/oxygen to burn out completely. This burn out of the large particles is significantly improved by the presence of fine particles which are thought to devolatilise providing the fuel for the initial flame front. The larger particles then fall behind the flame front and burn in the hot gasses. This is backed up by the results from **Figure 7.15** and **Figure 7.16** where in the absence of fine material, with no significant size variation between the particles in the mixture there is no shift in the size distribution of the post combustion residue. This is supported by the K_{st} generated in the $1m^3$ vessel where similarly to the Hartmann test results the K_{st} appears to be dictated by the finer particles in the mixture. This is shown by <500µm oak producing nearly identical K_{st} to 63-150µm oak (**Fig. 6.11**), the size fraction that shares nearly identical values of d 0.1 (**Table 4.1**) for particle size distribution.

8 Further discussion and comparisons

It was hoped that the Hartman vessel could be used for preliminary testing of dust samples to locate the MEC and most reactive concentration (K_{st}) prior to testing on the $1m^3$ vessel. This was due the waste of milled material that takes place if concentrations below the MEC are injected (recovery of the material was not possible due to preferential loss of fine particles to the vacuum cleaner bags) in the $1m^3$ vessel. If the Hartman vessel could be used to predict these values prior to testing on the $1m^3$ this would save time and effort.

8.1 Hartmann comparison against $1m^3$

As 6 identical material samples were tested in both vessels for MEC, K_{st} and a comparison between the vessels is possible.

Table 8.1 $1m^3$ MEC against hartmann MEC

Particle size	MEC Hartmann Ø	MEC Hartmann Ø corrected	$1m^3$ MEC Ø	Hartman /$1m^3$ - %
<63 oak	0.2	0.5	0.45	44.4 or 111
63 - 150 oak	0.17	0.51	1.1	15.5 or 46
150 -300 oak	1.4	2.8	4.3	31.3 or 65.1
<500 oak	0.6	1.8	2.3	25.3 or 78.3
<500 pine	1.3	2.6	1.8	68.8 or 144
EFB (empty fruit bunches)	1	2.5	2.3	40.8 or 109

The $1m^3$ gave consistently higher MEC values than those from the Hartmann apparatus (in this study), no values of <0.45Ø were found with this apparatus unlike Wilén (1999) who reported MEC's of 0.14Ø (wood) and 0.15Ø (bark) values in this apparatus and Field (1983) who reported a value of 0.14Ø for Spruce from undisclosed apparatus. The data collected from the Hartman apparatus (in this study) did produce results in this area for the finer fractions of oak and pine. However high speed video analysis showed that these tests were ignited before

mixing of the dust and air was complete (**Fig. 5.17**). Maisey (1965) recognised that the Hartman apparatus does not create a uniform mixture in the vessel, instead stating that the un-uniformity was constant throughout the tests. Therefore it is thought that these results (Wilén, 1999, Field, 1983) arose through unequal distribution of the dust within the vessel. While the $1m^3$ produced repeatedly higher MEC results for the same materials (in this study) there is no current method of determining the concentration of material around the ignition source as there is for the Hartman apparatus in the form of the high speed video footage. Therefore there is no way of guaranteeing that the injected concentration is the actual concentration the flame front propagated through. However circumstantial evidence exists to indicate that this may be the case-

- When tests were run on the distribution in the $1m^3$ vessel using flame speeds to determine if an even distribution existed the flame speeds were uniform in both directions indicating that this was the case. If the concentration was different in different parts of the vessel it would have been expected to be seen as differing flame speeds in different parts of the vessel as was shown in **Figure 5.13.**
- When the MEC from the Hartmann apparatus is corrected for the percentage of the tube actually occupied by the dust at the time of ignition the result is almost identical to the value from the $1m^3$ for the same material <63µm oak- 0.2 * 2.5 = 0.5Ø while the $1m^3$ gave 0.456Ø.

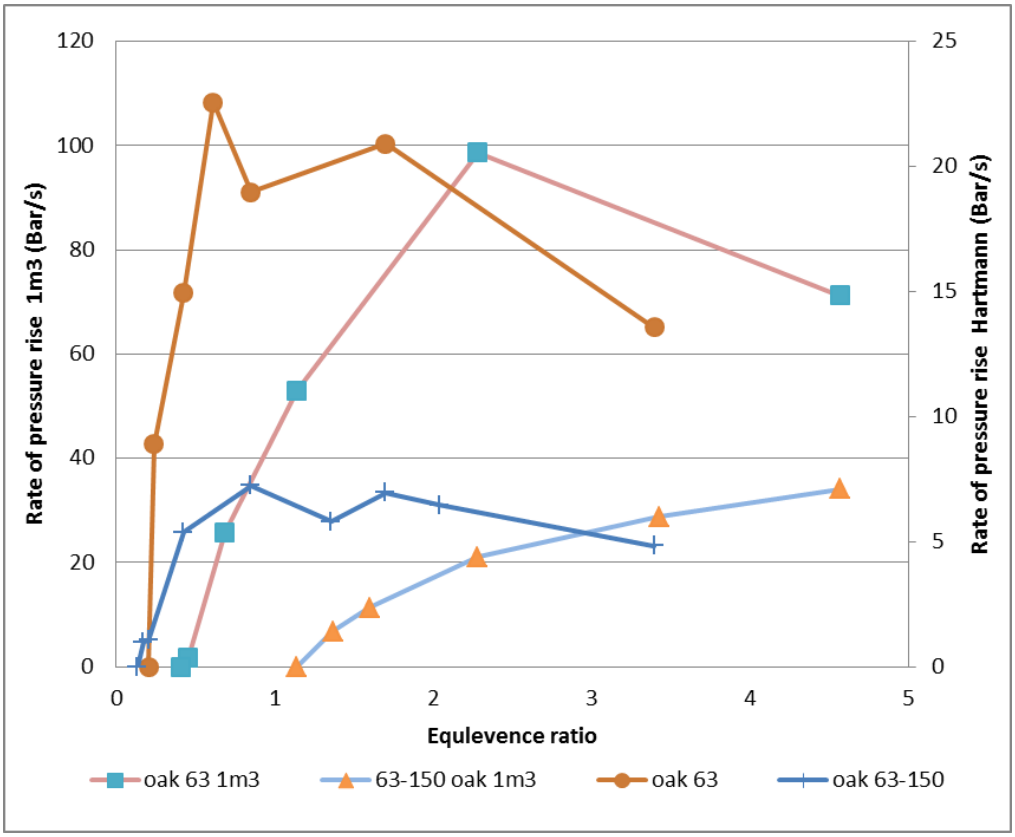

Fig 8.1 Hartmann and 1m^3 rate of pressure rise nominal concentration

When the maximum rate of pressure rise generated from 1m^3 and Hartmann were plotted against concentration there was an off set on the concentration at which the most reactive mixture occurs as would be expected from the unequal distribution. Different concentration gaps were found for both particle size materials indicating that they do not behave the same way in each vessel.

The unequal distribution was corrected for (by multiplying by 2.5 as the dust was only distributed over around 40% of the vessel at the time) and the data now show a far better correlation for this particle size, however not all the data produced such a good correlation.

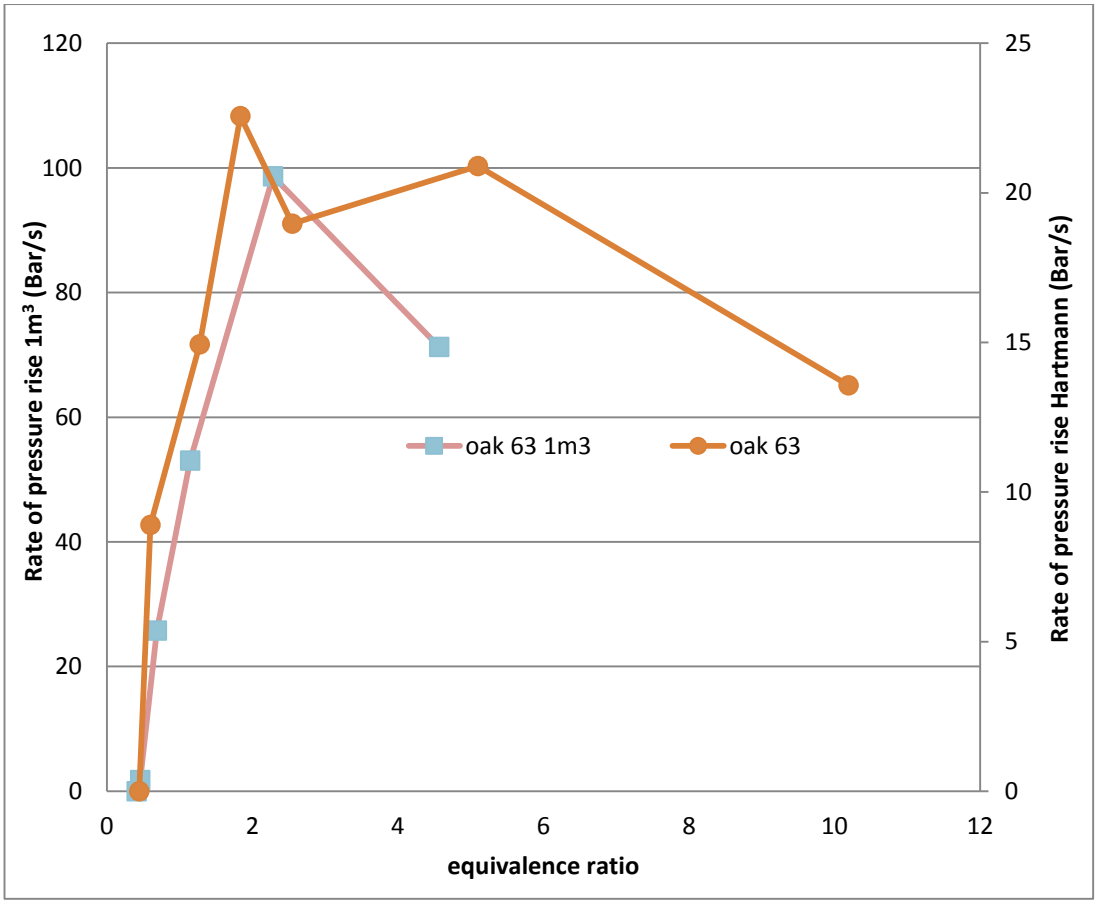

Fig 8.2 Hartmann and 1m³ rate of pressure rise corrected concentration

When the maximum rate of pressure rise generated from 1m³ and Hartmann tests is compared, (**Fig. 8.3** and **8.4**) there is a weak correlation between them with the 1m³ giving values on average 6 times higher than the Hartmann (**Fig. 8.3**).

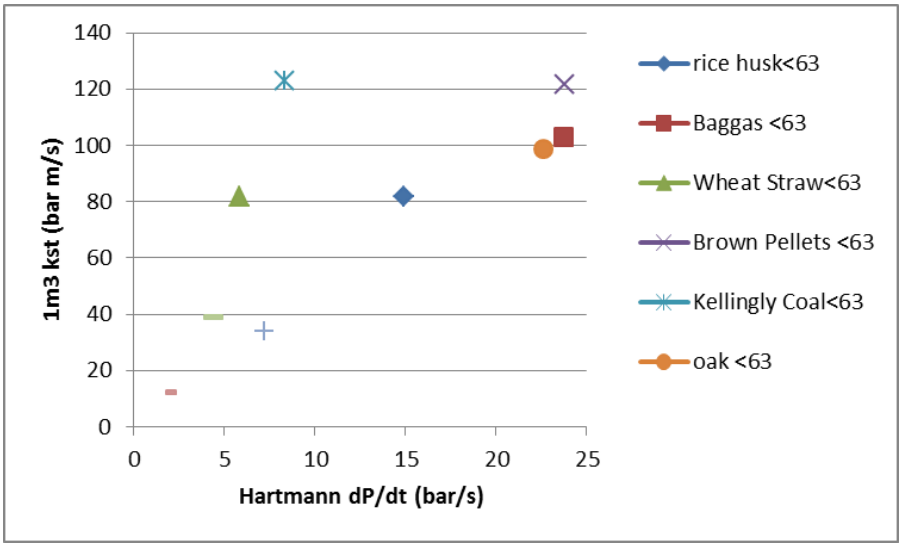

Fig 8.3 Maximum rate of pressure rise <u>recorded</u>

While there appears to be agreement on the maximum rate of pressure rise there is a large issue in that the data from which this is generated (**Fig. 5.9** and **6.11**) are in a large number of cases not the “maximum rate of pressure rise” but the maximum rate of pressure rise recorded as the rate of pressure rise is still increasing with concentration for many size ranges. However due to insufficient dust ($1m^3$) or insufficient data (Hartmann) no comparison of values could be created. When the maximum rate of pressure rise is plotted for those samples (where this was reached in both pieces of apparatus) there is no correlation (**Fig. 8.4**).

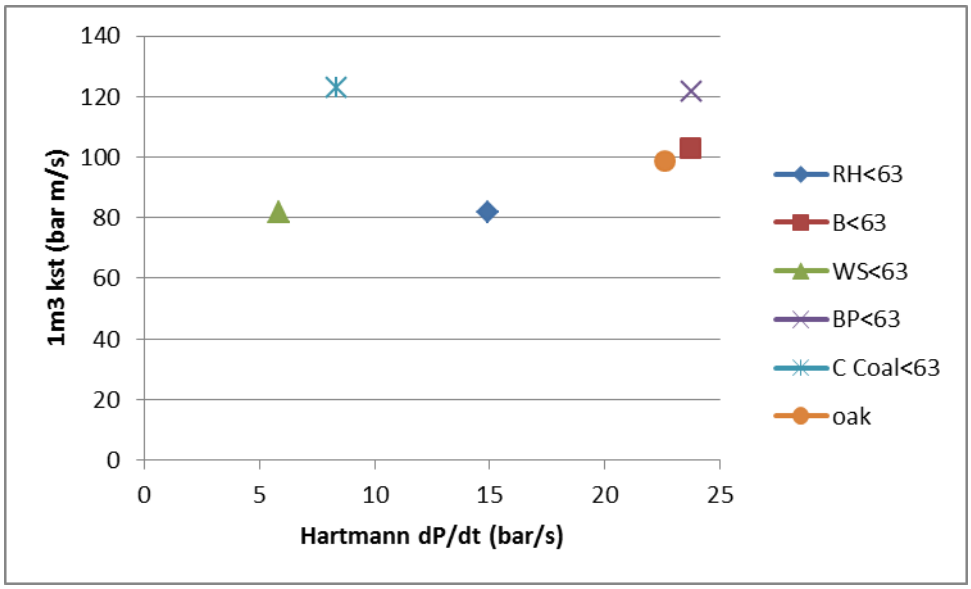

Fig 8.4 Maximum rate of pressure rise from vessels

When concentration (corrected nominal for Hartmann and nominal for $1m^3$) is used to plot the resulting dp/dt of the different vessels this becomes even clearer, with the disparity between vessels in dp/dt, ranging between 0.7 – 9 times greater in the $1m^3$ vessel than the Hartmann (**Fig. 8.5**).

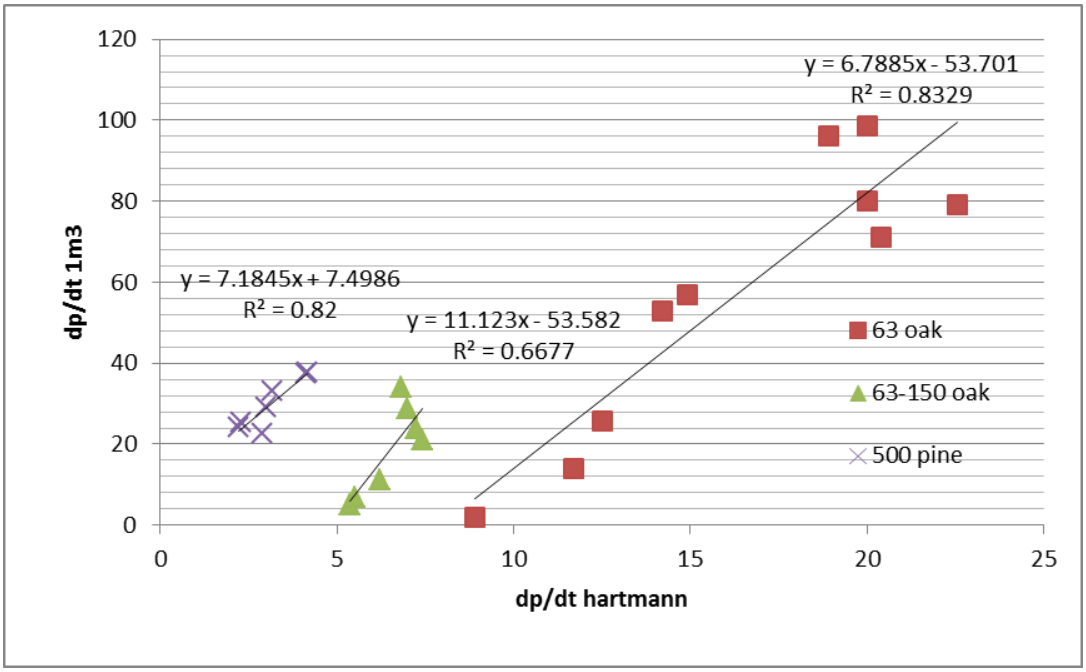

Fig 8.5 Rate of pressure rise from different vessels at different concentrations

Therefore at this time both pieces of equipment have issues and are, at this point incomparable to each other in regards to rate of pressure rise generated as a function of the concentration. It should be noted that in **Figure 5.9**, 5 out of the 8 dusts tested had not reached their most reactive concentration by the time the maximum concentration was reached. While in the $1m^3$, the maximum rate of pressure rise been reached for 9 out of 11 dusts tested. This is due to the Hartmann primarily being used to generate MEC data prior to the decision to try to use it to predict the most reactive concentration for a dust. Unfortunately by the time this was done there was insufficient time to perform more tests.

It had been hoped to be able to use the Hartmann vessel to get a measure of where the maximum reactivity would be found on the concentration scale for a given material without the need to mill and size separate the large mass of material needed for tests on the $1m^3$ apparatus. However at this time that appears impossible. More tests on the Hartmann apparatus at richer concentrations could improve this situation.

Although the different vessels produced different correlations for dp/dt and MEC with concentration, when the dp/dt and MEC were plotted out as function of the average volume/surface area ratio D 3/2 a very good correlation was found. Both the dp/dt and MEC scaled with the D 3/2 of the dust tested, and correlated very well with the trend line from each vessel.

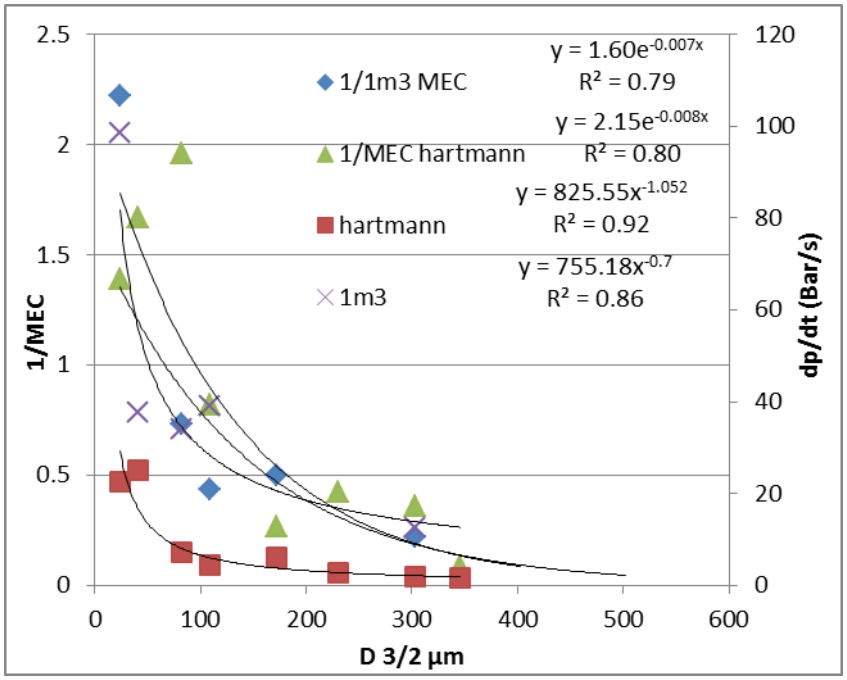

Fig 8.6 Maximum rate of pressure rise recorded and 1/MEC for Hartmann and 1m³ vessel as a function of D 3/2.

It is thought that the dp/dt from each vessel did not correspond as well as the MEC results did because not all the points are maximum values (especially for the Hartmann) as was mentioned earlier, therefore the correlation between dp/dt from the vessels may improve when this is carried out. Additionally the MEC values are all the intrinsic MEC so would be expected to correlate better than the dp/dt values.

In terms of MEC it is believed that the Hartmann apparatus produced the most reliable results, after adjustment from the high speed video to allow for unequal distribution. This is because the distribution of the dust can actually be measured at the time of ignition using high speed video, while no tool of that nature is presently available in the 1m³ vessel.

Flame speed data between the vessels is at this time incomparable as 1m³ didn't produce usable flame speed data for the majority of large particle tests and the turbulence factor in the Hartmann is presently unknown.

Chapter 9. Conclusions and future work.

One of the stated aims of this research was to compile a complete list of explosion data for future use including- particle size (d.1,d.5,d.9), elemental, proximate analysis, MEC and a full set of Pressure and K_{st} as a function of concentration as per the ISO standard.

It is believed that this has been done for oak at 4 separate particle size distributions (<63µm, 63-150µm and <500µm), pine at <500µm and EFB at <500µm, these materials were also run in the Hartmann apparatus for comparison with the $1m^3$. Moreover a method and the equipment for the dispersion and explosion of very coarse particle sizes has been established, tested and proven to work allowing for the characterisation of more material when it is sourced. It is believed that this is the first vessel to be fitted with this disperser and as such one of the few capable of dispersing coarse fibrous biomass particles. The only two other vessels capable of doing this is the Chilworth 20L sphere with internal placement of dust and a report of the use of the rebound nozzle in the $1m^3$ by Wilén (1999) that cannot be reproduced. Additionally a procedure for determining the concentration of material lost during combustion has also been established.

Although wood was also tested in the $1m^3$ the particles were too big to fit through the size analysis machine and therefore could not be compared on particle size to the other materials. Although there were other machines that would process particles of this size they operated on a different method to the mastersizer and therefore the results generated would not be comparable to the other data. Additionally the different machines had different minimum and maximum particle size ranges; therefore it was impossible to run all the samples through one machine without missing out the largest or finest particles.

As was covered in section 2.3.1 the MEC results in the literature are the result of the extremely crude method of MEC determination in the ISO standards. As such, reported measurements are not real MEC determinations, but are the last mixture that did explode in 50% intervals. An MEC in the literature of $60g/m^3$ could mean that the real MEC lies between 30 and $60g/m^3$. Where possible the MEC was recorded accurately during this work resolving it to 10% of the last mixture where a flame propagated.

9.1 Effect of particle size on the combustion behaviour of biomass with reference to coal.

Biomass was found to be more reactive in terms of equivalence ratio MEC, than coal in these tests (MEC of 0.45Ø against 0.7Ø). However when these values are turned into actual masses coal is more dangerous as its MEC is 80g/m^3 while oak is 98g/m^3. This combined with the very fine particle sizes that coal dust can create, would appear to make coal the more dangerous material in terms of housekeeping and cleaning/maintenance. This is due to the ease with which the finer particles will become airborne and the time they will spend in suspension.

This work found that biomass particles of 300-500µm would ignite and propagate a flame. Previous work (Man and Harris, 2014, Cook, 1977, Zabetakis, 1965, Wong, 2013) indicates that coal particles of 150–212µm would not explode and the same for a liquid sprays/mists of kerosene mist with a particle size >300µm. While biomass samples run in this work with a particle size of 300-500µm were ignited in the Hartman apparatus for a sample of pine wood and biomass samples with average particle sizes of 1227µm were found from the literature to propagate a flame by Wong (2013). This suggests that biomass has a higher reactivity than coal and that the particle size at which flame propagation is no longer possible will be larger for biomass than for coal. Biomass appears to have a maximum flammable particle size (300-500µm with d_{10} = 250µm) similar to liquid mists (300µm), probably due to its large volatile composition relative to coal.

Particle shape is also significant as biomass particles are cylindrical as opposed to coal which produced roughly spherical particles. As the height/radius ratio is increased for cylindrical particles the surface area : volume ratio reduces, however it is lower than for spherical particles of the same radius after a height : radius ratio of 2 (lowest average height : radius ratio for tested samples was around 3). For biomass the finer the particle size the higher the height : radius ratio is and therefore the less reactive the material should be in reference to another spherical particle of the same radius.

Further, it was determined that the biomass particles were the diameter of the sieve mesh's used to separate them by SEM (**Fig. 4.2- 4.5**) and particle size analysis (**Table 4.1**), this was done as the fibrous biomass particles could have been being separated based on their height instead of their diameter. This was prevented from

occurring by running the sieve shaker at the maximum allowable speed for a long time to ensure the particles were sufficiently agitated to allow them to fall through the size mesh vertically (diameter) instead of horizontally (height). It was confirmed through the size analysis that the desired particle sizes were being achieved as the d_{10} of the size separated material is almost the same as the bottom mesh size for all samples.

9.2 Combustion behaviour of biomass.

From previous publications (Han et al., 2000, Han, 2001, Gao, 2015) as well as the high speed video footage, it is believed that the combustion of biomass takes place homogeneously with a double flame structure as was observed for lycopodium. This means that all dust combustion above this size is likely to be in a devolatilization-controlled regime. A flammable atmosphere of devolatilised material is created ahead of the flame front by convective and radiative heat transfer that the flame front then propagates through. Large particles or particle agglomerations are then burnt in an envelope diffusion flame that surrounds the particle, which are then burnt in an oxygen controlled environment. The fineness of the particles in the dust cloud appears to dictate the gas concentration of the initial flame front and the structure of the flame. For fine particles (<63µm) it appears as if most of the particles are devolatilised ahead of the flame producing a rich mixture of gaseous material through which the flame front propagates uniformly. For coarse particles (>150µm) the mixture of devolatilised material is much leaner (visually less luminous due to less soot formation) as a result of the larger particles need more energy to be devolatilised to the same extent as the fine material due to larger thermal inertia as well as smaller surface area : volume ratios. Therefore the flame shape is far less uniform and corresponds with the locations of individual particles in the distribution as the volatile gas radius around the particles is much smaller.

The fact that MEC values of 0.13 – 0.3Ø are regularly encountered in the literature (**Table 2.13** and **Table 2.14**) suggests that unequal distribution within explosion vessels may be an issue. This is supported by the fact that pure hydrogen (the leanest burning gas species) has a MEC of 0.14Ø, therefore it is unlikely that the materials tested would have an MEC near this. While test vessels have in the past been used to test the MEC of materials for reference against other dusts (Maisey, 1965) the aim in this work is to produce an accurate MEC based off the mass of material and the volume of air in which it is distributed/burnt. Therefore the most

suitable method to display MEC in is equivalence ratio (for the last concentration that DID ignite (NFPA, 2013) as is done for gasses) as opposed to g/m^3 concentration, DAF or otherwise. It is therefore thought that the literature sources that report MEC's = 0.13 – 0.35Ø are most likely suffering from unequal distribution of the dust prior to ignition as was found for the Hartmann vessel in this work.

Biomass samples investigated in the 1m^3 vessel in this work had a minimum MEC of 0.45Ø, around the MEC of most CH gases. This compares to a generally accepted value of 80g/m^3 for Pittsburgh coal (Cashdollar, 1996, Chawla et al., 1996), Bureau of Mines identifies 90 g/m^3 as the lean limit for Pittsburgh coal (Jensen, 1994) putting the MEC =0.72 - 0.645Ø even though this material was milled to smaller particle size than the biomass. However when the volatile content is allowed for, (Kobayashi et al. (1977) demonstrated that at real heating rates coal has a volatile content of 60-65%) this becomes close to that of its stated devolatilised gas species CH_4, (0.65 x 0.65 = 0.42). The main difference is the availability of Hydrogen in the fuel with biomass having a H/C ratio of 1.5-1.7 and coal 1-1.5, however if biomass is nearly 100% volatiles and coal is 60-65% and the hydrogen is all released with the volatiles leaving the fixed carbon and ash behind the H/C ratio for coal volatiles is 1.7-2.5. This appears to be the reason that biomass produces mainly CO (Commandré, 2011, Corella, 1988, Lewellen, 1977) while coal produces CH_4 and CO_2 (Solomon et al., 1988). This would allow biomass to propagate a flame at leaner stoichiometric mixtures than coal can in terms of fuel mass while the volatile products have similar flammability ranges 0.4 – 0.5Ø.

However the MEC for the H_2/CO mixture released from pyrolysis of wood is 0.258Ø or less (Commandré, 2011) and the MEC's for this study are >0.42 for all materials tested (with high speed video adjustment of the Hartmann tests) even lycopodium, when tested, produced an MEC of 0.364Ø (corrected to 0.728Ø). This biomass had approximately 50% more hydrogen content than any of the other biomasses tested and as such would be expected to produce the lowest MEC if preferential release of hydrogen were occurring. This did not happen and the MEC was actually higher than for oak and pine at <63µm in equivalence ratio terms. The only significant difference (increased carbon content as found for coal shows no corresponding lowering of the MEC limits) between this material and other biomass's is the fuel bound oxygen content (**Table 4.2**) and the temperature at which it releases its volatile content (**Fig. 4.1**) which are believed to have led to this. Additionally

Commandré (2011) noted that the ratio of H_2/CO got smaller at lower heating rates, so at MEC conditions the flame front will be at its weakest with low flame temperatures and will be expected to produce less H_2 and more CO therefore pushing the gaseous MEC above 0.258Ø, further away from the 0.14 -0.25Ø values found in the literature.

It is therefore theorised that the woody biomass is producing predominantly CO but also other CH volatiles upon which the flame front is propagating this is supported by the lack of any evidence for preferential hydrogen loss in the residue and an MEC that is at no point observed to go below the 0.4Ø which is the flammability limit of CO.

Figure 8.6 shows that for both explosion vessels the K_{st} decreased faster than 1/MEC with increasing particle size. This indicates that the K_{st} is more sensitive to the fine particle composition of a mixture than the MEC this is supported by the fact that the R^2 value for 1/MEC corresponded well to both the d_{10} and d_{50} in different vessels but the dp/dt corresponded to the d_{10} best in both vessels (**Fig. 6.16, 6.15, 5.30** and **5.10**) with the $1m^3$ having a noticeable difference between the correlation for d_{10} and the other 2. This is thought to be due to the dp/dt (a reaction rate controlled situation) being generated by the finer particles that can instantly devolatilise into gas and not so much by the slower burning particles that burn behind this which have a far slower pressure release rate. While for the MEC (a fuel controlled environment) is governed by the mass of particles that can interact with and participate in the combustion regardless of the rate at which they do so.

9.3 Reasons for extended rich limit in biomass.

In the literature and in the tests carried out here the phenomenon of no degradation of the maximum pressure generated with increasing mass load is observed. This is believed to be due to the formation of a cake of material on the inside of the vessel, therefore isolating/excluding a large amount of material from the flame front, therefore lowering the energy loss to the unburnt material by reducing its surface area. This has the effect of lowering the concentration of material reported to have been burnt/used in these tests. For this reason a recommendation of this work is that all dust explosion literature in future report the mass burnt during a test instead of the nominal mass loaded into the disperser.

It was theorised at the beginning of this work that this phenomenon might be caused by the solid to gas transformation of more material with higher dust loading and that the energy loss to the additional dust mass was cancelled out by the corresponding pressure rise of this extra devolatilised material. However this can be shown not to be happening (**Fig. 6.28**), **Figure 6.28** also promoted the idea of a cake formation within the vessel as without it the mass lost should increase in line with the mass injected as material and therefore mass will be lost from any biomass material exposed to or passed over by a flame front.

It is thought the reason for coarse biomass particles having its maximum reactivity at ~2Ø is that at that point the closet mixture to stoichiometric in terms of devolatilised volatile concentration is being released ahead of the flame. It has been seen that the finer the particle size is made the closer to 1Ø the maximum reactivity is found in mass burnt.

This suggests that the solid material's ability to release its devolatilised mass is the reason for the maximum reactivity being found for >1Ø and as this scales with surface area to volume ratio, the larger the particle the further from 1Ø the maximum reactivity will be found.

It is theorised that the reason behind the exceptionally wide dust flammability limits compared to gasses is 2 fold –

- Firstly the dust displaces no air, therefore the displacement of oxygen by gaseous fuel does not happen.
- Secondly the nominal dust mass is not the mass of material that is devolatilised and burnt, an amount of this is due to the cake trapping material. Additionally, it appears as if the percentage of fuel that is not trapped in the cake, that does devolatilise, is dictated by the particle size of this material. For <40µm material the whole particle appears to devolatilise ahead of the flame front resulting in a flame propagation similar to that of gas combustion. While for larger particles the flame front devolatilises a part of its mass ahead of the flame front and the remaining particle mass burns in an envelope of flame behind this flame front with the remaining oxygen. The Ø concentration of the initial flame front is determined by the particle size, the closer the particles are to <40µm the closer the devolatilised fuel concentration will be to the dust concentration it passed through. Therefore the closer the particle size is to <40µm the less particles will be burning

behind the initial flame front and the thinner the flame front will be. This was demonstrated by the differing sharpness of the different rates of pressure rise for <63µm and <500µm oak in **Figure 6.14**.

If this is true it means that very simplistically the flammability limits for a given dust are the same as those of its devolatilised gas species if no air was displaced by the fuel with the mass of gaseous fuel = (injected concentration - concentration of cake) x the mass percentage of these particles that will devolatilise in time to burn in the flame front.

9.4 1m^3 improvements

The most important improvement on the work to date needs to be to improve the injected mass for the disperser at high mass loading as it currently only injects a maximum of 1250g. This is particularly important as 300-500µm material was found to ignite in the Hartmann explosion vessel at a nominal concentration of 1300g/m^3, when this is corrected it becomes approximately 2600g/m^3, far above the maximum concentration injectable at present.

One of the main problems is that when a different type or mass of material is loaded into a pre-set injection device it will be injected differently due to different friction coefficients but most importantly the differing mass load (**Fig. 6.30**). Another issue is that with higher dust loading more work will be being done by the injection air; therefore it should be creating differing levels of turbulence with different mass loads. This will become especially significant at mass loadings of >5000g/m^3.

This comes about as the same force is used for injection across the concentration ranges and while it is sufficient to inject and disperse nearly 100% of material at 500-750g/m^3 it is insufficient at 3000g/m^3. This is significant as the results of Wong (2013) indicate that some materials have MEC values as high as >5000g/m^3 which in the equipment now is beyond its maximum dispersible concentration. However changing the air pressure or vessel volume (work currently being undertaken by Azam Saeede) of air used alters the turbulence and therefore K_{st} and flame speed's generated. If this is to be corrected an extensive set of tests altering the mass of air used for injection would have to be carried out (while also changing the pre-dispersion vessel pressure to ensure the same mass of air is present in each test). This should be carried out for each mass of material requiring testing.

It highly recommended that optical probes are used in the future to determine the dust concentration in multiple locations at once as is shown in **Figure 8.8**, fitting optical probes to the $1m^3$ vessel would allow for more confidence to be put in the distribution of the dust within this vessel.

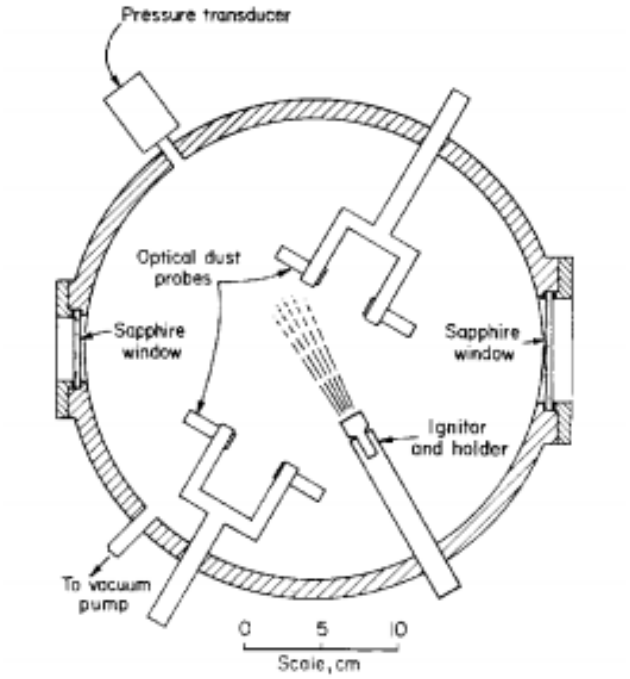

Fig 9.1 USBM 20 L explosibilty test chamber (Cashdollar, 1996).

This would also enable any injection calibration to be carried out with far more confidence as the distribution of the dust within the vessel could then be readily compared at different areas within the vessel.

The formation of a “cake” of material being formed in this vessel for rich mixtures would appear to be unavoidable due to the nature of the phenomenon itself and could go a long way to explaining the apparent lack of a lowering in the pressure results with increased mass of fuel.

If collection of the residue after combustion is continued after this work it is highly recommended that work is undertaken to seal off the ports attached to the vessel on the inside. This would avoid non spherical propagation and prevent dust loss when collecting the residue. Furthermore it would be highly advantageous to attach a tube to the side of the vessel at 90^o to the bottom of the vessel to collect some of the material forced against wall before it falls off. This would allow a cross section of

the cake formed to be examined and may answer some of the questions this work raised, such as-

- Is the loss of fine particles in the <63µm size fractions due to preferential combustion or as a result of devolatilization when the flame quenches on the cake against the wall?
- Do the large particles get preferentially thrown against the wall at the final stage of combustion? Are there any left to do so?

A cross section of the cake could answer these questions.

Due to the destruction of the igniter outer casings during some tests (**Fig. 6.32**) it is thought that it would be beneficial to create an igniter cup that contains the igniters themselves to stop then breaking; possibly causing non-centred ignition.

It was hoped to compare the rate of pressure loss of fine particles to large particles, however due to differences in maximum pressure and therefore flame temp this was not possible.

9.5 Hartmann improvements

The Hartmann apparatus needs to be calibrated for an ignition delay where the material is completely and evenly dispersed at the time of ignition. The high speed video equipment could be used to determine the point in time at which the dust is evenly dispersed throughout the vessel. However it should be noted that it is thought that different mass loads and different particle sizes of material will require different time delays for this to take place. Murillo et al. (2013) puts the Hartman ignition delay at for this at 60ms for all materials and concentrations, however it is thought that a longer ignition delay may be needed for very coarse particles than for fine ones.

It highly recommended that optical probes should be used in the future to determine the dust concentration in multiple locations at once as was proposed with the $1m^3$ vessel. Fitting optical probes to the Hartmann vessel would allow for more confidence to be put in the distribution of the dust within this vessel as it has already been shown that at 0 seconds ignition delay the dust distribution is unequal. As the thermocouples have been shown to generate erroneous flame speeds due to the flame being shot out of the vessel when the vent bursts it is thought that

optical dust probes could be fitted at these locations. However these optical probes would need to be either external or very small so as not to obstruct the flame propagation in the vessel or provide obstacles for the generation of turbulence as the flame front interacts with the structure of the probe.

It would be good to assess the degree of unequal distribution within the Hartman at the time of ignition. To re-calculate the separation distances between particles based on the actual volume of the tube they occupy at the time of ignition.

It would be good to measure the particle velocity relevant to gas during distribution and combustion in this vessel to try and confirm that the Biot number affects the observed difference in the flame behaviour between <63µm and >63µm materials believed to signify the transition from thermally thin to thermally thick particles.

9.6 Future work

1. A set definition of MEC must be decided on (the last concentration that DID propagate a flame as for gas MEC definition seems logical as it allows for comparison) and the definition used given, as at present there are 2 definitions and some people do not mention which one is used. Further the limit should be defined to 10% of the MEC as for gas explosions.
2. Carry out richer tests in Hartmann apparatus to get maximum dp/dt values to improve the quality of the data used in the prediction of maximum dp/dt with D3/2 in the Hartmann apparatus.
3. Finer size segregation of the material – 250 -300µm, 300 - 350µm, 350 - 400µm, 400 -450µm, 450 -500µm. This will allow for a clearer definition of the maximum flammable particle size.
4. Run the same series of tests that were carried out here but run with large particle size spherical biomass particles such as nut dust to compare the effect of particle shape on reactivity.
5. Run the same series of tests that were carried out here but run with <10µm particle size biomass particles to compare the effect of particles with aerodynamic drag against those with none. This will allow for determination of whether or not this affects the formation of the cake at the vessel wall.
6. Porosity determination of raw materials and explosion residues using the nitrogen adsorption method (BET surface area) to investigate if there is any

change in the porosity of the explosion residue compared to the original material.

7. Investigate the effect of solid suppressants on the maximum pressure, deflagration index and flame speeds and lean limits for biomass dust explosions.
8. Develop a burner test facility for pulverised biomass that would enable gas analysis probes to travers a stable flame to be undertaken to determine the flame front volatile species. This may reveal what gasses are produced during devolatilization of biomass in a real combustion situation.
9. Extend the work on pulverised biomass explosions into explosion venting, so that existing guidance can be tested on fibrous biomass.
10. Investigation of the effect of turbulence levels on the lean limits of dusts at different (narrow) particle sizes by varying the ignition delay in the Hartmann and in the ISO 1m^3 vessel.
11. Make mixtures of <63µm, 300 - 500µm and >500µm dust varying the concentrations of each particle size but with the overall mass of material constant this should allow for much more precise identification of the percentage of fines needed for combustion to take place. As well as possibly allowing for the determination of the contribution of the large particles that will not burn on their own to the pressure generation in a mixture.
12. Make particle size distributions of <500µm, 63 -500µm, 150 -500µm, 225 - 500µm and 300 -500µm this should allow for much more precise identification of the effect of removing fines from a mixture and its effect on combustion. As well as possibly allowing for the determination of the contribution of the large particles that will not burn on their own to the pressure generation in a mixture and how this effected by the minimum particle size of this mixture.
13. Calculate difference between large and fine particle velocity ahead of flame front based on drag coefficient of particles, this would be best done after the QICPIC equipment has been sources to ensure more accurate calculations.
14. It would be useful to carry out some isothermal TG experiments to investigate the effect of particle size on thermal decomposition rate, to do this tests should be carried out on individual particles to avoid generating a bulk surface area reactivity. If the particles have constant heat of gasification then when exposed to a constant heat flux one would expect the time for complete gasification to be proportional to particle size. Unfortunately this is not possible with the current apparatus.

9.7 Equipment improvements

If more work on large particle size and large size range biomass materials is to be continued it is highly recommended that a piece of size analysis apparatus (QICPIC) is purchased. With QICPIC particle sizes between 1 µm and 20 mm are able to be analysed, therefore preventing the problem that was encountered where the size analysis machines used at present have too narrow a range of operation. Additionally the QICPIC apparatus takes pictures of the actual particle shape instead of approximating the obscuration to that of a spherical particle as the present equipment does. This would enable a far more accurate modelling/ measurement of the particles surface area : volume ratio and particle shape.

References

6184-1:1985, I. 1985. Explosion protection systems -- Part 1: Determination of explosion indices of combustible dusts in air.

A. GARCIA-MARAVER, J. A. P.-J. 2015. *Biomass Pelletization: Standards and Production*, WIT Press.

ABBASI, T. & ABBASI, S. A. 2007. Dust explosions–Cases, causes, consequences, and control. *Journal of Hazardous Materials,* 140**,** 7-44.

ANDREWS, G. E. & BRADLEY, D. 1972. Determination of burning velocities: A critical review. *Combustion and Flame,* 18**,** 133-153.

ANDREWS, G. E. & BRADLEY, D. 1973. Limits of flammability and natural convection for methane-air mixtures. *Proceedings of the Fourteenth Symposium of Combustion***,** 1119-1128

ANDREWS, G. E. P., HERODOTOS N. 2010. Explosion Safety. *Handbook of Combustion.* Wiley-VCH Verlag GmbH & Co. KGaA.

ARBON, I. 8th International Conference on Sustainable Energy and Environmental Protection, 2015. University of West of Scotland, Key note lecture.

BARTKNECHT 1981 *Explosion's prevention protection. ,* Berlin, Springer-Verlag.

BARTKNECHT, W. 1989. *Dust explosions,* Berlin, Springer-Verlag

BBC. 2011. Fire crews tackle wooden pellets blaze at Port of Tyne. Available: http://www.bbc.co.uk/news/uk-england-tyne-15511691.

BBC. 2014. Bosley mill explosion: HSE finds 'dust issues' at blast site. Available: http://www.bbc.co.uk/news/uk-england-33887081.

BEC, B. E. C. 2005. Co-firing fuels. Available: http://www.biomassenergycentre.org.uk/portal/page?_pageid=75,41192&_dad=portal&_schema=PORTAL.

BECK, N. G., C. MOHLMAN 1997. Combustion and explosion characteristics of dusts (BIA-Report 13/97).

BERGMAN, A. R. B., J.H.A. KIEL, M.J. PRINS, K.J. PTASINSKI, F.J.J.G. JANSSEN 2011. Torrefaction for entrained-flow gasification of biomass. *Energy research Centre of the Netherlands*.

BIAGINI, E., BARONTINI, F. & TOGNOTTI, L. 2006. Devolatilization of Biomass Fuels and Biomass Components Studied by TG/FTIR Technique. *Industrial & Engineering Chemistry Research,* 45**,** 4486-4493.

BIDABADI, M. & RAHBARI, A. 2009. Modeling combustion of lycopodium particles by considering the temperature difference between the gas and the particles. *Combustion, Explosion, and Shock Waves,* 45**,** 278-285.

BRADLEY, D., LAWES, M., LIAO, S. & SAAT, A. 2014. Laminar mass burning and entrainment velocities and flame instabilities of i-octane, ethanol and hydrous ethanol/air aerosols. *Combustion and Flame,* 161**,** 1620-1632.

BRADLEY, D. & MITCHESON, A. 1976. Mathematical solutions for explosions in spherical vessels. *Combustion and Flame,* 26**,** 201-217.

BSEN 2004. BS EN 14034-1. *Determination of explosion characteristics of dust clouds. Determination of the maximum explosion pressure pmax of dust clouds.*

BSEN 2011. Determination of the lower explosion limit LEL of dust clouds. EN 14034-3:2006+A1:2011. . *Part 3.*

BSI 1991. Explosion protection systems — Part 1: Method for determination of explosion indices of combustible dusts in air.

BSI 2012. Determination of explosion limits of gases and vapours.

BSI, B. S. I. 2006. I.S. EN 14034-2:2006 - Determination Of Explosion Characteristics Of Dust Clouds - Part 2: Determination Of The Maximum Rate Of Explosion Pressure Rise (dp/dt)[max] Of Dust Clouds.

BURGOYNE, J. H. & COHEN, L. 1954. *The Effect of Drop Size on Flame Propagation in Liquid Aerosols*.

CALLÉ, S., KLABA, L., THOMAS, D., PERRIN, L. & DUFAUD, O. 2005. Influence of the size distribution and concentration on wood dust explosion: Experiments and reaction modelling. *Powder Technology,* 157**,** 144-148.

CASHDOLLAR, K. L. 1996. Coal dust explosibility. *Journal of Loss Prevention in the Process Industries,* 9**,** 65-76.

CASHDOLLAR, K. L. 2000. Overview of dust explosibility characteristics. *Journal of Loss Prevention in the Process Industries,* 13**,** 183-199.

CASHDOLLAR, K. L. H. M. 1987 *Industrial Dust Explosions: Symposium on Industrial Dust Explosions : Pittsburgh, Pennsylvania, 10-13 June 1986*, American Society for Testing and Materials.

CETIN, E. M., B. GUPTA, R. WALL, T. F. 2004. Influence of pyrolysis conditions on the structure and gasification reactivity of biomass chars. *Fuel,* 83**,** 2139-2150.

CHAWLA, N., AMYOTTE, P. R. & PEGG, M. J. 1996. A comparison of experimental methods to determine the minimum explosible concentration of dusts. *Fuel,* 75**,** 654-658.

COMMANDRÉ, L., H. SALVADOR, S. DUPASSIEUX, N. 2011. Pyrolysis of wood at high temperature: The influence of experimental parameters on gaseous products. *Fuel Processing Technology,* 92**,** 837-844.

COOK, C., C. F. GOOD, A. J. 1977. The measurement of the flammability limits of mists. *Combustion and Flame,* 30**,** 309-317.

CORELLA, M., A. SANTAMARIA, J. GONZÁLEZ-CAÑIBANO, J. 1988. Ultra-Fast Biomass Pyrolysis in a High-Temperature (2200° C), Fluid-Wall Reactor. *Journal of Solar Energy Engineering,* 110**,** 10-13.

COUHERT, C., COMMANDRE, J.-M. & SALVADOR, S. 2009. Is it possible to predict gas yields of any biomass after rapid pyrolysis at high temperature from its composition in cellulose, hemicellulose and lignin? *Fuel,* 88**,** 408-417.

CSHIB 2008. INVESTIGATION REPORT. U.S. CHEMICAL SAFETY AND HAZARD INVESTIGATION BOARD.

DASTIDAR, A., AMYOTTE PAUL, GOING JOHN, CHATRATHI KRIS 2001. Inerting of coal dust explosions in laboratory- and intermediate-scale chambers. *Fuel,* 80**,** 1593-1602.

DASTIDAR, A. G., AMYOTTE, P. R. & PEGG, M. J. 1997. Factors influencing the suppression of coal dust explosions. *Fuel,* 76**,** 663-670.

DASTIDAR, A. G. A., P. R. 2002. Explosibility boundaries for fly ash/pulverized fuel mixtures. *Journal of Hazardous Materials* 92**,** 115-126.

DEBYE 1920. *Van der Waals cohesion forces.,* Physikalische Zeitschrift.

DECC, D. O. E. C. C. 2012. UK Bioenergy Strategy.

DEGUINGAND, B. & GALANT, S. 1981. Upper flammability limits of coal dust-AIR mixtures. *Symposium (International) on Combustion,* 18**,** 705-715.

DENKEVITS, A. 2007. Explosibility of hydrogen–graphite dust hybrid mixtures. *Journal of Loss Prevention in the Process Industries,* 20**,** 698-707.

DUKES, D. O. U. E. S. 2014a. Electricity. *Digest of UK energy statistics (DUKES).*

DUKES, D. O. U. E. S. 2014b. Renewable sources of energy Chapter 6 *Digest of UK energy statistics (DUKES).*

ECKHOFF, R. 2003. *Dust Explosions in the Process Industries: Identification, Assessment and Control of Dust Hazards*, Elsevier Science.

EISENSCHITZ, R. & LONDON, F. 1930. Über das Verhältnis der van der Waalsschen Kräfte zu den homöopolaren Bindungskräften. *Zeitschrift für Physik,* 60**,** 491-527.

EPRA, -. E. P. R. A. 2011. Dust Explosion Guidelines European Phenolic Resins Association.

ESSENHIGH, R. H. & CSABA, J. 1963. The thermal radiation theory for plane flame propagation in coal dust clouds. *Symposium (International) on Combustion,* 9**,** 111-125.

EU ENERGY POLICY 2010. Renewable energy directive. *In:* POLICY, E. (ed.). European Commission.

FENELONOV, V. B. M. G., MAXIM SERGEEVICH PARMON, VALENTIN N. 2010. The Properties of Cenospheres and the Mechanism of Their Formation During High-Temperature Coal Combustion at Thermal Power Plans. *KONA Powder and Particle Journal,* 28**,** 189-208.

FIELD, P. 1983. *Explosibility assessment of industrial powders and dusts*, HMSO, Dept. Env., BR

FIELD, P. P. F. 1982 *Dust explosions. ,* Amsterdam Elsevier.

FONIOK, R. 1985 Hybrid dispersive mixtures and inenized mixtures of coal dust - explosiveness and ignitability. *Luft* 45(4) 151-154.

FORUM, T. E. Explosion at biomass plant kills three. The Electricity Forum: electricity forum.

FOULKE, E. G. 2007. Combustible Dust National Emphasis Program. *In:* ADMINISTRATION, O. S. H. A. O. S. H. (ed.).

GAO, W. M., TOSHIO YU, JIANLIANG YAN, XINGQING SUN, JINHUA DOBASHI, RITSU 2015. Flame propagation mechanisms in dust

explosions. *Journal of Loss Prevention in the Process Industries,* 36**,** 186-194.

GLINKA, W., WANG, X., WOLANSKI, P., & XIE, L. . Velocity and structure of laminar dust flames. pp. 6.1–6.18. 6th International Colloquium on Dust Explosion, 1996 Brgen, Norway. pp. 6.1–6.18.

GLOR, M. 2003. Ignition hazard due to static electricity in particulate processes. *Powder Technology***,** 223 - 233.

HACKETT, D. L. 2015. Drax CCS Energy Institute.

HAN, O.-S., YASHIMA, M., MATSUDA, T., MATSUI, H., MIYAKE, A. & OGAWA, T. 2000. Behavior of flames propagating through lycopodium dust clouds in a vertical duct. *Journal of Loss Prevention in the Process Industries,* 13**,** 449-457.

HAN, O.-S. Y., MASAAKI, MATSUDA, TOEI, MATSUI, HIDENORI, MIYAKE, ATSUMI, OGAWA, TERUSHIGE 2001. A study of flame propagation mechanisms in lycopodium dust clouds based on dust particles' behavior. *Journal of Loss Prevention in the Process Industries,* 14**,** 153-160.

HARKER, J. H., J. R. BACKHURST 1981. *Fuel and energy,* the University of Michigan, Academic Press.

HAYHURST, A. N. 2013. The kinetics of the pyrolysis or devolatilisation of sewage sludge and other solid fuels. *Combustion and Flame,* 160**,** 138-144.

HAYNES, W. M. & LIDE, D. R. 2011. *CRC handbook of chemistry and physics : a ready-reference book of chemical and physical data,* Boca Raton, Fla., CRC Press.

HERRIN, J. M. & DEMING, D. 1996. Thermal conductivity of U.S. coals. *Journal of Geophysical Research: Solid Earth,* 101**,** 25381-25386.

HERTZBERG, M. C., KENNETH L. LAZZARA, CHARLES P. SMITH, ALEX C 1982. *Inhibition and extinction of coal dust and methane explosions,* the University of Michigan, U.S. Dept. of the Interior, Bureau of Mines.

HERTZBERG, Z. C. 1992. Metal dust combustion. *Pittsburgh PA combustion institute,* 24th synopsis**,** (p.p 1827-1835).

HOEKSTRA, G. 2012 Fatal sawdust blast in B.C. comes after five explosions at similar plants since 2009. Available: http://news.nationalpost.com/news/canada/fatal-sawdust-blast-in-b-c-comes-after-five-explsions-at-similar-plants-since-2009.

HUESCAR, C., PHYLAKTOU, H. N., ANDREWS, G. E. & GIBBS, B. M. Determination of the minimum explosible and most reactive concentrations for pulverised biomass using a modified Hartmann apparatus. Proceedings of the IX International Seminar on Hazardous Process Materials and Industrial Explosions, 2012a Krakow, Poland.

HUESCAR, C., SATTAR, H., PHYLAKTOU, H. N., ANDREWS, G. E. & GIBBS, B. M. Explosibility of biomass and torrefied biomass powders: Determination of Minimum Explosible Concentrations. Proceedings of 20th European Biomass conference, 2012b Millan, Italy.

HUILING, D., QINGQING REN, JUNLI JIAN, LONGFEI PENG, FENG SUN, RUNCANG LIU, GUOLIANG 2015. Effect of structural characteristics of corncob hemicelluloses fractionated by graded ethanol precipitation on furfural production. *Carbohydrate Polymers,* 136**,** 203-209.

JECHURA, J. 1987. *API Technical Data Book*.

JENSEN, S. G. Review of coal dust explosibility research. The AusIMM Proceedings, 1994.

JOHNSON, K., K. ROBERTS, A. D. 1971. *Surface Energy and the Contact of Elastic Solids*.

JUN, D., ZHENMIN, L., XIAOCHUN, W. & YAOYUAN, H. 2010. Explosive limits of mixed gases containing CH4, CO and C2H4 in the goaf area. *Mining Science and Technology (China)* 20**,** 557–562.

KANG PU, Y., JAROSINSKI, J., SHENG TAI, C., WILLIAM KAUFFMAN, C. & SICHEL, M. 1989. The investigation of the feature of dispersion induced turbulence and its effects on dust explosions in closed vessels. *Symposium (International) on Combustion,* 22**,** 1777-1787.

KEESOM 1921. Die van der Waalsschen Kohasionskrafte. *Physik.,* 22**,** pp. 643-644.

KOBAYASHI, H., HOWARD, J. B. & SAROFIM, A. F. 1977. Coal devolatilization at high temperatures. *Symposium (International) on Combustion,* 16**,** 411-425.

L. W. KULA, M. M. Y. 1991. Characteristic Length of Complex Bodies for Transient Conduction.

LADDHA, S. Coal Dust. *http://www.suprememinerals.in/coal-dust.htm.* supream minerals: supream minerals.

LENTINI, J. J. 2006. *Scientific Protocols for Fire Investigation*.

LEWELLEN, P. C. P., W. A. HOWARD, J. B. 1977. Cellulose pyrolysis kinetics and char formation mechanism. *Symposium (International) on Combustion,* 16**,** 1471-1480.

LEWIS, G. V. E. 1987 *Combustion, flames and explosions of gases,* Hartcourt Brace Jovanovich, New York.

LEWIS, G. V. E., PH.D. 1938. Combustion, flames, and explosions of gases. *Journal of the Society of Chemical Industry,* 57**,** 475-477.

LI, G., YUAN, C. M., FU, Y., ZHONG, Y. P. & CHEN, B. Z. 2009. Inerting of magnesium dust cloud with Ar, N2 and CO2. *Journal of Hazardous Materials,* 170**,** 180-183.

LIVINGSTON. 2013 The firing and co-firing of biomass in large pulverised coal boilers.

M. TRAORÉ, O. D., LAURENT PERRIN, S. CHAZELET, DOMINIQUE THOMAS 2009. Dust explosions: How should the influence of humidity be taken into account? *PROCESS SAFETY AND ENVIRONMENTAL PROTECTION*.

MACLEAY, K. H., ANWAR ANNUT 2015. Digest of United Kingdom Energy Statistics 2015. Department of energy and climate change.

MAIL, D. 2012. Tilbury Power Station. Available: http://www.dailymail.co.uk/news/article-2107082/Tilbury-Fire-100-firefighters-tackle-huge-blaze-Europes-biggest-biomass-power-station.html.

MAISEY 1965. Chemical and Process Engineering *Chemical and Process Engineering* 46 662-672.

MALAV, D., GANGULI, R., DUTTA, S. & BANDOPADHYAY, S. 2008. Non-impact of particle size distribution on power generation at a pulverized coal power plant burning low rank Alaska coal. *Fuel Processing Technology,* 89**,** 499-502.

MAN, C. K. & HARRIS, M. L. 2014. Participation of large particles in coal dust explosions. *Journal of Loss Prevention in the Process Industries,* 27**,** 49-54.

MASON, P. E. D., L. I. JONES, J. M. POURKASHANIAN, M. WILLIAMS, A. 2015. Single particle flame-combustion studies on solid biomass fuels. *Fuel,* 151**,** 21-30.

MOHAN, D., PITTMAN, C. U. & STEELE, P. H. 2006. Pyrolysis of Wood/Biomass for Bio-oil: A Critical Review. *Energy & Fuels,* 20**,** 848-889.

MURILLO, C., DUFAUD, O., LOPEZ, O., PERRIN, L., VIGNES, A. & MUNOZ, F. CFD modelling of nanoparticles dispersion in a dust explosion apparatus. 14. International Symposium on Loss Prevention and Safety Promotion in the Process Industry, 2013-05-12 2013 Florence, Italy. AIDIC. Milano, 889-894.

NFPA 2012. NFPA 654: Standard for the Prevention of Fire and Dust Explosions from the Manufacturing, Processing, and Handling of Combustible Particulate Solids.

NFPA 2013. NFPA® 68 Standard on Explosion Protection by Deflagration Venting.

PHYLAKTOU, C. L. G. A. G. E. A. 2010. Flame Speed Measurements in Dust Explosions. *FEH6.*

PHYLAKTOU, G. A. A. 2001. charicteristics of confined turbulent gas explosion with refference to protection methodologys. *18 ICDUS*.

PILÃO, R., RAMALHO, E. & PINHO, C. 2004. Influence of initial pressure on the explosibility of cork dust/air mixtures. *Journal of Loss Prevention in the Process Industries,* 17**,** 87-96.

PILÃO, R., RAMALHO, E. & PINHO, C. 2006. Overall characterization of cork dust explosion. *Journal of Hazardous Materials,* 133**,** 183-195.

POLYMEROPOULOS, C. E. 1984. Flame Propagation in Aerosols of Fuel Droplets, Fuel Vapor and Air. *Combustion Science and Technology,* 40**,** 217-232.

PROUST, C. Experimental Determination of the Maximum Flame Temperatures and of the Laminar Burning Velocities for Some Combustible Dust-Air Mixtures. Fifth International Colloquium on Dust Explosions, 1993 Pultusk, Poland.

PROUST, C. 2006. A few fundamental aspects about ignition and flame propagation in dust clouds. *Journal of Loss Prevention in the Process Industries,* 19**,** 104-120.

RAMÍREZ, Á., GARCÍA-TORRENT, JAVIER AGUADO, PEDRO J. 2009. Determination of parameters used to prevent ignition of stored materials and to protect against explosions in food industries. *Journal of Hazardous Materials,* 168**,** 115-120.

SATTAR, H. S., D.J.F. ANDREWS, G.E. GIBBS, B.M PHYLAKTOU, H.N.,. Pulverised Biomass Explosions: Investigation of the Ultra Rich Mixtures that give Peak Reactivity. Proceedings of the IX International Seminar on Hazardous Process Materials and Industrial Explosions, 2012 Krakow, Polland.

SHAO, Y. 2008. *Physics and Modelling of Wind Erosion,* Holland, springer

SOLOMON, P. R., HAMBLEN, D. G., CARANGELO, R. M., SERIO, M. A. & DESHPANDE, G. V. 1988. General model of coal devolatilization. *Energy & Fuels,* 2**,** 405-422.

STANDARD, E. 2003. Limits of Flammability Measurement Standard for Gases and Vapours. *BS EN 1839:2012.*

STEPZINSKI, T. 2011. Overheated assembly caused Georgia Biomass explosion. Available: http://jacksonville.com/news/georgia/2011-07-13/story/overheated-assembly-caused-georgia-biomass-explosion.

TILLMAN, D. A. 1978. Wood as an Energy Resource. *In:* TILLMAN, D. A. (ed.) *Wood as an Energy Resource.* Academic Press.

TOMINAGA, T. M., S. ; KOMAI, T. ; ISEI, T. 1987. Coal Dust Explosion Characteristics under Atmosphere with Methane Gas Coexistence. *Safety in mines research 22nd International conference*

TOOLBOX, T. E. Thermal Conductivity of some common Materials and Gases. *In:* TOOLBOX, T. E. (ed.).

TORTOSA MASIÁ, A. A., BUHRE, B. J. P., GUPTA, R. P. & WALL, T. F. 2007. Characterising ash of biomass and waste. *Fuel Processing Technology,* 88**,** 1071-1081.

TRAORÉ, M., DUFAUD, O., PERRIN, L., CHAZELET, S. & THOMAS, D. 2009. Dust explosions: How should the influence of humidity be taken into account? *Process Safety and Environmental Protection,* 87**,** 14-20.

UBHAYAKAR, S. K., STICKLER, D. B., VON ROSENBERG, C. W. & GANNON, R. E. 1977. Rapid devolatilization of pulverized coal in hot combustion gases. *Symposium (International) on Combustion,* 16**,** 427-436.

UPDEGRAFF, D. M. 1969. Semimicro determination of cellulose inbiological materials. *Analytical Biochemistry,* 32**,** 420-424.

VAN LOO, J. K. 2002 *Handbook of Biomass Combustion and Co-Firing*, Twente University Press.

VERAKIS, V. J. N. U. H. C. 1983. *Development and Control of Dust Explosions. ,* New York.

WAYNE. 2011. Green FAIL – FOIA shows dangerous university biomass power plant fraught with problems, closures, explosion. Available: http://wattsupwiththat.com/2011/10/09/green-fail-foia-shows-

dangerous-university-biomass-power-plant-frought-with-problems-closures-explosion/.

WILÉN, C., MOILANEN, A, RAUTALIN, A, TORRENT, J, CONDE, E, LÖDEL, R, CARLSON, D, TIMMERS, P, BREHM, K. 1999. Safe handling of renewable fuels and fuel mixtures. *VTT Publications, Finland* 1-117.

WILÉN, C. & RAUTALIN, A. Safe handlimg of biomass fuels in IGCC power production. 9th European Bioenergy Conference, 1996 Copenhagen. 170-175.

WILLIAM SIMPSON, A. T. 1999. *Wood handbook—Wood as an engineering material.* , U.S. Department of Agriculture, Forest Service, Forest Products Laboratory. .

WILLIAMS, P. T., BESLER, S. & TAYLOR, D. T. 1990. The pyrolysis of scrap automotive tyres: The influence of temperature and heating rate on product composition. *Fuel,* 69**,** 1474-1482.

WONG, S. H. 2013. Sawmill Wood Dust Sampling Analysis and Explosibility. fpi nnovations.

YAO B. YANG, V. N. S., JIM SWITHENBANK, LIN MA, LEILANI I. DARVELL, & JENNY M. JONES, M. P., AND ALAN WILLIAMS*, 2008. Combustion of a Single Particle of Biomass. *Energy & Fuels,* 22**,** 306-316.

ZABETAKIS, M. G. 1965. Flammability characteristics of combustible gases and vapors. Bureau of Mines, U.S.

ZABETAKIS, M. G. 1965. Flammability Characteristics of Combustible Gases and Vapors.: US Bureau of Mines.

ZANZI, R., SJÖSTRÖM, K. & BJÖRNBOM, E. 1996. Rapid high-temperature pyrolysis of biomass in a free-fall reactor. *Fuel,* 75**,** 545-550.

ZINK-SHARP, A. 1997. particle board. *In:* BOARD, P. (ed.). woodmagic.vt.edu.